Measuring and Modelling Human Response to Foot-transmitted Vibration Exposure

by

Katie Anne Goggins

A thesis submitted in partial fulfillment
of the requirements for the degree of
Doctor of Philosophy (PhD) in Natural Resources Engineering

The Faculty of Graduate Studies
Laurentian University
Sudbury, Ontario, Canada

THESIS DEFENCE COMMITTEE/COMITÉ DE SOUTENANCE DE THÈSE
Laurentian Université/Université Laurentienne
Faculty of Graduate Studies/Faculté des études supérieures

Title of Thesis Titre de la thèse	Measuring and Modelling Human Response to Foot-transmitted Vibration Exposure	
Name of Candidate Nom du candidat	Goggins, Katie Ann	
Degree Diplôme	Doctor of Philosophy	
Department/Program Département/Programme	Natural Resources Engineering	Date of Defence July 16, 2019 Date de la soutenance July 16, 2019

APPROVED/APPROUVÉ

Thesis Examiners/Examinateurs de thèse:

Dr. Tammy Eger
(Supervisor/Directrice de thèse)

Dr. Brent Lievers
(Co-supervisor/Co-directeur de thèse)

Dr. Marc Arsenault
(Committee member/Membre du comité)

Dr. Markus Timusk
(Committee member/Membre du comité)

(Committee member/Membre du comité)

Dr. Peter W. Johnson Dean, Faculty of Graduate Studies
(External Examiner/Examinateur externe)

Dr. Judith M. Horrigan
(Internal Examiner/Examinateur interne)

Approved for the Faculty of Graduate Studies
Approuvé pour la Faculté des études supérieures
Dr. David Lesbarrères
Monsieur David Lesbarrères

Doyen, Faculté des études supérieures

ACCESSIBILITY CLAUSE AND PERMISSION TO USE

I, **Katie Ann Goggins**, hereby grant to Laurentian University and/or its agents the non-exclusive license to archive and make accessible my thesis, dissertation, or project report in whole or in part in all forms of media, now or for the duration of my copyright ownership. I retain all other ownership rights to the copyright of the thesis, dissertation or project report. I also reserve the right to use in future works (such as articles or books) all or part of this thesis, dissertation, or project report. I further agree that permission for copying of this thesis in any manner, in whole or in part, for scholarly purposes may be granted by the professor or professors who supervised my thesis work or, in their absence, by the Head of the Department in which my thesis work was done. It is understood that any copying or publication or use of this thesis or parts thereof for financial gain shall not be allowed without my written permission. It is also understood that this copy is being made available in this form by the authority of the copyright owner solely for the purpose of private study and research and may not be copied or reproduced except as permitted by the copyright laws without written authority from the copyright owner.

shall not be allowed without my written permission. It is also understood that this copy is being made available in this form by the authority of the copyright owner solely for the purpose of private study and research and may not be copied or reproduced except as permitted

Abstract

Foot-transmitted vibration (FTV) occurs when a worker is exposed to vibration through the feet and can occur when operating vibrating equipment such as bolters, jumbo drills, or crushers, or standing to operate mobile equipment such as locomotives and forklifts. Exposure to FTV has been linked to the development of vibration-induced white feet, a vascular disorder with reduced circulation to the toes causing blanching. Vibration research has been focused on whole-body vibration (WBV) and hand-arm vibration, with FTV being lumped in to standing WBV. This research includes, but is not limited to, resonant frequency identification, development of international standards governing safe exposure limits, personal protective equipment design, and model development. It is the intention of this research to initiate research specifically for FTV.

The first step to preventing harmful exposure is to identify the resonant frequencies at different anatomical locations on the foot (Objective 1). The resonance of 24 anatomical locations on the foot was identified for 21 participants, where the most notable differences in the average peak frequency occurred between the toes (range: 99-147Hz), midfoot (range: 51-84Hz), and ankle (range: 16-39Hz).

As workers do not normally stand in a completely natural position, it was equally important to measure how altering the location of the centre of pressure (COP) changes resonance and the transmissibility of vibration through the foot (Objective 2). The resonance at the same 24 anatomical locations was identified when the COP was pushed forward (towards toes) and backward (towards heels). Generally, resonance at the measurement location increased when the COP was concentrated to a particular portion of the foot.

The third objective of this research was to reduce the measurements at 24 anatomical locations, from the first two objectives, down to a representative subset (Objective 3). Multiple correspondence analysis was conducted on the peak transmissibility magnitude in order to assess

structure displacement leading to increases in potential injury risk. Transmissibility results were analysed based on two magnitude thresholds: at 2.0 indicating 100% amplification of the input signal, and at 2.5 indicating 150% amplification. Results indicate that transmissibility measurements at the nail bed of first phalange, head of first metatarsal, head of second metatarsal, and the lateral malleolus may be sufficient to effectively measure foot-transmitted vibration when participants changed their COP location from natural, forward and backward.

Then a K-means analysis was conducted to minimize the anatomical locations necessary to capture the transmissibility response from 10 to 200 Hz, and using the reduced locations, a lumped-parameter model was designed and validated (Objective 4). Three locations (the nail of the big toe, the third metatarsal, and the lateral malleolus) were found to be sufficient for summarizing FTV transmissibility modulus. A three segment, four degrees-of-freedom lumped-parameter model of the foot-ankle system (FAS) was designed to model the transmissibility response at three locations when exposed to vertical vibration from 10 to 60 Hz. Reasonable results were found at the ankle, midfoot, and toes in the natural standing position and forward COP. However, when the COP is backward, the model does not sufficiently capture the transmissibility response at the ankle.

Determining the resonant frequencies of the FAS is important for the prevention of vibration-induced injury. Resonance needs to be incorporated into the design of equipment, tools (e.g. anti-vibration drills, isolated platforms), and personal protective equipment (e.g. anti-vibration insoles or boots) can be modified to reduce vibration at the frequencies where tissue resonance occurs. These findings could also inform the development of new international standards for measuring/reducing exposure to FTV.

Co-Authorship Statements

The enclosed dissertation has been written in a manuscript-based format. For the purposes of this document, the original manuscripts have been re-formatted to disseminate the research in one cohesive work. A list of the manuscripts, including their journal submission information and author institutions, is provided here. The nature and scope of the work of the individual co-authors for each manuscript is summarized in the associated tables.

Chapter 3

Katie A. Goggins*[1,2], Marco Tarabini[3], W. Brent Lievers[1,2], Tammy R. Eger[2,4]. (2018). Biomechanical response of the human foot when standing in a natural position while exposed to vertical vibration from 10-200 Hz. *Ergonomics.* doi: 10.1080/00140139.20181559362

[1]*Bharti School of Engineering, Laurentian University, Sudbury, Canada*
[2]*Centre for Research in Occupational Safety and Health, Laurentian University, Sudbury, Canada*
[3]*Department of Mechanics, Politecnico di Milano, Lecco, Italy*
[4]*School of Human Kinetics, Laurentian University, Sudbury, Canada*

Author Contribution	K. Goggins	M. Tarabini	B. Lievers	T.Eger
Study Design	✓			
Data acquired/collected	✓	✓		✓
Supervision			✓	✓
Advice		✓	✓	✓
Organised study	✓	✓		✓
Provided equipment		✓		
Programming	✓	✓		
Statistical analysis	✓			
Manuscript preparation	✓			
Manuscript revision			✓	✓
Technical assistance		✓		
Financial support		✓	✓	✓
Institutional support		✓		

Chapter 4

Katie A. Goggins*[1,2], Marco Tarabini[3], W. Brent Lievers[1,2], Tammy R. Eger[2,4]. (2019). Standing centre of pressure alters the vibration transmissibility response of the foot. *Ergonomics.* (under review)

[1]*Bharti School of Engineering, Laurentian University, Sudbury, Canada*
[2]*Centre for Research in Occupational Safety and Health, Laurentian University, Sudbury, Canada*
[3]*Department of Mechanics, Politecnico di Milano, Lecco, Italy*
[4]*School of Human Kinetics, Laurentian University, Sudbury, Canada*

Author Contribution	**K. Goggins**	**M. Tarabini**	**B. Lievers**	**T.Eger**
Study Design	✓			
Data acquired/collected	✓	✓		✓
Supervision			✓	✓
Advice		✓	✓	✓
Organised study	✓	✓		✓
Provided equipment		✓		
Programming	✓	✓		
Statistical analysis	✓			
Manuscript preparation	✓			
Manuscript revision			✓	✓
Technical assistance		✓		
Financial support		✓	✓	✓
Institutional support		✓		

Chapter 5

Katie A. Goggins*[1,2], Bruce E. Oddson[2,3], W. Brent Lievers[1,2], Tammy R. Eger[2,4]. (2019). Anatomical locations for capturing magnitude differences in foot-transmitted vibration exposure determined using multiple correspondence analysis. *Theoretical Issues in Ergonomics Science.* (Submitted)

[1]*Bharti School of Engineering, Laurentian University, Sudbury, Canada*
[2]*Centre for Research in Occupational Safety and Health, Laurentian University, Sudbury, Canada*
[3]*Laurentian Research Institute in Aging, Laurentian University, Sudbury, Canada*
[4]*School of Human Kinetics, Laurentian University, Sudbury, Canada*

Author Contribution	**K. Goggins**	**B. Oddson**	**B. Lievers**	**T.Eger**
Study Design	✓			
Data acquired/collected	✓			
Supervision			✓	✓
Advice		✓		
Organised study	✓			
Provided equipment				
Programming	✓	✓		
Statistical analysis	✓	✓		
Manuscript preparation	✓			
Manuscript revision		✓	✓	✓
Technical assistance		✓		
Financial support			✓	✓
Institutional support		✓	✓	✓

Chapter 6

Katie Goggins*[1,2], Delphine Chadefaux[3], Marco Tarabini[3], Brent Lievers[1,2], Tammy Eger[2,4]. (2019). Three segment, four degrees-of-freedom lumped parameter model of the foot-ankle system exposure to vertical vibration. *Journal of Sound and Vibration.* (to be submitted)

[1]*Bharti School of Engineering, Laurentian University, Sudbury, Canada*
[2]*Centre for Research in Occupational Safety and Health, Laurentian University, Sudbury, Canada*
[3]*Department of Mechanics, Poloitecnico di Milano, Lecco, Italy*
[4]*School of Human Kinetics, Laurentian University, Sudbury, Canada*

Author Contribution	**K. Goggins**	**D. Chadefaux**	**M. Tarabini**	**B. Lievers**	**T.Eger**
Study Design	✓				
Data acquired/collected	✓				
Supervision				✓	✓
Advice		✓	✓		
Organised study	✓				
Provided equipment			✓		
Programming	✓	✓			
Statistical analysis	✓	✓		✓	
Manuscript preparation	✓				
Manuscript revision		✓	✓	✓	✓
Technical assistance		✓	✓		
Financial support			✓	✓	✓
Institutional support			✓		

Acknowledgements

In order to thank those who helped me through these last four years, in classic Katie fashion, I have listed everyone (in no particular order – they're not numbered).

Tammy and Brent
Thank you for your supervision throughout my PhD process. I am grateful for your guidance, dedication to providing me revisions, commitment to challenging me to grow as a researcher, and for offering me countless experiences to further develop my academic and professional portfolio. From working in Italy each year, to the international conferences I was able to attend and present at, to meeting industry experts – I thank you both for never holding me back from any opportunity. I had an amazing, well-rounded experience as a PhD student – thank you.

Marco, Francesco, Delphine, and Pietro
My new friends from Italy, thank you for offering your expertise, access to equipment and personnel that was foundational to completing my thesis work. I truly admire how hard-working and dedicated all of you are to your research. I could not have finished this dissertation without your technical expertise and willingness to help.

Bruce
Thank you for all of your help with my statistical analysis. I really value all of our discussions and conversations that challenged me to think and approach my research in new ways. I truly appreciated the days when you would come into the CROSH lab to check on my progress and wellbeing. You are a true advocate for student academics.

Leah
Thank you for helping me with my graphical abstracts for journal publications. Your expertise in graphic design was very much appreciated and led to some fantastic visualizations.

Mom
Thank you for always supporting me in my decisions – even when you thought they were crazy. And for constantly making homecooked food to keep me fueled so that I could focus and dedicate myself to my research.

Family
Dad, Shelby and Maggie
Tracy (Tim), Dayna (Mallory, Ethan, and Camden)
Thank you for always showing up. Regardless of what the presentations were for, you were all always there to sit, listen, and support me. You all have been showing up to watch me for years.

Emily
Thank you for pushing me to be a more well-rounded student by getting me involved in more than just my research. Thank you for all of your help with designing my presentations, making my rough sketches come to life as actual graphics, and for listening to me practice my presentations. Thank you for always encouraging me to pursue my hobbies and take breaks regularly.

Mallorie, Caleb and the Girls
Thank you for always being ready for a coffee break and offering your support throughout the thesis dissertation process. I love that the girls know how to make me a fancy coffee whenever I stop by, and playing (skating, colouring, legos, and watching dance routines) with the girls offered a much needed mental break for me.

Brandon
Thank you for always being ready to help me with any of my projects whenever I asked. Our work breaks to play squash were always necessary, and I really appreciated our friendship and ability to talk honestly.

Lisa & Izzy
Thank you for helping me redo my data analysis, with a newborn baby in-toe, when I had a meltdown, needing to fix my entire data set. Thanks for always having me over, feeding me regularly, and letting me play with Izzy.

Mike
Thank you for asking me to coach basketball with you. At first I thought it would be too much to take on, but I really appreciate being able to spend time with you and the kids we coach. This time was always a very welcome break from work.

Table of Contents

List of Tables

List of Figures

List of Appendices

Glossary of Abbreviations, Terminology and Nomenclature

Abbreviation	Long Form
A(8)	8-hr frequency-weighted r.m.s. acceleration
a_{hv}	vibration total value (frequency-weighted for hand-arm vibration exposure)
AM	apparent mass
ANOVA	analysis of variance
ASD	auto-spectral density
COP	centre of pressure
CPT	current perception threshold
CSD	cross-spectral density
DFT	discrete Fourier transform
DOF	degrees of freedom
DPR	driving-point response
EMG	Electromyography
EU	European Union
FRF	frequency response function
FTV	foot-transmitted vibration
HAV	hand-arm vibration
HAVS	hand-arm vibration syndrome
HTV	hand-transmitted vibration
ISO	International Organization for Standardization
LP	lumped-parameter
MCA	multiple correspondence analysis
MI	mechanical impedance
NIOSH	National Institute for Occupational Safety and Health
PPE	personal protective equipment
PSD	power spectral density
RMS	root-mean squared
SNR	signal-to-noise ratio
VDV	vibration dose value
VIWF	vibration-induced white finger
VIWFt	vibration-induced white foot
WBV	whole-body vibration
VR	vibration-reducing
W_d	weighting filter for x and y-axis of seat surface for WBV exposure (ISO 2631-1)
W_k	weighting filter for z-axis of seat surface for WBV exposure (ISO 2631-1)
W_h	weighting filter for hand-arm system (ISO 5349-1)

Terminology

Definitions were drawn from International Standard (ISO) 2041 – *Vibration and Shock Vocabulary* (1990).

Amplification: An increase in amplitude and intensity of a signal.

Apparent mass: The apparent mass at a certain frequency corresponds to the force divided by the acceleration. For rigid systems the apparent mass is the same as the mass of the system. For systems such as the human body, the equation is a function of frequency such that the apparent mass is greater at some frequencies than others.

Attenuation: A reduction in amplitude and intensity of a signal.

Biodynamic/biomechanical response: The science of the physical, biological and mechanical properties and responses of the human body (tissues, organs, parts and systems) to an external force (vibration) or in relation to the internal forces, produced by an interplay of external forces and the body's mechanical activity.

Cross-spectral density: Measures the relationship between two signals, including the phase difference between them.

Dominant frequency: A frequency at which a maximum value occurs in a spectral density curve.

Duration: The duration of vibration exposure is simply the measure of the total time of the exposure.

Frequency: The frequency of vibration is expressed as cycles of motion per second with a standard international (S.I.) unit of Hertz (Hz).

Frequency-weighted: A term indicating that a wave-form has been modified according to some defined frequency-weighting.

Frequency-weighting: A transfer function used to modify a signal according to a required dependence on vibration frequency.

Foot-transmitted vibration: Vibration that is transmitted to the feet and legs of operators from vibrating tools or vibrating machinery.

Hand-transmitted vibration: Vibration that is transmitted to the hands and arms of operators from vibrating tools or vibrating machinery.

ISO 2631-1: The International Standard for Mechanical Vibration and Shock – Evaluation of human exposure to whole-body vibration.

ISO 5349-1: The International Standard for Mechanical Vibration and Shock – Measurement and evaluation of human exposure to hand-transmitted vibration.

ISO-10819: The International Standard for Mechanical Vibration and Shock – Hand-arm Vibration – Measurement and evaluation of the vibration transmissibility of gloves at the palm of the hand.

Lumped-parameter model: Combination of masses, springs, and dampers used to model a mechanical system.

Magnitude: Vibration magnitude is quantified by its displacement (m), its velocity (m/s) or its acceleration (m/s^2).

Mechanical impedance: A measure of how much a structure resists motion when subjected to a harmonic force. The mechanical impedance of a point on a structure is the ratio of the force applied at a point to the resulting velocity of that point.

Power spectral density: A measure of a signal's power intensity in the frequency domain and is typically computed from the Fast Fourier Transform (FFT) spectrum of the signal.

Resonant frequency: The frequency at which the response magnitude is at its maximum. The resonant frequency is the point at which maximum displacement between organs and skeletal structures occurs, thereby placing strain on the body tissues involved.

Root-mean-square: For a set of numbers, the square root of the average of their squared values.

Transmissibility: Transmissibility is defined as the ratio of the vibration measured between two points.

Vibration: An oscillatory motion about a fixed reference point.

Whole-body vibration: Vibration that is transmitted into the human body through the buttocks, back and/or feet of a seated person, the feet of a standing person, or the supporting area of a recumbent person.

Nomenclature

Chapters 3 and 4

x, y, z	Cartesian coordinate system
a	acceleration (stimulus)
v	velocity (response)
f	frequency
S_a	complex spectra of a (stimulus)
S_v	complex spectra of v (response)
$\bar{S}_{aa}(f)$	auto-spectral average of a (stimulus)
$\bar{S}_{vv}(f)$	auto-spectral average of v (response)
$\bar{S}_{av}(f)$	cross-spectral average of a and v
$j\omega$	angular velocity
$H_1(f)$	H_1 estimator frequency response function
T	transmissibility
φ	phase angle
γ^2	coherence
n	participants
l	measurement (anatomical) location
$\bar{T}_l(f)$	average transmissibility
$\bar{\varphi}_l(f)$	average phase angle
$\overline{\gamma^2}_l(f)$	average coherence
$ReS_{av}(f)$	real component of the cross-spectral density function
$ImS_{av}(f)$	imaginary component of the cross-spectral density function
$PA_{n,l}$	peak amplitude
$Pf_{n,l}$	peak frequency
$\overline{PA}_l$	average peak amplitude
$\overline{Pf}_l$	average peak frequency
$PA_{avg,l}$	peak amplitude of the average transmissibility of all the participants
$Pf_{avg,l}$	peak frequency of the average transmissibility of all the participants
β_0	intercept (regression analysis)
β_1 to β_5	coefficients (regression analysis)

Chapters 5

N	binary evaluation of participant
L	binary evaluation of measurement (anatomical) location
$\boldsymbol{Z}$	probability matrix
B	total of the factor scores from the correspondence analysis
$\boldsymbol{J}$	N x L indicator matrix
$\boldsymbol{R}$	row factor scores
$\boldsymbol{C}$	column factor scores
$\boldsymbol{n}$	vector of the row totals of $\boldsymbol{Z}$
$\boldsymbol{l}$	vector of the columns totals of $\boldsymbol{Z}$
$\boldsymbol{D_n}$	$diag\{\boldsymbol{n}\}$
$\boldsymbol{D_l}$	$diag\{\boldsymbol{l}\}$
$\boldsymbol{L}$	factor score for the anatomical locations
$\boldsymbol{N}$	factor score for the participants
Δ	diagonal matrix of the singular values
$\boldsymbol{d_n}$	squared distance from the rows barycenter
$\boldsymbol{d_l}$	squared distance from the columns barycenter
$\boldsymbol{\ell}$	factor
$o_{n,\ell}$	angular similarity between row n and factor $\boldsymbol{\ell}$
$o_{l,\ell}$	angular similarity between column l and factor $\boldsymbol{\ell}$

Chapters 6

σ^2	total variance
g	group
σ_g^2	sum of the variance in each group
$T(f)$	average transmissibility response over the frequencies, f
$T_i(f)$	individual transmissibility curve
$\bar{T}_g(f)$	group average transmissibility curve
L	length
m	mass
J	moment of inertia
k	spring stiffness
c	damper dampening
θ	angle
$\oplus$	centre of mass
$\boldsymbol{r}_F$	free degrees-of-freedom matrix
$\boldsymbol{r}_C$	constrained degrees-of-freedom matrix
$\boldsymbol{r}$	generalized degrees-of-freedom matrix
y_{input}	single steady-state vibration input for platform excitation
ω	angular frequency
$j\omega$	angular velocity
t	time
E	kinetic energy
U	potential energy
D	dissipative energy
$[M]$	mass matrix
$[C]$	damping matrix
$[K]$	stiffness matrix
ε	reconstructed quadratic error

CHAPTER 1: DOCUMENT OVERVIEW

Miners are exposed to foot-transmitted vibration (FTV) when operating vibrating equipment such as locomotives, bolters, jumbo drills and/or drills attached to platforms on which they stand [1]. Case studies suggest exposed miners experience pain, discomfort, and blanching in the toes more often than co-workers who are not exposed to FTV [2]. If interventions are not introduced, tissue damage can be permanent and lead to a medical diagnosis of vibration-induced white-foot (VIWFt). In order to develop prevention strategies for occupational FTV exposure, an understanding of the biomechanical response of the foot, when exposed to vibration, is necessary. To understand differences in the biomechanical response of different regions of the foot, the resonant frequencies at different anatomical locations of the foot need to be identified.

A large body of research exists regarding the development of hand-arm vibration syndrome (HAVS). Dong and colleagues [3] proposed an elegant conceptual model of factors they believed to influence the cause-effect relationship for hand-transmitted vibration (HTV) exposure. Their model identified vibration source factors (magnitude, frequency, direction, duration), environmental factors (temperature, noise), and other factors (hand-arm postures, applied hand force, contact geometry, anthropometrics) as determinants of the biodynamic (transmissibility, apparent mass, power absorption) and physiological response (finger blood flow, temporal numbness, vibrotactile perceptions) of the hand-arm system to HTV. However, limited research has been published on FTV.

The development of a conceptual model for FTV exposure, similar to the one developed by Dong et al. [3] for HTV, requires the identification of potential parameters and a systematic evaluation to confirm their importance in determining the biomechanical

response of the human foot. Previous work by Tarabini et al. [4] suggests that posture and location of centre of pressure (COP) are influential parameters for determining vibration transmissibility because changes to either can alter the distribution of forces on the feet for a standing human. Therefore, research is required to understand the influence of posture and COP location on the transmission of vibration through the feet.

1.1 STRUCTURE OF THIS DOCUMENT

The proposed research will build off previous work reporting the characteristics of FTV exposure and the biodynamic response of the foot to vibration [1, 5], with an overall aim to develop a biomechanical model to simulate the human response to FTV. The four objectives of the research are presented briefly in the following section, with each objective corresponding to a refereed journal publication (Figure 1.1). This chapter concludes with the research objectives and the anticipated impact of this research. The second chapter of this document provides a summary of the necessary literature regarding: human vibration exposure, epidemiological evidence of injury from vibration exposure, FTV exposure, and previously developed lumped-parameter models. Chapters three to six are four research paper manuscripts, as outlined in the co-authorship statements, which form the novel contributions of this thesis. Finally, the seventh chapter contains a global discussion, summarizes the conclusion and implications of the research, and identifies future research directions related to FTV exposure.

1.2 RESEARCH OBJECTIVES

In order to complete the Doctor of Philosophy (PhD) in Natural Resources Engineering, the objectives (or purposes) of this research included the following:

1. To measure the transmission of vibration through the foot when standing in a natural upright position;
2. To measure the transmission of vibration through the foot when altering the COP location to the forefoot and rearfoot;
3. To determine the minimal number of unique measurement points required to document vibration transmissibility through the foot; and,
4. To develop a lumped-parameter model to model the transmission of vibration through the foot-ankle system.

1.3 RESEARCH IMPACT

This research has both an experimental (Objectives 1-3) and a modelling component (Objective 4). Findings from the experimental portion of the thesis could inform the design of equipment, tools (e.g. anti-vibration drills, isolated platforms), and personal protective equipment (e.g. anti-vibration insoles, boots or mats) to focus on reducing vibration at frequencies where tissue resonance in the foot/toes occurs. These findings could also inform the development of new international standards for measuring exposure to FTV. The development and calibration of a biomechanical model of the human foot exposed to FTV will give engineers the opportunity to evaluate materials with different stiffness and damping characteristics without involving human participants in testing.

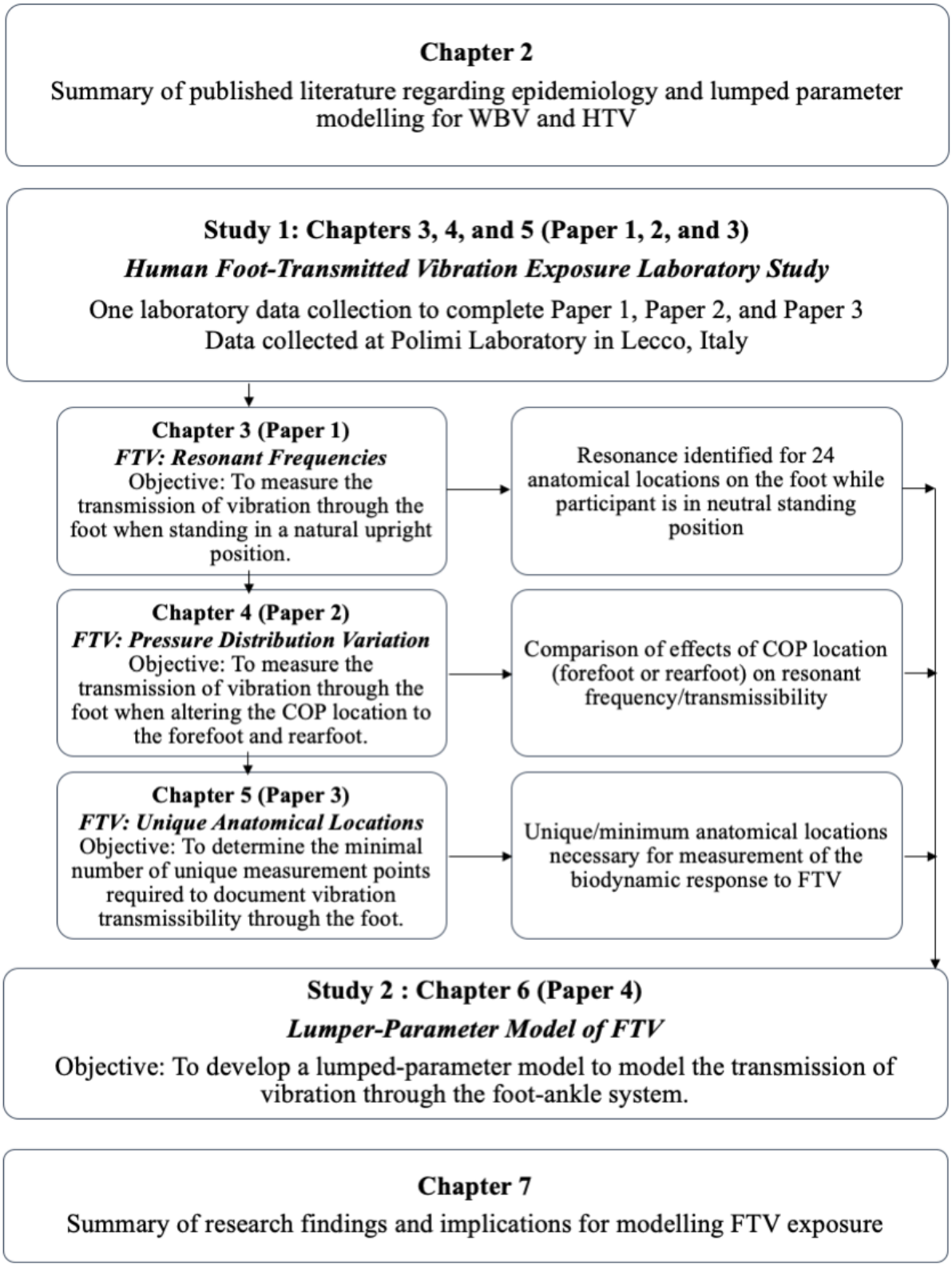

Figure 1.1: Overview of the relationships between the four papers for this PhD dissertation.

CHAPTER 2: LITERATURE REVIEW

Occupational vibration exposure is a health risk for humans and, traditionally, research has focused mainly on whole-body vibration (WBV) and hand-transmitted vibration (HTV). However, attempts to reduce HTV by increasing mechanization of mining has created a third type of vibration exposure: foot-transmitted vibration (FTV). By creating equipment that humans stand on to operate (e.g. jumbo drills, bolting platforms, raised platforms) the contact and exposure points associated with occupational exposure to vibration have changed. FTV has a similar symptomology to hand-arm vibration (HAV) including pain and numbness in the toes and feet, increased sensitivity to cold, blanching in the toes, and joint pain; prolonged exposure can result in a condition known as vibration-induced white foot (VIWFt) [2].

2.1 HUMAN VIBRATION EXPOSURE OVERVIEW

In order to fully understand the complexities of the human response to vibration, it is imperative to understand the interactions between the component areas (human, response, vibration). As previously mentioned, there are three categories of human vibration exposure (WBV, HTV, and FTV) with the focus of this research being FTV. Within this introductory section, four core concepts —vibration, biodynamic response, transmissibility, and resonant frequency— will be outlined, including their definitions and relevant terminology.

2.1.1 Vibration Basics

Vibration is defined as a mechanical movement that oscillates (repeats itself after an interval of time) about a fixed point [6, 7]. Vibration is often complex, contains many frequencies,

occurs in several directions, and changes over time [8]. Consequently, in order to properly categorize the human response to vibration exposure, the axis, frequency, magnitude, and duration of vibration exposure must be taken into consideration [9]. Linear vibration can be measured in the x-axis (fore and aft), y-axis (lateral), z-axis (vertical), and rotational vibration can be measured about the same axes — roll (rotation around x-axis), pitch (rotation around y-axis) and yaw (rotation around z-axis) —resulting in a 6 degrees-of-freedom (DOF) signal.

Vibration can be transmitted to the human body through any member in contact with a vibrating surface, such as the hands when operating hand-held vibrating tools, the buttocks through the seat in transport vehicles, or the feet from vibrating platforms [1, 9-11]. When investigating a vibratory system (machine or human), it must be understood that the system includes a component for storing potential energy (spring or elasticity), a component for storing kinetic energy (mass or inertia), and a component that dissipates energy (damper) [7]. This method of defining the three components of a vibratory system is the basis of system modelling.

2.1.2 Biomechanical Response

The biomechanical response can be defined as the human mechanical response to a dynamic environment [6, 9, 12]. The biomechanical response of the human body has traditionally been captured in two ways: measuring the force-motion (mechanical impedance, apparent mass, and absorbed power) relations at the human-machine interface, and measuring the vibration transmissibility through the human body [13-15]. However, there are many factors, intrinsic and extrinsic, that influence the human response to vibration, as summarized in Table 2.1.

Variation in any of these components can change the human's biomechanical response when exposed to vibration.

Understanding the biomechanical response of the human body to WBV, HTV, and FTV is required for designing and assessing vibration isolation methods. Due to human anthropometric and physiologic variation, the response of the human body is nonlinear and it can be nearly impossible to control all of the variables that influence the biomechanical response. Therefore, the experimental portion of this research selected control variables based on equipment availability and variation in anthropometrics, discounting physiological variables such as blood flow and muscle contraction, as these variables will not be incorporated into a model. The dissertation research focused on identifying the human biomechanical response with regards to FTV, in order to design a preliminary lumped-parameter (LP) model. Expanded understanding of the biomechanical response of the foot to FTV exposure will improve methods for measuring and analyzing FTV exposure and will assist the design of possible isolation strategies.

Table 2.1: Summary of intrinsic and extrinsic factors influencing the human response to vibration.

Intrinsic Factors
▪ Age ▪ Sex ▪ Anthropometrics [16, 17] ▪ Previous health condition [8]

Extrinsic Factors		
Personal	***Environmental***	***Vibration Exposure Profile***
▪ Experience ▪ Motivation ▪ Expectations ▪ Financial involvement ▪ Personal protective equipment ▪ Posture [4, 18-20] ▪ Muscle tension [21] [8, 22]	▪ Temperature ▪ Noise ▪ Light [8, 9, 23]	▪ Magnitude ▪ Frequency [9, 17] ▪ Orientation/Axis ▪ Duration [18, 24]

*Note: References beside bullet points are specifically for the corresponding bullet point. References below the section are for the factors listed in the section.

2.1.3 Transmissibility

Transmissibility is defined as the ratio of the vibration measured between two points [6]. Vibration attenuation is indicated when the resulting transmissibility value is below one (or unity), and amplification is indicated when the transmissibility value is above one. More specific to human vibration exposure, transmissibility is a measure of the ability of the body to either attenuate or amplify an input vibration signal. A variety of biodynamic responses, particularly those between the point at which the vibration enters the body and the point at which it is measured, are reflected in the transmissibility of the human body. For WBV exposure, a common transmissibility metric is the seat-to-head or foot-to-head measurement [12, 18, 25].

Transmissibility is also commonly termed a transfer function, and there are two specific transfer functions used frequently in human vibration studies: the power spectral density (PSD) transfer function, and the cross-spectral density (CSD) transfer function. PSD is a measure of a signal's power intensity in the frequency domain and is computed from the discrete Fourier transform (DFT) spectrum of the signal. The PSD method is the most common technique for analyzing the frequency content for human vibration exposure, because it is ideally suited to characterize the amplitude versus frequency content of a random signal [26].

The CSD method measures the relationship between two signals, including the phase difference between them. A function using the CSD method is limited to the vibration signals measured at two locations, and can therefore be very useful for measuring transmissibility between two points on the human body. Typically, the CSD functions are represented with modulus, phase, and coherence. The modulus is the transmissibility amplitude. The phase angle represents the difference in phase equivalent to one complete cycle. Finally, coherence is the correlation between an input and an output signal. Low coherence values can be used to identify experimental measurement issues and eliminate spurious readings. Explanation of the calculations for both the PSD and CSD methods will be explained in the experimental methodology of Chapters 3 and 4.

2.1.4 Resonant Frequency

Resonance occurs when the external excitation matches the natural frequency of a structure, leading to excessive deflections and structural failure [7]. For human exposure, the resonant frequency is where transmissibility is highest, leading to maximum displacement occurring between organs and skeletal structures, thus placing strain on the body tissue involved and

increasing injury risk [11, 27]. Understanding human resonance behaviour is difficult because stimulating the natural frequency of an isolated organ without exciting the whole-body resonances is almost impossible [28]. The inability to isolate means experimental studies must attempt to control as many variables (excluding anthropometrics and physiological differences) as possible. More specifically, laboratory studies need to have the ability to maintain the vibration exposure magnitude while varying the frequency in order to isolate the frequency effects.

Currently, FTV exposure remains the least studied type of human vibration exposure and the resonant frequencies of different areas of the foot have not yet been systematically identified. A laboratory study of FTV identified the possible resonant frequency of the hallux to be 50Hz or higher, and the ankle to be lower than 25Hz [5]. The major limitation of this study was that the frequencies of exposure were only from 25 to 50Hz (at 5Hz intervals), and the vibration magnitude was not held constant across the different exposure frequencies. Nevertheless, these results suggest that the toes respond differently than the ankle, similar to the differences observed between the fingers and palm of the hand [29]. It is imperative to identify the resonant frequencies of the foot in order to model FTV, develop appropriate international standards specific to FTV that set exposure limits to decrease the risk of developing VIWFt, create an appropriate sampling protocol for measuring occupational exposure to FTV, and to develop engineering controls and personal protective equipment (PPE) to mitigate FTV and decrease risk of developing VIWFt [5, 30].

2.2 EPIDEMIOLOGICAL EVIDENCE OF INJURY FROM VIBRATION EXPOSURE

The following section outlines the epidemiology and known injury information associated with exposure to FTV. As there is very little documented about the specific epidemiology of FTV, the epidemiology of WBV and HTV are presented first as workers' exposure to FTV typically have concurrent exposure to HAV and/or WBV.

2.2.1 Whole-Body Vibration Epidemiology

Exposure to WBV is a wide-spread occupational risk factor [31]. It has been estimated that 4-7% of all workers in the United States, Canada, and some European countries are exposed to potentially harmful WBV [32]. The adverse health effects are often evident in drivers of trucks, fork-lifts, tractors, cranes, loaders, and helicopter pilots [31]. There is strong epidemiological evidence that occupational exposure to WBV is associated with an increased risk of low back pain, sciatic pain, and increased vertebral and intervertebral disc diseases [33-37]. Exposure to WBV may also lead to neck and shoulder problems, changes in joint stability, circulatory disorders, auditory effects (e.g. hearing loss), and effects to reproductive system [22, 35, 37].

Additional factors such as prolonged sitting, awkward postures, stress, fatigue, and individual health factors, may also contribute to an increased risk of the development of injury. Due to these additional risk factors, it can be difficult to differentiate the relative role of WBV in the etiology of certain disorders and pathological changes. In addition to the strong evidence of harmful effects and risk factors associated with WBV, a number of researchers have focused on the effects and risk factors related specifically to segmental vibration exposure [22, 38-40]. Comprehension of the nuances of the effects of WBV on the

human body is the foundation of understanding how FTV could affect the standing human body.

2.2.2 Hand-Transmitted Vibration Epidemiology

In the United States, Canada, and Europe, approximately 1.7-5.8% of workers are exposed to HTV [22]. The acute and chronic effects of segmental vibration exposure to the hands are well documented [41]. Acute exposure to HTV can cause an increase in sympathetic nervous system activation of the heart, resulting in artery dilation and reduced blood flow in the fingers and toes [42]. Chronic exposure to HTV results in hand-arm vibration syndrome (HAVS), which is a condition affecting the digital arteries, peripheral nerves, and musculoskeletal system of the upper limbs [41]. HAVS includes a complex of neurological, vascular, and musculoskeletal disorders, which can affect other organ systems, including the lower extremities [2]. The occurrence of HAVS and the rate of degeneration have been attributed to several physical and biodynamic factors, such as intensity, frequency and direction of HTV, duration and pattern of exposure, grip force, and position/orientation of the hand and arm [43].

The principle vascular disorder associated with HTV is vibration-induced white finger (VIWF), a type of secondary Raynaud's phenomenon. VIWF is a disorder characterized by complete episodic closure of digital blood vessels which can cause blanching, a condition where the digit turns white due to loss of circulation [44]. VIWF is a peripheral neuropathy with sensory impairment comprising the neurologic component, and degenerative changes of the bones and joints of the upper extremities, particularly the wrists and elbows, characterizing the osteoarticular element [22]. Epidemiologically, the prevalence of VIWF ranges from 0-5% in geographic areas with warm climates, to 80-100% of exposed

workers in northern climates. Given the similar anatomical structures of the hand and foot, exposure to FTV in a similar frequency range could lead to VIWFt. The hand-arm system can therefore be used to gain a better understanding of the potential risk factors associated with FTV.

In order to explore the injury mechanisms associated with the development of HAVS, rat tail models have been deemed to provide reasonably similar results to those of the fingers at midrange to high frequencies [45]. Long-term (4 consecutive hours) daily vibration exposure (for 10 or 28 days) was found to alter the current perception threshold (CPT) sensitivity and myelinated axons in a rat-tail model [46]. Using rat tail models, it has been deduced that vibration exposure above 100 Hz, induces the greatest stress and strain on the tail, resulting in vascular damage indicative of dysfunction [47]. Consequently, it can be hypothesized that the vascular and neurological damage to the toes will also occur at midrange to high frequencies (>100 Hz).

2.2.3 Foot-Transmitted Vibration Epidemiology

Workers who stand on platforms or equipment that vibrate, such as locomotives, bolting platforms, jumbo drills, raise drilling platforms, and crushers, are exposed to FTV [1]. Unfortunately, epidemiological data has not classified FTV independently from WBV; therefore, published exposure data have not been reported for worker exposure to FTV. However, workers in mining, farming, forestry, and construction are known to be exposed to FTV [2, 48-50]. Adding to the challenge of classifying FTV exposure, researchers have found that workers with HAVS can have corresponding neurological and vascular symptoms in the feet, despite only being exposed to HAV [2].

Segmental vibration exposure to the feet may result in VIWFt, a condition that is similar to vibration-induced white finger [2]. VIWFt or Raynaud's phenomenon of the feet (Figure 2.1), has been examined mostly in conjunction with HAVS [51-54]. Hedlund [52] determined that the prevalence of Raynaud's phenomenon in both the fingers and toes was greater in workers exposed to vibration than individuals who had no vibration exposure. A number of researchers have examined the effects of HTV frequency and magnitude on the blood flow of the fingers and toes [42, 55, 56]. All three studies showed a significant reduction in blood flow to the fingers of both the exposed and non-exposed hands. Egan et al. [42] showed a reduction in toe blood flow and an increase in heart rate, concluding HAV exposure produced a generalized increase in sympathetic tone in the heart and extremities. This may be a factor in the development of vasospastic disease with long-term use of hand-held vibrating tools.

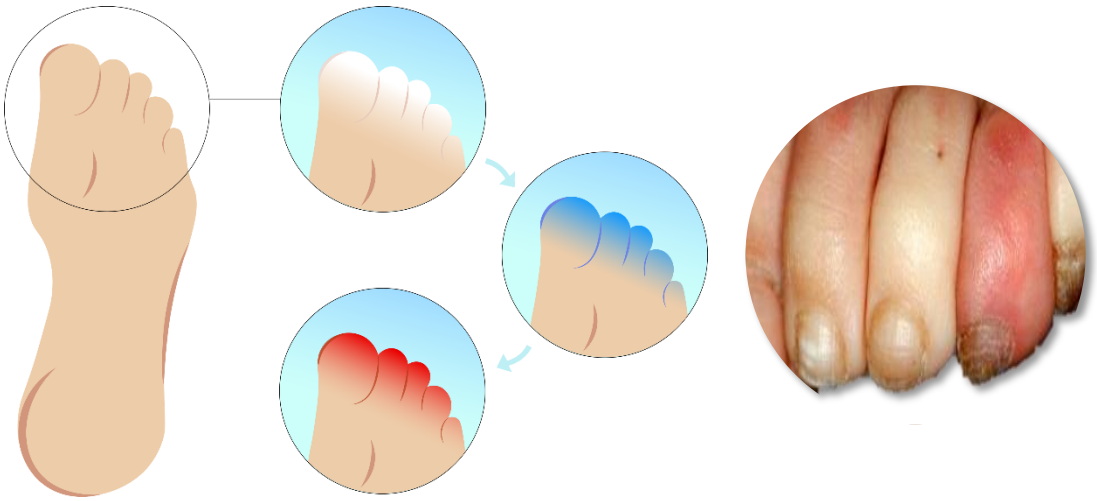

a b

Figure 2.1:Graphical representation of a toe blanching attack from Raynaud's phenomenon (a) and the effects of long-term exposure and tissue damage (causing necrosis) (b).

Hashiguchi et al. [51] examined the pathology of vibration syndrome in the upper and lower extremities and showed thickening of the medial muscular layer of the small arteries or arterioles and an increase of collagen fibres in the connective tissue, especially in the perivascular region in the fingers and the toes. It was concluded that these results in the toes could be attributed to not only direct vibration exposure of the foot itself, but also to long-term repeated circulatory disturbances and vasoconstriction caused by the sympathetic nervous system activation from HTV exposure. Hashiguchi et al. [51] also suggested that more severe circulatory disturbances of the hand correlate to a greater likelihood of circulatory disturbances to the foot. This observation is consistent with early findings that the more frequent the attacks of Raynaud's phenomenon in the fingers, the greater the likelihood of complaints of coldness to the feet [53]. There is further evidence presented by Schweigert [57] that suggests that individuals with HAVS may have concurrent vascular symptoms in the feet, which usually appeared after hand symptoms are already present. The vascular symptoms in the feet of individuals with HAVS are primarily due to autonomic dysfunction and sympathetic hyperactivity [58].

To the author's knowledge, the literature on VIWFt, without corresponding HAVS, is limited to two published case studies [2, 59]. In the case study by Thompson et al. [2], a diagnosis of vibration-induced Raynaud's phenomenon was determined based on exposure history, compatible symptoms, negative work-up for other secondary causes of Raynaud's phenomenon and plethysmographic findings. These observations suggest that local vascular pathology secondary to direct vibration exposure may be the principal pathophysiological mechanism in some cases.

Singh [60] examined vibration transmissibility via the feet in standing individuals to determine if gender played a role in transmissibility and subjective reports of discomfort. Results indicated that there was no significant difference in floor-to-ankle transmissibility by gender. The results further indicated that anatomical structures, such as the heel fat pad, might play a role in attenuating FTV from the floor through the foot to the ankle.

Understanding symptomatology of different types of vibration exposure (WBV, HTV, and FTV) is essential for recognizing the risk factors associated with the development of long-term vibration disorders. However, strictly relying on symptomatology is a lagging indicator, or retrospective indication, which means the worker has already been exposed to the hazard. The proposed research is focused on identifying resonant frequencies and modelling, in order to improve understanding of how FTV affects the human foot. Knowledge of which frequencies are associated with the most damage (the resonant frequencies) will be an indicator of which exposure frequencies need to be reduced or eliminated. This knowledge will assist in the development of interventions and engineering controls, an appropriate frequency-weighting curve for creating an international standard for measuring FTV, and exposure guidelines to protect workers from negative health outcomes.

2.3 MEASURING HUMAN VIBRATION EXPOSURE

The measurement of occupational human vibration exposure is not explicitly legislated in Ontario. There are no requirements for employers to measure or document occupational exposures, as there are for other occupational exposures in industrial hygiene (e.g. asbestos, silica, noise, etc.). However, there are guidelines provided by the International Standards Organization (ISO) and European Union Directive (EU) for measuring occupational exposures to WBV and HTV.

The measurement of WBV exposure is guided by ISO 2631-1 [8] and EU Directive 2002/44/EC [61]. Both of these standards have methods for extrapolating the 8-hr frequency-weighted r.m.s. acceleration (A(8)) and vibration dose values (VDV_{total}) for comparison with their respective guidelines to determine likelihood of health risks (Table 2.2). Similarly, the measurement and evaluation of HAV exposure is guided by ISO 5349-1 [62] and EU Directive 2002/44/EC [61]. HAV measurements result in sum values incorporating all three axes (x, y, and z) and are based on the vibration acceleration values in m/s^2. From ISO 5349-1 [62], symptoms of HTV are rare for a vibration total value (a_{hv}) less than 2 m/s^2, and from the EU Directive 2002/44/EC [61], the daily exposure action value it 2.5 m/s^2 and the daily exposure limit value is 5 m/s^2 for the a_{hv}.

Table 2.2: Summary of the Health Guidance Caution Zone (ISO 2631-1, 1997) and Exposure Action and Limit Values (EU 2002/44/EC).

ISO 2631-1 Health Guidance Caution Zone (HGCZ)			Terminology used to describe the Predicted Health Risks	**EU Directive 2002/44/EC**		
Assessment of Adverse Health Effects	A(8) (m/s^2 r.m.s.)	VDV_{total} ($m/s^{1.75}$)		Exposure Action Value (EAV) Exposure Limit Value (ELV)	A(8) (m/s^2 r.m.s.)	VDV_{total} ($m/s^{1.75}$)
For exposure below the HGCZ, health effects have not been clearly documented and/or objectively observed	< 0.45	< 8.5	Low	*EAV*	< 0.5	< 9.1
In the HGCZ, caution with respect to potential health risks is indicated	0.45 – 0.9	8.5 – 17	Moderate	*Between EAV and ELV*	0.5 – 1.15	9.1 – 21
Above the HGCZ health risks are likely	> 0.9	> 17	High	*ELV*	> 1.15	> 21

Frequency weighted filters are used to process and present human vibration exposure data. The term, frequency weighting, is defined as a frequency response function that models the response function of the body to a wave phenomenon [6]. Frequency weightings are developed as an inversion of an equal response (e.g. perception or pain) curve. For example,

since it has been observed in seated WBV that the body is 10 times more sensitive to vibration at 5 Hz than at 100 Hz, then the frequency weighting in this case would reduce measurements at 100 Hz by a factor of 10 in comparison to measurements at 5 Hz. The most commonly used frequency weightings in WBV are W_k and W_d, and HTV is W_h.

Three limitations to using frequency-weightings have previously been identified [6]:

1. Frequency weightings are developed from meta-analysis of studies of equal sensation curves, making them representative of a population, not an individual. As such, using weighting techniques makes it difficult to reproduce inter- and intra-individual differences.
2. Frequency weightings assume a linear relationship between frequency and perception, there is only one weighting curve for high and low magnitudes.
3. The current frequency weightings were derived with techniques based on vibration perception (or ratings of equal comfort); thus, they assume that perception ratings (psycho-physiological response of the visual, vestibular, somatic, and auditory systems) can be used to predict injury (pathological response of the tissue).

Although these limitations have been identified, alternative methods for assessing complex vibration with components at multiple frequencies have yet to be applied. Knowledge of the limitations is important for understanding when it is appropriate to use the frequency weightings for FTV exposure.

2.4 FOOT-TRANSMITTED VIBRATION EXPOSURE

2.4.1 Human Foot Anatomy

The human foot functions to allow stable stance, ambulation, and the effective transfer of force through the lower limb [63]. As such, the foot is a very complex anatomical structure with 26 bones (7 tarsals, 5 metatarsals, and 14 phalanges) (Figure 2.2). The foot is often divided into three sections, including the forefoot (metatarsals and phalanges), the midfoot (navicular, cuneiforms, and cuboid), and the rear foot (talus and calcaneus). Two commonly referred to bony processes include the medial and lateral malleolus (Figure 2.3).

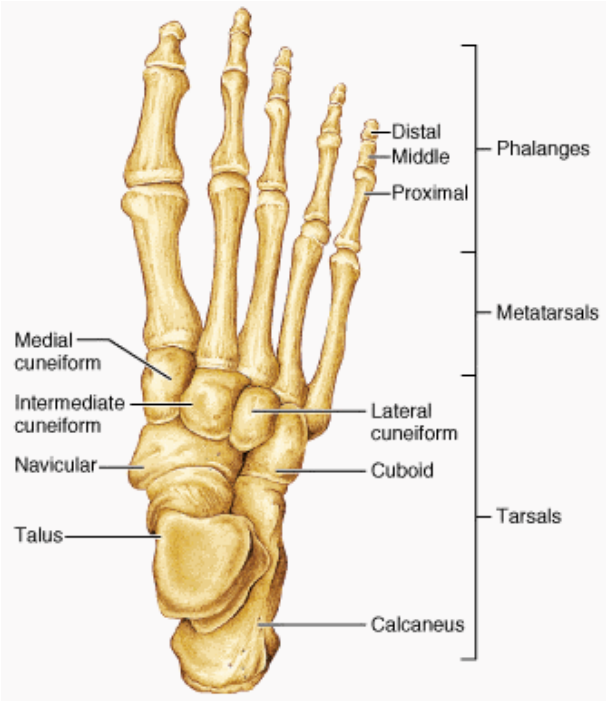

Figure 2.2: Superior view of the bones of the right foot [64].

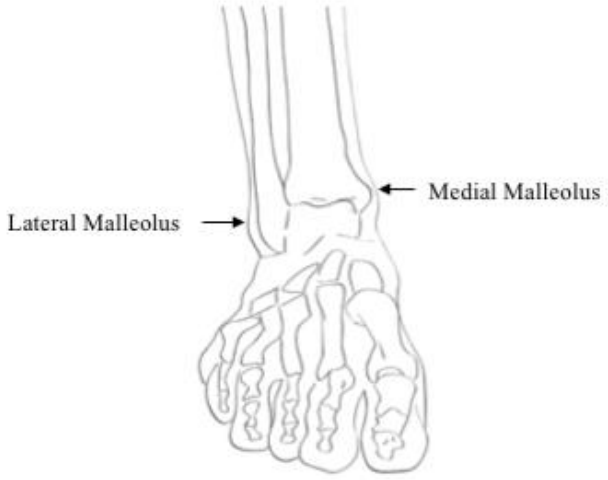

Figure 2.3: Anterior view of the bony processes of the malleolus (lateral and medial).

2.4.2 Biomechanics during Bipedal Standing

Biomechanically, the foot is comprised of two longitudinal arches (medial and lateral), where the plantar fascia (Figure 2.4) anchors the forefoot and rear foot. There are two models of the medial longitudinal arch: the beam (Figure 2.5a) and the truss model (Figure 2.5b) [63]. The beam model assumes arch stability from bony contact and ligamentous support, whereas the truss model relies on the triangular arrangement of structures where the bones of the arch are able to pivot about their apex and the tough plantar fascia (dotted line) forms the third side. Recognizing how the foot absorbs impact forces and dissipates energy from contact with the ground will form a basis for understanding variations in vibration response from different components of the foot.

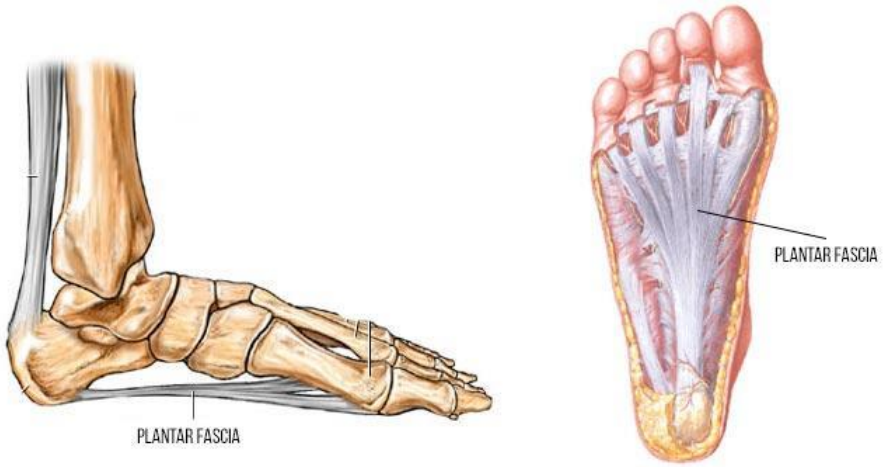

Figure 2.4: Medial and bottom view of the plantar fascia [65].

Often workers are exposed to FTV during bipedal standing while operating equipment [1], where each foot supports approximately one-half of the individual's body weight. During bipedal standing, the center of mass is typically positioned anterior to the ankle joint axis, which causes a dorsiflexion moment across the ankle joint axis [66]. Changes in position, as small as 2mm, between the subtalar joint axis and plantar aspect of the foot can alter balance of moments. A basic understanding of the anatomy and biomechanics of the human foot in a standing position is essential for interpreting vibration transmissibility results, as vibration exposure may cause muscle contraction to remain balanced during the exposure. Knowledge of how the feet react to changes in stimuli will assist the development of a model for FTV exposure.

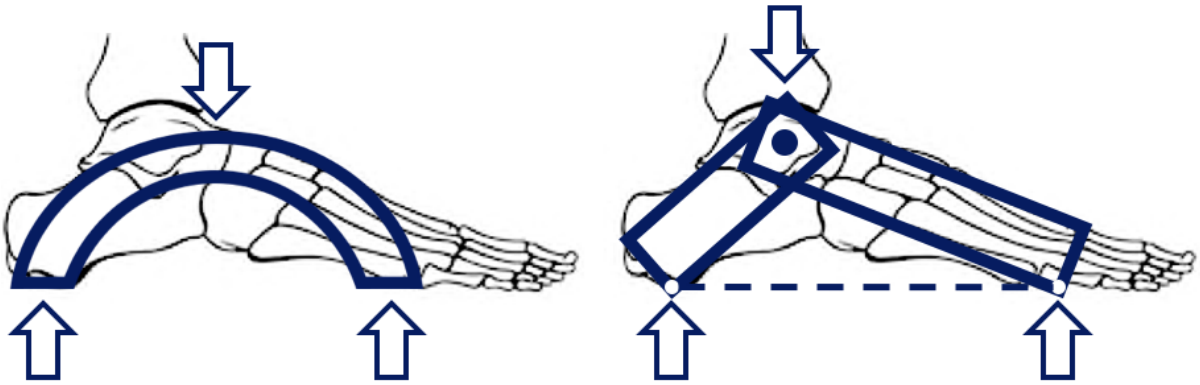

a b

Figure 2.5: Images reproduced from Dawe [63] showing (a) the beam model and (b) the truss model of the medial longitudinal arch.

2.4.3 Summary of Previous Laboratory Studies Involving Transmissibility Measurement(s) on the Foot

The majority of studies on standing vibration have focused on vibration transmissibility from the feet to the lumbar spine, cervical spine, and head [9, 67]. A study conducted by Harazin and Grzesik [68] investigated vertical WBV to six body segments while standing, including the metatarsus, ankle, knee, hip, shoulder, and head. Results showed the magnitude of vibration being transmitted by the foot is amplified in the frequency range of 31.5-125Hz at the metatarsus and 25-63Hz at the ankle, which implies the formation of a local resonance. Transmissibility measurements at the metatarsus had similar responses regardless of posture, with the exception of when the participant was asked to load their weight onto one leg. Ankle measurements where participants were asked to stand on their toes resulted in decreased transmissibility from 16-160 Hz when compared to the other nine postures. Results from this study suggest changes to the way the participant is weight-bearing, or the centre of pressure (COP), affect the transmissibility at different locations on the foot.

Tarabini et al. [4] conducted a study measuring the static pressure distribution and apparent mass while participants adopted five different body postures on three different

plantar supports. The general effects of vibration on the static pressure distribution included: the largest fraction of the load was concentrated on the rearfoot and the weight distribution became more uniform when the knees were bent; the plantar support increased the weight percentage on the midfoot; and vibration increased the weight percentage on the forefoot. Unfortunately, transmissibility was not directly measured on the foot and exposure frequencies were limited to 30Hz, which is lower than the resonant frequency of the toes [5].

In 2016, Goggins et al. [5] measured FTV transmissibility on the distal head of the first metatarsal and on the lateral malleolus with 30 male participants exposed to vibration from 25-50 Hz (at 5 Hz intervals). Statistical comparisons for the three-way interactions of both measurement location, frequency, and arch type (low, neutral, high), and measurement location, frequency, and mass were not significant. However, the difference in average transmissibility between locations was significant, with the greatest transmissibility magnitude occurring at 50 Hz for the metatarsal and 25-30Hz for the lateral malleolus. These findings suggest that pressure distribution may lead to an increased ability to predict changes in transmissibility at various locations on the foot, as the anatomical measurement of arch index was not sufficient.

To the author's knowledge, there have been five laboratory studies conducted involving a vibration transmissibility measurement at a location on the foot [5, 60, 68-70]. In those five studies, transmissibility was measured exclusively on the metatarsus and either the medial or lateral malleolus (Table 2.3). Unfortunately, there does not appear to be an experimental justification for using just one or two anatomic locations to characterize the response of the foot, nor is there justification for those particular points being the optimal locations. Further research is needed to first quantify the overall response of the foot in

different regions and then identify the unique measurement locations required to accurately capture the foot's biodynamic response to vibration.

Table 2.3: Summary of experimental locations previously reporting foot-transmitted vibration transmissibility.

Author(s) (Year)	**Acceleration Measurement on the Human Foot**			**Vibration Excitation**			**Participant #**
	#	Anatomical Location(s)	Method	Type and Direction	Magnitude	Frequency Range (Hz)	
Harazin & Grzesik [68]	2	Metatarsals Medial malleolus	ACC	Random Vertical (z-axis)	R.M.S. acceleration $4m/s^2$	4-250	10 males
Kiiski, Heinonen, Jarvinen, Kannua, & Sievanen [69]	1	Medial malleolus	ACC	Sinusoidal Vertical (z-axis)	Reported as displacement: 0.05, 0.5, 1, 3mm	10-90 (at 5Hz intervals)	4 males
Singh, Eger, Dickey, House, & Oliver [60]	1	Lateral malleolus	ACC	NR	R.M.S. acceleration $7\text{-}13m/s^2$	31.5Hz	5 males, 5 females
Wee & Voloshin** [70]	1	Medial malleolus	ACC	Harmonic Vertical (z-axis)	Peak-to-peak acceleration $17.9m/s^2$	10-50 (at 5Hz intervals)	13 males 7 females
Goggins, Godwin, Lariviere, & Eger [5]	2	Distal head of first metatarsal Lateral malleolus	ACC	NR	NR	25-50 (at 5Hz intervals)	30 males

** Denotes seated vibration study
Note:
ACC = Accelerometer
NR = Not Reported
R.M.S.= Root-mean squared

2.5 LUMPED-PARAMETER MODELLING OF HUMAN VIBRATION EXPOSURE

Lumped-parameter (LP) models use a combination of masses, springs, and dampers to represent the human body [6, 14] and can be used to model the biological response to vibration. Variation in the complexity of LP models can be dependent on the DOF of the system, where DOF is defined as the minimum number of independent coordinates required to completely determine the positions of all parts of the system at any instant in time [7].

Basic LP models begin at 1-DOF [6, 71] and incorporate single axis vibration exposures, typically in the vertical direction.

Once a model has been created, the constants associated with the model elements (e.g., stiffness or dampening coefficient) must be determined. This step is referred to as calibration and is typically done by fitting the predicted response to a set of experimental data or reference functions. Factors that influence the reliability of a LP model calibration can include:

1. Model structure;
2. Sufficiency of the reference functions;
3. Accuracy of the reference functions and parameter constraints;
4. Representativeness of the reference functions
5. Integrity of modeling equations, programs and results;
6. Goodness of curve fitting; and
7. Validity of model parameters and predicted responses [72].

The reference functions for the calibration of vibration models typically include experimental data measured on human or non-human primate subjects [73] and may include (1) the vibration transmissibility (including mass information), (2) driving-point responses (DPR) (either apparent mass or mechanical impedance), or (3) use of both the transmissibility and DPR functions [72]. Experimental data sets to create the reference functions have included as few as three and as many as 60 participants [74].

Lumped-parameter models have been created to model WBV and HTV; however, a FTV model for standing vibration exposure, has yet to be designed and calibrated. Therefore, existing WBV and HTV models were reviewed (Section 2.5.1 and 2.5.2) to serve as a basis for the development of a LP model for FTV.

2.5.1 Whole-Body Vibration Lumped-Parameter Models

The first LP model for WBV was a 1-DOF system created by Coermann in 1962 [12]. This model represented the entire human body in either a sitting erect, sitting relaxed, or standing erect position, and was tested against experimental results from eight subjects. Since its development, five more variations of the 1-DOF model have been created [24, 74-77]. While the equation of motion for the 1-DOF model does not necessarily change, the masses and configurations of the masses in the model change to represent different portions of the human body. For instance, a seated human body can be modelled with [78] or without the influence of a backrest on the seat [79, 80].

Lumped-parameter models of human WBV exposure have been developed from 1-DOF to as many as 15-DOF (Table 2.4). Experimentally-measured mechanical impedance (MI), apparent mass (AM) or transmissibility data have been used to validate WBV LP models [81, 82] using curve-fitting techniques to minimize the error between the computed and measured biomechanical response functions [14]. These techniques highlight the human body's nonlinear response to WBV exposure [4].

Whole-body vibration LP models typically highlight the effects of vertical vibration (z-axis) exposure on the human body. Four LP models have previously been created for the standing human body: 1-DOF [12], 4-DOF (Figure 2.6) [83], 5-DOF and 7-DOF [84] (Figure 2.7). These models focused on the standing body as a whole, with masses representing very large portions of the body; where only the 5-DOF and 7-DOF model used a single mass to represent the foot as a distinct component. These models used the apparent mass function (Table 2.4), which is a measurement of the change in force at the vibration platform. Knowledge of how the human body has been previously modelled with regards to WBV

(standing human body model) will assist in development of FTV LP models, with the specific focus on the biodynamic response of the human foot.

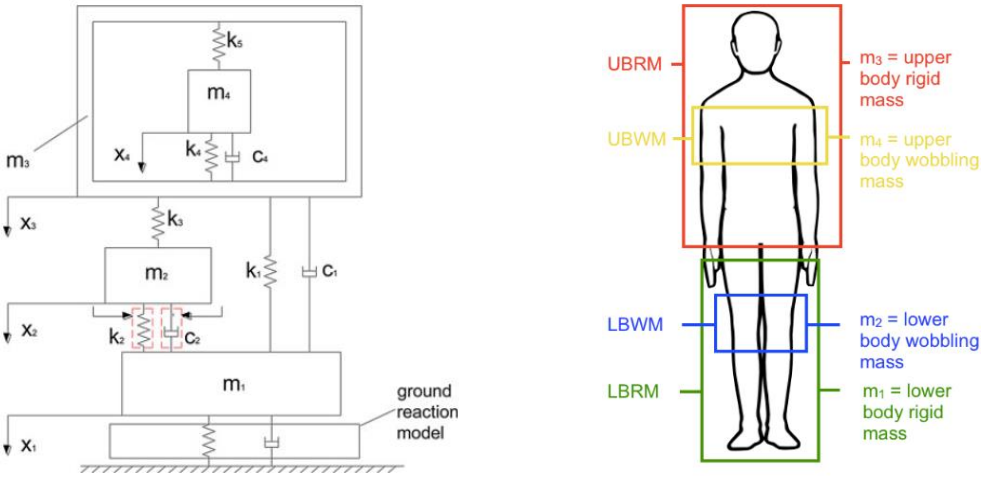

Figure 2.6: Schematic drawing of the improved 4-DOF model (modified from [85]) to study the effects of shoe hardness on the loading of the human body during running [83].

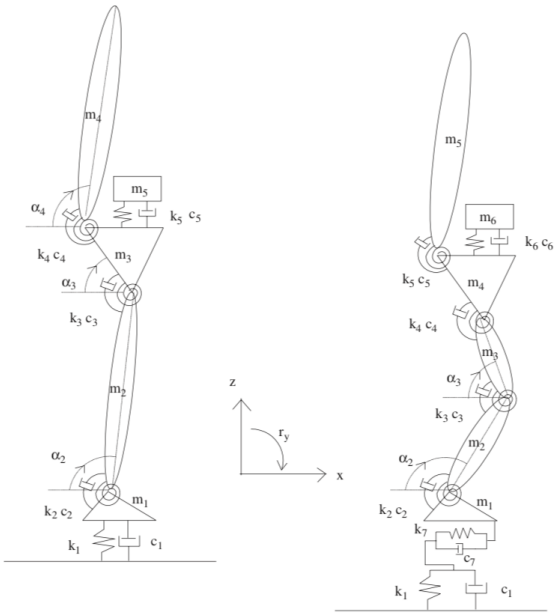

Figure 2.7: Schematic diagrams of five-degrees-of-freedom (left) and seven-degrees-of-freedom (right) lumped-parameter models of the standing human body [84].

The vibration exposure profile is also very important to take into consideration, as the exposure profile should cover the known or suspected resonant frequencies. As the principle resonance of the human body is reported at 4-6Hz in most literature, with experimental

studies finding the resonant frequencies of most organs to be between 1-10 Hz [86], most WBV LP models are limited to a peak exposure frequency of 20Hz, regardless of the number of DOF [24, 73, 87-89]. Since the resonance of the hand and fingers occurs at 40-120 Hz, and resonance of the toes occurs at 50Hz or higher [5], an understanding of the foot's response to higher frequency vibration will be imperative for understanding FTV.

Table 2.4:Summary of whole-body vibration lumped-parameter models, including the degrees-of-freedom, calibration method, frequency range (Hz), and whether it was a standing or seated model.

DOF	***Author(s)***	***Year***	***Calibration Method***	***Frequency Range (Hz)***	***Standing or Seated***
1	Coermann [12]	1962	MI	1-20	Both
	Wei & Griffin [74]	1998	AM	0.25-20	Seated
	Barauskas & Krusinskiene [76]	2007	COP	NR	Standing
	Coe et al. [77]	2009	AM	0-10	Seated
	Zhou and Griffin [90]	2014	AM	1, 1.25, 1.6, 2, 2.5, 3.15, 4, 5, 6.3, 8, 10, 12.5 and 16	Seated
2	Smith [73]	1994	MI	3-20	Seated
	Wei & Griffin [74]	1998	AM	0.25-20	Seated
	JianHua et al. [91]	2011	AM	1-20	Seated
3	Muksian & Nash [87]	1976	T	1-30	Seated
	Boileau et al. [92]	2002	MI	0.5-20	Seated
	Nawayseh & Griffin [93]	2009	AM	1-10	Seated
	Wang & Ramatalla [94]	2013	T	0.5-10	Seated
4	Wan & Schimmels [79]	1995	T	1-80	Seated
	Boileau & Rakheja [80]	1998	MI	0.625-10	Seated
	Matsumoto & Griffin [81]	2001	AM and T	0.5-10	Seated
	Zadpoor & Nikooyan [83]	2010	GRF	N/A	Standing
	Nikooyan & Zadpoor [95]	2012	GRF	N/A	Standing
5	Smith [96]	2000	MI and T	0-21.5	Seated
	Matsumoto & Griffin [81]	2001	AM and T	0.5-10	Seated
	Subsahi et al. [84]	2008	AM	2-20	Standing
6	Muksian & Nash [78]	1974	T	1-30	Seated
	Choi & Han [97]	2007	T	0.1-100	Seated
7	Kim et al. [98]	2005	AM and T	1-20	Seated
	Kubo et al. [88]	2001	T	2, 5, 8, 11, 14, 17, and 20	Seated
	Subsahi et al. [84]	2008	AM	2-20	Standing
	Zheng et al. [99]	2011	AM	0.25-20	Seated
9	Cho and Yoon [100]	2001	T	1-25	Seated
	Harsha et al. [101]	2014	T	1, 2, 2.5, 3, 3.5, 4, 4.5, 5, 5.5, 6, 8, 10, 12.5, 16 and 20	Seated
11	Qassem et al. [102]	1994	T	5-500	Seated
14	Liang & Chiang [103]	2008	T and AM	0-40	Seated

*Note: DOF = degrees-of-freedom, MI = mechanical impedance, AM = apparent mass, COP = centre of pressure, T = transmissibility, NR = not reported, N/A = not applicable.

2.5.2 Hand-Transmitted Vibration Lumped-Parameter Models

Lumped-parameter models of HTV are not as thoroughly developed as those of WBV. The reasons for the more primitive state of these models may include the difficulty in modelling more structures, and the fact that HTV is not necessarily uniaxial. To date, there is one 1-DOF model of HTV, which was published by Reynolds and Soedel [104], which has served as the foundation to further create numerous 2-DOF to 8-DOF models from (Table 2.5). In order for Reynolds and Soedel [104] to model the effects of all three axes on the hand while gripping a power tool, the frequency range (20 to 500Hz) had to be split into two regions, low being 20-73Hz and high being 73-500Hz. Then, for each region and direction, a second-order differential equation (1-DOF) mass-spring-damper system was curve-fit to the experimental data. Thus, there were six separate results for the model parameters of the 1-DOF model. Grip tightness and the amount of pressure applied to the handle were found to significantly influence the response of the hand-arm system [104].

As previously mentioned, while the anatomical structures are similar for the hand and foot, their physiology is different. Understanding how the hand structures are represented in previously validated LP model is helpful for creating FTV LP models; however, the formations of these models must be approached with caution as the foot is primarily for weight-bearing and not for manipulating forces and gripping objects like the hand. In the case of FTV, a 1-DOF model may not be the best representation, since previous research suggests the toe and ankle have very different responses [5], or the frequency range may need to be split into low and high regions [104].

Table 2.5: Summary of hand-transmitted vibration lumped-parameter models, including the degrees-of-freedom, calibration method, and frequency range (Hz).

DOF	*Author(s)*	*Year*	*Calibration Method*	*Frequency Range (Hz)*
1	Reynolds & Soedel [104]	1972	MI	20-500
2	Mishoe & Suggs [105]	1977	MI	20-2000
	Wood et al. [106]	1978	MI	30-1000
	Miwa et al. [107]	1979	MI	10-1000
3	Reynolds & Falkenberg [108]	1982	MI	5-1000
	Daikoku & Ishikawa [109]	1990	MI	1/3 octave bands, from 8-200
	Gurram et al. [110]	1995	MI	10-1000
4	Reynolds & Falkenberg [108]	1982	MI	5-1000
	Gurram et al. [110]	1995	MI	10-1000
	Dong et al. [111]	2007	MI	16-1000
5	Reynolds & Angevine [112]	1977	T	5-1000
	Dong et al. [111]	2007	MI	16-1000
	Dong et al. [113]	2008	MI	10-1000
6	Panaitescu-Liess & Bausic [114]	2012	NR	NR
	Adewusi et al. [115]	2012	MI and T	2.5-500
8	Bausic [116]	2013	NR	NR

*Note: DOF = degrees-of-freedom, MI = mechanical impedance, T = transmissibility, NR = not reported. Greyed rows were inaccessible studies for the author.

2.5.3 Lumped-Parameter Models of the Foot

Thus far, modelling of the foot-ankle system (FAS) has focused on gait analysis, with clinical applications for foot injuries such as impaired plantar fascia function [117, 118], low or high arches [119], and force distribution on the metatarsals [120]. The major support areas of the foot have been found to be concentrated under the tuberosity of the calcaneus and the heads of five metatarsals, with metatarsals 1 and 5 baring the highest fraction of the total load, regardless of the heel height from the ground [120]. The results indicate that these two support areas need be incorporated into a FTV LP model.

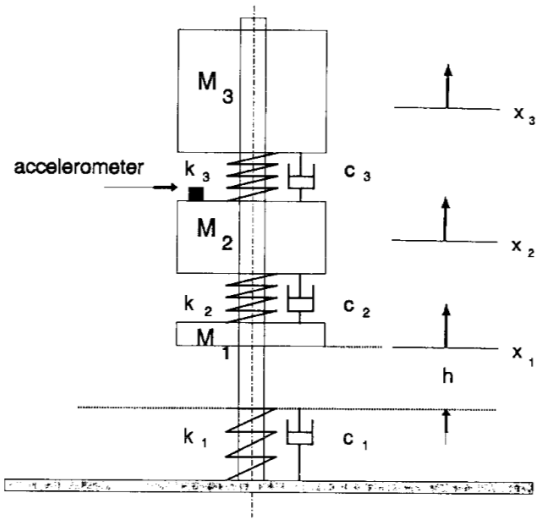

Where,

M_1 = mass of foot
M_2 = mass of tibia
M_3 = mass of rest of body
k_1 = stiffness constant landing cushion
k_2 = stiffness constant tibia and ankle
k_3 = stiffness constant knee and above
c_1 = damping constant landing cushion
c_2 = damping constant tibia and ankle
c_3 = damping constant knee and above
x_1 = vertical displacement of M_1
x_2 = vertical displacement of M_2
x_3 = vertical displacement of M_3

Figure 2.8: Three-degree-of-freedom lumped-parameter model of the lower extremity, to model heel strike transients during running [121].

A LP model of the lower extremity (foot, tibia, rest of the body) has been created in 3-DOF (Figure 2.8), using the acceleration of m_2 (measured at the tibial tuberosity) as the model output, to model heel strike transients during running [121]. The model analysis focused on the effect of the ground and footwear damping and spring constants on the dynamic loading of the human body. This study revealed that the damping constant was the most dominant factor for controlling impact to the human body resulting from the heel strike of running. Although these findings are specific to a single impact from running, they suggest that the soft tissues of the foot will be important to incorporate when modelling FTV.

In terms of vibration modelling, a five mass LP model of the foot has been designed [122]. However, this model was validated using transmissibility data from seated subjects with load placed on the knees, with a frequency range of 10-50Hz at 5Hz increments, at the medial malleolus and tibial tuberosity [70]. Moreover, the Wee model [122] used seated transmissibility data, as such, is incapable of accounting for the effects of different COP positions in a standing worker.

As demonstrated by the variations in the model responses based on calcaneal angle changes [119] and the height of the calcaneus [120], it is not unreasonable to expect changes to an FAS model's parameters based on changes in transmissibility response of the foot with changes in the COP location. Given the additional evidence for regional differences in the response of the human foot to vibration [5], a model incorporating FTV transmissibility measurements at different anatomical locations on the foot is necessary. Therefore, this research will build off previous model studies with the aim to establish a baseline model of the FAS in order to model the effects of altering the centre of pressure on vertical vibration exposure.

2.6 CONCLUSIONS

This chapter aimed to present the relevant literature for: (1) understanding the basics of human vibration exposure, (2) outlining the epidemiological evidence of injury from vibration exposure, (3) the state of current standards for measuring human vibration exposure, (4) specifics regarding FTV exposure, and (5) where the research is currently with regards to modelling of FTV exposure. There is ample evidence to suggest FTV exposure can cause damage to the vascular, neurological, and muscular systems; however, there has been very little focus on FTV exposure specifically as it has been lumped in with standing WBV exposure.

Based on this review of the literature, four gaps in the literature have been identified:

1. A thorough mapping of the regional responses of foot's response to vibration exposure has not been completed for standing vibration exposure;
2. The effects of differences in the COP position on the foot's response to vibration has not been considered;

3. There is no evidence-based justification for the number and location of the measurement points needed to characterize the response of the foot to vibration; and,
4. A lumped-parameter model to predict the foot's response of a standing person exposed to FTV has yet to be designed.

The subsequent four chapters describe the attempts to address each of these gaps in turn.

CHAPTER 3: RESONANT FREQUENCY IDENTIFICATION

Biomechanical response of the human foot when standing in a natural position while exposed to vertical vibration from 10-200Hz

Exposure to foot-transmitted vibration (FTV) can lead to pain and numbness in the toes and feet, increased cold sensitivity, blanching in the toes, and joint pain. Prolonged exposure can result in a clinical diagnosis of vibration-induced white foot. Data on the biomechanical response of the feet to FTV is limited; therefore, this study seeks to identify resonant frequencies for different anatomical locations on the human foot, while standing in a natural position. A laser Doppler vibrometer was used to measure vertical (z-axis) vibration on 21 participants at 24 anatomical locations on the right foot during exposure to a sine sweep from 10-200Hz with a peak vertical velocity of 30 mm/s. The most notable differences in the average peak frequency occur between the toes (range: 99-147Hz), midfoot (range: 51-84Hz), and ankle (range: 16-39Hz).

Keywords: foot-transmitted vibration; standing; resonant frequency

The contents of this chapter have been published as "Goggins, K.A., Tarabini, M., Lievers, W.B., Eger, T.R. (2018). Biomechanical response of the human foot when standing in a natural position while exposed to vertical vibration from 10-200 Hz. *Ergonomics*. doi: 10.1080/00140139.2018.1559362"

Graphical Abstract

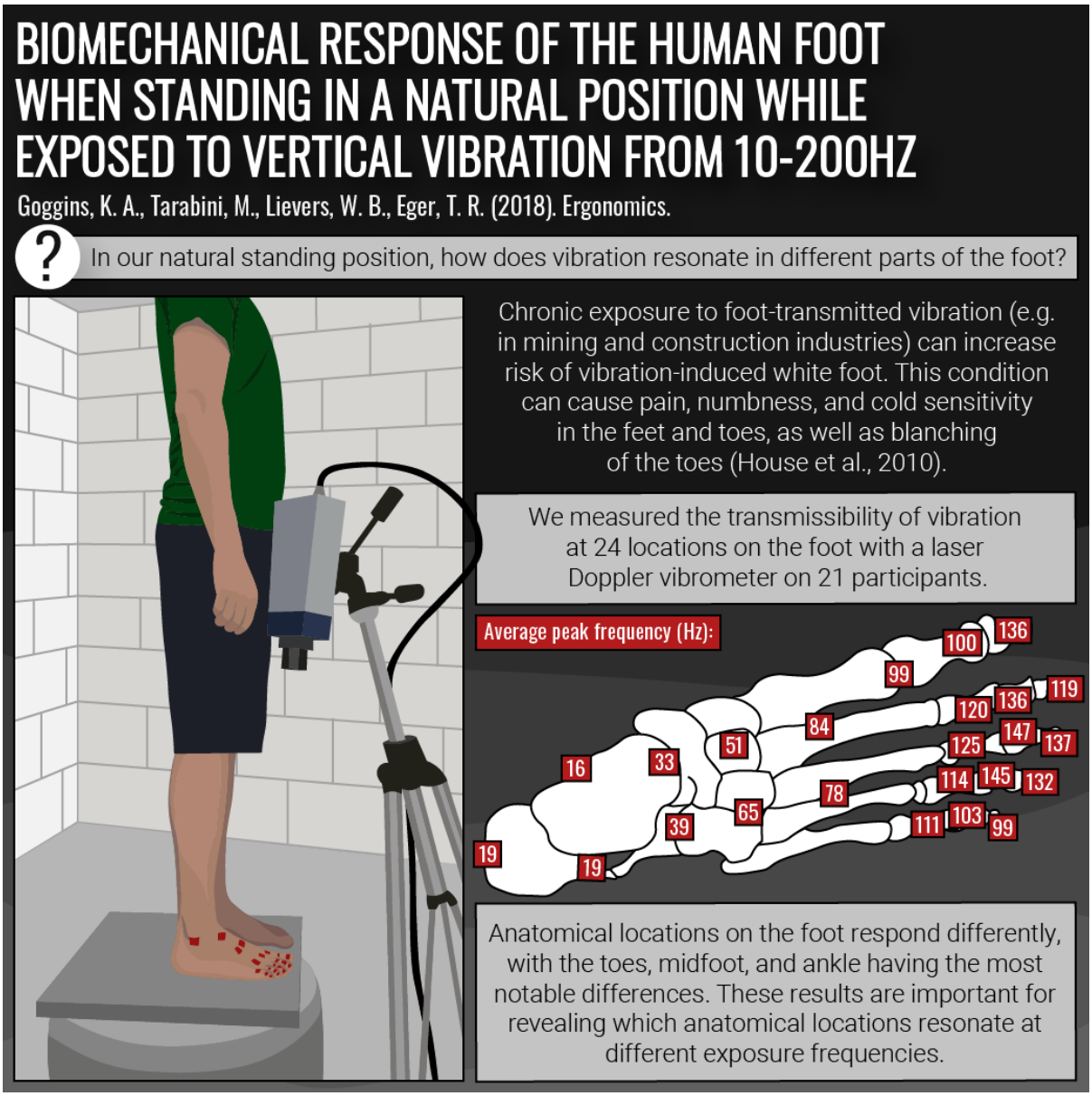

3.1 INTRODUCTION

Occupational exposure to vibration can be associated with negative health effects. The severity of these health effects can be affected by a number of factors such as the point of contact with the vibration source, vibration amplitude, exposure frequency, and in some cases the worker's posture [6, 9]. More specifically, a worker exposed at resonant frequency, which is the point where vibration transmissibility is highest and can result in maximum deformation of tissues in the human body, is at greatest risk [11, 80]. In order to prevent and mitigate injury risk from vibration exposure, it is imperative to understand how vibration is transmitted and resonates through different body segments.

Traditionally, occupational vibration research has focused on whole-body vibration (WBV) and hand-arm vibration (HAV). Vibration transmitted through the buttocks of a seated person, the back of a recumbent person, or the feet of a standing person, is typically classified as WBV [8]. Exposure to WBV has numerous health risks including back and neck disorders, vascular issues, hearing loss, gastrointestinal disorders, and motion sickness [33, 35, 36]. Since the consequences of WBV on health can have immediate effects on the lower back, neck, or head, the majority of studies on standing vibration have focused on vibration transmissibility from the platform to these regions [9, 67]. Vibration transmitted through the hands, commonly associated with the operation of power tools, is termed HAV. Chronic exposure to HAV places workers at risk for hand-arm vibration syndrome (HAVS), a complex of osteoarticular, neurological, and vascular disorders [22, 38, 39]. The vascular symptoms of HAVS can also be referred to as vibration-induced white finger (VIWF) [123], where prolonged vibration exposure can result in decreased blood flow and blanching in the fingers [124].

Various prevention/isolation strategies have been developed for WBV and HAV. International standards have been designed specifically to protect workers from vibration exposure [8, 62]. Personal protective equipment (PPE) has also been developed specifically for WBV and HAV. Mobile equipment seats are now designed with suspensions to attenuate vibration or impacts [125-127] and anti-vibration gloves have been developed in accordance with guidelines in ISO-10819 [128]. Additionally, engineering controls have been implemented to prevent occupational exposure; for example, jumbo drills have replaced hand-held jack-leg drilling in mining in order to minimize HAV exposure [1].

An unintended consequence of replacing the jack-leg with a jumbo drill to reduce HAV exposure is that exposure to FTV has increased as the worker is now standing on a vibrating platform [1, 2]. The health effects associated with FTV have a similar symptomology to HAVS, including pain and numbness in the toes and feet, increased sensitivity to cold, blanching in the toes, and joint pain [1]. Tingsgard & Rasmussen [59], who documented cold-induced blanching in the toes of a farmer who had a 12-year history of FTV exposure, termed the condition vibration-white-toes. The term vibration-induced white foot (VIWFt) was subsequently used to describe the vascular symptoms experienced by a miner with prolonged exposure to FTV [2]. The timing of the technological changes and the chronic exposure required suggests that VIWFt is an emergent condition whose incidence is expected to increase over the coming years. In order to prevent FTV injury, the resonant frequencies of different anatomical areas of the foot need to be systematically identified, as has been done with WBV and HAV [13].

The research measuring the vibration response of the foot has been limited to date. Harazin and Grzesik [68] investigated the transmission of vertical WBV with a frequency

range of 4-250Hz at a amplitude of 4m/s^2, to six body segments (metatarsus, ankle, knee, hip, shoulder and head) for 10 standing postures. Transmitted vibration was amplified from 4-10Hz and 31.5-125Hz at the metatarsus and 4-10Hz and 25-63Hz at the ankle, implying the formation of a local resonance. Similarly, a laboratory study of FTV conducted on 30 male participants, identified the resonant frequency of the hallux to be 50Hz or higher, and the ankle to be lower than 25Hz [5]. The major limitation of this study was that only exposure frequencies from 25 to 50Hz were evaluated (at 5Hz intervals). Nevertheless, both of these papers found different transmissibility responses for the forefoot and rearfoot. This observation is consistent with previous HAV work, which has reported differences in the vibration response at the fingers and palm of the hand [13, 29, 129]. These regional differences suggest that a systematic identification of resonant frequencies for the foot must include more locations to fully capture the foot's response.

Therefore, the objective for this study was to determine resonant frequencies at 24 anatomical landmarks on the human foot under natural upright standing. Twenty-one volunteers were subjected to a vibration sine sweep from 10-200 Hz. A laser Doppler vibrometer (LDV) was used to determine the vibration at each of the 24 locations, from which the resonant frequencies were identified. This work was intended to contribute to a larger body of ongoing research intended to characterize the vibration response of the foot, ultimately leading to the development of engineering controls, PPE, and FTV-specific international standards that set exposure limits to decrease the risk of developing VIWFt.

3.2 METHODOLOGY

This study was performed in accordance with the ethical guidelines of both Politecnico di Milano and Laurentian University (Appendix A).

3.2.1 Participants

Twenty-one participants (6 females, 15 males) with an average (± standard deviation) age of 24 (±7.8) years, height of 175.6 (± 9.1) cm, mass of 70.1 (± 14.0) kg, and total foot length of 25.8 (± 2.0) cm participated in the study. Participants were eligible to participate if they could communicate in English. Participants were excluded from the study if they self-reported having diabetes, a concussion, a current pregnancy, problems with motion sickness, or a lower body musculoskeletal injury in the previous six months.

3.2.2 Vibration Platform Set-Up

Vertical vibration input was supplied by a 50 x 50cm steel plate mounted to an electromagnetic shaker (LDS V830), with a maximal displacement of ±50 mm and a maximal force close to 10 kN. The upper frequency limit was the one for which the frequency response function (FRF) of the plate itself increased more than 10% at one of the points where the transmissibility was measured; more details about the experimental setup arranged for single-axis are reported elsewhere [130]. The vibration platform acceleration was measured using a uni-axial (100mV/g) piezoelectric CCLD accelerometer (Bruel & Kjaer 4508B).

3.2.3 Vibration Exposure Profile

The stimulus included a peak vertical vibration of 30 mm/s, with a sine sweep from 10-200Hz, lasting 51 seconds. The choice of the constant velocity profile was governed by the necessity of having a constant signal-to-noise ratio (SNR) on the laser, in order to have a constant measurement noise in the presence of constant vibration transmissibility. The large

sweep rate was chosen in order to limit the total testing time and participant exposure to vibration. The general set-up of equipment is illustrated in Figure 3.1.

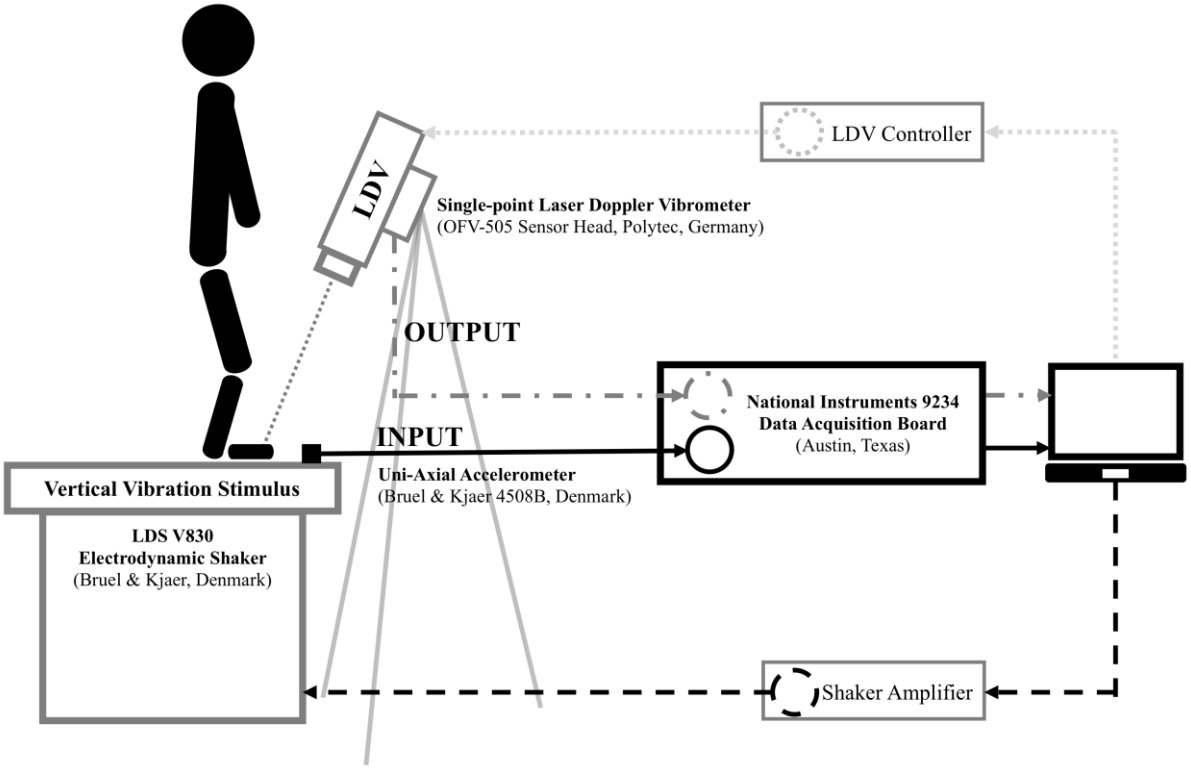

Figure 3.1: Illustration of experimental set-up and equipment connections.

3.2.4 Vibration Transmissibility Measurement

Twenty-four small reflective markers (3M retro-reflective tape) were placed on the desired anatomical location on the right foot as follows: three on each toe (15 in total), six on the mid-foot, two on the ankle, and one on the heel (Figure 3.2) (Appendix B). A Polytec LDV, with a OFV-505 Sensor Head, was used to measure the velocity at one of 24 anatomical locations on the foot while the participant was standing in their natural upright standing position. After each 51s exposure the participant had a 10 to 20s rest period before the measurements at the next anatomical location were taken. In total, the participant was

exposed to vibration for 20 minutes and 24s. Data were acquired at a sampling rate of 2048Hz using a National Instruments 9234, 24-bit data acquisition board.

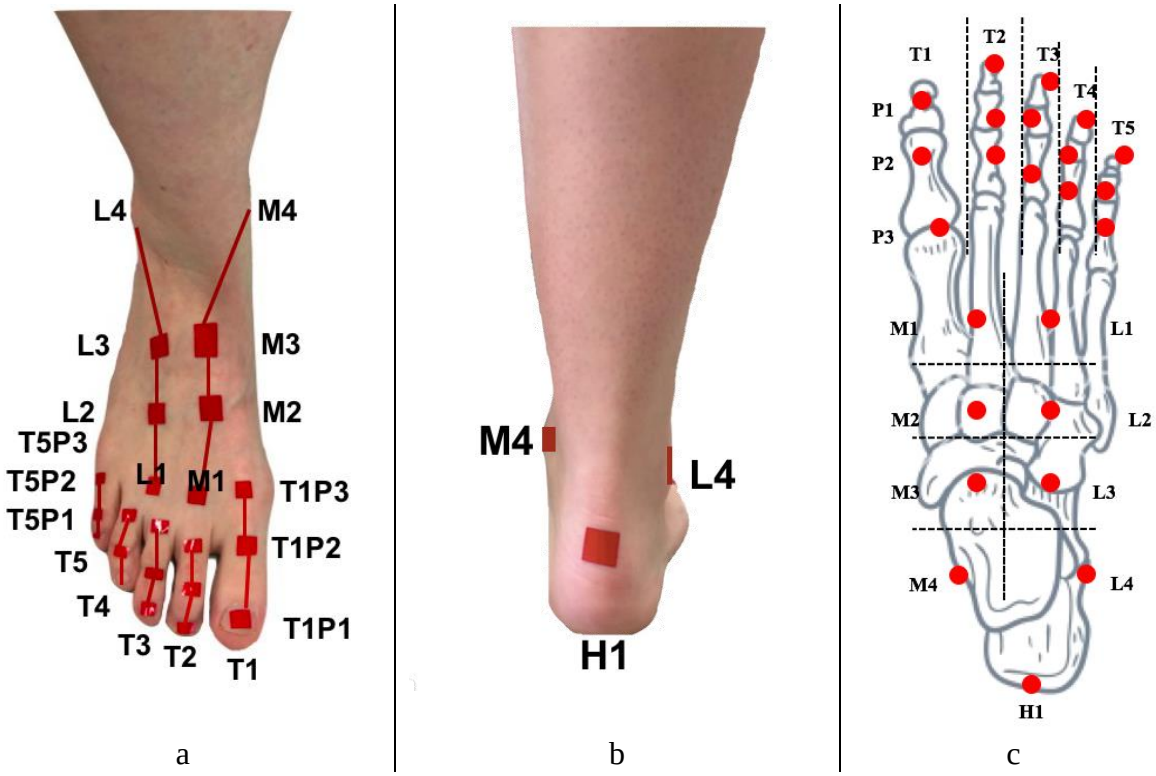

Figure 3.2: Reflective marker set-up (a) anterior view, (b) posterior view, (c) top view of anatomic representation.

For vertical HAV measurements, the LDV can be positioned directly above the hand to capture vibration transmissibility at the desired anatomical locations [13]. In the current study it was not possible to have the LDV positioned directly above all the measurement points on the foot because the position of the knee and lower leg impeded the laser when participants stood in a natural upright position with both feet on the platform. Therefore, the LDV had to be positioned at an angle to measure vibration transmissibility at all points of interest with the exception of T1P1, T2P1, and T3P1.

In order to enable the calculation of a correction factor, to adjust for the non-vertical position of the LDV, the LDV was moved individually to one of four positions (Figure 3.3).

Using a permanent marker, the location of the LDV beam on the platform was marked and identified as LDV laser points (LP) 1 (LP1), 2 (LP2), 3 (LP3), and 4 (LP4). Pilot testing confirmed the four points were sufficient to enable transmissibility measurements at the 24 anatomical locations for feet ranging from size 6-12 US. The detector of the LDV was positioned 65 cm above the vibration platform (Figure 3.1). The exact vertical distance from the reflective markers varied with the foot anthropometry of the participant, the anatomic location being measured, and the point on the platform (LP1 to LP4) where the measurement was taken. The measurement distance is a non-factor as this measurement technology offers properties that are independent of the measurement distance [131].

During vibration transmissibility measurement, each participant was asked to position their foot on the platform so that one of the 24 points of interest was located at LP1, LP2, LP3, or LP4. The LDV location at which measurements were taken was recorded for each of the 24 points on the foot (Appendix C).

Previous research has been conducted to quantify noise associated with vibration measures when the LDV beam is on an angle [132]. In order to account for the error associated with the angle of the LDV at LP1-LP4, the FRF was compensated using correction factors determined by measuring the transmissibility of the rigid plate using the tilted LDV. The inverse of the H_1 function (Equation 3.4) were 1.06, 1.16, 1.16, and 1.16 respectively. The values were compatible with the angle secant.

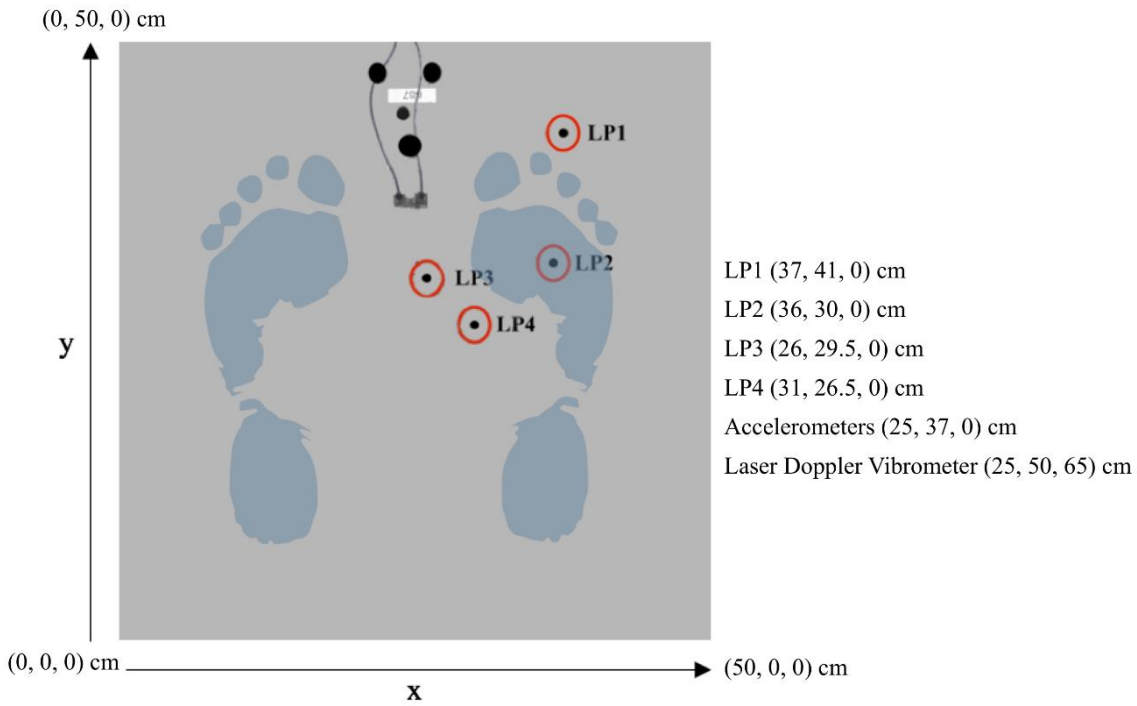

Figure 3.3: Top view of the four permanently marked laser point locations on the vibration platform, used for the laser Doppler vibrometer measurements. The foot was repositioned for each test to ensure the anatomic location being measured was situated over one of these four points. Laser points (LP) from 1 to 4, LP1-LP4, correspond to the locations on the platform for the four laser locations used in the study.

3.2.5 Data Analysis

All vibration data were processed using LabVIEW (National Instruments, 2015). The vibration time histories of the stimulus (acceleration, hereinafter *a*) and of the response (velocity, hereinafter *v*) were split according to the Bartlett method into 26 buffers of 4096 samples lasting 2s without overlap. Complex spectra of *a* and *v* (S_a and S_v) were computed on each buffer (i) using the rectangular window, to preserve most of the original signal content (best at reducing noise while maintaining edge sharpness) [133]. The derivative of the velocity was computed in frequency domain by multiplying the signal spectrum times the imaginary unit and angular velocity ($j\omega$). The auto-spectral averages ($\bar{S}_{aa}(f)$ and $\bar{S}_{vv}(f)$) and cross-spectral average ($\bar{S}_{av}(f)$) are:

$$\bar{S}_{aa}(f) = \frac{\sum_{i=1}^{26} S_{a,i}(f) \cdot S_{a,i}^{*}(f)}{26} \tag{3.1}$$

$$\bar{S}_{vv}(f) = \frac{\sum_{i=1}^{26} S_{v,i}(f) \cdot S_{v,i}^{*}(f)}{26} \tag{3.2}$$

$$\bar{S}_{av}(f) = \frac{\sum_{i=1}^{26} S_{a,i}(f) \cdot S_{v,i}^{*}(f) \cdot j\omega}{26} \tag{3.3}$$

The FRF was evaluated across the frequency range (10-200Hz) for all 24 locations using the H_1 estimator:

$$H_1(f) = \frac{\bar{S}_{av}(f)}{\bar{S}_{aa}(f)} \tag{3.4}$$

FRF estimators are typically used with random stimuli, but their usage with a deterministic stimulus removes the non-deterministic components from the FRF [130]; the latter are the ones that, in each specific buffer used for averaging, have a frequency different from that of the stimulus (Appendix D).

The coherence ($\gamma^2(f)$) was computed for all 24 locations as:

$$\gamma^2(f) = \frac{|\bar{S}_{av}(f)|^2}{\bar{S}_{aa}(f) \cdot \bar{S}_{vv}(f)} \tag{3.5}$$

Coherence is a value between 0 and 1 where a larger number indicates a greater correlation between the two signals being measured [6]. The coherence function can drop below unity for a number of reasons including contaminating noise on the input or output signals, leakage measurement errors not reduced by windowing, system non-linearities, or because there are non-measured inputs affecting the output [130]. Tests where the average coherence in the range 10-200Hz dropped below 0.5 were redone, as this was used as an indication that the laser beam left the reflective marker.

When *n* is the number of the participant and *l* the measurement location, the average transmissibility ($\bar{T}_l(f)$), phase angle ($\bar{\varphi}_l(f)$) and coherence ($\overline{\gamma^2}_l(f)$) are defined as:

$$\bar{T}_l(f) = \frac{\sum_{k=1}^{21} \left|H_{1,n,l}(f)\right|}{21} \tag{3.6}$$

$$\bar{\varphi}_l(f) = \frac{\sum_{k=1}^{21} arg\left(H_{1,n,l}(f)\right)}{21} \tag{3.7}$$

$$\overline{\gamma^2}_l(f) = \frac{\sum_{k=1}^{21} \varphi^2{}_{n,l}(f)}{21} \tag{3.8}$$

Of the 504 measurements (24 locations × 21 participants), only five tests were excluded from the analysis due to their inconsistent behaviour (low coherence or obvious artifact).

For each participant, the resonance at each location was identified using the peak amplitude (maximum of $H_{1,n,l}(f)$) and the corresponding frequency.

$$PA_{n,l} = \max(\left|H_{1,n,l}(f)\right|) \tag{3.9}$$

$$Pf_{n,l} = \text{frequency at } PA_{n,l} \tag{3.10}$$

These two quantities were averaged to identify the average peak amplitude ($\overline{PA}_l$) and peak frequency ($\overline{PA}_l$) at each location (*m*):

$$\overline{PA}_l = \frac{\sum_{k=1}^{21} PA_{n,l}}{21} \tag{3.11}$$

$$\overline{Pf}_l = \frac{\sum_{k=1}^{21} Pf_{n,l}}{21} \tag{3.12}$$

The peak amplitude and frequencies were also computed on the average transmissibility curve ($\bar{T}_l(f)$) as:

$$PA_{avg,l} = max\left(\bar{T}_l(f)\right) \tag{3.13}$$

$$Pf_{avg,l} = frequency\ at\ PA_{avg,l} \tag{3.14}$$

these quantities will be referred to as peak amplitude of the average ($PA_{avg,l}$) and peak frequency of the average ($Pf_{avg,l}$).

3.3 RESULTS

The individual transmissibility responses of each participant at all 24 anatomical locations are presented in Appendix E. The average (± standard deviation) of the entire transmissibility, phase and coherence of 21 participants are plotted for 24 anatomical locations in Appendix F. Two measurements were removed from the analysis due to their low coherence (participant 8 at location H1, and participant 17 at location M4) (Appendix G), and an additional three measurements were excluded based on obvious measurement artifact (participant 11 at T2P1, participant 12 at T3P1, and participant 14 at M4). The average coherence was maintained at unity for most points, with the exception of M4, L4, and H1, where the average coherence gradually decreases to 0.6 at frequencies above 130Hz.

3.3.1 Transmissibility

Vibration transmissibility varied across the 24 measurement points (Figure 3.4). The most notable differences are observed between three larger areas: the toes (15 locations), midfoot (M1, M2, L1, and L2), and ankle (M3, M4, L3, L4, and H1). As such, these anatomically grouped areas will continue to be referenced throughout the text. Vibration transmissibility was amplified at the toes, midfoot, and ankle at almost all frequencies (10-200Hz), between 10-110Hz, and between 10-50Hz, respectively (Figure 3.4).

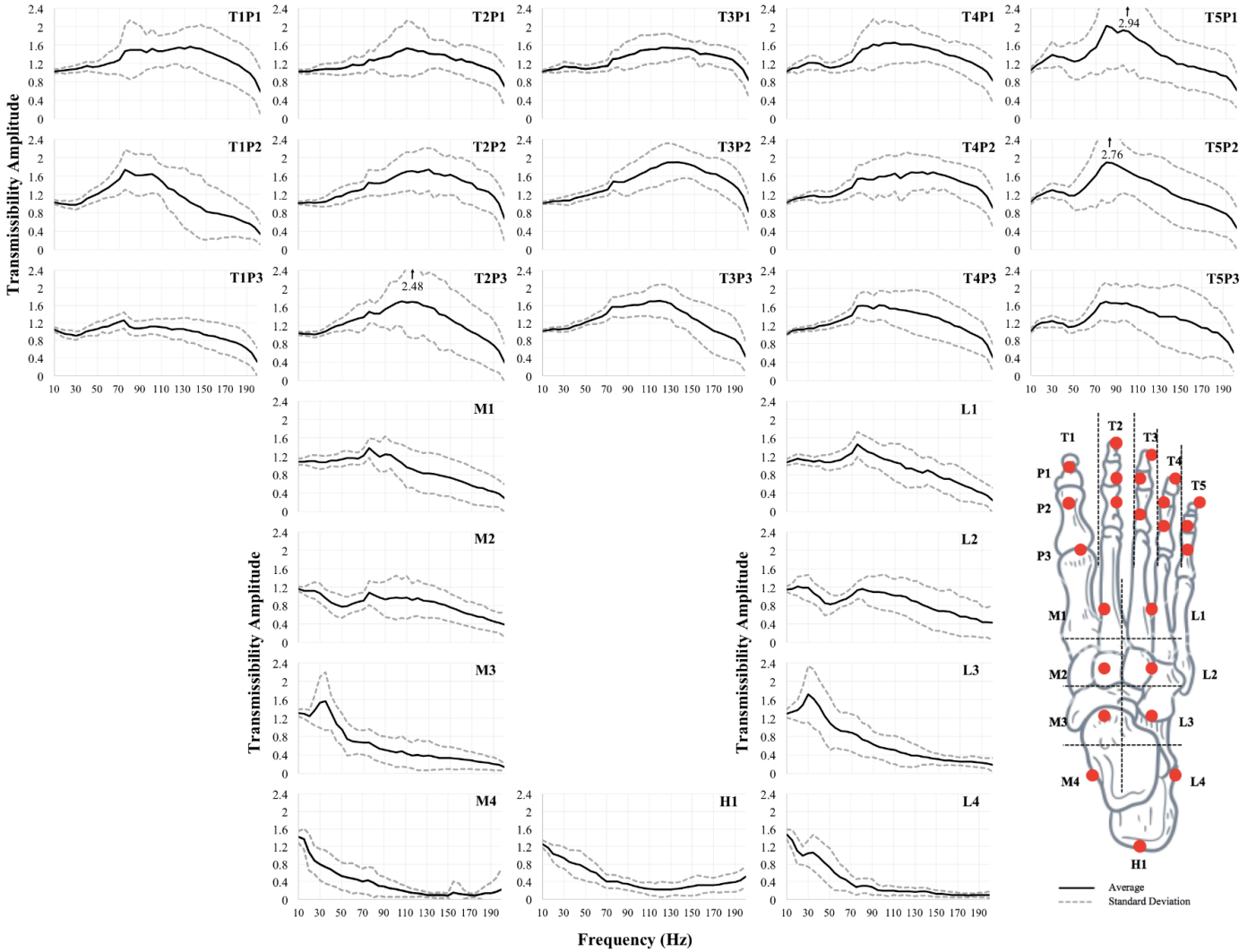

Figure 3.4: Average (± standard deviation) of the entire FTV transmissibility response of 21 participants plotted for measures taken at 24 anatomical locations across a frequency range of 10-200Hz. Excluded measurements include: one participant at T2P1, T3P1, and H1 and two participants at M4.

3.3.2 Phase

The phase angle had two very distinct categories depending on the anatomical location (see graphs in Appendix F). The average phase angles for the toes and upper portion of the midfoot were initially very close to zero in the range 10-80Hz, but decreased rapidly at higher frequencies. The five points around the ankle (M3, M4, L3, L4, and H1) do not exhibit a similar low frequency-high frequency transition; the phase shift decreases continuously with increasing frequency, reaching angles as high as -500.2^{o} for M4.

3.3.3 Resonant Frequency

The average peak amplitude, $\overline{PA}_l$, and frequency, $\overline{Pf}_l$, of the 21 participants at 24 locations on the foot are reported in Figure 3.5, together with the peak amplitude of the average, $PA_{avg,l}$, and peak frequency of the average, $Pf_{avg,l}$. There were notable differences in peak FTV resonance frequency and associated transmissibility amplitude by measurement location (Figure 3.5). The average peak transmissibility frequency (amplitude) for the toes ranged from 99-147Hz (1.40-2.56), for the midfoot from 51-84Hz (1.42-1.59), and for the ankle from 16-39Hz (1.31-2.10). The maximum average peak transmissibility frequency (147Hz) occurred at T3P2, and the lowest (19Hz) occurred at L4 and H1. The large variability of the transmissibilities, $\bar{T}_l(f)$, leads to large differences between $\overline{PA}_l$ and $PA_{avg,l}$, and between $\overline{Pf}_l$ and $Pf_{avg,l}$.

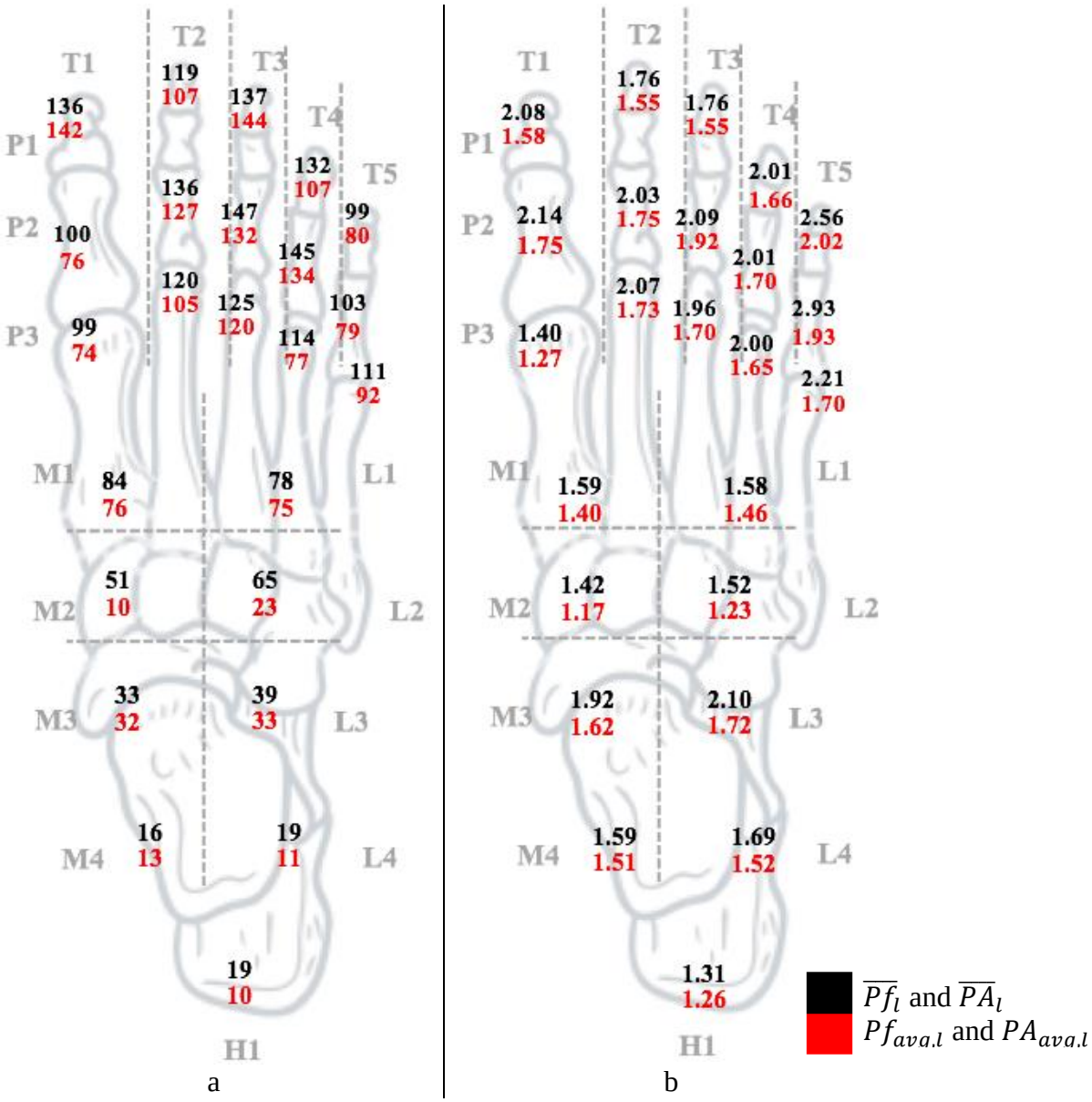

Figure 3.5: (a) Average peak frequency, $\overline{Pf_l}$, and peak frequency of the average, $Pf_{avg,l}$, and, (b) average peak amplitude, $\overline{PA_l}$, and peak amplitude of the average, $PA_{avg,l}$, measured at 24 locations on the foot.

3.4 DISCUSSION

The transmissibility response was found to differ for various anatomical locations on the foot, which could be qualitatively divided into three regions: toes, midfoot, and ankle (Figure 3.4). In general, resonance occurred at higher frequencies at the toes (less mass, soft tissue,

and weight bearing) and at lower frequencies at the ankle (increased mass, soft tissue and weight bearing necessities). These results are similar to regional differences observed in HAV exposure measurements, where resonance occurred at higher frequencies at the fingertips than the palm [13, 29, 129]. The fundamental resonant frequency at each location on the foot-leg system has some similarity to that at the corresponding location on the hand-arm system. Specifically, the resonant frequency range found at the toes (99-147 Hz) (based on Figure 3.5) is similar to that reported for the fingers [134]. Moreover, the resonant frequency range found at the mid-foot (51-88 Hz) (based on Figure 3.5) is similar to that reported for the hand dorsum [135] and that found for the ankle (19-39 Hz) is similar to that previously reported at the wrist [135, 136]. Evidence that the foot does not respond as a uniform structure is imperative for the development of vibration isolation strategies and protective measures. These regional differences warrant further study.

Comparing the current results with published results is complicated by the limited research specific to FTV. Three previously completed studies reported accelerometer measurements on the metatarsus (Figure 3.6a), medial malleolus (Figure 3.6b) and lateral malleolus (Figure 3.6c). Results from the studies by Goggins et al. [5] and Wee & Voloshin [70] were available for direct comparison, whereas the data from the Harazin & Grzesik [68] study was extracted using a plot digitizer. Two measurement locations in this study (T1P3 and L4) were also used by Goggins et al. [5] and yielded approximately a 0.3 decrease in transmissibility magnitudes (Figure 3.6a and Figure 3.6c). Equipment differences (accelerometers versus LDV) are likely responsible for the magnitude offsets observed.

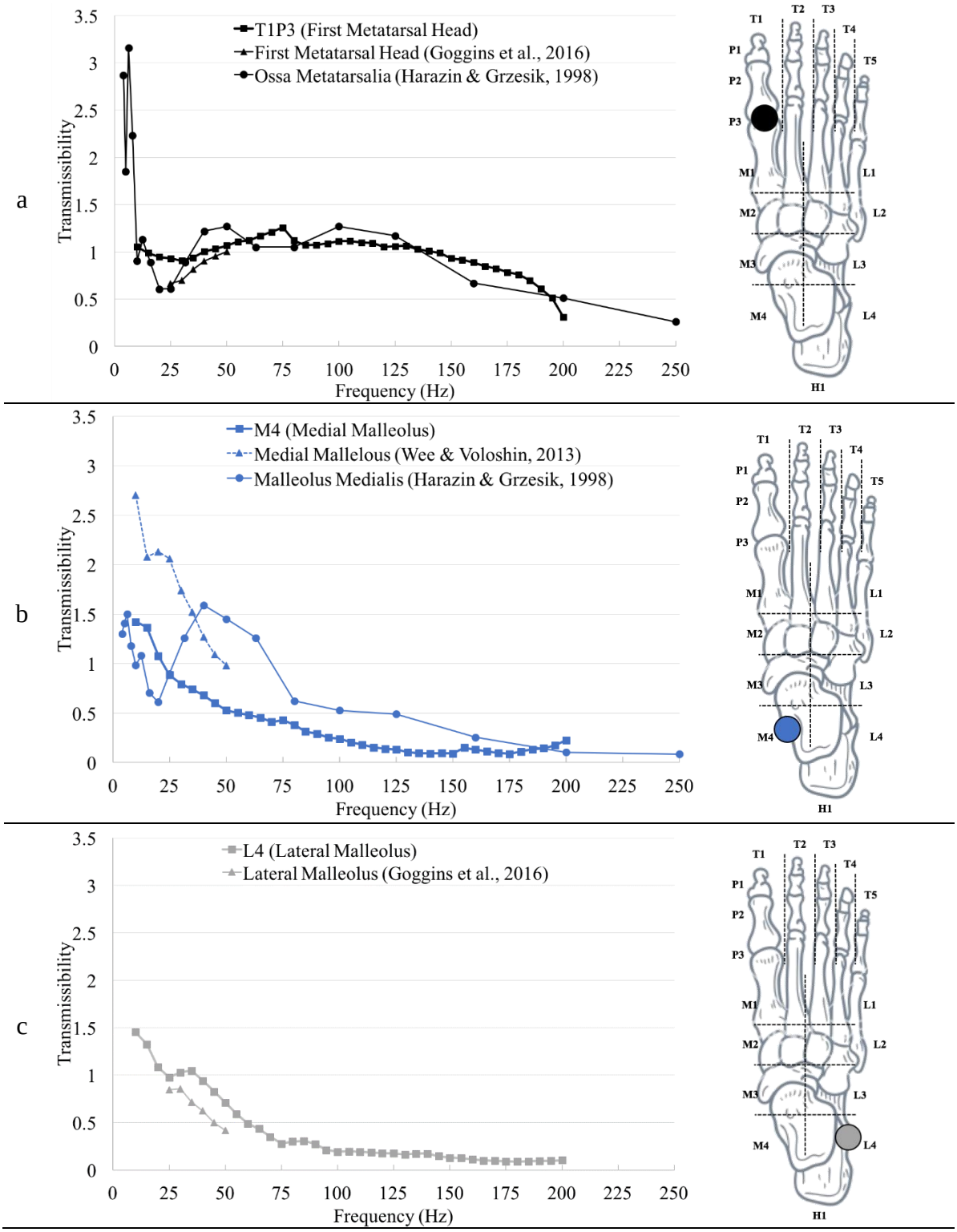

Figure 3.6: Comparison of transmissibility results at the first metatarsal head (a), medial malleolus (b), and lateral malleolus (c) from three previously completed studies [5, 68, 70].

The linear phase response from the toes and the upper portion of the midfoot (Figure 3.7a) was to be expected because these portions of the feet have a simple transmission path with very little damping from excess tissue. The average phase angle measured at the medial malleolus (M4) is identical to the phase angle measured from 10-50Hz for a seated participant [70]. However, the drastic phase changes observed (Figure 3.7b) at the five locations around the ankle (M3, M4, L3, L4, and H1) have two potential explanations. It is possible that, because the transmissibility magnitudes are below 0.2 between 110 to 200Hz, the large uncertainty on the phase may be due to the poor SNR, as suggested by Smith [133]. The phase change may also result from the greater number of anatomic elements between the vibration input and measurement location compared to the forefoot and midfoot. Vibration can pass through the heel fat pad, talus, calcaneus and one of two leg bones (tibia or fibula), as well as various tendons, ligaments, and muscles. Each of these components introduces structural dampening in the kinematic chain. This more complicated transmission path amounts to multiple mechanical elements in series, which may result in the greater variability observed.

Results indicated that the average coherence was close to 1 for most points, with the exception of M4, L4, and H1, where the average coherence decreased to 0.6 above 130Hz. Coherence drops from unity for four main reasons: system non-linearity, presence of non-measured inputs, leakage, or noise. The effect of the first three causes is minor for the following reasons:

1. The effect of spectral leakage is limited in the presence of high modal damping [137];
2. The risk of non-measured inputs is small, given that the only input in the frequency range of interest is the vibration provided by the shaker; and,

3. The adoption of a non-linear model, which included quadratic and cubic terms described by Tarabini et al. [130], did not increase the coherence value by more than 10%, the coherence increase was not homogeneous in different tests, and the response at frequencies different from the one of the stimulus was trivial.

a

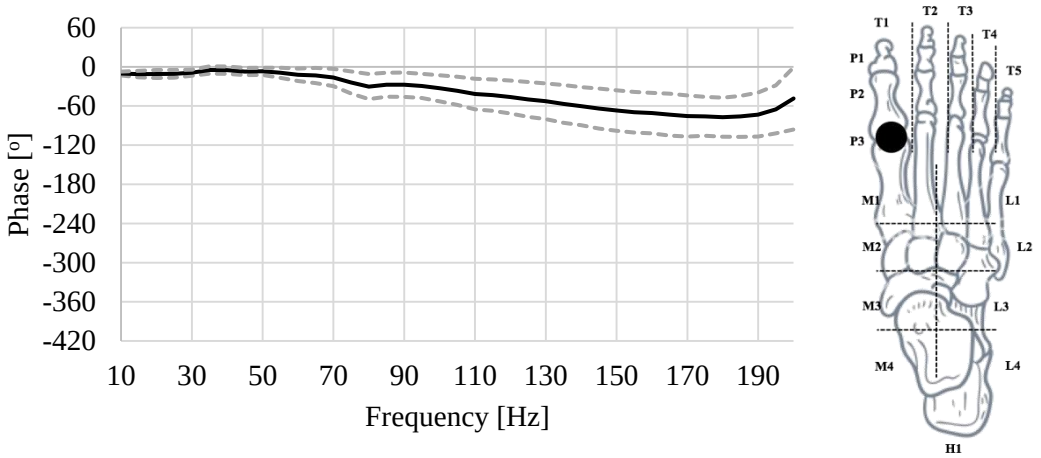

b

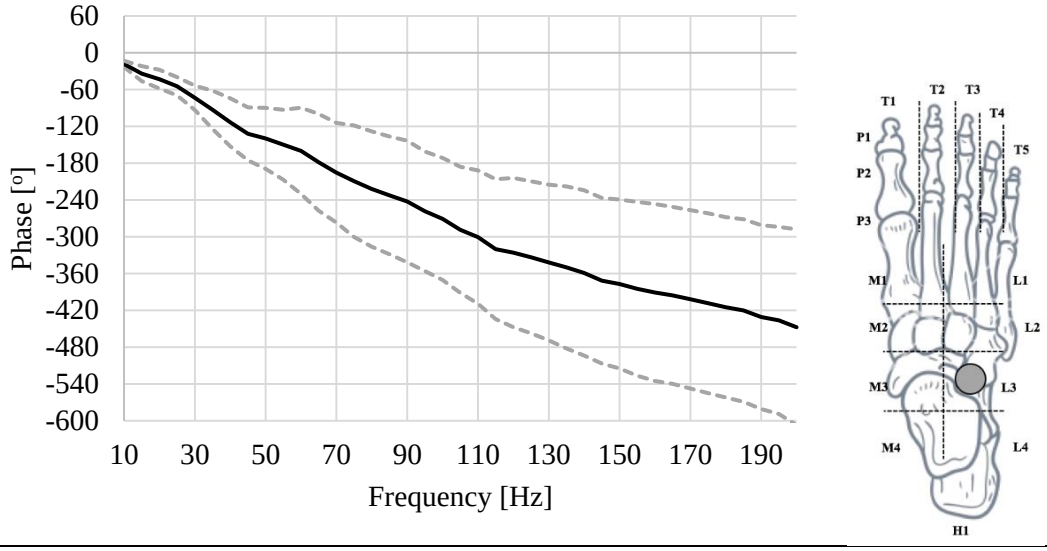

Figure 3.7: Average phase angle plots for 21 participants at T1P3 (a) and L3 (b).

Therefore, the low coherence can be reasonably attributed to the presence of measurement noise resulting from the constant velocity imposed by the shaker, which decreases the FRF magnitude, which in turn decreases the SNR at high frequencies.

Additionally, recording a vertical measurement of a point within a horizontal plane can cause a reflection artifact which reduces the light measured by the LDV and decreases the SNR.

The human response to vibration is non-linear, with many influencing factors [21]. Anthropometric differences as well differences in the underlying anatomy, such as muscle mass and the amount of adipose tissue, may have had a significant effect on the person-to-person variability observed in this study. In the case of hand-arm vibration, transmission of vibration occurs primarily through the bones and joints (<20% of the body mass); however, the soft tissues have been identified as being more influential in determining the overall response [138]. Certainly the influence of soft tissue, including the relative motion of the skin and the underlying tissues, becomes an important consideration when vibration transmissibility is measured on the skin. It is reasonable to assume that some of the reported resonances arose solely from relative motion between the skin and the underlying tissues. With the current set-up of this study the authors cannot rule this out. Future studies could consider the use of bone pins with a tri-axial accelerometer to determine transmissibility to the underlying bony structures.

Previous HAV studies have shown an increase in resonant frequency with increases in muscle tension [75, 139]. Although tension was not specifically measured in this study, it is interesting to note that involuntary muscle contraction was observed in some participants on the anterior portion of the ankle (L3, L4, M3, and M4) for frequencies beyond 20 Hz. Since the ability of participants to maintain a natural standing position without losing balance is confounded by individual factors (e.g. muscle control, muscle fatigue, or previous experience on vibration platforms), future research should measure differences in muscle activation and contraction with changes in FTV exposure frequency and magnitude.

Data from the localized transmissibility responses of the foot can contribute to improving the safety of industrial workers. For example, the current data could be used to develop more effective biodynamic models of the foot, as has been done with HTV models of the hand [115]. Once an appropriate model has been developed, the initial design and analysis of engineering controls to mitigate FTV exposure could be performed without human exposure testing. Furthermore, the findings from this study suggest that the toe, midfoot and ankle regions of the foot respond differently to the same FTV exposure input. Therefore, development of PPE with a single uniform material, such as anti-vibration insoles, boots, or mats, may be ineffective at mitigating FTV exposure to different areas of the foot.

The main limitations of this study derive from the constraints of the experimental setup. First, the LDV could not be positioned vertically above each measurement point on the foot because the knee and lower-leg blocked the path of the laser when participants stood on the vibration platform. The LDV measures the vibration along the laser axis and, in an ideal set-up, should be located directly above each measurement position and aligned with the vertical stimulus. To compensate for this limitation, correction factors were applied to correct for the off-axis error. However, the resulting compensation is only error-free in the presence of a good SNR (that was verified by the signal quality indicated by the LDV conditioning unit) and if the direction of motion is perpendicular to the LDV laser ray. Given that in the presence of a vertical stimulus the horizontal motion of the foot is expected to be smaller than the vertical one, the error should be small in comparison to inter-and intra- subject variability. Future research could evaluate horizontal foot motion when exposed to a vertical vibration stimulus.

Further limitations include the fact that the vibration stimulus (sweep rate with a constant velocity profile) was chosen in order to have a predictable SNR and to limit the overall test duration. The adoption of different stimuli (stepped sine, noise), of different sweep rates and of different amplitudes, could lead to different FRF estimations in the presence of system non-linearity and should be evaluated in future FTV studies. This study was also limited to the use of barefoot participants in a natural standing position only. Typically, workers exposed to vibration will be wearing socks and footwear, and operating some form of equipment which will take them out of a natural standing position. Future studies should consider the impact of different footwear conditions on FTV and consider the physiological effects. Changes in muscle activation and blood flow during the exposure may be more indicative of the onset for muscle fatigue and vascular damage.

As suggested by Dong and colleagues [15], an increased knowledge of the foot's response to vertical vibration may also be used to quantify vibration exposures for risk assessments. Moreover, as researchers learn more about the biomechanical response of the foot and lower leg segment, members of the ISO committee for human health should consider the development of a standard to evaluate health risks associated with occupational exposure to FTV. The current study found the resonant frequencies for the toes, midfoot, and ankle ranged from 99-147Hz, 51-84Hz, and 16-39Hz, respectively. These results may suggest that the current method of evaluating standing WBV exposure [8] may not be appropriate for evaluating health/injury risk specifically to the feet, as the weighting curve (W_k) decreases the influence of frequencies above 10Hz. The HAV standard [62] may be more appropriate for identifying health/injury risk to the feet as it does not apply such a negative weighting (W_h) to the higher frequencies where the toes are known to resonate.

Nevertheless, future research, including studies examining impedance and apparent mass, will be required before alternative frequency-weighting curves appropriate for determining health effects associated with exposure to FTV can be recommended.

3.5 CONCLUSIONS

This study identified the vibration transmissibility response at 24 anatomical locations on the feet of 21 volunteers when maintaining an upright natural standing position under exposure to FTV from 10 to 200Hz. Overall, the average transmissibility response was found to vary across anatomical locations with different average peak transmissibility frequencies for the toes (range: 99-147Hz), midfoot (range: 51-84Hz), and ankle (range: 16-39Hz). The corresponding average peak transmissibility amplitudes were found to be: toes (1.40-2.56), midfoot (1.42-1.59), and ankle (1.31-2.10).

Acknowledgements

This work was supported by a Natural Science and Engineering Research Council of Canada Discovery Grant (RGPIN/4252-2015) and by Regione Lombardia within the project "PORFESR 2014-2020: "Smart Fashion and Design". Dr. Lievers is an IAMGOLD Research Fellow and gratefully acknowledges the financial support of the IAMGOLD Corporation.

The authors would also like to acknowledge the instrumental contributions of Francesco Corti (Department of Mechanics, Politecnico di Milano, Lecco, Italy) in assisting with data collection, and for sharing his expertise in mechanical sampling. A sincere thank you as well to all of the willing participants in this study that supported our ability to contribute to the FTV literature.

CHAPTER 4: EFFECTS OF COP POSITION ON RESONANCE

Standing centre of pressure alters the vibration transmissibility response of the foot

Vibration white foot as an occupational disease has underscored the need to better understand the vibration response of the foot. While vibration transmissibility data exists for a natural standing position, it is anticipated that weight distribution will affect the response. The purpose of this study was to determine the effects of changes in centre of pressure (COP) on the foot's biomechanical response. Twenty-one participants were exposed to vertical vibration of 30 mm/s, with a sine sweep from 10-200 Hz. Z-axis (vertical) vibration was measured at 24 locations on the right foot, with the COP shifted forward or toward the heel. A mixed model analysis at each location revealed significant differences ($p<.001$) in the transmissibility response when the COP was altered to the forefoot and rearfoot. In general, when the COP was shifted toward a region of the foot (forward, backward), the peak frequency of the average vibration response for a region of the foot increased and the peak magnitude of the average vibration response decreased.

Keywords: foot-transmitted vibration; resonant frequency; centre of pressure

The contents of this chapter have been accepted as "Goggins, K.A., Tarabini, M., Lievers, W.B., Eger, T.R. (2019). Standing centre of pressure alters the vibration transmissibility response of the foot. *Ergonomics.* DOI: 10.1080/00140139.2019.1626490"

Graphical Abstract

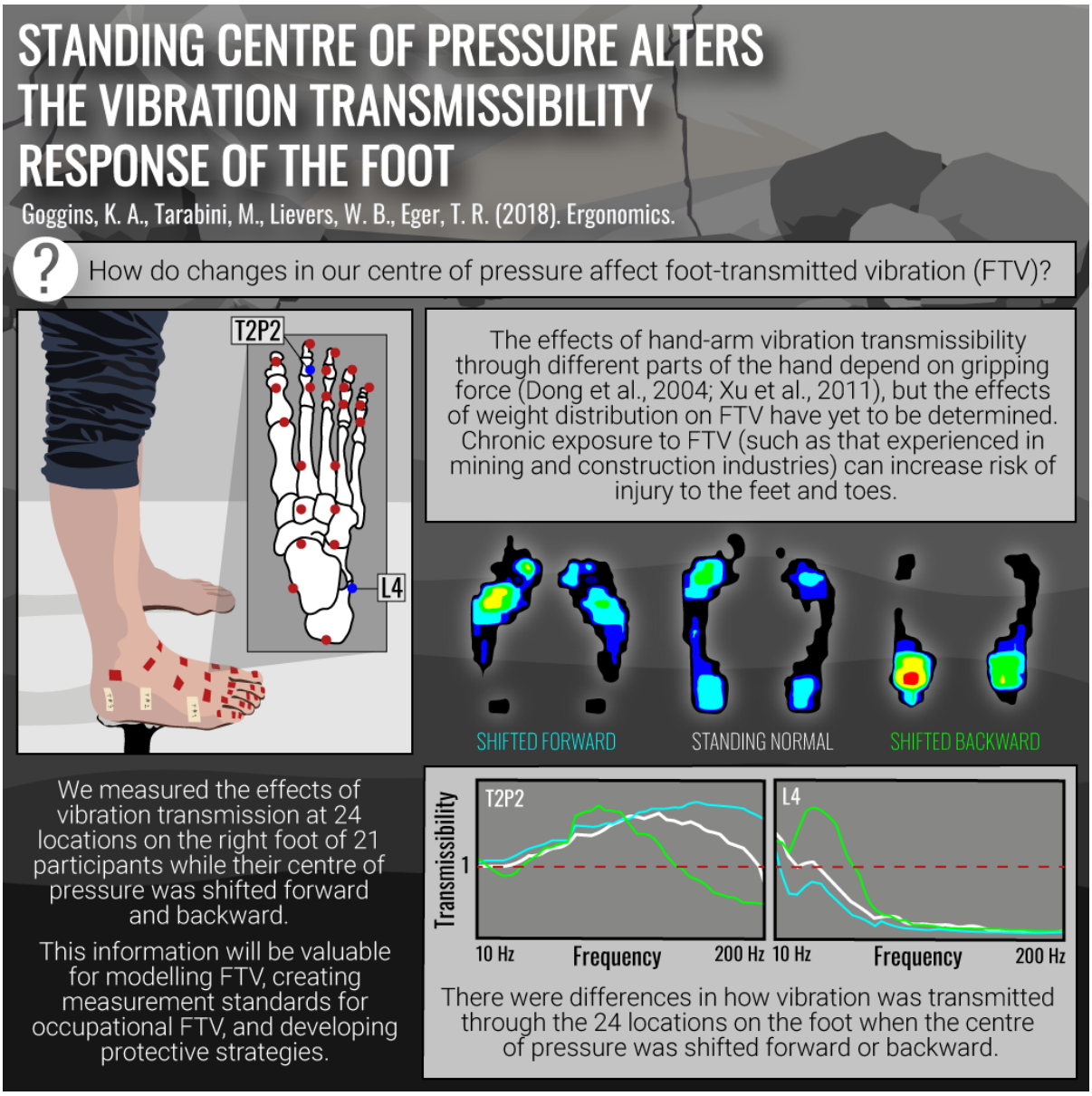

4.1 INTRODUCTION

Workers who stand on vibrating platforms or equipment —including those in mining, farming, forestry, and construction— are exposed to foot-transmitted vibration (FTV) on a daily basis [1, 2, 48-50]. This chronic exposure puts them at an increased risk of developing vibration-induced white-foot (VIWFt), a condition that can include symptoms such as pain and numbness in the toes and feet, increased sensitivity to cold, blanching in the toes, and joint pain, and in extreme cases complete loss of circulation resulting in necrosis and possible amputation [2, 124]. Unfortunately, very little is known about the vibration behaviour of the foot and few studies have reported the biomechanical response of a standing human exposed to FTV [4, 5, 68]. In order to further understand the link between occupational FTV exposure and injury, improved measures of FTV transmissibility are needed.

A major short-coming of most previous studies is that they have been limited to upright standing [5, 20, 28]; the effects of weight distribution on FTV have not been studied explicitly [4]. This omission is unfortunate because workers will routinely alter their footing and weight distribution in order to manipulate tools or equipment. For example, operators of a jackleg drill will often assume a lunge position, with one foot forward and one foot backward, and push forward on their toes when drilling into a rock face. It is reasonable to assume that, under such conditions, the vibration response of the toes will change, compared to neutral standing, as a person leans forward and their centre of pressure (COP) shifts toward their forefoot. In hand-arm vibration (HAV) studies, transmissibility through different structures of the hand [135] has been shown to depend on both gripping force [13, 129, 140] and on arm position [139]. Due to the anatomical and physiological similarities between the hands and feet, it is anticipated that the biomechanical response of the latter would be

affected by comparable factors such as the COP location and pressure distribution through the foot [13].

Several studies further support the hypothesis that body position and COP should be considered in detail. Harazin and Grzesik [68] found that transmissibility measurements at the metatarsus had similar responses regardless of posture, except when participants were asked to load their weight onto one leg. Similarly, ankle transmissibility measurements decreased when participants were asked to stand on their toes. Tarabini et al. [4] showed that different body postures did alter the weight distribution through the foot. Unfortunately, transmissibility was not measured directly and the vibration exposure frequencies were limited to 30Hz [4], which is notably lower than the resonant frequencies of the toes and midfoot [141]. These studies suggest that changes in weight distribution during standing FTV exposure can affect the vibration response of the foot.

A better understanding of the factors that affect the foot's response will assist in the development of human isolation strategies, through interventions and engineering controls, which could ultimately lead to improved protection and comfort for workers against occupational vibration exposure. Thus, the goal of the current work is to determine how changes in COP affect the vibration response of the foot. In addition to the previously published natural standing position data set [141], the same 21 participants were asked to assume two other standing positions (forward-lean and backward-lean) while exposed to vertical vibration in a sine sweep from 10-200 Hz.

4.2 METHODOLOGY

The study methodology was approved independently by the research ethics board of Laurentian University (Sudbury, Canada) (Appendix A) and ethical procedures for the MetroSpace Lab at Politecnico di Milano (Lecco, Italy).

4.2.1 Participants

Twenty-one participants, 15 males and 6 females, with an average (± standard deviation) age of 24 (±7.8) years, height of 175.6 (± 8.9) cm, mass of 70.1 (± 13.7) kg, and total foot length of 25.8 (± 2.0) cm participated in the study [141]. Participants were eligible to participate if they could communicate in English. Due to the effects of vibration exposure on the vascular and neurological systems, exclusion criteria included: self-reported diabetes, a concussion, a current pregnancy, problems with motion sickness, or a lower body musculoskeletal injury in the previous six months.

4.2.2 Centre of Pressure Measurement

Participants were asked to stand on the Pedar-Expert insoles (Version 11.3.12, Munich, Germany), to measure their COP in two deviations (forward lean and backward lean) from the previously collected natural standing position [141] (Table 4.1). Prior to the COP measurement, participants practiced holding each of the desired positions with a plumb line attached at their hip and the corresponding location on their foot was marked (Figure 4.1). The marked locations served as a guide for the participant to reassume their position when measuring COP, and then again for transmissibility measurements on the vibration platform. The ability to return to a particular position was needed because the COP measurements could not be taken simultaneously with the vibration transmissibility measurements due to

the insole bandwidth of 50 Hz [142]. The participant's COP (x, y-coordinates (cm)) and vertical force (N) were recorded while the participant maintained their position for five seconds. The axial location (y-coordinate) of the COP was normalized with regards to participant's foot length, and the normalized y-coordinate (%) was used for analyses.

Table 4.1: Centre of pressure position descriptions given to the participants.

Standing Position	**Instructions Given to Participant**
Forward Lean	Stand in a forward leaning position, that shifts your weight forward to your toes. From your natural position, you can bend your knees approximately 10^{o} and lean forward.
Backward Lean	Stand in a backward leaning position, that shifts your weight backward into your heels. From your natural position, you can bend your knees approximately 10^{o} and lean backward.

Figure 4.1: Example of participant using Pedar-Expert insoles and plumb line combination to capture pressure distribution and COP showing backward lean position (left), natural position (center)[141], and forward lean position (right).

4.2.3 Instrumentation and Data Analysis

Detailed information, including the specifications of the instrumentation and data analysis procedure can be found in Figure 4.2. An electrodynamic shaker with a mounted 50 x 50 cm steel plate delivered the vertical vibration stimulus, with maximal displacement and force of ±50 mm and 10 kN respectively. The stimulus included a sine sweep vertical vibration of 30 mm/s from 10-200 Hz and lasted 51 seconds [141]. The input was measured with a uni-axial accelerometer to measure the vertical vibration from the platform. The output was measured with a laser Doppler vibrometer (LDV) to capture the velocity at 24 anatomical locations on the foot (Figure 4.3), while the participant assumed each of the three standing positions (Table 4.1). Retro-reflective tape (3M) was placed on the desired anatomical locations to aid in reflecting the laser light for the LDV measurement. The natural position was tested first and is reported in [141], and the order that the forward lean and backward lean positions were adopted was then randomized for all participants. From both experiments, the participants were exposed to vibration for approximately 61 minutes, resulting in 72 transmissibility measurements (24 anatomical locations, in the natural [141], forward and backward COP positions).

All vibration data were processed using LabVIEW (National Instruments, 2015). The acceleration of the foot was calculated by differentiation of the velocity measured by the LDV and the acceleration of the platform were measured with the accelerometer mounted directly on the platform. Transmissibility was calculated for the forward and backward lean position, across the frequency range (10-200 Hz) for all 24 locations on the right foot. The modulus was calculated using the $H_1(f)$ frequency response function (FRF) [130]:

$$H_1(f) = \frac{\bar{S}_{av}(f)}{\bar{S}_{aa}(f)} \tag{4.1}$$

where $\bar{S}_{av}(f)$ is the averaged cross-spectral density; and $\bar{S}_{aa}(f)$ is the auto-spectral density function of the input signal. Cross-spectral density was calculated using a discrete Fourier transform (DFT) that had a size of 2048 samples, used a rectangular window with no overlap, and had a spectral frequency resolution of 0.5 Hz. As the participants' legs obstructed the LDV, a totally vertical measurement was not possible. The maximum tilt of the LDV was limited (< 20°) and the bias error deriving from the tilt was compensated for as described in the previous study [141] using the laser point locations (Appendix G).

The phase angle was calculated at each measurement location (m) [130]:

$$\varphi_l(f) = arctan\left(\frac{ReS_{av}(f)}{ImS_{av}(f)}\right) \tag{4.2}$$

where $ReS_{av}(f)$ is the real component of the cross-spectral density function; and $ImS_{av}(f)$ is the imaginary component of the cross-spectral density function.

The coherence (the degree of correlation between the input and output) was calculated according to [130]:

$$\gamma^2(f) = \frac{|\bar{S}_{av}(f)|^2}{\bar{S}_{aa}(f) \cdot \bar{S}_{vv}(f)} \tag{4.3}$$

where $|S_{av}(f)|^2$ is the modulus of the cross-spectral density function; $S_{aa}(f)$ is the auto-spectral density function of the input signal; and $S_{vv}(f)$ is the auto-spectral density function of the output signal.

During the vibration exposure testing, there were trials with noticeable instantaneous decreases in coherence data from the laser ray not remaining on the reflective marker. Coherence was monitored during testing and trials where coherence distinctively dropped below 0.5 were repeated. As not all decreases in coherence were strictly caused by the

reflective marker and laser [141], during data analysis, additional measurements were discarded based on their coherence. Discarded measurements included: data for one participant in the backward lean position, two measurements in the natural position, nine in the forward lean position, and six in the backward lean position (Appendix H). The average peak transmissibility frequency and amplitude were also computed, as an indication of resonance.

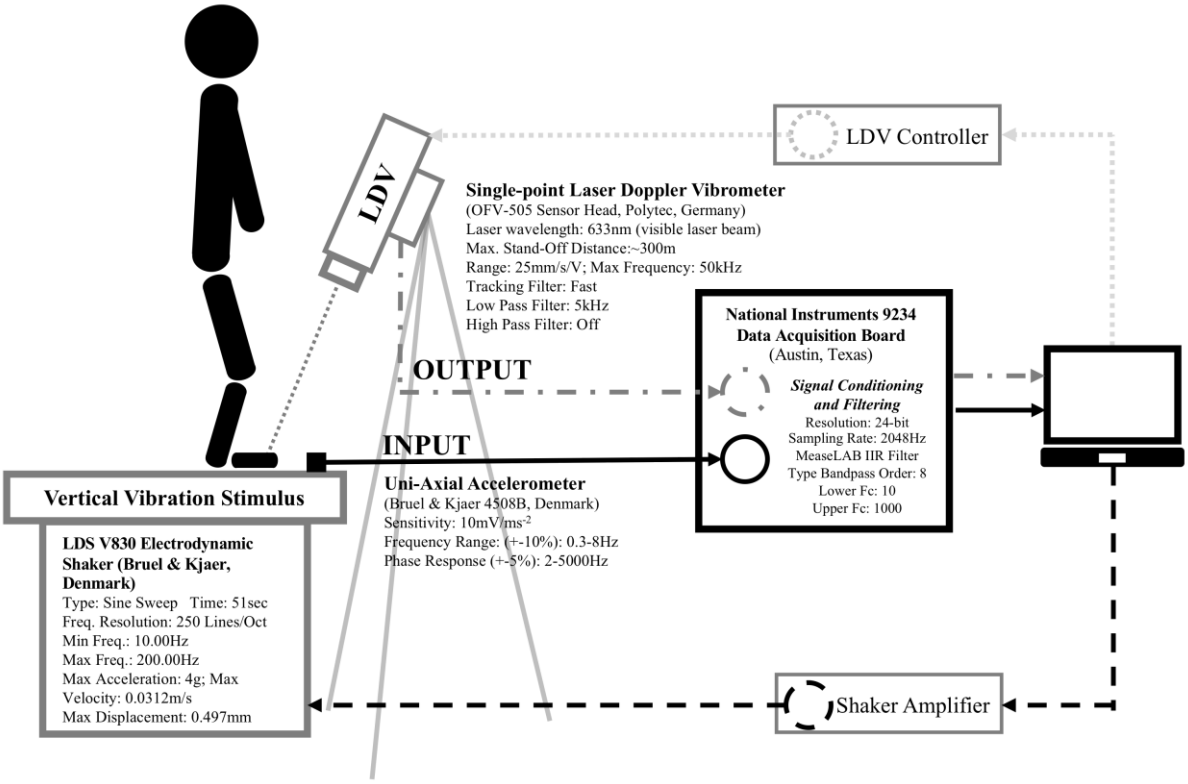

Figure 4.2: Outline of the data collection instrumentation specifications and data analysis technique with corresponding equations. Examples figures of the modulus, coherence, and phase are results from anatomical location T1P3 in the natural standing position.

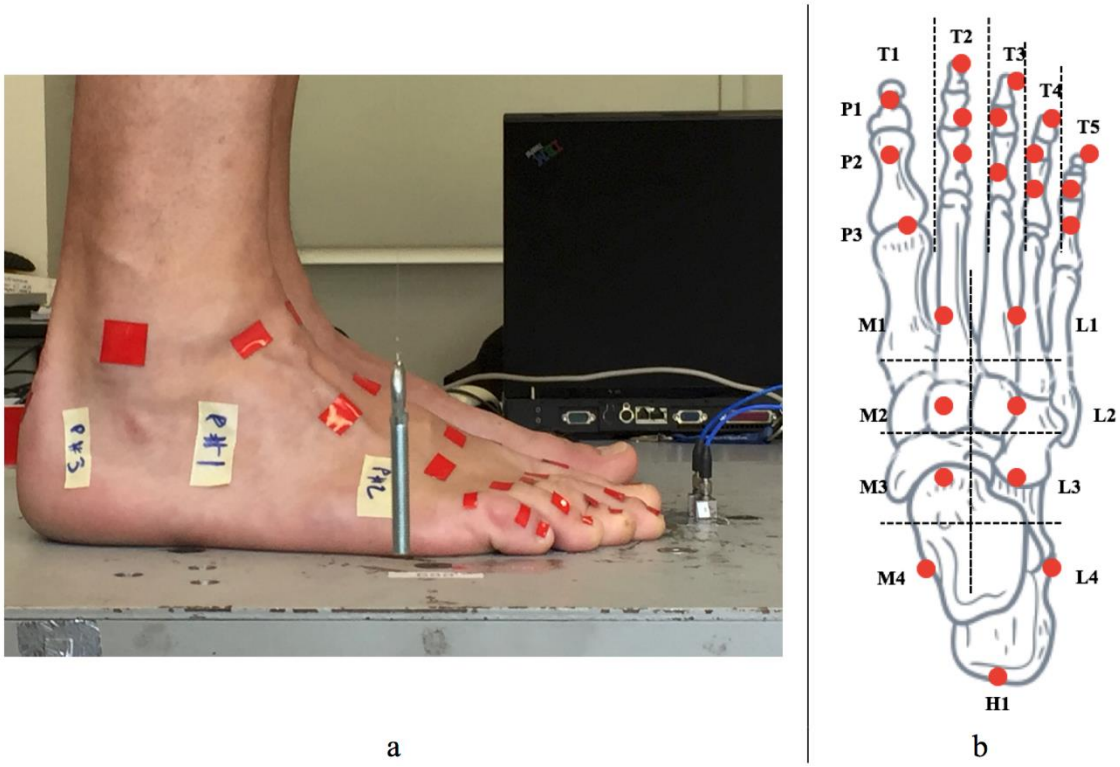

Figure 4.3: Reflective sticker set-up (a) lateral view with LDV measurement at T4P2, and (b) topical anatomic representation.

4.2.4 Statistical Analysis

Initially, a one-way independent analysis of variance (ANOVA) with Tukey's pairwise comparisons was conducted on the normalized y-coordinate of the COP, in order to ensure a statistically significant ($p<0.05$) difference between the natural, forward lean, and backward lean positions. After confirming the COP location changed significantly, the changes in transmissibility response in the three positions could be treated separately for comparison.

The differences in transmissibility based on the COP location were evaluated at each anatomical location using fifth degree polynomial regressions given by:

$$T = \beta_0 + \beta_1 f + \beta_2 f^2 + \beta_3 f^3 + \beta_4 f^4 + \beta_5 f^5 \qquad (4.4)$$

where T is the transmissibility, f is the frequency, β_0 is the intercept, and β_1 to β_5 are the coefficients. Initially, a fifth degree polynomial regression was completed on the natural position and then the regressions in the forward and backward lean positions were evaluated for significant differences ($p<.05$). Each anatomical location was treated separately, and no correction factor for type I error was applied [143] since this would make the likelihood of type II error unacceptable in this case.

4.2.5 Resonance Analysis

Resonance occurs at the frequency associated with the maximum transmissibility amplitudes [6, 9]. In order to assess resonance, the peak amplitude and frequencies were also computed on the average transmissibility curve $\bar{T}_l(f)$ for each location (l) as:

$$PA_{avg,l} = max\left(\bar{T}_l(f)\right) \tag{4.5}$$

$$Pf_{avg,l} = frequency\ at\ PA_{avg,l} \tag{4.6}$$

These quantities are referred to as peak amplitude of the average ($PA_{avg,l}$) and peak frequency of the average ($Pf_{avg,l}$) [141].

4.3 RESULTS

4.3.1 COP and Position

The COP x and y-coordinates were measured for each participant when standing in a natural, forward and backward lean position (Appendix I). As an indication of the longitudinal location of the COP from the origin (back edge of the heel), the normalized y-coordinate (%) of the COP is reported in a histogram for all three positions (Figure 4.4). The one-way independent ANOVA revealed there was a significant effect of position on the normalized y-

coordinate (%) of COP ($p < .001$). Post hoc testing with Tukey's pairwise comparisons revealed the natural position was significantly different from the forward lean ($p < .001$) and backward lean ($p < .001$) positions. The forward lean position was also significantly different to the backward lean position ($p < .001$). In the forward lean, natural and backward lean positions, the normalized y-coordinate (%) of the COP ranged from 46.42 to 80.28%, 12.84 to 62.73%, and 8.10 to 29.06%, respectively.

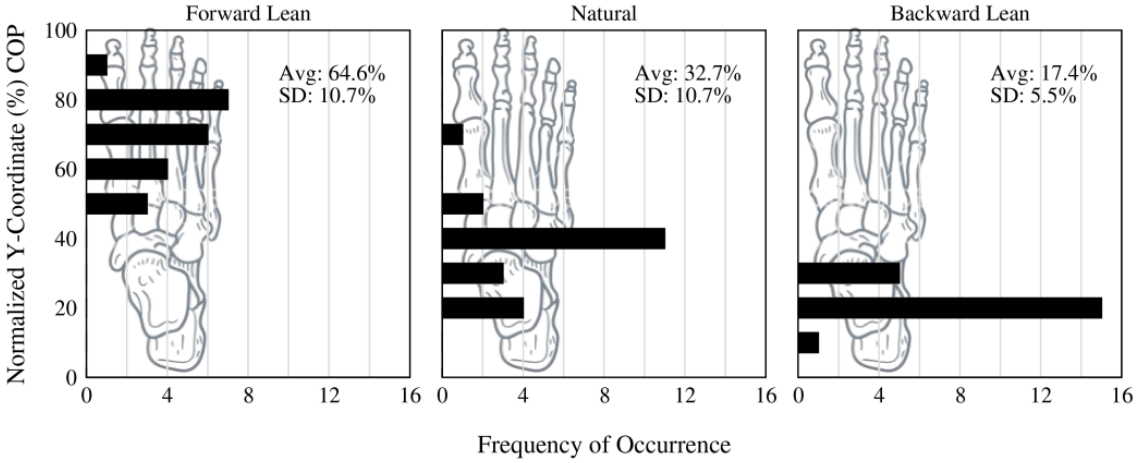

Figure 4.4: Histogram of each participant's normalized y-coordinate (%) of the COP in the forward lean (top), natural (middle), and backward (bottom) lean positions. Avg = Average, SD = Standard Deviation.

4.3.2 COP and Transmissibility

Forty-one, including 24 measurements from one participant in the backward COP position, of the 1512 individual measurements taken were omitted for low (<0.5) coherence. Of the remaining 1471 measurements, most had coherence values near unity. The coherence for most measurements during testing was near unity and they were considered acceptable. The individual transmissibility responses of all participants in the forward and backward COP locations at all 24 anatomical locations are presented in Appendix J. The average (± standard deviation) transmissibility, phase and coherence for each location from the 21 participants are plotted in the forward (Appendix K) and backward (Appendix L) leaning positions.

Average transmissibility, phase and coherence data for the natural upright standing position were reported previously [141]. Differences in average transmissibility amplitude were observed for the natural, forward, and backward positions (Figure 4.5).

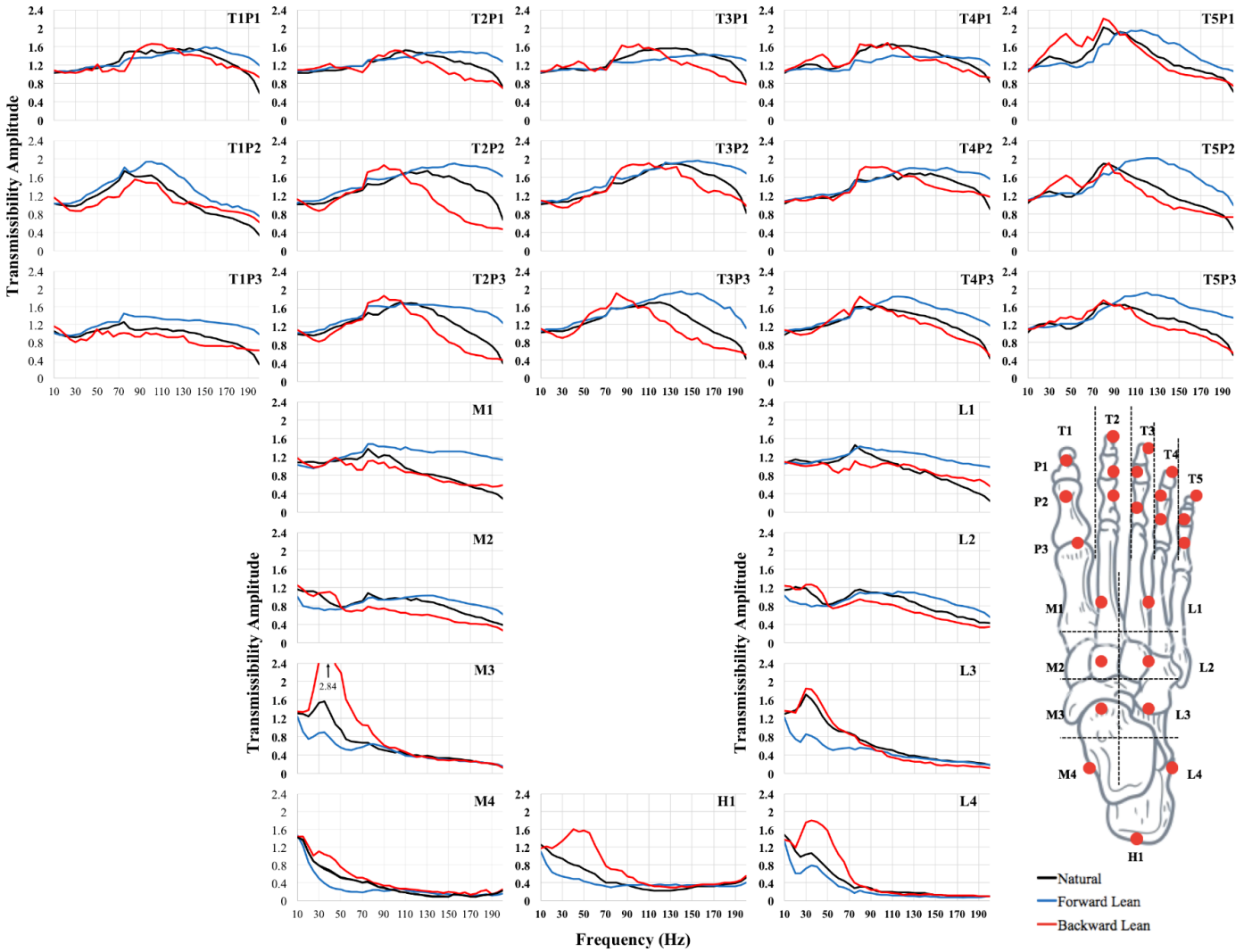

Figure 4.5: Vibration transmissibility was measured at 24 locations on the foot, under 3 standing conditions (natural [141], forward lean, backward lean) for 21 participants exposed to FTV across a frequency range of 10-200 Hz. The average transmissibility amplitude for each measurement location is plotted for each condition.

Overall, the transmissibility response in the forward lean position was similar to that in the natural standing position at low frequencies (10-80 Hz), but at higher frequencies (80-200 Hz) the transmissibility response of the forward lean position was more amplified than natural standing. Forcing the COP into the forefoot, generally decreased the transmissibility response (10-200 Hz), compared to the natural standing position, at the anatomical locations around the ankle (M3, M4, L3, L4 and H1). Concentrating the COP in the rearfoot led to an increase in transmissibility amplitude at low frequencies (10-60 Hz), with little difference observed at higher frequencies (90-200 Hz).

Forward Lean Position

The fifth degree polynomial regressions revealed that positioning the COP in the forefoot, significantly ($p<.001$) altered the transmissibility response compared to when the participant was standing in their natural position at all anatomical locations. Generally, the forward lean position produced a similar transmissibility response to natural standing at low frequencies (10-80 Hz), but at higher frequencies (80-200 Hz) the transmissibility response was more amplified than natural standing. For the anatomical locations around the ankle (M3, M4, L3, L4 and H1), pushing the COP to the forefoot, decreased the majority of the transmissibility response (10-200 Hz) from that of the natural standing position.

Backward Lean Position

At all anatomical locations except L1 ($p=.765$), the polynomial regressions revealed the transmissibility when in the backward lean position was significantly different ($p<.001$) from the natural standing position. The negative result at L1 is likely due to the response of one participant (see participant #12 in L1 Appendix E). No outlier testing was performed; all tests that satisfied the coherence criterion were included in the analysis. In general,

concentrating the COP in the rearfoot led to amplification at low frequencies (10-60 Hz), and attenuation at higher frequencies (90-200 Hz), when compared to the natural COP position.

4.3.3 Resonance

The peak frequency of the average ($Pf_{avg,l}$) (Figure 4.6a) and peak amplitude of the average ($PA_{avg,l}$) (Figure 6b) are reported for the natural standing [141], forward lean and backward lean positions. Generally, the highest $Pf_{avg,l}$ occurred in the forward lean position and lowest in the backward lean position, at all measurement locations except at the rearfoot (M3, M4, L3, L4, and H1). At these five locations around the ankle, the backward lean position resulted in a higher average peak frequency than the natural and forward lean positions.

All measurement locations and COP positions resulted in vibration amplification ($PA_{avg,l}$> 1) (Figure 4.6b). The $PA_{avg,l}$ was highest in the backward lean position at all measurement locations at four of the five measurement locations around the ankle (excluding M4). Transmissibility amplitude was found to be the lowest at the first measurement point on all of the toes, for the forward lean position, whereas the remainder of the measurements on the toes recorded the lowest transmissibility amplitudes in the natural or backward lean position.

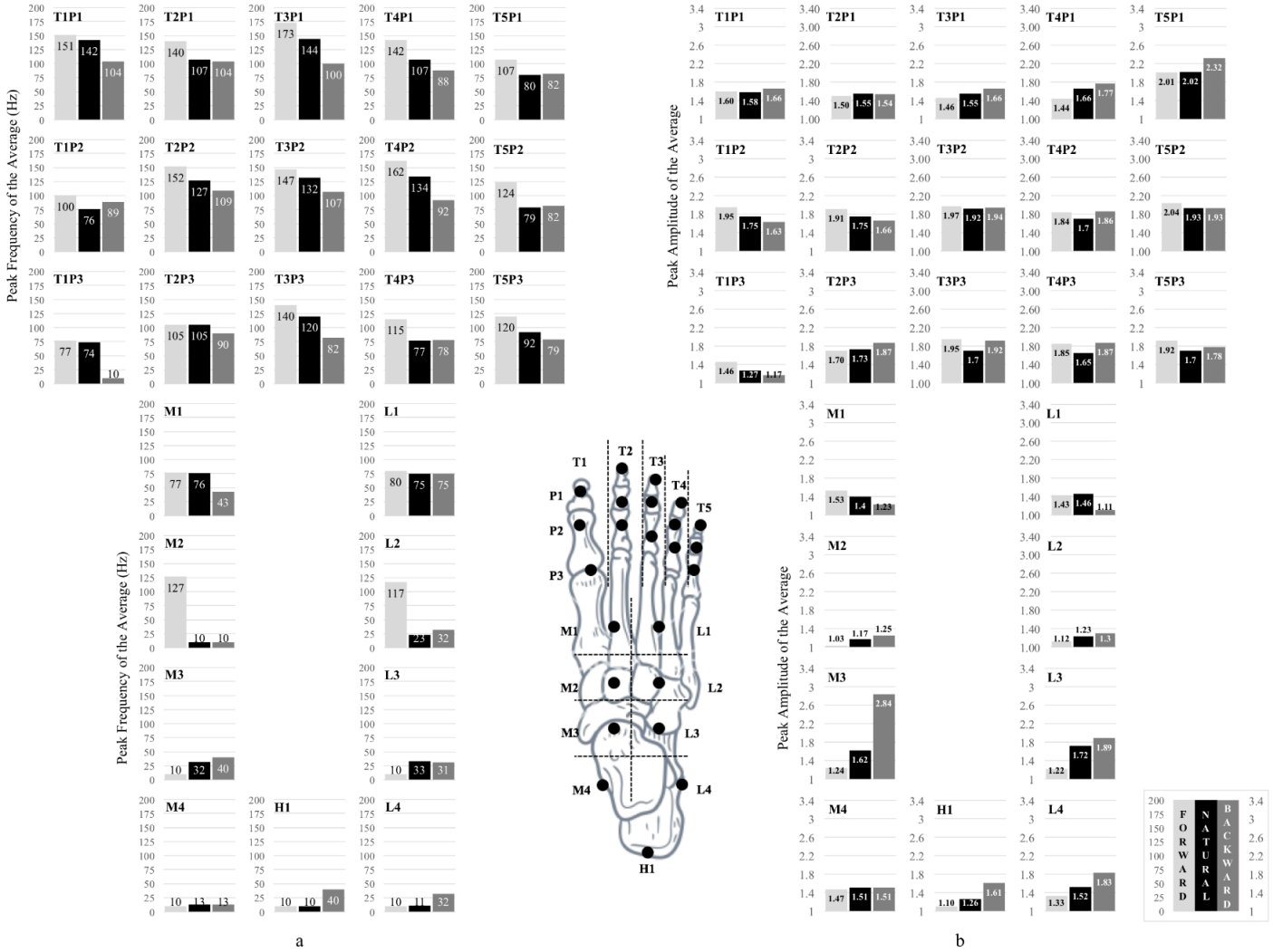

Figure 4.6: The peak frequency of the average ($Pf_{avg,m}$) (a), and peak amplitude of the average ($PA_{avg,m}$) (b), of 21 participants exposed to vertical vibration from 10-200 Hz, under 3 standing conditions (natural [141], forward lean, backward lean) from 24 anatomical locations.

4.4 DISCUSSION

Participants were asked to assume two standing positions (forward lean and backward lean) which caused deviations in the COP from their natural standing position, in order to evaluate the effects of altering the COP on the vibration transmissibility response of the foot. Analysis revealed that the resulting COP locations measured for each position were significantly different ($p<.001$). The normalized y-coordinate of the COP ranged from 46.4 to 80.3%, 12.8 to 62.7%, and 8.1 to 29.1% in the forward, natural and backward lean positions, respectively. Overall, concentrating the mass to a particular portion of the foot resulted in an increase in the peak frequency at the corresponding anatomical locations.

Since FTV literature is limited, and the hands are anatomically similar to the feet, comparison of transmissibility results to the larger hand-transmitted vibration (HTV) literature is warranted. However, the difference in experimental conditions between FTV and HTV studies are significant and cannot be understated. For instance, the force acting on the foot from the full body weight of a participant are much higher than the maximum grip force that same participant can achieve with their hand. Concettoni and Griffin [13] used a LDV to measure HTV at 41 locations from the fingertips to the elbow. Participants were exposed to HTV in seven conditions, involving variations of how much of the palm and fingertips were directly on the vibration platform. The greatest mean transmissibility (2.9 at 22 Hz) for the fingertips occurred when the palm was in contact with the vibrating plate (push force 25 N). These results are similar to those from the backward lean position, where the greatest mean transmissibility at the toes ranged between 3.0 at 89 Hz (average maximum force on the right foot 308 N). Concentrating the mass in the heel resulted in a larger transmissibility amplitude

at the toes (Figure 4.6b), similar to the increases at the finger tips observed when greater force is placed on the palm [13].

In another HTV study, Aldien et al. [144] conducted a laboratory experiment which exposed seven male participants to random vibration between 8-1000 Hz, using three handles, and different grip (10, 30, and 50 N) and push forces (25, 50, and 75 N), in two different postures. The study found that increasing the push and grip force tended to shift the peak impedance to a higher frequency in both postures. These results are also comparable with the current study where concentrating the standing pressure to a certain portion of the foot (average maximum force in natural, forward, and backward positions are 259, 270, and 308 N, respectively) resulted in a shift in peak frequency of the average curves (Figure 4.6a).

The average transmissibility results are also similar to those of an HTV study conducted by Welcome and colleagues [134], where the transmissibility of seven participants at six locations on the left and right hands, with grip forces of 15, 30, and 50 N, were measured using a 3D LDV. For example, from the bare hand condition, the transmissibility on the proximal phalanx of the middle finger, anatomically comparable to the T3P3 location from this study, increases from ~1 (at 16 Hz) until ~1.7 (at 120Hz) and then decreases to ~0.5 (at 400 Hz) [128, 134]. Whereas, at T3P3 in the natural bare foot condition, transmissibility increased from 0.99 (at 10 Hz) to 1.70 (at 120 Hz) and decreases to 0.79 (at 200 Hz). As the goal of [134] was to evaluate the effect of vibration-reducing (VR) gloves on finger vibration, different levels of grip force were also evaluated [128] and were found to influence the effect of the VR gloves. In order to create personal protective equipment for FTV exposure (e.g. boots and insoles), transmissibility response differences based on changes in

the COP location should be incorporated, as workers standing on vibrating platforms are rarely stationary and often adjust foot position in order to balance themselves.

Resonance can result in maximum deformation of the tissue and, as such, has been recognized as the most influential exposure frequency causing human injury [11, 27]. Traditionally, resonance has been identified as the frequency with the greatest transmissibility amplitude [6, 9]. When participants were asked to lean forward, concentrating the COP in the forefoot, a shift to a higher resonance frequency occurred at the toes and midfoot, similar to the trends seen in the hand [29, 145], and the transmissibility amplitude decreased. However, the reverse occurred when concentrating the COP in the rearfoot: the transmissibility amplitude increased near the heel (M3, M4, L3, L4, and H1) and resonance shifted to a lower frequency. These results are consistent with previous findings showing that transmissibility amplitude measured at the ankle decreased when participants stood on their toes [68]. Furthermore, an HTV study has shown that increased the contact pressure can increase the soft tissue stiffness and consequently the natural frequency [136], similar to the changes observed herein with shifting COP.

Important regional differences (e.g. between the toes, midfoot and ankle) in vibration response were observed due to changes in COP. In general, vibration amplification occurred in the forward lean position when participants were exposed to FTV above 100 Hz; transmissibility amplitudes consistently reached around 2 (Figure 4.5). While in the backward lean position, vibration transmissibility amplitudes decreased above 100 Hz, gradually reaching attenuation levels of approximately 0.8. The transmissibility response was the opposite for the five measurement locations around the ankle (M3, M4, L3, L4, and H1). When participants were exposed to FTV below 80 Hz, vibration amplification occurred in the

backward lean position, with maximum amplification at the M3 location (Figure 4.5). Conversely, exposure below 80 Hz in the forward lean position resulted in vibration attenuation with transmissibility levels constantly below 1.

Understanding regional differences in vibration transmissibility response to FTV is necessary for developing an appropriate measurement and assessment standard, and for creating practical isolation strategies, such as those developed for HTV [128]. VIWFt has previously been documented for a 54-year old worker primarily operating a vehicle-mounted bolter [2], which exposed him to a dominant z-axis vibration at 40 Hz. Results from the current study indicate toe resonance to occur at higher frequencies in the forward lean position (113-167 Hz) than in the backward lean position (78-126 Hz). This knowledge, combined with the effects of resonance on artery stiffness [146], would indicate that in order to advance understanding of VIWFt studies need to consider more than the resonance of the ankle. The higher frequency resonance of the toes must also be properly measured and evaluated.

While quantifying the vibration response at 24 locations provides a detailed description of the behavior of the foot, such a large number of measurement points is not without shortcomings. For example, there were not enough participants in the current study to support an appropriate multivariate statistical test over all 24 anatomical locations. Moreover, measuring the transmissibility response at 24 anatomical locations is not practical in the field. Incorporating an increased number of measurement locations also limits potential for testing different combinations of conditions (e.g. postures, COP positions, insoles, outsoles, boots, etc.) in the laboratory setting while minimizing participants' daily exposure to FTV. In the future, minimizing measurement locations to appropriately represent the

biodynamic response of the foot will allow for practical FTV measurements in the field (e.g. underground), reduce exposure times in the laboratory, and allow for testing a larger variety of conditions for the same daily exposure limit. Additionally, minimizing measurement locations will better guide numerical model development by identifying which points must be incorporated to accurately represent the biodynamic response to FTV [13].

One of the major shortcomings of this research was that the COP could not be measured directly while on the vibration platform due to the frequency range limitations of the insoles [142]. However, statistical analysis confirmed the participants were able to create statistically different COP profiles for forward, natural and backward. Thus, conclusions about the effects of the COP are based on the assumption that the participants were able to replicate and hold their COP position on the vibrating platform, as they did during the static measures of COP. As the changes in COP location had significant effects on the transmissibility response, future FTV laboratory studies should aim to measure COP simultaneously with vibration exposure.

Findings from this study also suggest that the entire transmissibility response curve (Figure 4.5) should be evaluated in the future because limiting analysis to resonance, including peak frequencies and amplitudes, can ignore other important changes to the biodynamic response as a result of COP. Most notably, the differences in transmissibility response before resonance at locations around the ankle and after resonance for the midfoot and the toes, need to be addressed as workers are exposed to a range of exposure frequencies and amplitudes. Future research could also evaluate the effects of different vibration amplitudes and waveforms on transmissibility and apparent mass.

4.5 CONCLUSIONS

Vibration transmissibility was measured at 24 locations on the foot for three standing position with different COP locations. Regression analysis at each anatomical location revealed significant differences ($p<.001$) in the transmissibility response when the COP was shifted toward the forefoot and rearfoot, with the exception of anatomical location L1 ($p=.765$) in the backward lean position. Generally, concentrating the COP to a particular portion of the foot produced an increase in peak frequency of the average to the corresponding anatomical area. The results of this study have direct implications for creating a foot specific International Standard for measuring FTV exposure, modelling FTV, and developing control strategies to mitigate FTV exposure.

Acknowledgements

This work was supported by a Natural Science and Engineering Research Council of Canada Discovery Grant (RGPIN/4252-2015) and by Regione Lombardia within the project "PORFESR 2014-2020: "Smart Fashion and Design". The authors would also like to thank Francesco Corti (Department of Mechanics, Politecnico di Milano, Lecco, Italy) in assisting with data collection, and Dr. Bruce Oddson (Department of Human Kinetics, Laurentian University, Sudbury, Canada) in assisting with statistical analysis. Dr. Lievers is an IAMGOLD Research Fellow and gratefully acknowledges the financial support of the IAMGOLD Corporation.

CHAPTER 5: UNIQUE ANATOMICAL LOCATIONS

Anatomical locations for capturing magnitude differences in foot-transmitted vibration exposure determined using multiple correspondence analysis

To facilitate research and safety studies, it is desirable to identify the minimum number of measurement points needed to characterize the biodynamic response of the foot to vibration exposure. In previous experiments, transmissibility measurements were taken at 24 anatomical locations on the foot when 21 participants were standing with their centre of pressure (COP) in a natural, forward and backward location. Multiple correspondence analysis was performed using the peak transmissibility magnitudes from these data in order to identify clusters of behaviour that might be used to reduce the total number of measurement locations. Peak transmissibility was analysed based on two magnitude thresholds: at 2.0 (100% amplification of the input signal), and at 2.5 (150% amplification). Results indicate that transmissibility measurements at the nail bed of the first phalange (T1P1), the head of first metatarsal (T1P3), the head of second metatarsal (M1), and the lateral malleolus (L4) may be sufficient to effectively measure foot-transmitted vibration across the range of COP locations analyzed (natural, forward and backward).

Keywords: foot-transmitted vibration, standing vibration, vibration-induced white-foot

The contents of this chapter have been published as "Goggins, K.A., Oddson, B.E., Lievers, W.B., Eger, T.R. (2019). Anatomical locations for capturing magnitude differences in foot-transmitted vibration exposure determined using multiple correspondence analysis. *Theoretical Issues in Ergonomics Science.* (Submitted)."

5.1 INTRODUCTION

Foot-transmitted vibration (FTV) exposure occurs in mining, farming, forestry, construction, and in other industries where workers stand on vibrating platforms or equipment [2, 48, 50]. Unfortunately, prolonged occupational exposure to FTV can result in neurological, vascular, or musculoskeletal symptoms in the feet and lower limbs. The vascular symptoms are termed vibration-induced white-foot (VIWFt), a condition characterized by pain and numbness, increased sensitivity to cold, and blanching in the toes [2, 124]. To date, a limited number of field and laboratory studies have measured the biodynamic response of the human foot to standing vibration exposure. A better understanding of the FTV response is needed.

One shortcoming common to many previous studies is that transmissibility measurements have been limited to a few anatomical locations on the foot: the head of the first metatarsal, the medial malleolus, and the lateral malleolus [5, 60, 68-70]. Whereas the response of the hand to HTV is typically captured with anywhere from 20 [140] to 41 measurements [13]. For example, the biodynamic response of the hand has been shown to vary with anatomic location, individuals, and applied hand forces [3, 140]. Since the palm of the hand and the fingers have different resonant frequencies, it is impossible to identify a single resonance band that reflects the entire hand-arm system [140]. Similarly, assuming a single resonance in the foot does not appear to be applicable [141].

Recent FTV work [141, 147] has addressed this issue of limited spatial resolution by measuring the transmissibility response at 24 locations on the foot. Clear differences in the response of the toes, midfoot, and rearfoot were observed which supports the notion that two or three unique measurement positions may be insufficient to fully characterize the foot's behaviour under exposure to vibration. Of course, having too many points is undesirable also.

Using all 24 anatomic locations measured by Goggins et al. [141, 147] either greatly increases the amount of vibration exposure each participant receives or limits the total number of test conditions that can be studied. A greater number of locations also makes it more difficult to perform studies on barefoot volunteers. Finally, understanding how to incorporate excess data into predictive modelling efforts becomes more difficult with more locations. Identifying a minimal subset of measurement locations has the potential to greatly simplify future experimental and modelling investigations of FTV.

In order to assess the structural displacement of the foot, the transmissibility magnitude (e.g. displacement severity) was considered instead of the traditionally used frequency analysis [145, 148, 149]. Analyses based on the frequency response are beneficial for understanding the exposure frequencies which will cause maximum tissue deflection and may result in injury; however, these results are specific to the exposure frequency and magnitude. The benefit of analysing transmissibility based on the magnitude is that regardless of the exposure frequency, the anatomical locations with the greatest displacement can been categorized.

An optimal set of measurement locations, one that ensures the foot's response is properly characterized while minimizing the measurements required, would be a huge asset for FTV research. Not only would a minimal set ensure that sufficient data is captured to characterize the foot's response to FTV, but it would also minimize data collection time and thereby reduce the risk for study participants in laboratory testing. Determining the minimum number of data collection points could also be important for practitioners conducting field exposure measures and those developing models of FTV response. Thus, the objective of this work is to identify clusters of similar behaviour within the 24 points on the foot where

transmissibility data were previously collected by Goggins et al. [141, 147], so that the total number of measurement locations can be reduced.

5.2 METHODOLOGY

5.2.1 Experimental Data Set

The transmissibility measurements of 21 participants (15 males and 6 females) at 24 anatomical locations (Figure 5.1) gathered in previous studies [141, 147] were analyzed. In these experiments, participants were exposed to a sine sweep vertical vibration of 30 mm/s, from 10-200 Hz, lasting 51 seconds, for each measurement. The centre of pressure (COP) was also varied from a natural standing position [141], forward (concentrating mass in the toes), and backward (concentrating mass in the heels) position [147]. From this experimental data, the transmissibility values at each anatomical location were evaluated based on different thresholds. As transmissibility is indicative of vibration attenuation (<1.0) or amplification (>1.0), and thus potential injury by tissue deformation [9, 80], it is reasonable to use it for characterizing the foot's response to vibration exposure.

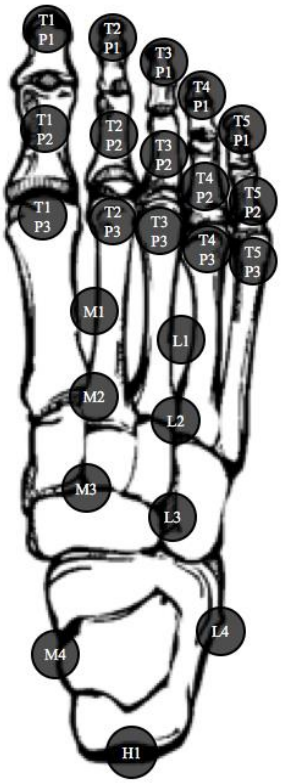

Figure 5.1: Illustration of the 24 anatomical locations used for vibration measurement, including location labels [141].

5.2.2 Data Analysis

Multiple correspondence analysis (MCA), which is a form of geometric modelling with descriptive statistics [150], was used to identify clusters of points that show similar transmissibility magnitudes. This test was selected as the number of participants does not limit the statistical test [151].

The MCA analysis was focused on two specific transmissibility magnitudes: 2.0 (100% amplification of input signal) and 2.5 (150% amplification of input signal) (Figure 5.2). Denoting N as the set of n participants (total 21) and L as the set of anatomical locations (total 24), binary data tables were created using the $N \times L$ matrix, where the entry in cell

(n, l) was either 0 (no) or 1 (yes) based on whether the transmissibility at anatomical location n for participant l exceeded the threshold [150].

From the binary categorical data $N \times L$ indicator matrix, the probability matrix is computed as $\boldsymbol{Z} = B^{-1}\boldsymbol{J}$ where B is the total of the factor scores from the correspondence analysis and $\boldsymbol{J}$ is the $N \times L$ indicator matrix. From here a singular value decomposition is conducted to attain the factor scores:

$$\boldsymbol{D_l}^{-\frac{1}{2}}(\boldsymbol{Z} - \boldsymbol{n}\boldsymbol{l}^{\mathrm{T}})\boldsymbol{D_n}^{-\frac{1}{2}} = \boldsymbol{L}\boldsymbol{\Delta}\boldsymbol{N}^{T} \tag{5.1}$$

where $\boldsymbol{n}$ is the vector of the row totals of $\boldsymbol{Z}$, $\boldsymbol{l}$ is the vector of the columns totals of $\boldsymbol{Z}$, $\boldsymbol{D_n} = diag\{\boldsymbol{n}\}$, $\boldsymbol{D_l} = diag\{\boldsymbol{l}\}$, $\boldsymbol{L}$ is the factor score for anatomical locations, $\boldsymbol{N}$ is the factor score for participants, and Δ is the diagonal matrix of the singular values. Then the row and column factor scores are computed as:

$$\boldsymbol{R} = \boldsymbol{D_n}^{-\frac{1}{2}}\boldsymbol{L}\boldsymbol{\Delta} \quad \text{and} \quad \boldsymbol{C} = \boldsymbol{D_l}^{-\frac{1}{2}}\boldsymbol{N}\boldsymbol{\Delta} \tag{5.2}$$

Then the squared (χ^2) distance from the rows and columns to their respective barycenter is:

$$\boldsymbol{d_n} = diag\{\boldsymbol{R}\boldsymbol{R}^{\mathrm{T}}\} \quad \text{and} \quad \boldsymbol{d_l} = diag\{\boldsymbol{C}\boldsymbol{C}^{\mathrm{T}}\} \tag{5.3}$$

Finally, the angular similarity was obtained as the squared cosine between row n and factor ℓ and column l and factor ℓ:

$$o_{n,\ell} = \frac{r_{i,\ell}^2}{d_{n,i}^2} \quad \text{and} \quad o_{l,\ell} = \frac{c_{j,\ell}^2}{d_{l,j}^2} \tag{5.4}$$

where $d_{n,i}^2$, and $d_{l,j}^2$, are the i-th element of $\boldsymbol{d_n}$ and the j-th element of $\boldsymbol{d_l}$, respectively [152]. The geometric data were then exported as symmetric variable plots where the first two factors (axes) were included. From the symmetric variable plots, the anatomical locations

from the first factor were clustered based on their proximity to each other and consistency with their physical anatomical proximity to each other.

Anatomical locations in which all of the transmissibility measurements (21 participants) did not reach the transmissibility magnitude threshold (2.0 or 2.5), did not have any variability and were excluded from the symmetric variable plots. Although the excluded anatomical locations were not plotted, they were included as a group as they had the same transmissibility response magnitude. From the clustered anatomical locations and the group of excluded anatomical locations, a single location from each group was chosen to represent the group based on the ease at which it can be measured using an accelerometer or laser Doppler vibrometer (LDV).

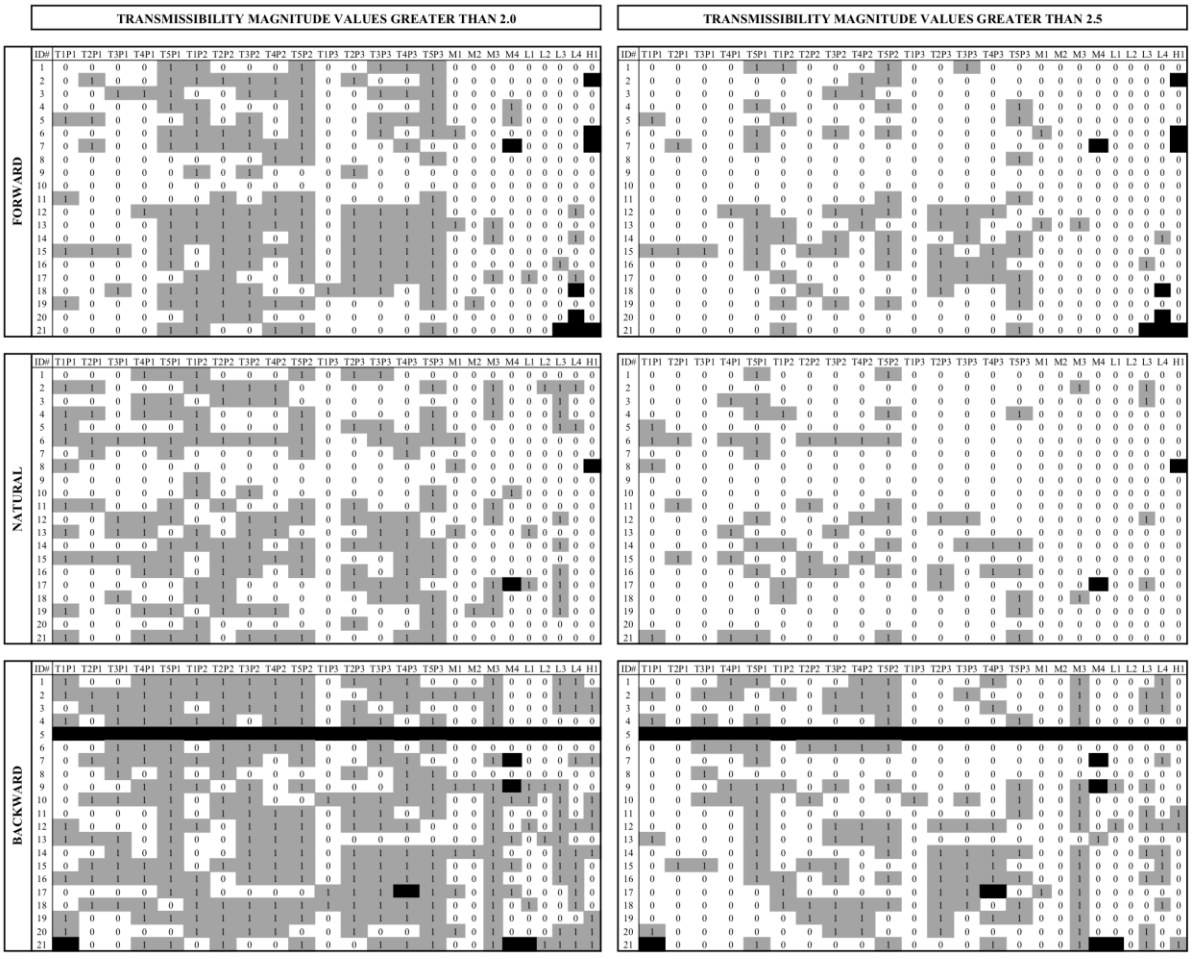

Figure 5.2: Summary of the peak transmissibility magnitude divided according to the peak transmissibility magnitudes (>1.5, >2.0, >2.5, and >3.0) and positions (natural, forward, and backward) with the anatomical locations (24) and participants (21), using a binary system where 1 indicates a transmissibility magnitude value above the threshold, and 0 is below. The black square represents data that were not analyzed due to low coherence.

5.3 RESULTS

The symmetric variable plots, using the two largest factors (F1 and F2) from the MCA analysis, are presented in Figure 3. The plots shown are for two transmissibility magnitude thresholds (2.0 and 2.5) and for three variations in standing centre of pressure (natural, forward, and backward). As this type of analysis was binary, with certain thresholds for inclusion, there are anatomical locations omitted in each case because at no frequency from 10 to 200 Hz across all test participants did the transmissibility magnitude exceed the set threshold. At the threshold of 2.0 (input vibration has been amplified by 100%), two locations in the natural position (T1P3, H1) and three in the forward COP position (T1P3, L2, H1) were omitted. While at the higher threshold of 2.5 (input vibration amplified by 150%), nine (T1P3, T3P1, M1, L1, M2, L2, M4, L4, H1), six (T1P3, L1, M2, L2, M4, H1), and two (M2, L2) measurements were omitted in the natural, forward, and backward COP positions, respectively.

At a transmissibility magnitude threshold of 2.0, there are four, two and three groupings of anatomical locations in the natural, forward, and backward COP positions based on the MCA analysis (Figure 5.3). The anatomic positions in each cluster are identified on a schematic of the foot in Figure 5.4; black measurement points indicate those that were omitted. Generally, at this threshold the toes tend to be clustered together as the first area and the locations around the ankle are located further from the origin and form their own groups. Regardless of the centre of pressure position, all of the toe measurements, except T1P3, can be grouped together as one measurement location. Greater variability in clustering at this threshold occurs in the midfoot and ankle; however, it would appear that taking a measurement at either M1 or L1, along with an ankle location (M4 or L4), should be

sufficient for capturing the variation in transmissibility magnitude at this threshold. The most notable difference occurs in the backward COP position: almost all anatomical locations are grouped as one cluster.

Whereas, at a transmissibility magnitude threshold of 2.5 there are three, three and four groupings of anatomical locations in the natural, forward, and backward COP positions, respectively (Figure 5.5). At this threshold there are differences in the clustered anatomical locations based on COP, but overall it would appear that the toes are split into two groups in each position and the remaining locations at the midfoot and ankle tend to be outlying on their own further from the origin (Figure 5.3). Again, T1P3 is clustered differently than the remainder of the toe measurements.

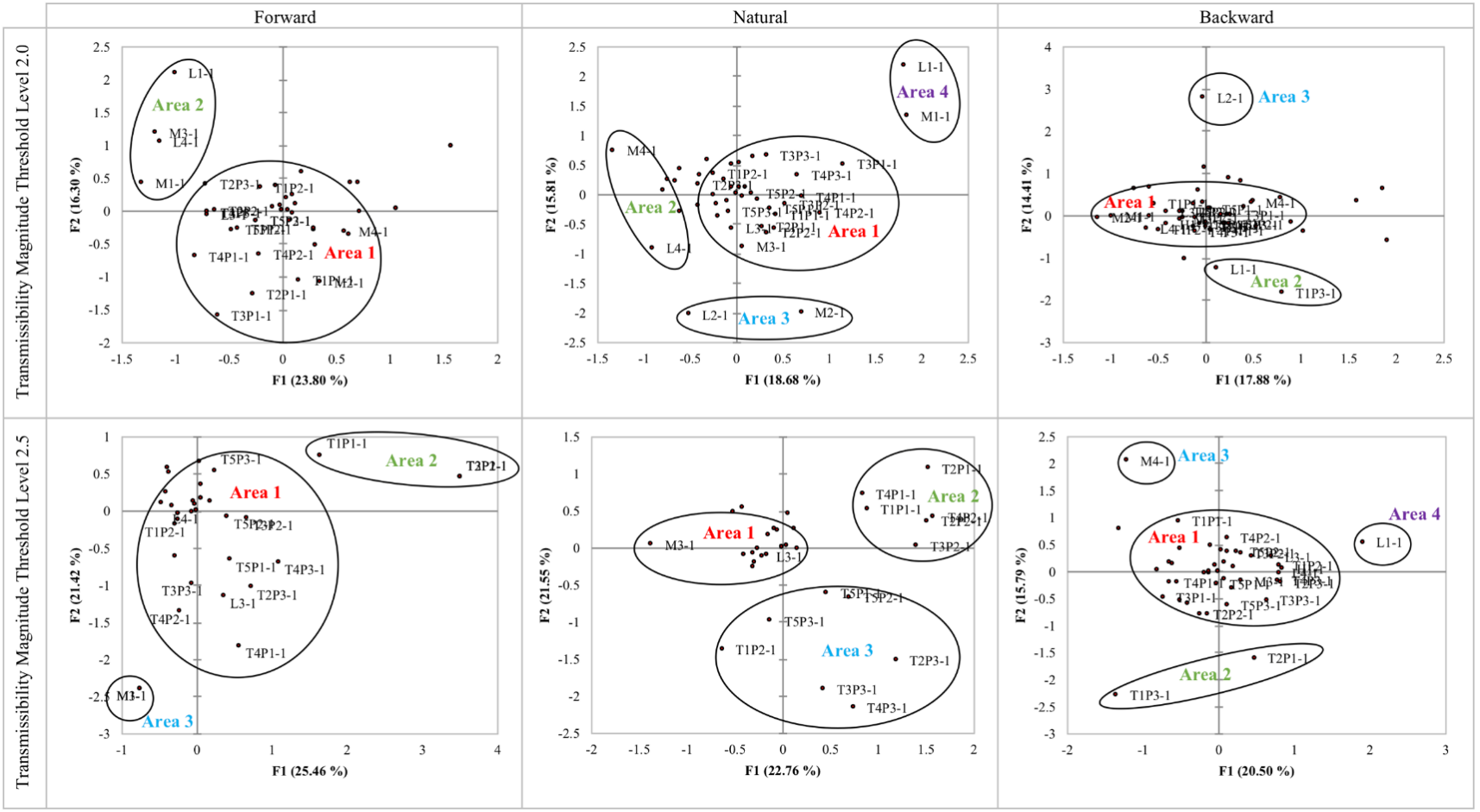

Figure 5.3: Symmetric variable plots using first two axes (factors) from MCA including anatomical locations above transmissibility magnitude thresholds of 2.0 (top) and 2.5 (bottom) for three variations in standing centre of pressure (natural, forward, backward). The percentages listed on the axes indicate the amount of variation accounted for by factor 1 or factor 2. Unlabeled data points are excluded from clustering as they are from the second factor.

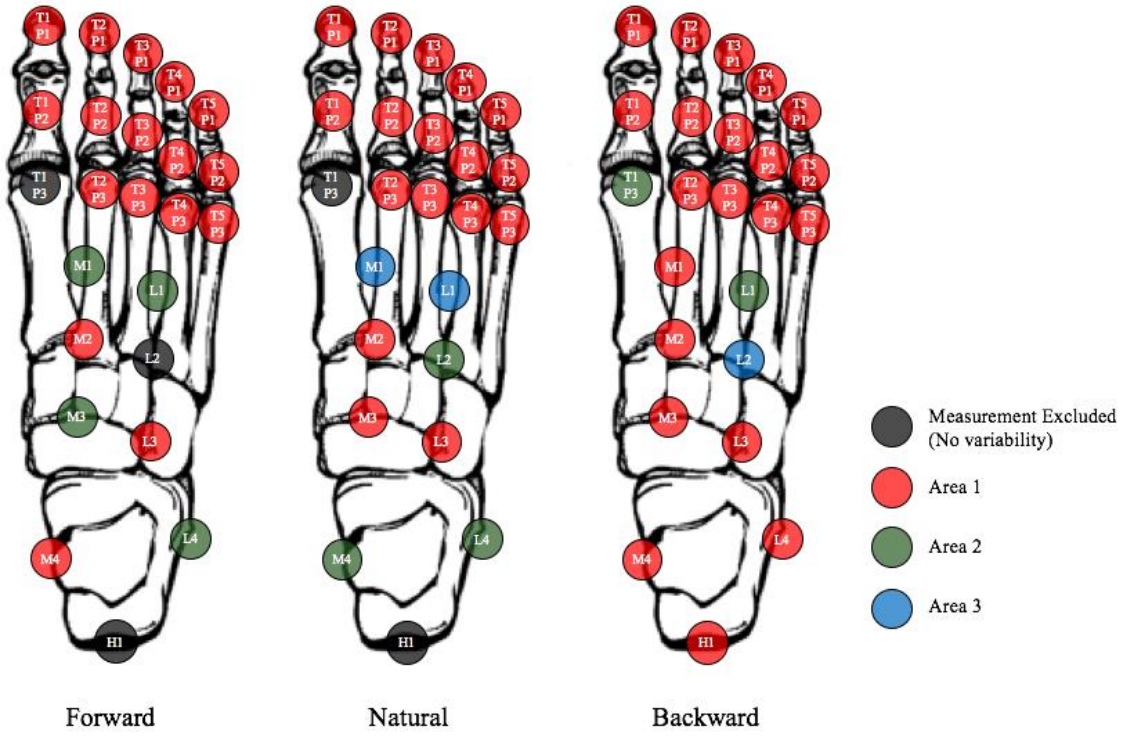

Figure 5.4: Anatomical representation of the measurement locations clustered in a group from the MCA conducted at a transmissibility magnitude threshold of 2.0. The transmissibility measurements at anatomical locations represented in black did not reach the transmissibility magnitude threshold (no variability).

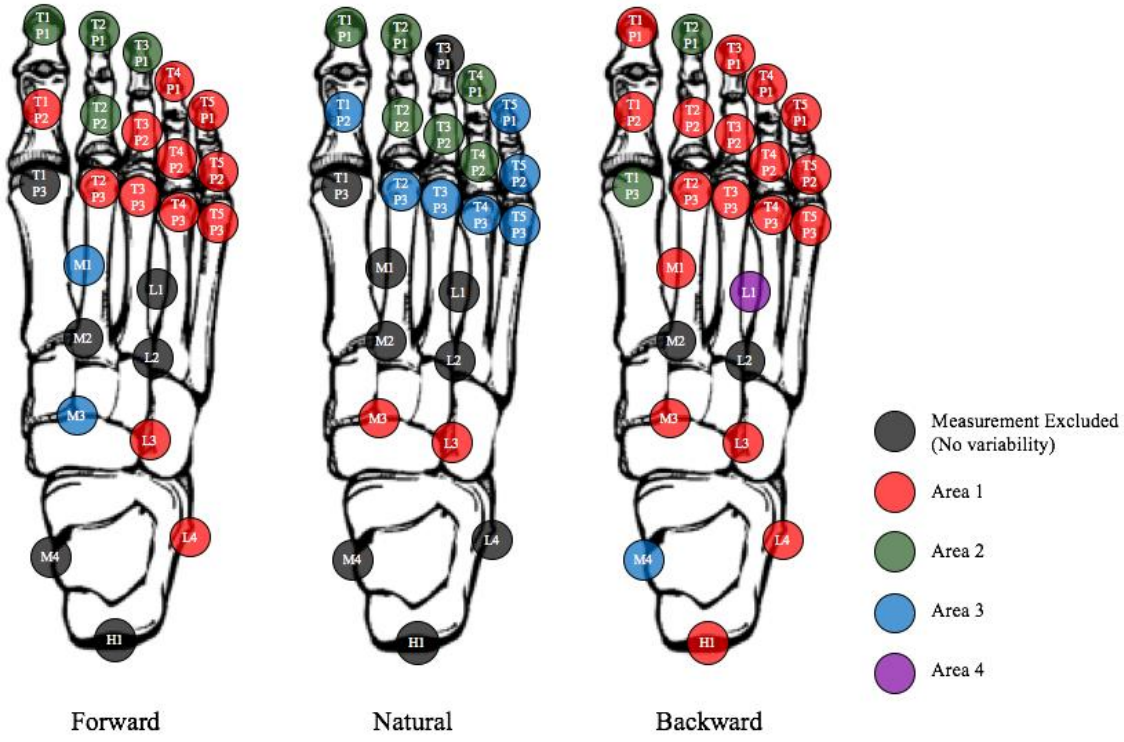

Figure 5.5: Anatomical representation of the measurement locations clustered in a group from the MCA conducted at a transmissibility magnitude threshold of 2.5. The transmissibility measurements at anatomical locations represented in black did not reach the transmissibility magnitude threshold (no variability).

The minimum anatomical locations required to capture differences in transmissibility magnitude are summarized in Table 5.1. These locations considered ease of identification and measurement, along with the vibration response. Taking all of these measurements into account, if transmissibility measurements are taken at T1P1, T1P3, M1 and L4, then potentially tissue damaging transmissibility magnitudes, with greater than 100% amplification could be captured.

Table 5.1: Minimal anatomical locations required to capture differences in transmissibility magnitude in three centre of pressure positions.

Forward		Natural		Backward	
2.0	2.5	2.0	2.5	2.0	2.5
T1P1	T1P1	T1P1	T1P1	T1P1	T1P1
T1P3	T1P3	T1P3	T1P3	T1P3	T1P3
L4	L4	L4	T5P3	L2	L1
	M1	M1	M3		L2
					M4

5.4 DISCUSSION

Published transmissibility data measured at 24 locations on the foot, from 21 participants in three COP positions, were used to identify clusters of behaviour to determine the minimum locations required to capture the FTV biodynamic response. Using the magnitude of the transmissibility response focuses the analysis on the displacement of the anatomical structures, which is strongly associated with increased injury risk [6, 55]. In order to prevent FTV exposure injury, transmissibility measurements need to be taken on the most appropriate locations for capturing the differences in displacement of the foot's anatomical structures.

While taking any measurement point from within each cluster should capture the range of transmissibility magnitudes, there are practical considerations that make particular locations more feasible for laboratory and field FTV measures. One must consider, for example, the ease with which that site can be measured using an accelerometer or LDV, as well as the repeatability of identifying an anatomic landmark. The MCA analysis revealed that at the 2.0 transmissibility magnitude threshold, there were four, three, and three clusters of anatomical locations in the natural, forward, and backward COP positions required to capture the response of the foot to vibration. At the 2.5 transmissibility magnitude threshold,

more clusters were needed to summarize the three positions. There were four, four, and five clusters of anatomical locations in the natural, forward, and backward COP positions, respectively. The minimal measurement points for each of these scenarios are summarized in Table 5.1; however, a single set of locations is needed that is able to capture the range of potential biodynamic responses that occur in the field. Taking all of the MCA results into account, transmissibility measurements taken at T1P1, T1P3, M1 and L4 should effectively summarize the potentially tissue damaging transmissibility magnitudes for the parts of the foot for FTV exposure below 200 Hz.

The results would indicate that there are differences in the transmissibility magnitude depending on COP position (natural, forward and backward). As the toes are the primary area of concern for vascular damage associated with VIWFt [2, 124], understanding how vibration exposure influences the displacement of these structures is essential. Concentrating the COP towards the heel resulted in more transmissibility measurements above the magnitude thresholds in the toes, whereas concentrating the COP towards the toes resulted in less measurements reaching the thresholds (Figure 5.2). Overall it would appear that regardless of the magnitude threshold, the response of the toes is consistently above the threshold, with the exception of measurements at T1P3 (Figure 5.4 & Figure 5.5) and these results should not be ignored given the injury risk [1, 2].

The responses of the midfoot and ankle are very similar throughout, with the backward COP position resulting in the most measurements above the magnitude threshold (Figure 5.2). In the natural standing position, all of the measurements in the midfoot and ankle, with the exception of M3 and L3, are below the 2.5 transmissibility magnitude threshold. It is not until participants concentrate their mass in their heels that the groupings

change and more locations in the midfoot and ankle are above the magnitude threshold (Figure 5.4 & Figure 5.5). Some of the difference in transmissibility amplitude between the forefoot and rearfoot could be explained by the plantar fat pad [153]. Any increased loading disturbances to the plantar fat pad can stimulate a significant modification to the tissue, causing an increased stiffness and lowering its damping capabilities [153, 154]. In the backward COP position, forcing an increased concentration of mass on the heel could have caused an alteration to the plantar fat pad, which in turn resulted in an increased resonant frequency and magnitude.

The current results enable the suitability of the measurement locations used in earlier studies of FTV to be assessed. For example, the MCA clustering analysis indicates that the transmissibility magnitude at T1P3 is grouped separately from the rest of the toes in all cases. This location has previously been considered as representative of the transmissibility response at the toes [5]; however, these results suggest that transmissibility measurements at T1P3 will underestimate the amplitude elsewhere on the toes. This behaviour is comparable to the results of hand-transmitted vibration studies which showed that the average transmissibility amplitudes at the base of the thumb are lower than those on the other four fingers [13, 135, 140].

Vibration measurements have also previously been taken on the medial (M4) [68, 70] and lateral (L4) malleoli [5]. The results from the MCA analysis would indicate that the transmissibility magnitudes at these two locations are uniform in the natural position, but differ slightly in the forward and backward COP position depending on the applied transmissibility magnitude threshold. The maximum transmissibility amplitudes of the average (21 participants) remained at approximately 1.5 [141], with the exception of the

spike in amplitude (1.8) at L4 in the backward COP position [147]. As L4 has greater amplitudes, and because it is easier to measure than the medial malleolus, this location was chosen as more appropriate for capturing amplitude differences at the ankle. Therefore, it is recommended that M4 be used in the future.

The data set used in the current work was gathered from 21 participants at 24 locations on the foot [141, 147]. Traditional statistical analyses would have required a much larger number of participants (almost 1000, assuming a minimum of 40 per measurement point) in order to detect significant differences [151]. The MCA used herein is ideal for identifying the underlying structure in categorical data within a smaller number of participants. The creation of this categorical data requires that a transmissibility threshold amplitude be set. Since the selection of a value is arbitrary, different thresholds were considered to account for this effect. One shortcoming of this approach is that it ignores the overall frequency response and the frequency at which maximum transmissibility occurs. While the subset of measurement points identified herein are sufficient for assessing risk in the foot, future work should evaluate whether another set should be used for characterizing the overall vibration response.

Lab-based data are easier to collect, but it is field experiments that will provide the best means of evaluating occupational risk to FTV. Future work must evaluate the feasibility of the proposed anatomic locations to measure FTV in industrial environments when workers are wearing industrial footwear (e.g. steel toe work boots). Exposure to FTV from different machinery should also be investigated, along with assessing the protection offered by different footwear and insoles combinations, in order to improve the safety of workers.

5.5 CONCLUSIONS

Peak transmissibility values measured at 24 anatomical locations [141, 147] were evaluated at two magnitude thresholds: 2.0 indicating 100% amplification of the input signal, and 2.5 indicating 150% amplification of the input signal. Results of the MCA indicate that transmissibility measurements at T1P1 (nail bed of first phalange), T1P3 (distal head of first metatarsal), M1 (proximal head of second metatarsal) and L4 (lateral malleolus) summarize the potentially tissue damaging transmissibility magnitudes. These measurement locations should be sufficient to assess the safety risk posed by FTV.

CHAPTER 6: LUMPED-PARAMETER MODEL

Three segment, four degrees-of-freedom lumped parameter model of the foot-ankle system exposed to vertical vibration

Modelling the foot-ankle system (FAS) while exposed to foot-transmitted vibration (FTV) is essential for designing prevention methods to inhibit occupational exposure and prevent the effects of vibration-induced white-foot. A K-means analysis was conducted on the transmissibility response of 24 anatomical locations, and three locations (the nail of the big toe, the third metatarsal, and the lateral malleolus) were found to be sufficient for summarizing FTV. A three segment, four degrees-of-freedom lumped-parameter model of the FAS was designed to model the transmissibility response at these three locations when exposed to vertical vibration from 10-60 Hz. Reasonable results were found at the ankle, midfoot, and toes in the natural standing position and forward centre of pressure (COP). However, when the COP is backward, the model does not sufficiently capture the transmissibility response at the ankle.

Keywords: foot-ankle vibration model, foot-transmitted vibration

The contents of this chapter will be published as "Goggins, K.A., Chadefaux, D., Tarabini, M., Lievers, W.B., Eger, T.R. (2019). Three segment, four degrees-of-freedom lumped parameter model of the foot-ankle system exposure to vertical vibration. *Journal of Sound and Vibration.* (to be submitted)."

6.1 INTRODUCTION

Prolonged occupational foot-transmitted vibration (FTV) exposure can cause neurological, vascular, and osteoarticular symptoms in the feet [1, 2, 124]. Workers in industries such as underground mining, where they are required to stand on vibrating platforms, are particularly at risk. Models of the human foot are important for predicting the structural behaviour of their components [155], as they can aid in the diagnosis, treatment and prevention of foot pathologies [66, 120]. Two-dimensional lumped-parameter (LP) models of the feet have been developed to investigate specific behaviours of the foot, such as its deformation with various applied loads [120], the energy storage of the longitudinal arch [119], and the role of the plantar fascia in load bearing [118]. Unfortunately, the vibration response of the foot has yet to be modelled in detail.

LP models use a combination of masses, springs, and dampers to represent different elements of physical systems such as the human body [14, 26]. LP modelling of the biological response to vibration has previously been completed for both standing whole-body vibration (WBV) [12, 84] and hand-transmitted vibration (HTV) [104-106, 111, 156]. Standing WBV LP models typically highlight the effects of vertical vibration exposure on the human body. These models are used to model the resonance of the standing human body as a whole [68, 84], only one standing WBV model [84] has included a distinct component for the foot. Research specifically modelling the effects of vibration exposure on the foot has yet to evolve.

A three degree-of-freedom (DOF) model has previously been established for modelling the heel strike transients during running [121], where the components were stacked vertically. This model was limited to masses representing the landing cushion, tibia

and ankle, and the knee and above. Clinical research does try to measure changes in the COP with vibration exposure because these results can provide valuable information on the health and physical condition of a patient [76]. Using a controlled inverted pendulum model with 1-DOF, the COP signal was found to be highly dependent on the cumulative disturbance torque of the model [76]. This study did not measure vibration transmissibility at any locations on the exposed foot, and was limited to the use of a single subject to validate the model of the COP signal; however, these findings suggest the COP of a standing participant will be affected by FTV exposure.

As the transmission of vibration through the feet is becoming an increasing occupational hazard [1, 30, 124], the overall purpose of this paper is to create a two-dimensional LP model of the foot exposed to vertical vibration. Lumped-parameter models can be calibrated with transmissibility data (including mass information), driving-point responses (DPR) (either apparent mass or mechanical impedance), or both responses as the reference functions [72]. The most comprehensive data set available for the biodynamic response of the foot is a transmissibility data-set including measurements at 24 anatomical locations of the foot, under three loading conditions, from 21 participants [141, 147].

The development and calibration of the LP model proceeded as follows. First, K-means analysis was used to determine which anatomical locations are a priority for modelling. Based on the clustering results, a three-segment, 4-DOF model was proposed. The model was then calibrated with the human biodynamic response data. This model can serve as the baseline for establishing how to model FTV exposure.

6.2 METHODOLOGY

The model of the foot-ankle system (FAS) was created using a vertical vibration transmissibility data-set, from 10-200Hz, that includes measurements at 24 anatomical locations of the foot, under three loading conditions, from 21 participants [141, 147] (Figure 6.1). One challenge when developing a LP model is determining how many segments to include. As modelling 24 locations is not practical, a modified K-means clustering analysis was performed to provide guidance about which unique anatomical regions should be represented in the foot model and which measurement points are representative of those regions.

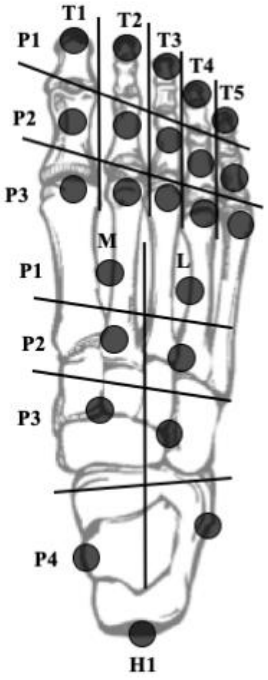

Figure 6.1:Twenty-four anatomical locations where transmissibility measurements were taken [141, 147].

6.2.2 K-means analysis: identify anatomic regions

K-Means Analysis: Algorithm

K-means clustering is typically performed to minimize the total variance [157], σ^2, that is, the sum of the variance in each group, σ_g^2. One curve, $T(f)$, the average transmissibility response over the frequencies, f, from 10-200 Hz, was taken as representative of the behaviour at each of the 24 locations. The variance of a group, σ_g^2, was then calculated as the sum of the variances of the individual curves, $T_i(f)$, relative to the group average, $\bar{T}_g(f)$.

Since the intent was to identify regions of the foot having comparable responses, an additional spatial constraint was added. A connectivity network was superimposed on the measurement points that described their positions relative to one another. Groups were constrained to be connected so as to ensure, for example, that the big toe and the heel were not found to be part of the same "regional" group.

The pseudo-code for the K-means clustering algorithm with superimposed regional constraints is as follows, assuming an initial grouping for each point:

1. Calculate the averages and variance for each group;
2. Calculate the total variance;
3. Identify the "edge points", the measurement points adjacent to another group;
4. Sort the edge points, based on their individual variance from the group average, largest to smallest;
5. Go through each edge point and attempt to switch it to each adjacent group
6. Calculate the updated total variance;
7. Keep a switch if it reduces the total variance and maintains group connectivity, otherwise revert it and try the next edge point in 5; and

8. If an edge point switches group, return to step 1, otherwise a local minimum has been found.

A common issue with K-means clustering techniques is that they can only guarantee a local, and not a global, minimum. Therefore, for each clustering attempt, 100 random initial groups were assigned using an initial seeding and region growing approach that ensured group connectivity. The clustering algorithm was then applied. The result with the lowest total variance was identified as the final solution.

One further simplification was made. Nine measurement points were excluded (white circles in Figure 6.2) based on their difficulty to measure with a laser Doppler vibrometer (LDV) or accelerometer. The excluded points included all measures on the fourth and fifth toes (T4 and T5 in Figure 6.1) due to a very small surface area for measurement, and two measurement locations on the midfoot and one on the heel which can be influenced by skin artifact from ligament contracture.

K-Means Analysis: Findings

Using the algorithm described above, clustering of the transmissibility responses was performed separately for the forward, natural, and backward data published previously [141, 147]. The minimum variance findings are presented with the COP in the forward (Figure 6.2), natural (Figure 6.3), and backward (Figure 6.4) positions for two, three, and four solution groups.

Results of the modified K-means cluster analysis suggest that three groups (toes, midfoot, ankle) provides the most consistent results. While increasing the number of groups

does decrease the total variance, at K=4, isolated clusters begin to appear, where only a single anatomical location represents a group.

Any of the measurement points within these three groups could be taken as representative of that region; however, certain anatomic locations are easier to landmark and measure with an accelerometer or LDV (Chapter 5). Therefore, the nail of the big toe (T1P1), the third metatarsal (L2), and the lateral malleolus (L4) are recommended and will be used in subsequent analyses as the reference functions.

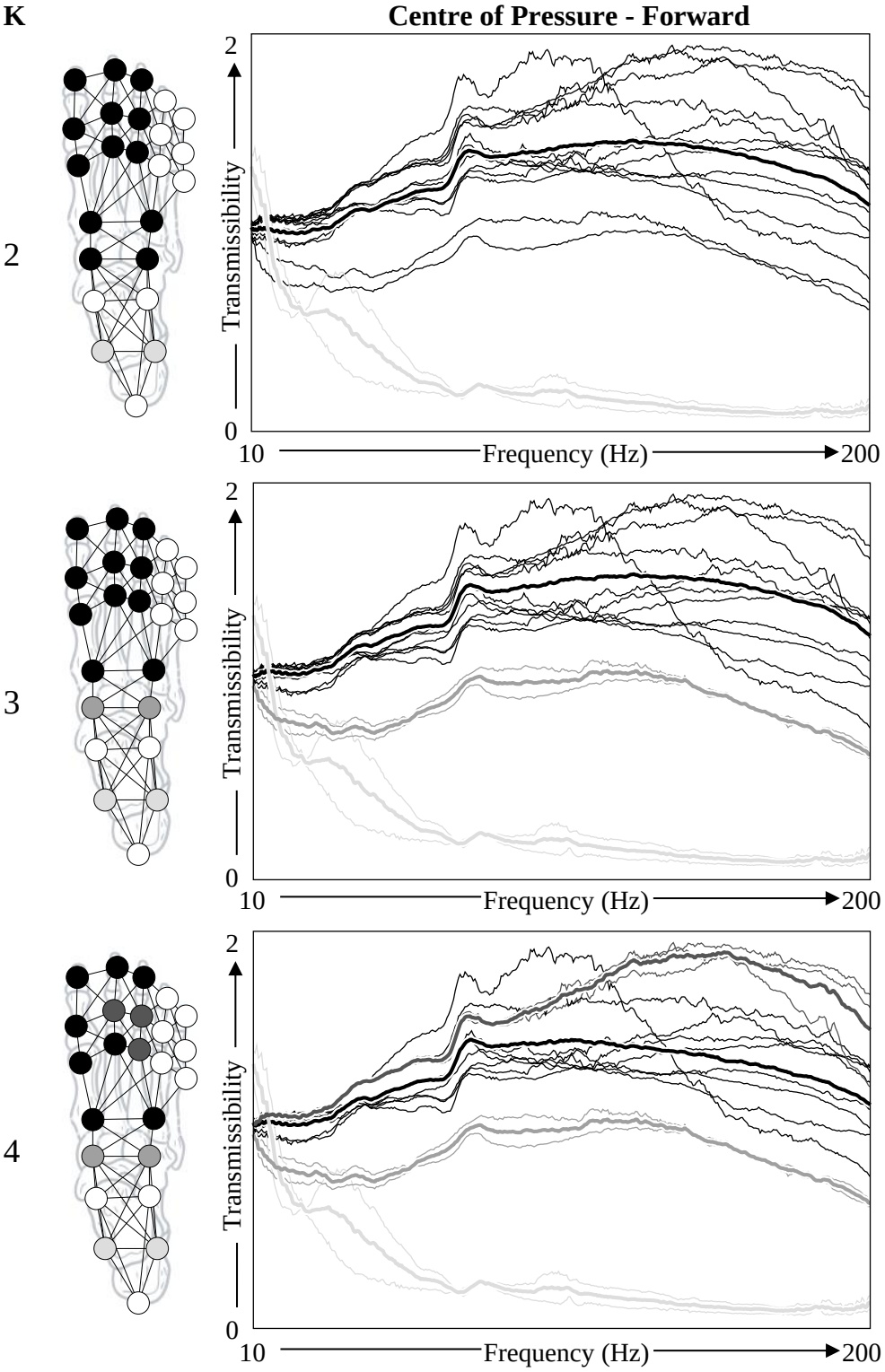

Figure 6.2: Total variance results from K-Means cluster analysis conducted on transmissibility results with the centre of pressure in the forward position [147]. White circles are excluded locations. Thin transmissibility lines are experimental measurements, and the corresponding thick transmissibility line is the average of the group of locations.

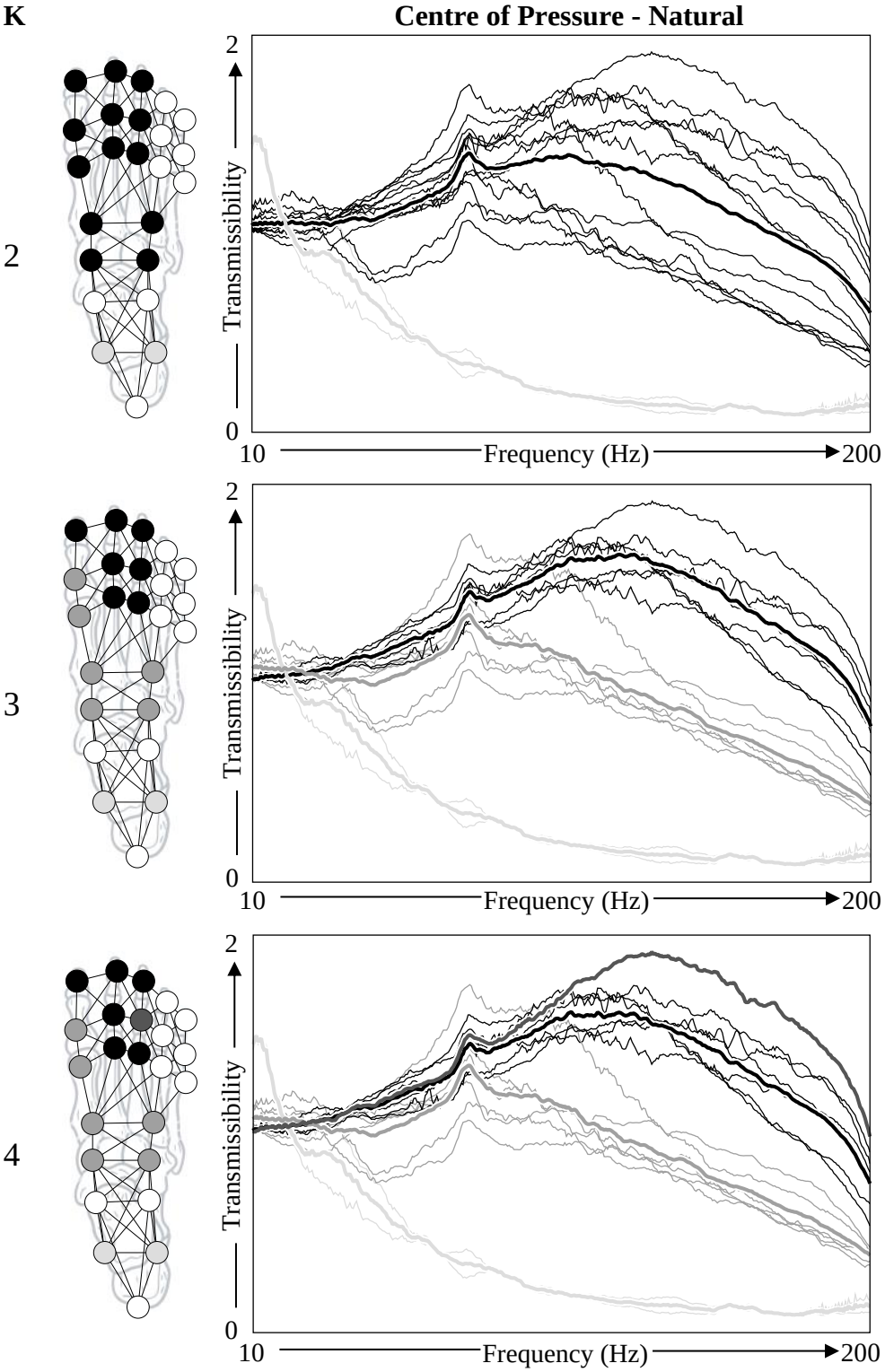

Figure 6.3: Total variance results from K-Means cluster analysis conducted on transmissibility results with the centre of pressure in the natural position [141]. White circles are excluded locations. Thin transmissibility lines are experimental measurements, and the corresponding thick transmissibility line is the average of the group of locations.

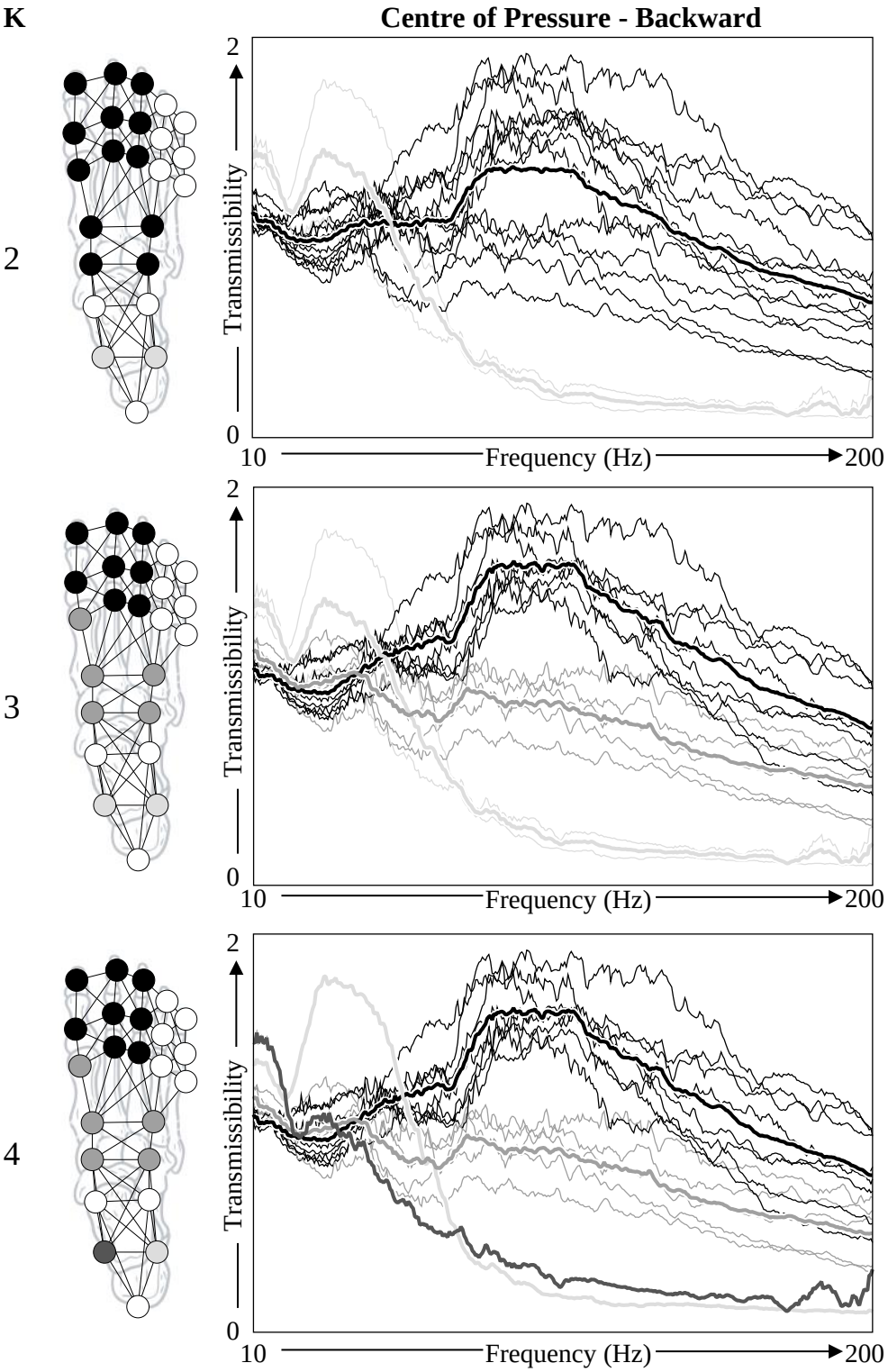

Figure 6.4: Total variance results from K-Means cluster analysis conducted on transmissibility results with the centre of pressure in the forward position [147]. White circles are excluded locations. Thin transmissibility lines are experimental measurements, and the corresponding thick transmissibility line is the average of the group of locations.

As indicated from the results of the K-means analysis, the LP model was designed to incorporate three transmissibility responses —ankle, midfoot, and toes— as the reference functions (Figure 6.3). The two-dimensional model describes the dynamic behaviour of one foot supporting a mass (35 kg) corresponding to the half of the total human body mass (m_1), averaged from 21 participants exposed to standing FTV [141, 147]. The medial longitudinal arch, consisting of the calcaneus, talus, navicular, three cuneiforms, and the heads of the first three metatarsals, can be simplified into a truss structure [117, 118]. As such, the model was composed of two homogenous segments, referring to the rearfoot (2) and forefoot (3). Both segments were assumed to be rigid bodies described by their length (L_2 and L_3), mass (m_2 and m_3), and moment of inertia (J_2 and J_3) (Table 6.1).

Table 6.1: Geometric and inertial characteristics of the two foot segments represented in the two-dimensional model of the foot-ankle system [158-160].

		Segment 2 (Rearfoot)	Segment 3 (Forefoot)
Length	L (m)	79.3 x10^{-3}	10.6 x 10^{-2}
Mass	m (kg)	0.147	0.343
Inertia	J (kg·m^2)	28 x10^{-5}	55.54 x10^{-7}

The motion of the human body centre of mass ($y_1(t)$) and midfoot ($y_3(t)$) were assumed to be vertical and connected by a spring-damper (k_3, c_3). The plantar aponeurosis was represented by a spring-damper system (k_1, c_1) connecting the calcaneus and metatarsophangeal articulation [118, 122]. Additionally, the fat pads at each of the support locations were assumed to be viscoelastic materials and are described with a Kelvin-Voigt model of properties (k_2, c_2 and k_4, c_4).

The model of the FAS included four DOF, the displacements of the midfoot $y_3(t)$ and of the remainder of the body $y_1(t)$, which were assumed to be vertical, and the two rotations between the segments (θ_1 and θ_2) (Figure 6.3). The static values of the FAS posture

for θ_1 and θ_2 were 69° and 68° [119]. An imposed harmonic displacement ($y_{input}(t)$) drove the sole of the foot. Within the x,y frame of reference, the FAS response using 4-DOF was estimated at the ankle ($x_2(t)$ and $y_2(t)$), the midfoot ($y_3(t)$), and the toes ($x_4(t)$ and $y_4(t)$).

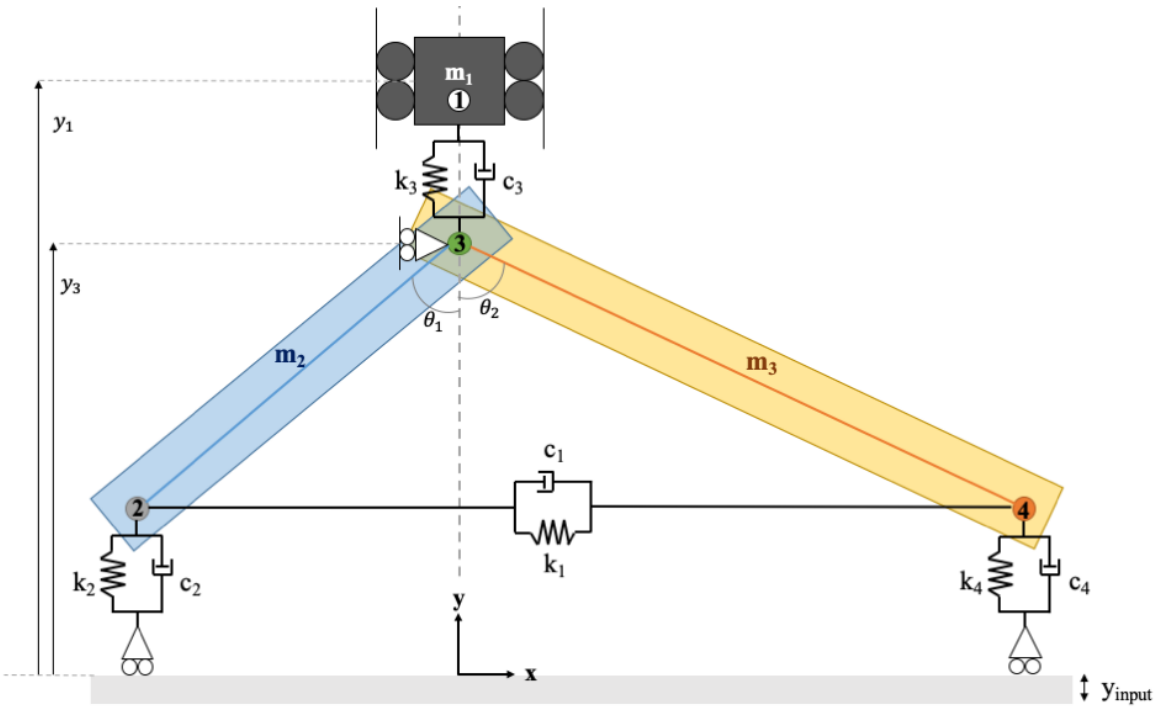

Figure 6.5: Two-dimensional model of the foot-ankle system. The mass of half the total body (m_1), and the two rigid body segments referring to the rearfoot (m_2) and forefoot (m_3). The dynamic properties of the spring-damper systems ($k_{1\ldots4}$ and $c_{1\ldots4}$) were used to describe tissue behaviour. The four degrees-of-freedom are represented with y_1, y_3, θ_1, and θ_2 and the vibration platform input is represent by y_{input}. The origin is not fixed to the top of the plate.

Equations of Motion

As previously mentioned, for the purposes of this model, the position of the total body ($x_1 = 0, y_1$) and top of the midfoot ($x_3 = 0, y_3$) were assumed to be in the vertical direction. The coordinates at the ankle (2) were:

$$\begin{aligned} x_2 &= -L_1 \sin(\theta_1) \\ y_2 &= y_3 - L_1 \cos(\theta_1) \end{aligned} \tag{6.1}$$

And the coordinates for the toes (4) was:

$$\begin{aligned} x_4 &= L_2 \sin(\theta_2) \\ y_4 &= y_3 - L_2 \cos(\theta_2) \end{aligned} \tag{6.2}$$

The position of the centre of mass of the rigid body comprising the mass of the rearfoot $\left(\oplus_{m_2}\right)$ was:

$$\begin{aligned} \oplus_{x_{m_2}} &= -\frac{L_2}{2}\sin(\theta_1) \\ \oplus_{y_{m_2}} &= y_3 - \frac{L_2}{2}\cos(\theta_1) \end{aligned} \tag{6.3}$$

And the centre of mass of the rigid body representing the forefoot $\left(\oplus_{m_3}\right)$ was determined where:

$$\begin{aligned} \oplus_{x_{m_3}} &= \frac{L_3}{2}\sin(\theta_2) \\ \oplus_{y_{m_3}} &= y_3 - \frac{L_3}{2}\cos(\theta_2) \end{aligned} \tag{6.4}$$

Assumptions

The system was assumed to be in static equilibrium prior to the linearization procedure, where the gravitational forces were balanced by the static deformation of the springs [72]. The forces were considered to be in the positive direction when the springs and dampers were in extension. To further simplify the analysis of this model, it was assumed that the vibration transmitted to the foot induced small perturbations around the equilibrium position (justified given the previously limited nonlinear effects in the biodynamic response of standing participants [130]) and as such the analysis was limited to the first two terms of the Taylor series expansion [7]:

$$\begin{gathered} \sin(\theta) \cong \sin(\theta_0) + \cos(\theta_0)\,(\theta - \theta_0) \\ \theta\ \epsilon\ (\theta_0 \pm \varepsilon) \\ \cos(\theta) \cong \cos(\theta_0) - \sin(\theta_0)\,(\theta - \theta_0). \end{gathered} \tag{6.5}$$

The free (r_F) and generalized (r) coordinates were expressed as:

$$\boldsymbol{r}_F = \begin{Bmatrix} y_1 \\ y_3 \\ \theta_1 \\ \theta_2 \end{Bmatrix} \text{; and } \boldsymbol{r} = \begin{Bmatrix} y_1 \\ y_3 \\ \theta_1 \\ \theta_2 \\ y_{input} \end{Bmatrix} \tag{6.6}$$

The vibration platform was assumed to be excited by a single steady-state vibration (y_{input}), which can be expressed as [72]:

$$y_{input} = y_i \cdot exp^{j\omega t} \tag{6.7}$$

where y_i is the vibration displacement, $j = \sqrt{-1}$, ω is the angular frequency (rad/s) and t is the time (s).

From the defined position vectors, the kinetic (E), potential (U), and dissipative (D) energies were calculated according to:

$$E = \frac{1}{2}\left(m_1\dot{y}_1^2 + m_2\dot{y}_2^2 + m_3\dot{y}_3^2 + J_2\dot{\theta}_2^2 + J_3\dot{\theta}_3^2\right) \tag{6.8}$$

$$U = \frac{1}{2}(k_1(\Delta x_4 - \Delta x_2)^2 + k_2(\Delta y_2)^2 + k_3(\Delta y_1 - \Delta y_3)^2 + k_4(\Delta y_4)^2) \tag{6.9}$$

$$D = \frac{1}{2}(c_1(\dot{x}_4 - \dot{x}_2)^2 + c_2(\dot{y}_2)^2 + c_3(\dot{y}_1 - \dot{y}_3)^2 + c_4(\dot{y}_4)^2) \tag{6.10}$$

where m is the mass (kg), x and y are the horizontal and vertical displacements (m), respectively, J is the moment of inertia (kg·m^2), $\dot{\theta}$ is the angular velocity (rad/s), k is the spring stiffness (N/m), c is the damper damping coefficient (N·s/m), and Δ represents the difference from the initial position.

Ultimately, the equations of motion were derived using the Lagrange equation [7, 71]:

$$\frac{d}{dt}\left(\frac{\partial E}{\partial \dot{\boldsymbol{r}}}\right) - \frac{\partial E}{\partial \boldsymbol{r}} + \frac{\partial U}{\partial \boldsymbol{r}} + \frac{\partial D}{\partial \dot{\boldsymbol{r}}} = \boldsymbol{0} \tag{6.11}$$

where the conservative generalized force was zero as there were no additional external forces.

The equations of motion of the 4-DOF linear model were then expressed in matrix form with the addition of the constrained DOF for the platform (y_{input}) as:

$$\boldsymbol{M\ddot{r} + C\dot{r} + Kr = 0} \tag{6.12}$$

where the mass matrix $\boldsymbol{M}$ (Appendix M) is:

$$\boldsymbol{M} = \begin{bmatrix} M_{FF} & M_{FC} \\ M_{CF} & M_{CC} \end{bmatrix} \tag{6.13}$$

the damping matrix $\boldsymbol{C}$ (Appendix N) is:

$$\boldsymbol{C} = \begin{bmatrix} C_{FF} & C_{FC} \\ C_{CF} & C_{CC} \end{bmatrix} \tag{6.14}$$

and the stiffness matrix $\boldsymbol{K}$ (Appendix O) is:

$$\boldsymbol{K} = \begin{bmatrix} K_{FF} & K_{FC} \\ K_{CF} & K_{CC} \end{bmatrix} \tag{6.15}$$

where F refers to the matrices of the four free DOF and C refers to the matrices of the constrained platform DOF (Appendix P).

The combination of equations 6.12 to 6.15, result in a final equation of motion:

$$\boldsymbol{M_{FF}\,\ddot{r}_F + C_{FF}\dot{r}_F + K_{FF}r_F = -C_{CC}\dot{y}_{input} - K_{CC}y_{input}} \tag{6.16}.$$

Vibration transmissibility

The vibration transmissibility was calculated based on the ratio between the input (vibration platform) and output (location on the foot) [141, 147] and from equation 6.16 the transmissibility at each location becomes:

$$\boldsymbol{T}_{2\ldots4} = \frac{\dot{\boldsymbol{r}}_F}{\dot{\boldsymbol{y}}_{input}} = \left[\boldsymbol{M}_{FF} + \frac{\boldsymbol{C}_{FF}}{\dot{\theta}} + \frac{\boldsymbol{K}_{FF}}{(\dot{\theta})^2}\right]^{-1}\left[\frac{\boldsymbol{C}_{CC}}{\dot{\theta}} + \frac{\boldsymbol{K}_{CC}}{(\dot{\theta})^2}\right] \tag{6.17}$$

where $\dot{\theta}$ is the angular velocity [72], resulting in three transmissibility functions computed between the vibrating platform (y_{input}) and the ankle (T_2), midfoot (T_3), and toes (T_4).

Parameter estimation and optimization

Initial values for each spring were set to $1x10^4$ N/m and set to be in the range of 100 N/m and $5x10^5$ N/m. Similarly, damping coefficients were initially guessed to be 10 Ns/m and set to be within the range of 0.1 Ns/m and $5x10^3$ Ns/m. To optimize the model parameters ($k_{1\ldots4}$ and $c_{1\ldots4}$), a nonlinear curve-fitting in least-squares sense was used (*lsqcurvefit* function implemented in *Matlab R2018a* software). Then the deviation between the modelled and measured transmissibility (equation 6.18) and phase (equation 6.19) responses at the three locations (reconstructed quadratic error) ($\mathcal{E}$) was calculated as [113]:

$$\mathcal{E}(T)_{2\ldots4} = \sqrt{\frac{1}{N}\sum_{f=10}^{60}\left|\tilde{T}_{2\ldots4}(f) - T_{2\ldots4}(f)\right|^2} \tag{6.18}$$

$$\mathcal{E}(P)_{2\ldots4} = \sqrt{\frac{1}{N}\sum_{f=10}^{60}\left|\tilde{P}_{2\ldots4}(f) - P_{2\ldots4}(f)\right|^2} \tag{6.19}$$

where f is the frequency, $\tilde{T}_{2\ldots4}$ and $T_{2\ldots4}$ are the modelled and measured transmissibility functions, $\tilde{P}_{2\ldots4}$ and $P_{2\ldots4}$ are the modelled and measured phase functions, and N is the length of the discrete transmissibility functions. The optimization was run on the transmissibility and phase functions to a maximum of $1x10^4$ iterations and stopped once residual deviations were below $1x10^{-10}$. After trials using the entire frequency range of the reference functions (10-200 Hz), it became evident that the frequency range need to be limited. As such, a

frequency range from 10-60 Hz was used to incorporate the frequencies at which equipment operators could be exposed to FTV [1].

Sensitivity analysis

Finally, to estimate the model sensitivity a Monte Carlo analysis was conducted using 100 randomized combinations of the stiffness and damping parameters to estimate the three transmissibility functions. The stiffness and damping parameters were varied based on an assumed normal distribution with a mean equivalent to its optimized value and a standard deviation of 20% of the mean. The variability between the optimized transmissibility function and the Monte Carlo simulated transmissibility functions were estimated with the percentage of deviation between the two values at 10 Hz intervals.

6.3 RESULTS

The estimated parameters of the three segment, 4-DOF lumped parameter model of the FAS (Figure 6.3) exposed to vertical vibration between 10-60Hz are presented in Table 6.2. Separate sets of parameters are given for each of the three COP positions (forward lean, neutral, backward lean) studied in the experiments.

The stiffness of the plantar aponeurosis (k_1) was the greatest in the natural standing position and the least when the COP was closer to the heel, while the damping (c_1) remained at the minimum (0.1 Ns/m) regardless of the COP location. The stiffness of the mass of the human body (k_3) was the largest in the natural standing position, and was the imposed minimum (100 N/m) in the forward and backward COP locations. The damping of the mass of the body (c_3) is the largest in the natural position, followed by the forward and then backward COP locations.

The stiffness of the calcaneus fat pad (k_2) is the greatest in the natural standing position, and the lowest in the backward COP position; and the damping of the calcaneus (c_2) is the greatest in the forward COP position, and the imposed minimum (0.1 Ns/m) in the natural and forward COP positions. Finally, the stiffness and damping of the tarsal fat pad (k_4, c_4) are opposites, where the stiffness is the great in the forward, natural, and backward COP location respectively; and the damping is greatest in the backward, natural, and forward COP location respectively.

Table 6.2: Estimated model parameters, using single location transmissibility responses T1P1, L2, L4), including the stiffness and damping coefficients of each model segment in the natural standing position and under two changes in centre of pressure location (towards the forefoot and rearfoot).

Parameter	Unit	COP Location			Description
		Forward	Natural	Backward	
k_1	N/m	$1.33x10^6$	$2.86x10^6$	$4.11x10^5$	stiffness of the plantar aponeurosis
k_2	N/m	$2.76x10^5$	$9.00x10^5$	$1.72x10^5$	stiffness of the calcaneus fat pad
k_3	N/m	100	$1.21x10^4$	100	stiffness of the mass of the body
k_4	N/m	$5.57x10^5$	$6.46x10^4$	102	stiffness of the tarsals fat pad
c_1	Ns/m	0.10	0.10	0.10	damping of the plantar aponeurosis
c_2	Ns/m	$1.26x10^4$	0.10	0.10	damping of the calcaneus fat pad
c_3	Ns/m	$2.24x10^3$	$5.09x10^3$	621	damping of the mass of the body
c_4	Ns/m	0.10	$7.89x10^3$	$2.52x10^5$	damping of the tarsals fat pad

The transmissibility and phase angle of the modelled and measured responses of the ankle, midfoot, and toes while in the natural standing position are presented in Figure 6.6. The mean-squared error (ε) percentage between the measured and modelled transmissibility response was 4.7, 8.9, and 47.1% at the toes, midfoot, and ankle respectively (Table 6.3). From the proposed model of the FAS, the greatest variance in transmissibility response occurred at the ankle. Whereas, the mean-squared error (ε) percentage between the measured and modelled phase angle response was 4.7, 14.1, and 1.0% at the toes, midfoot, and ankle respectively, with the greatest difference being at the midfoot (Table 6.3).

Table 6.3:Mean-squared error (ε) between the reference function and optimized modelled response of the three segment, four degrees-of-freedom lumped parameter model of the foot-ankle system.

	Modulus			Phase (radians)		
	Forward	Natural	Backward	Forward	Natural	Backward
Toes	0.057	0.047	0.039	0.081	0.047	0.081
Midfoot	0.058	0.089	0.219	0.275	0.141	0.109
Ankle	0.539	0.471	1.09	0.154	0.010	1.174

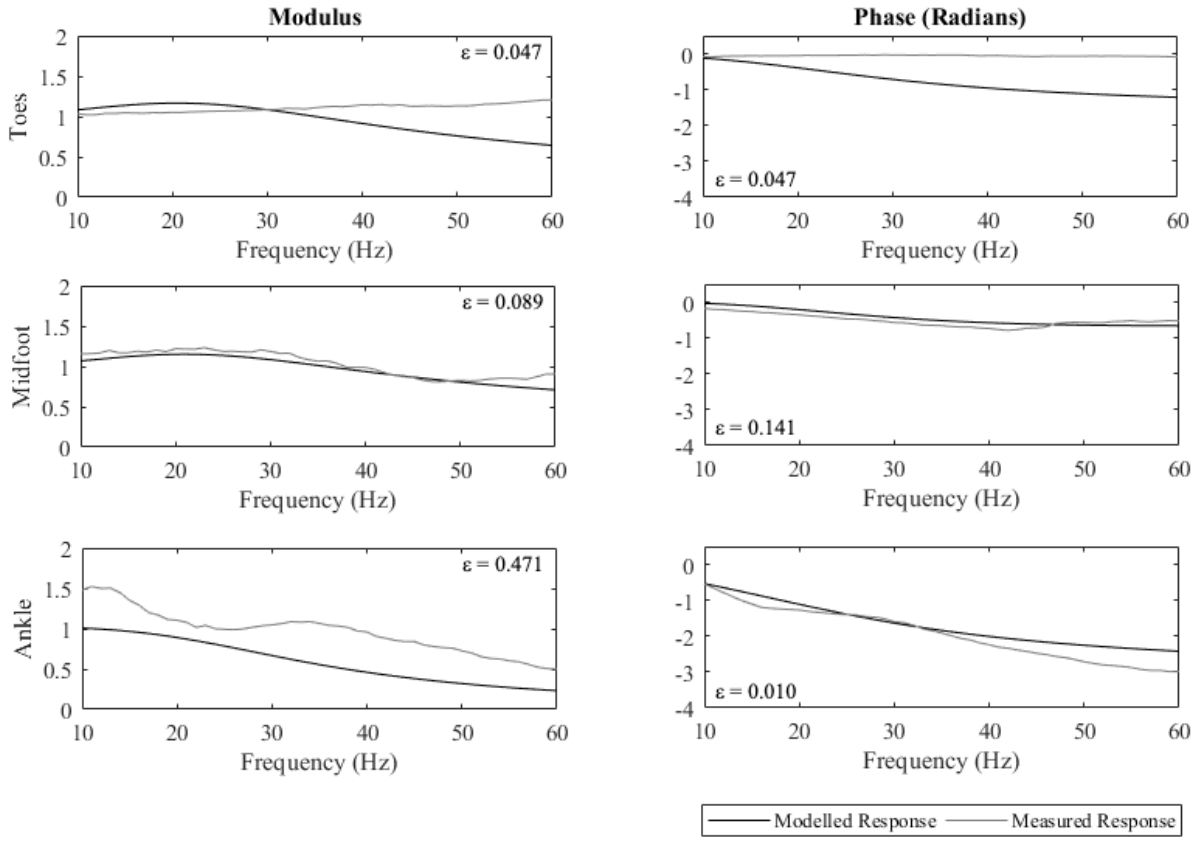

Figure 6.6: The modelled (black) and measured (grey) transmissibility modulus and phase responses of the ankle, midfoot, and toes of the barefoot in a natural standing position exposed to vertical vibration between 10-60Hz [141].

Similarly, the transmissibility and phase angle of the modelled and measured responses of the ankle, midfoot, and toes while in the standing forward COP position are presented in Figure 6.7. The mean-squared error (ε) percentage with the COP forward towards the toes, was 5.7, 5.8, and 53.9% at the toes, midfoot, and ankle respectively with the

greatest difference occurring at the ankle (Table 6.3). Whereas, the mean-squared error (ε) percentage between the phase angle responses were 8.1% (toes), 27.5% (midfoot), and 15.4% (ankle).

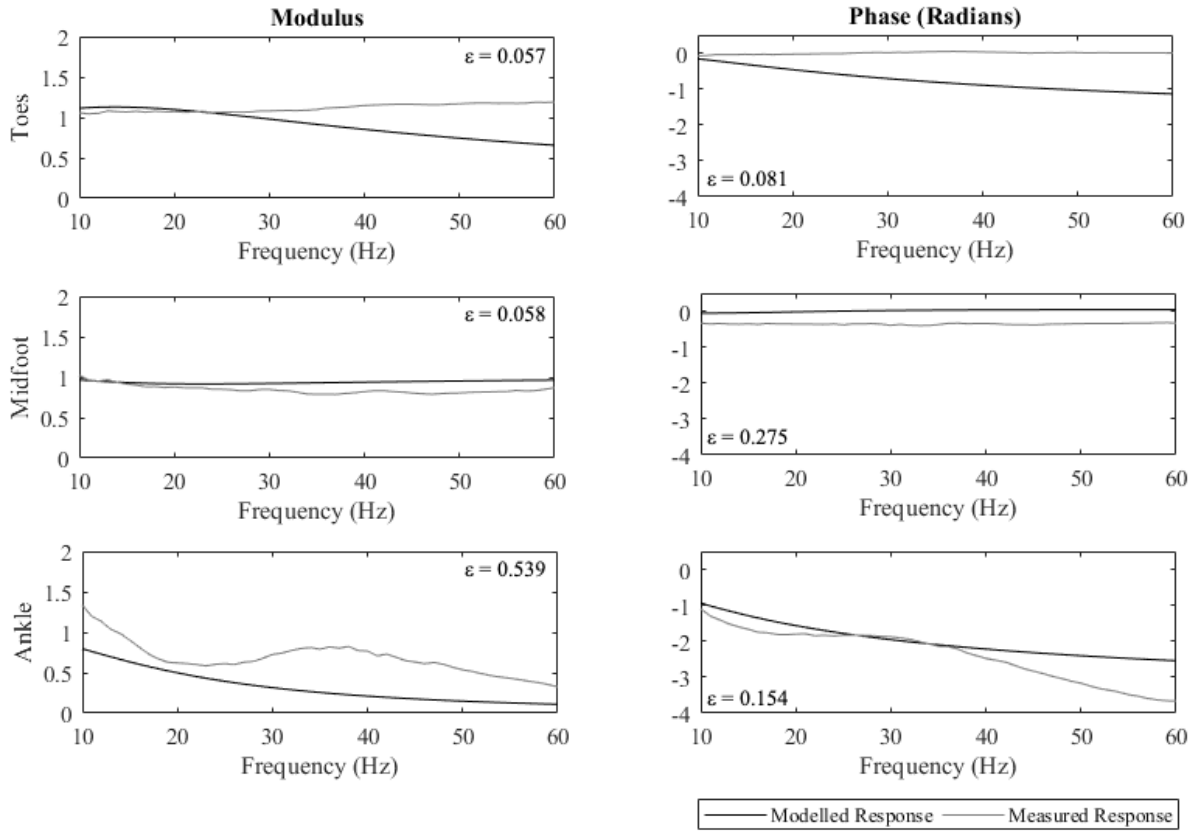

Figure 6.7: The modelled (black) and measured (grey) transmissibility modulus and phase responses of the ankle, midfoot, and toes of the barefoot standing with the COP towards the forefoot, while exposed to vertical vibration between 10-60Hz [147].

Of the three modelled COP positions, the backward COP had the poorest response at the ankle (ε = 109%) (Figure 6.8). The mean-squared error between the modelled and measured transmissibility responses is much smaller (ε = 21.9 and 3.9%) at the midfoot and toes respectively (Table 6.3). The mean-squared error (ε) percentage for the phase angle response were 8.1% (toes), 10.9% (midfoot), and 117% (ankle), again where the response at the ankle was modelled the poorest.

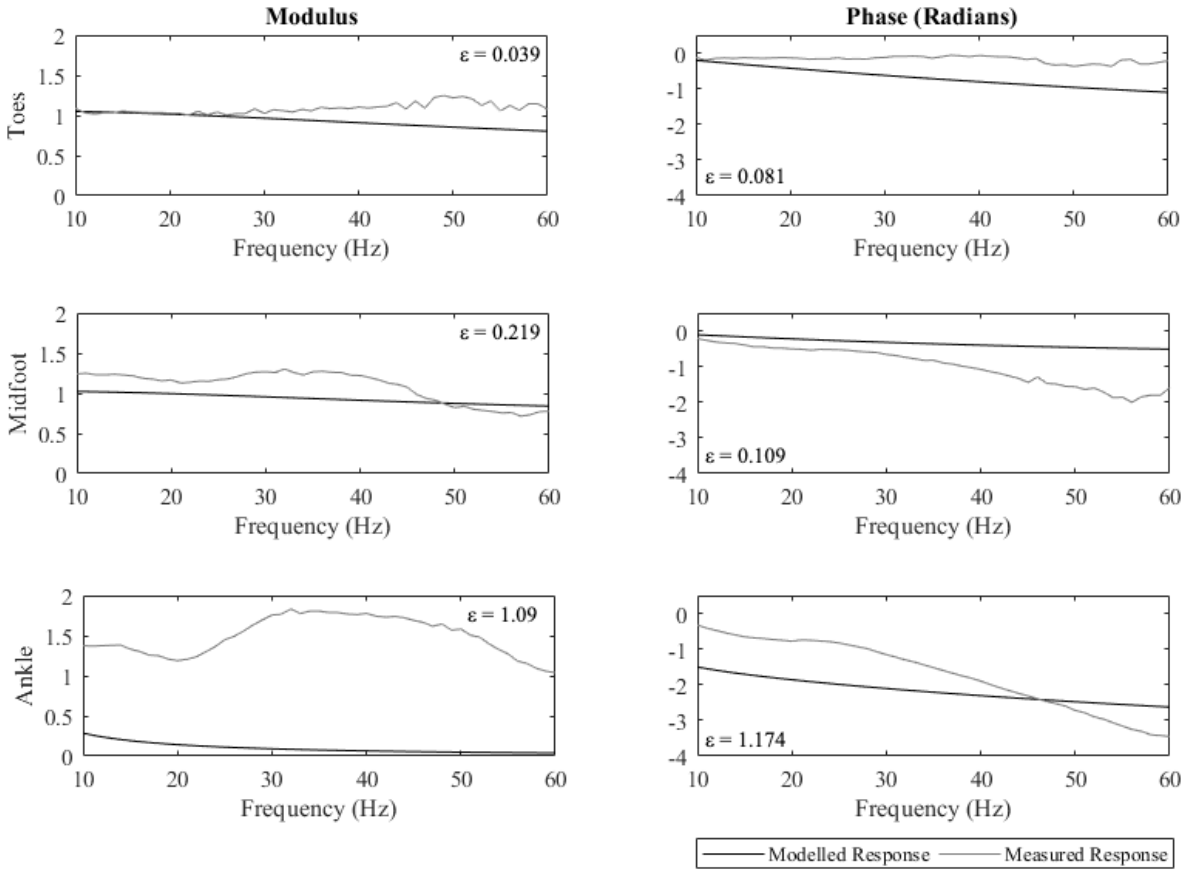

Figure 6.8: The modelled (black) and measured (grey) transmissibility modulus and phase responses of the ankle, midfoot, and toes of the barefoot standing with the COP towards the rearfoot, while exposed to vertical vibration between 10-60Hz [147].

6.3.1 Sensitivity Analysis

Results of the Monte Carlo sensitivity analysis are presented for the three segment, four-DOF LP model of the FAS are presented in the natural (Figure 6.9), forward (Figure 6.10), and the backward (Figure 6.11) COP positions. In general, the transmissibility function variability stimulated by the randomized deviation in the stiffness and damping coefficients (black lines) was always smaller than the measured variability of the participants (grey area) [141, 147].

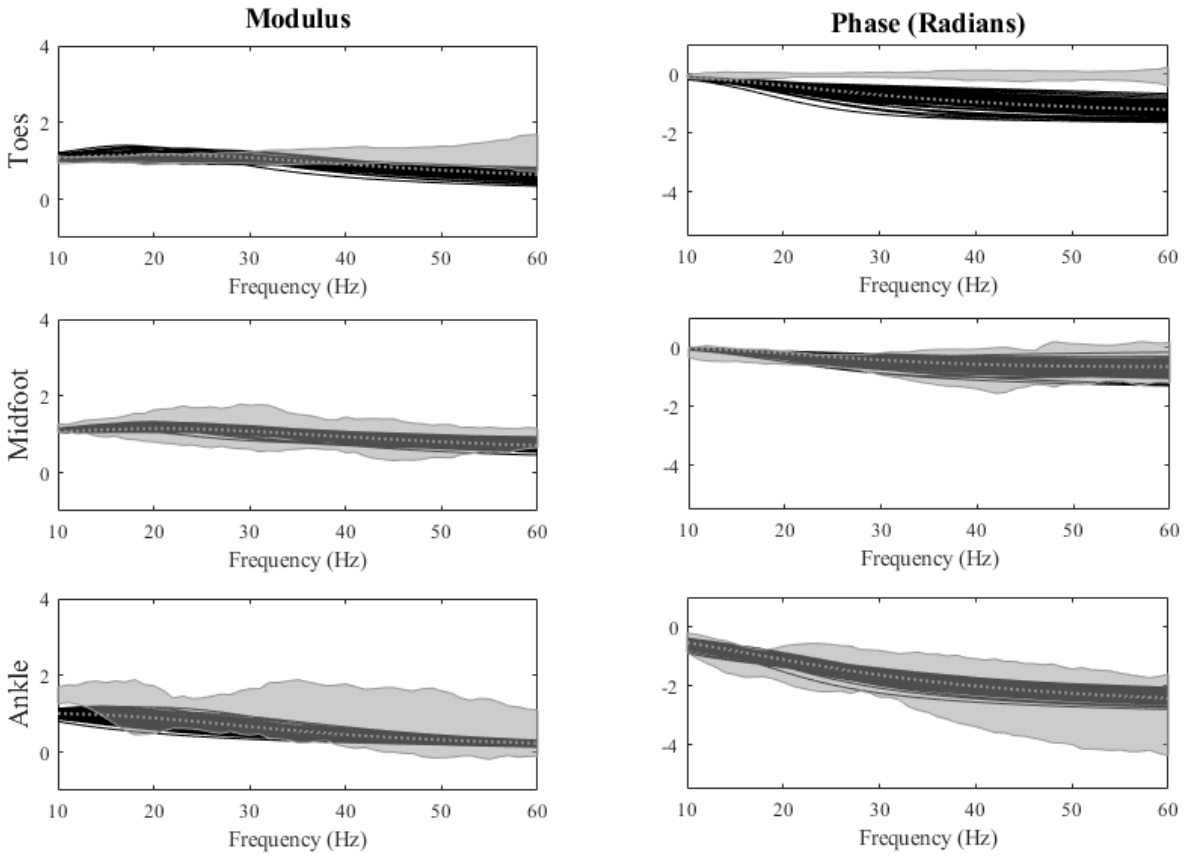

Figure 6.9: Model sensitivity (black curve) for the natural COP position (grey dotted line) and measured ± standard deviation (grey area) [141] of the transmissibility modulus and phase computed at three modelled locations (toes, midfoot, ankle).

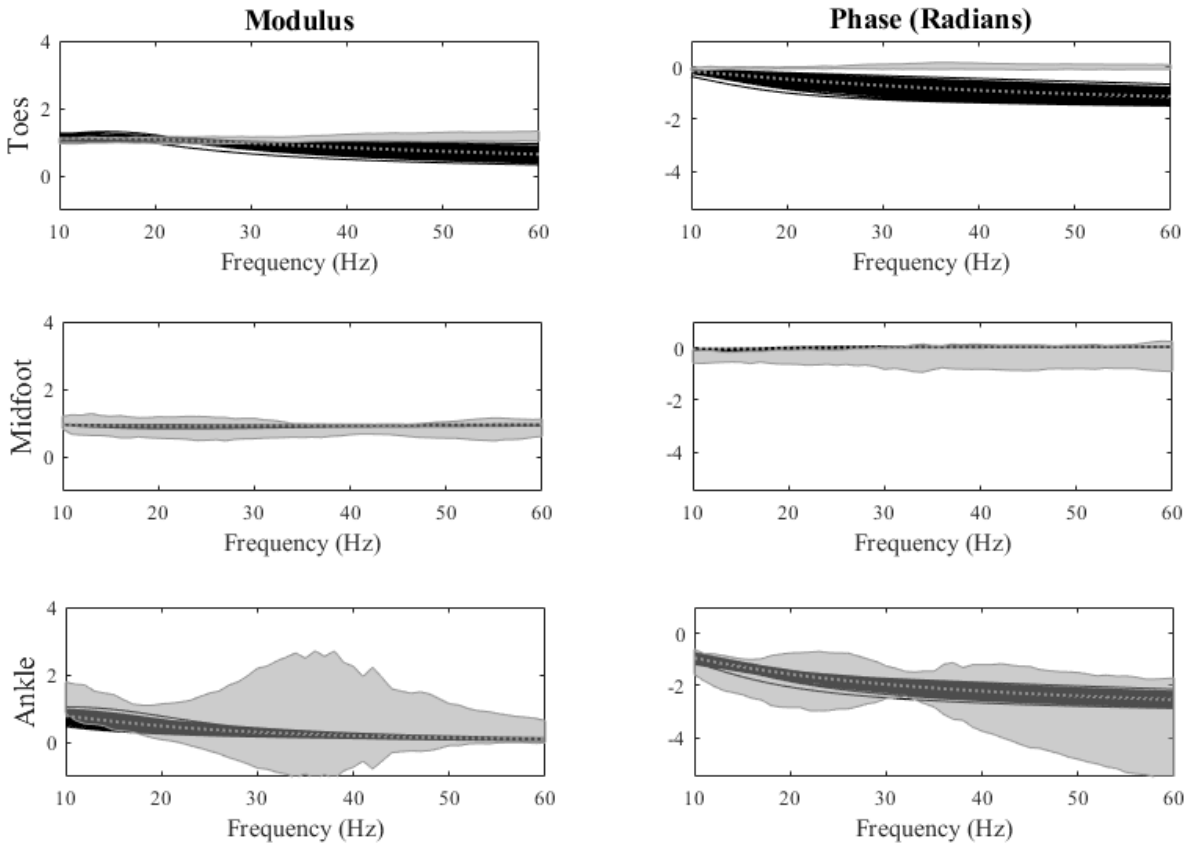

Figure 6.10: Model sensitivity (black curve) for the forward COP position (grey dotted line) and measured ± standard deviation (grey area) [147] of the transmissibility modulus and phase computed at three modelled locations (toes, midfoot, ankle).

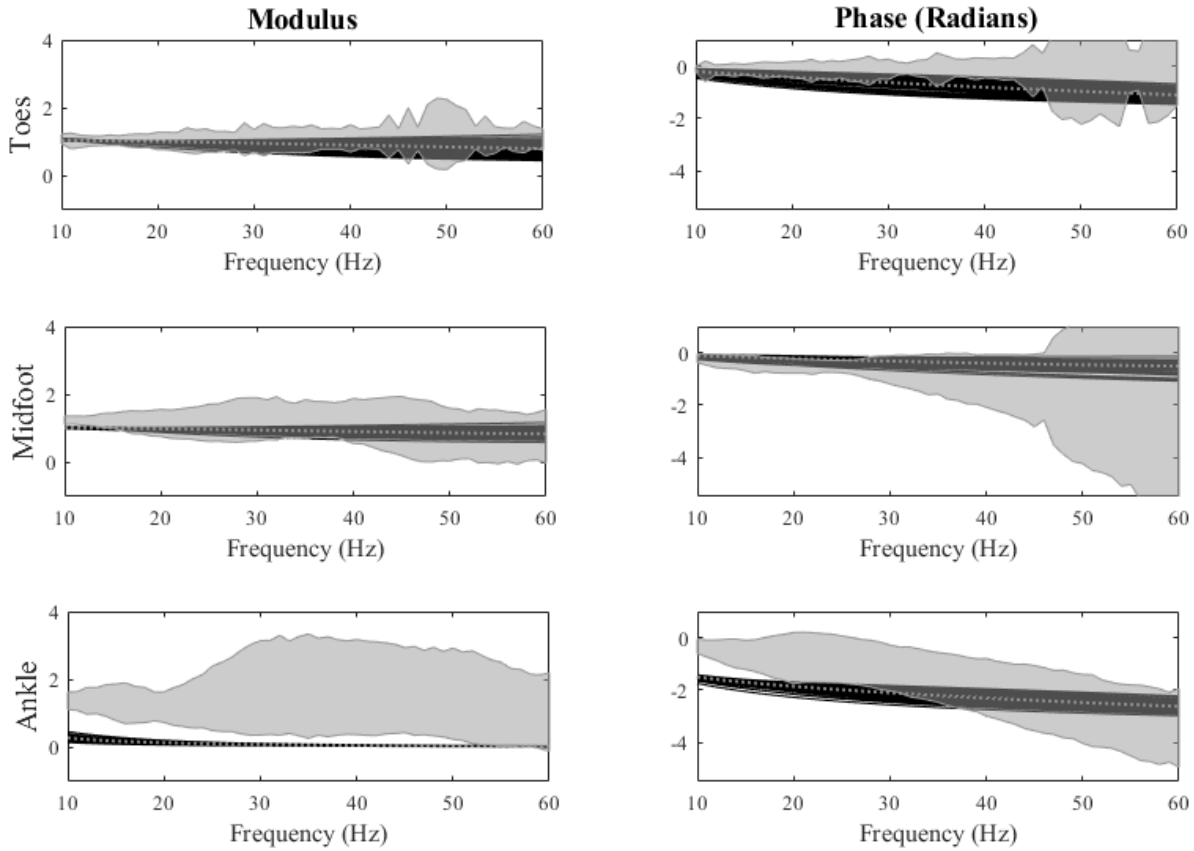

Figure 6.11: Model sensitivity (black curve) for the backward COP position (grey dotted line) and measured ± standard deviation (grey area) [147] of the transmissibility modulus and phase computed at three modelled locations (toes, midfoot, ankle).

The variability (as a percentage) between the optimized functions and the Monte Carlo simulated functions are presented for the transmissibility (Figure 6.12) and phase (Figure 6.13) at 10 Hz intervals. Overall, the variability was lower for the transmissibility (10.1 ± 6.2 %) than the phase (22.0 ± 14.9 %). As anticipated for the transmissibility sensitivity variance analysis, the variance was the highest at the ankle regardless of COP location. The ankle appeared to become less sensitive as the transmissibility increased, whereas the midfoot and toes became more sensitive as the transmissibility increase. While, the phase sensitivity variance analysis revealed the midfoot had the highest variance

regardless of COP location, and there was not a visible trend in sensitivity depending on the frequency.

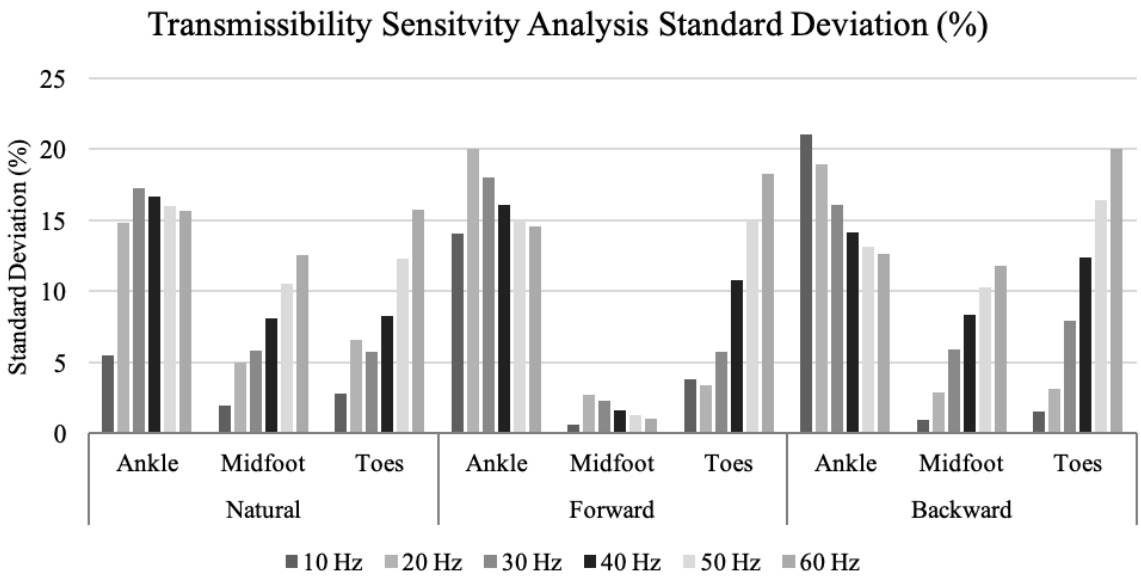

Figure 6.12: The percentage of deviation between the optimized transmissibility function and the Monte Carlo simulated transmissibility functions, in three COP locations (natural, forward, backward) at 10 Hz intervals.

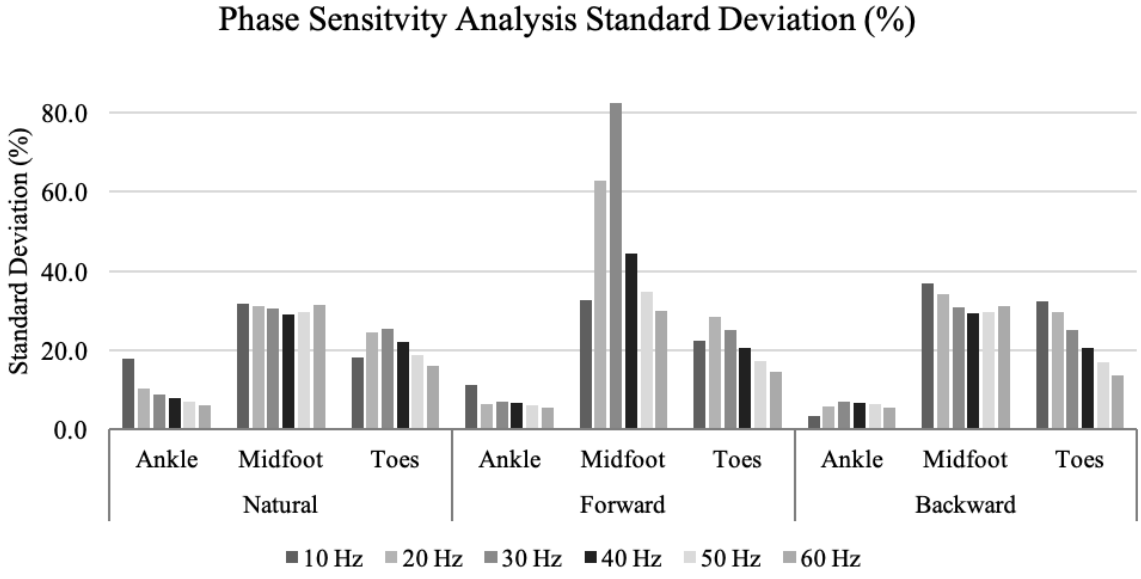

Figure 6.13: The percentage of deviation between the optimized phase function and the Monte Carlo simulated phase functions, in three COP locations (natural, forward, backward) at 10 Hz intervals.

6.4 DISCUSSION

The purpose of this paper was two-fold: (1) reduce a data-set, which included 24 anatomical locations [141, 147], using K-means analysis to determine which anatomical locations are a priority for modelling the FAS; and (2) create and calibrate a model of the FAS using the priority anatomical locations. From the K-means analysis, it was determined that the nail of the big toe (T1P1), the third metatarsal (L2), and the lateral malleolus (L4) would be sufficient for modelling the transmissibility response of the FAS. Using the truss-structure framework from Simkin & Leichter [119] and Kim & Voloshin [118], a three segment, 4-DOF LP model of the FAS exposed to vertical vibration from 10-60Hz was created. The model was then fit to the transmissibility measurements from 21 participants [141] in order to assess the effects of changing the COP location on the model parameters [147].

The anatomical measurement locations selected using the transmissibility magnitude analysis (multiple correspondence analysis) in Chapter 5 are similar to those selected using the transmissibility frequency analysis (K-means). This agreement is noteworthy given the different analyses and different experimental features from which they were obtained. From the transmissibility analysis, using three groups (T1P1, L2, and L4) is sufficient for summarizing the FTV biodynamic response, while the multiple correspondence analysis suggests four groups (T1P1, T1P3, M1, and L4). Though there are differences in the specific locations recommended, both approaches separate locations at the ankle, midfoot, and toes, with the T1P3 location being grouped in with the midfoot (Figure 6.2). In future models, the toes should be included as a separate component and T1P1 could be used to summarize the toes as a whole. Further to that, the toes could be separated with representation by three components: the first, the middle two and the last two metatarsals [120].

The large stiffness ($41.1x10^4$–$286.2x10^4$ N/m) and negligible damping (0.1 Ns/m) values of the spring-damper representing the plantar aponeurosis suggest that it does not play a significant role in vibration absorption. Similar results were found by Kim & Voloshin [118] when the foot was modelled with and without a plantar fascia; the absence of the fascia only caused a 10% change in the impact acceleration of the ankle joint, implying an insignificant role in shock absorption. Additionally, the difference between the stiffness in the forward ($133.2x10^4$ N/m) and backward ($41.1x10^4$ N/m) COP locations may be explained by the increased tension of the plantar aponeurosis [120]. Concentrating the pressure towards the toes could causes a flattening of the arch, with the pressure underneath the heel being released and the pressure increased underneath the first metatarsal head.

As the major support areas of the foot are concentrated under the tarsal heads and calcaneus [120], these two areas were represented in the model by spring-dampers. The stiffness and damping parameters at these two locations exhibited the largest changes based on COP location. When the COP location is pushed forward towards the toes, the stiffness at the tarsal fat pad increased from $64.6x10^3$ N/m (natural) to $55.6x10^4$ N/m and the damping decreased from $7.88x10^3$ Ns/m (natural) to the model minimum of 0.10 Ns/m. Conversely, when the COP location is pushed backward towards the heel, the stiffness at the tarsal fat pad is diminished to 102 N/m and the damping increases substantially ($25.2x10^4$ Ns/m). The nature of the observed changes suggests that increased loading on the soft tissues increases their stiffness and damping response. The reverse trend was observed in the calcaneus fat pad, with stiffness increasing and damping decreasing [154] as the COP was shifted towards the rearfoot.

Since the modelling of FTV response has been limited, comparison with earlier foot models is impossible. Instead, the current study will be compared to LP models evaluating the transmission of vibration through the hands. One of the first models of the hand gripping a tool in 1-DOF [104] was non-linear with two frequency regions, low frequency (20-73 Hz) and high frequency (100-500 Hz). Similarly, in order to achieve reasonable results with a lower DOF model, the frequency region of this FTV model was reduced to 10-60 Hz. Limiting the model to 60 Hz is reasonable as occupational exposures to standing vibration have been documented at dominant frequencies as high as 40 Hz [1].

Model simplifications, with assumptions at some level, are required for realistic simulation [155]. The model presented in this paper makes numerous simplifications and assumptions (e.g. three segments, non-linear, and vertical axis vibration only) in order to achieve a simplistic model of the FAS using practical measurement locations on the foot within an appropriate frequency range for FTV exposure [1]. This model is also limited by the experimental data, which lumps together people of different ages, sex, anthropometry, arch height, etc. As there may be additional factors that affects the foot's biodynamic response, future work could identify these factors and can be incorporated into a model.

Future modelling research can begin by completing a validation of this model. Model validation can include confirming results with other software, or using a new experimental data set as the reference functions. Enhancements to this model may reveal that more sophisticated models are necessary to capture the biodynamic response of the foot. More segments may need to be added to the model, for example, such as one to represent the toes; however, the increasing complexity needs to be approached with caution to ensure the model still answers specific questions regarding foot function [161]. Adding more segments may

result in a model that is capable of capturing a larger frequency range (greater than 60 Hz) to specifically incorporate the resonant frequencies of the toes. In addition to improvements to the LP model, future work should consider the effects of raising the heel above the plane of the metatarsals [120] to evaluate and reproduce the effects of insoles and footwear. Finally, the effects of vibration in multiple axes (x, z, and potentially the rotational axes) could be evaluated and modelled. Modelling can be an effective method of evaluating footwear designs, with incremental improvements [162] specifically engineered to reduce vibration exposure.

6.5 CONCLUSIONS

The three segment, 4-DOF LP model of the FAS exposed to vertical vibration from 10-60 Hz presented herein provides reasonable results at the ankle, midfoot, and toes in the natural standing position (ε = 0.471, 0.089, and 0.047) and with the COP pushed forward towards the toes (ε = 0.539, 0.058, and 0.057). However, when the COP is pushed backward toward the hindfoot, the model does not sufficiently capture the transmissibility response at the ankle (ε = 1.09, 0.219, and 0.039). While the current work represents a useful initial model of the vibration response of the foot, further refinements are needed to fully capture its behaviour under a variety of loading scenarios.

CHAPTER 7: SUMMARY & CONCLUSIONS

This final chapter seeks to tie together the material presented in the four manuscript chapters included in this dissertation. To that end, a summary of the research findings is presented along with the unique contributions of each to the research field, and practical implications for foot-transmitted vibration (FTV) measurement standards, design engineers, and ergonomists. Finally, recommendations for future research to advance learning in FTV exposure are outlined.

7.1 RESEARCH FINDINGS SUMMARY

There were four main research objectives with the overall purpose to enhance understanding of vibration transmissibility through the foot-ankle system (FAS) when standing in an upright position. The specific research objectives and key findings from each chapter are summarized in Table 7.1.

Table 7.1: Summary of the research objectives and key findings from the four papers included in the dissertation.

Chapter #	
3	**Objective:** To measure the transmission of vibration through the foot when standing in a natural upright position.
	Key Finding(s): The average resonant frequencies (where maximum amplification occurred) differ across anatomical locations on the foot: • Toes (range: 99-147Hz); • Midfoot (range: 51-84Hz); and • Ankle (range: 16-39Hz).
4	**Objective:** To measure the transmission of vibration through the foot when altering the centre of pressure (COP) location to the forefoot and rearfoot.
	Key Finding(s): Average resonant frequencies differ based on the COP location. Generally, concentrating the COP towards the toes caused an increase in the resonance frequency at the toes, and concentrating the COP towards the heel caused an increase in resonance frequency at the measurement locations around the ankle.
5	**Objective(s):** To determine the minimal number of unique measurement points required to document vibration transmissibility through the foot.
	Key Finding(s): Vibration transmissibility of the FAS can be represented with measurements taken at: T1P1, T1P3, M1, and L4.
6	**Objective(s):** To develop a lumped-parameter model to model the transmission of vibration through the FAS.
	Key Finding(s): A three segment, 4-DOF LP model of the FAS provides reasonable results in natural standing position.

7.2 CONTRIBUTIONS TO RESEARCH LITERATURE

Prior research regarding FTV exposure has traditionally been lumped in with standing whole-body vibration (WBV) exposure. The goal of this dissertation was to establish a foundation for FTV-specific research by making the following contributions:

- The biodynamic response of the FAS, under exposure to FTV, was determined at 24 locations on the foot. Previously published vibration transmissibility data for the foot-ankle had been limited to the first phalange and the medial and lateral malleolus (Table 2.2), so the inclusion of 21 new anatomical locations in the current work provides the most complete mapping of the vibration response of the foot to date.
- The biodynamic response of the foot was documented over a frequency spectrum of 10-200 Hz. Only one study, involving only two anatomical locations, used a larger frequency range (4-250 Hz) [68]. Such a large range is needed to properly characterize the response of the toes where the symptoms of vibration-induced white-foot (VIWFt) manifest themselves.
- Resonance was identified at 24 anatomical locations on the barefoot in a natural standing position, which up until this point was not documented for any locations on the foot, as the only other studies involving a transmissibility measurement on the foot were limited by the exposure frequency.
- The effects of altering the COP position on resonance were measured. When the COP was forward towards the toes the greatest amplitude of vibration transmissibility was at the toes, and similarly when the COP position was backward towards the heels the greatest amplitude of vibration transmissibility was at the ankle. Understanding how COP affects vibration response is critical for clinicians studying vibration-induced

white-foot, as well as engineers designing protective equipment, since workers assume a range of postures throughout their shift.

- The minimum number of locations required to capture the biodynamic response of the foot were identified. The fact that four points —first phalange (T1P1), first metatarsal (T1P3), second metatarsal (M1), and lateral malleolus (L4)— are capable of evaluating the transmissibility amplitude will inform the design of future laboratory and field experiments. The use of multiple correspondence analysis (MCA) to categorize anatomical locations is also a novel application of this analysis technique.
- K-means clustering with superimposed spatial constraints was used to identify regions of similar response based on the vibration response across the entire frequency range (10-200 Hz), rather than simply maximum transmissibility. The regions identified were used to reduce measurement locations and inform decisions for the lumped-parameter (LP) model creation. This analysis has confirmed that the forefoot, midfoot, and rearfoot have different biodynamic responses, which is an important finding for insole and boot development, where different dampening components or materials along the foot can be designed to ensure appropriate protection [163].
- A LP model of the foot's response to vibration exposure from 10-60 Hz was developed. The transmissibility response of the FAS was modelled with a three segment, four DOF model in three COP positions. This model is the first to use the previously designed truss model of the longitudinal arch, in order to simulate FTV exposure.

7.3 RESEARCH IMPLICATIONS

7.3.1 FTV Measurement Standards

International standards exist for evaluating WBV [8] and hand-transmitted vibration (HTV) [62]. Typically, the WBV standard and z-axis weighting curve (W_k) and x, y-axis weighting curve (W_d) are used to evaluate health effects associated with vibration exposure for a standing operator [8]. The highest dominant FTV exposure frequencies reported in the literature, for workers exposed to occupational vibration, are 40 Hz on a raise platform [1, 30]. Unfortunately, the reported data were processed according to ISO 2631-1 [8] and ISO 5349-1 [62], thus the actual dominant exposure frequency could be underestimated due to the weighting curves prescribed by those standards. The findings of this research reported differences in vibration transmissibility magnitude at different FTV exposure frequencies. This finding supports the earlier recommendation by Eger et al. [1] that field measures of FTV exposure should be reported both un-weighted and weighted in order to better understand which frequencies correlate to occupational disease and tissue damage.

Based on the research presented in this thesis, the current method of using the WBV W_k weighting filter to evaluate vibration for a standing person is not appropriate for FTV. As the resonant frequencies of the pelvis and lumbar spine are 3-5 Hz and 8-12 Hz, the only exposure frequencies to remain unweighted using the W_k weighting filter are from approximately 4 to 12.5Hz. The International standard for HTV exposure uses the W_h weighting filter, where frequencies between 8 to 16 Hz remain relatively un-weighted. In this study, the resonant frequencies of the foot ranged between 99-147 Hz at the toes, 51-84 Hz at the midfoot, and 16-39Hz at the ankle (Chapter 3). As such, neither of these existing weightings curves should be used for evaluating health risk and injury prevention for the feet

since both will underestimate the importance of the higher frequencies which have been shown to affect the midfoot and toes. A weighting curve specifically designed for FTV exposure is needed, where the un-weighted frequency range is larger (between 12.5 and 125 Hz).

7.3.2 Design Engineers

The hierarchy of controls has been established in order to protect workers from hazards which could potentially lead to occupational injuries/illnesses [164]. The hierarchy orders controls from most effective to least effective (elimination, substitution, engineering, administration, and personal protective equipment (PPE)) (Figure 7.1). Focusing specifically on the engineering component, design engineers can use the transmissibility findings from this research (Chapter 3 and 4) to prioritize exposure frequencies for human isolation. For instance, bolting platforms have already been measured to have dominant exposure frequencies between 30-40 Hz. As it is now known that these frequencies can be damaging to the ankle and midfoot, isolation platforms for the worker with active damping to avoid frequencies between 20-40 Hz could be designed.

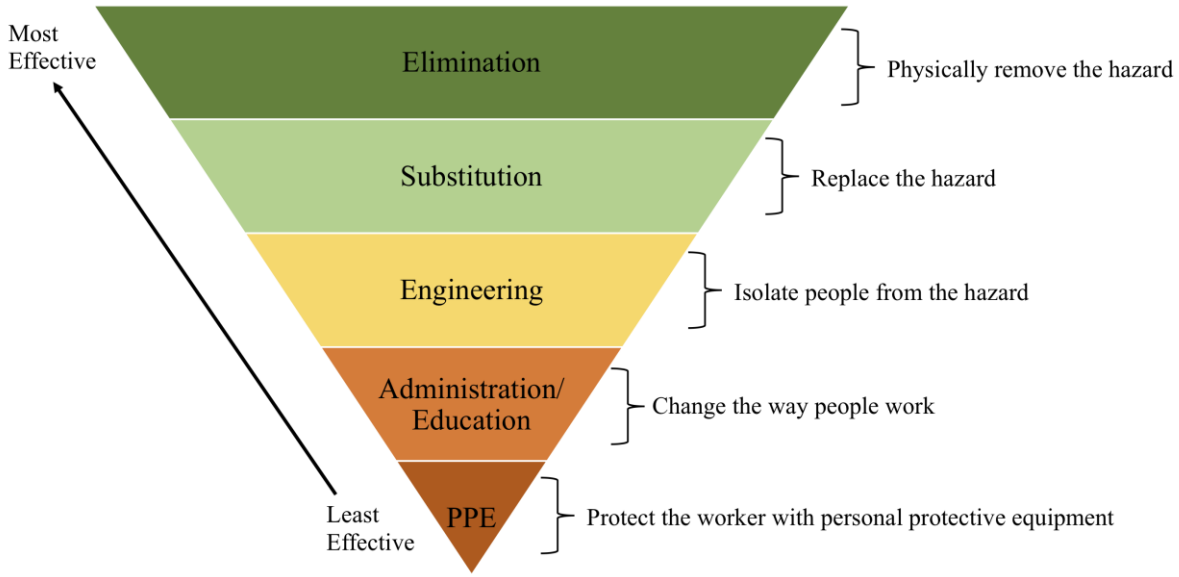

Figure 7.1: Hierarchy of controls and risk control effectiveness [164].

Similarly, the isolation concepts can also be used for PPE design. It has now been established that areas of the foot respond differently depending on exposure frequency (Chapter 3 and 4). With this in mind, insole and safety boot designs need to use a regional approach to attenuate vibration at the toe differently than vibration at the heel in order to provide optimal protection from FTV exposure.

7.3.3 Ergonomists

As an ergonomist measuring occupational exposure to vibration, the results of this research can specifically be incorporated into capturing FTV field measurements. Accelerometers can be used in the field to record measurements on the vibrating surface, directly on the worker, or both. Measurements on the vibrating surface should be taken as close to the standing worker as possible. Additionally, the transmissibility ratio between the platform (input) and the worker (output) can be derived much like what is done for WBV seat measurements, where the input below the seat and the output at the seat surface are measured to evaluate seat

effectiveness. This can be accomplished with FTV exposure to evaluate the effectiveness of interventions such as boots, insoles, and isolation platforms.

Results from this research indicate that the biodynamic response of the foot can be captured with measurements at four locations (T1P1, T1P3, M1, and L4). However, this may not be the most practical strategy, as having four accelerometers on a worker's foot inside their safety boot could be cumbersome. Alternatively, measurement at T1P1 and L4 will provide insight on the highest exposure risk to the toes (T1P1), where symptoms of VIWFt are first felt and noticed, as well as documenting the exposure at the ankle (L4), where mining platforms have previously been measured to have a dominant exposure frequency matching the resonance of the ankle.

7.4 RECOMMENDATIONS FOR FUTURE RESEARCH

This research is really just the beginning for understanding, assessing, and evaluating FTV exposure. The experimental data (Chapter 3 and 4) has characterized the barefoot resonance at 24 anatomical locations on the foot with three COP positions. However, there are numerous other intrinsic and extrinsic factors (Table 2.1) which can affect the biodynamic response to vibration exposure that still need to be studied. As COP position was found to alter the biodynamic response, future research should continue to consider anthropometric measures of the foot of participants being exposed to FTV. These could include platform contact surface area, arch type, pressure distribution, and soft tissue measurements of the fat pads.

It has been proven that minimally four anatomical locations (T1P1, T1P3, M1, and L4) can be used to account for differences in the biodynamic response of the foot (Chapter 5). The ability to reduce measurement time with a minimal set of data collection locations

will greatly improve the ability of researchers to systematically test different conditions and this will allow for a better understanding of the injury mechanisms from FTV exposure. Nevertheless, work is still needed to develop and validate a reliable experimental protocol based on these results.

The future of field studies of FTV exposure is also influenced by this research. Field measurements have yet to be taken directly on the foot, as this can prove to be difficult when wearing socks and safety boots. However, the locations for measuring FTV have been assessed and can now be prioritized depending on the technology to be used in the field. We now know that taking field measurements on T1P1 and L4 is important for capturing the biodynamic response, and combining these two measurements with a platform measurement would give an indication of the FTV exposure workers are experiencing while wearing their safety equipment.

More research is also needed to better understand the physiological changes that result from vibration exposure. For a better understanding of the cause of toe blanching (whiteness caused by decreased blood flow), the blood flow of the medial plantar (supplies first toe) and lateral plantar (supplies toes 2 to 5) arteries, and the dorsal pedal (supplies first and second) and dorsal metatarsal (supplies toes 2 to 5) arteries should be measured (Figure 7.3) before and after vibration exposure. Digital photocell plethysmography could also be conducted on the feet and hands before and after vibration exposure. This testing would involve a baseline blood flow measurement in the toes and fingers, then a measurement after cold water immersion (10°C for 2 minutes) [165]. Results from this type of testing would indicate whether there are immediate changes to the arteries circulating blood to the feet, as the longitudinal effects of prolonged vibration exposure have already been proven.

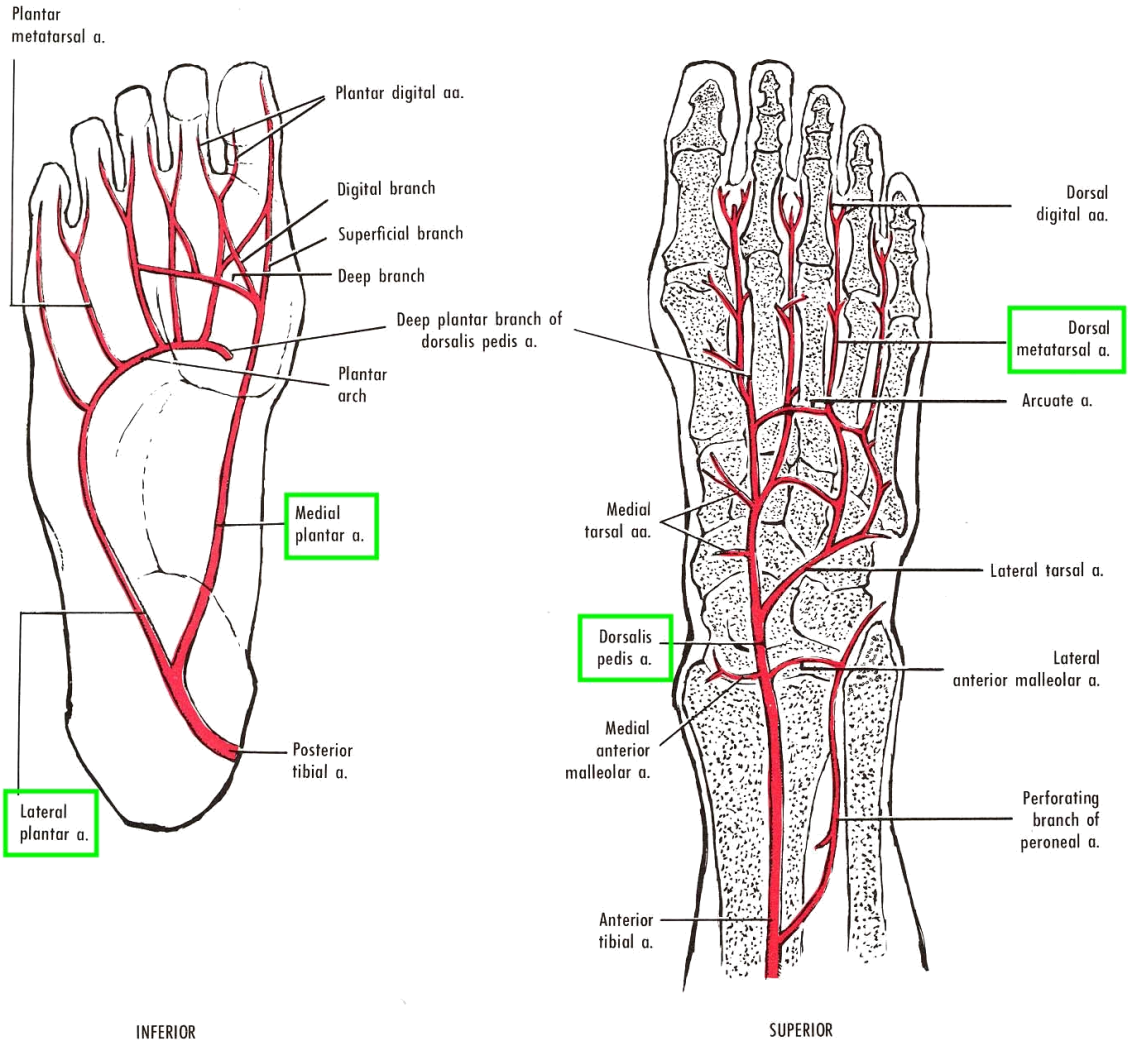

Figure 7.2: Arteries circulating blood to the foot and toes [166].

As vibration exposure is known to have not only vascular effects, but also neurological effects, with nerve conduction velocity tests or electromyography (EMG) to assess muscle health and innervation. EMG can reveal nerve dysfunction, muscle dysfunction, or problems with nerve-to-muscle signal transmission [167] and can be used to assess the influence of differences in muscle tension and activation on the biodynamic response of the foot. As the measurement locations for assessing vibration transmissibility

have been reduced, applying the EMG pads to the superficial locations on the lower limb will be easier to retrieve simultaneous measurements.

Since it has already been suggested that the WBV weighting curve (W_k) is not appropriate for evaluating health risks associated with FTV exposure, future research should focus on developing and evaluating a new weighting curve specifically designed for FTV exposure.

Finally, the LP model described within this dissertation (Chapter 6) simply sets the stage for future, more sophisticated, FTV model development. While the possible combinations of changes for future models are endless, some are suggested herein. Future LP models should add segments for the toes, divide the midfoot and ankle into more components, and include segments for the lower limb. Additionally, components can be added to test the effects of various materials underneath the foot (insoles, or boots) and determine what height, stiffness and damping characteristics of these materials would be the most effective. As boots typically have a higher component in the heel, the height at which the contact locations are exposed can also be altered, to change the angles of the foot to be more representative of a barefoot worker.

7.5 OVERALL CONCLUSIONS

The primary purpose of this dissertation research was to study the transmission of vibration through the FAS when standing in an upright position. The resonance of 24 anatomical locations was identified and found to vary with changes in COP. Measurement at T1P1 (first phalange), T1P3 (first metatarsal), M1 (second metatarsal), and L4 (lateral malleolus), were confirmed to be sufficient to document the biomechanical response of the FAS to FTV. This finding is important as it will make it easier to test epidemiological mechanisms of injury,

including blood flow and muscle tension, in the future. A LP model of FTV from 10-60 Hz established a baseline for continued model development. Expansions of this model to test additional components and different conditions will be imperative for continuing to prevent vibration-induced injury to the feet.

References

1. Eger, T., et al., *Vibration induced white-feet: Overview and field study of vibration exposure and reported symptoms in workers.* Work, 2014. **47**(1): p. 101-110.
2. Thompson, A., et al., *Vibration-white foot: a case report.* Occupational Medicine, 2010. **60**: p. 572-574.
3. Dong, R.G., J.Z. Wu, and D.E. Welcome, *Recent advances in biodynamics of human hand-arm system.* Industrial Health, 2005. **43**: p. 449-471.
4. Tarabini, M., et al., *Apparent mass distribution at the feet of standing subjects exposed to whole-body vibration.* Ergonomics, 2013. **56**(5): p. 842-855.
5. Goggins, K., et al., *Study of the biodynamic response of the foot to vibration exposure.* Occupational Ergonomics, 2016. **13**: p. 53-66.
6. Mansfield, N.J., *Human Response to Vibration*. 2004, London: CRC Press. 256.
7. Rao, S.S., *Mechanical Vibrations*. Fifth ed. 2011, 1 Lake Street, Upper Saddle River, New Jersey: Pearson Education, Inc. 1084.
8. ISO-2631-1, *Mechanical vibration and shock – Evaluation of human exposure to whole-body vibration – whole-body vibration – Part 1: General Requirements*. 1997, International Organization for Standardization: Geneva.
9. Griffin, M.J., *Handbook of Human Vibration*. 1st ed. 1990, London: Academic Press. 988.
10. Kitazaki, S. and M.J. Griffin, *Resonance behaviour of the seat human body and effects of posture.* Journal of Biomechanics, 1998. **31**: p. 143-149.
11. Adamo, F., et al., *Assessment of the uncertainty in human exposure to vibration: An experimental study.* IEEE Sensors, 2014. **14**(2): p. 474-481.
12. Coermann, R.R., *The mechanical impedance of the human body in sitting and standing position at low frequencies.* Human Factors, 1962: p. 227-253.
13. Concettoni, E. and M. Griffin, *The apparent mass and mechanical impedance of the hand and the transmission of vibration to the fingers, hand, and arm.* Journal of Sound and Vibration, 2009. **325**: p. 664-678.
14. Abbas, W., et al., *Optimization of biodynamic seated human models using genetic algorithms.* Engineering, 2010. **2**: p. 710-719.
15. Dong, R.G., et al., *Theoretical relationship between vibration transmissibility and driving-point response functions of the human body.* Journal of Sound and Vibration, 2013. **332**(24): p. 6193-6202.
16. Hinz, B., et al., *The significance of using anthropometric parameters and postures of European drivers as a database for finite-element models when calculating spinal forces during whole-body vibration exposure.* International Journal of Industrial Ergonomics, 2008. **38**: p. 816-843.
17. Gu, C. and M.J. Griffin, *Vibrotactile thresholds at the sole of the foot: Effect of vibration frequency and contact location.* Somatosensory and Motor Research, 2011. **28**(3-4): p. 86-93.
18. Zimmerman, C.L. and T.M. Cook, *Effects of vibration frequency and postural changes on human responses to seated whole-body vibration exposure.* International Archives of Occupational and Environmental Health, 1997. **69**: p. 165-179.

19. Simeonov, P., et al., *Postural stability effects of random vibration at the feet of construction workers in simulated elevation.* Applied Ergonomics, 2011. **42**: p. 672-681.
20. Ksiazek, M.A. and J. Tarnowski, *Experimental studies of the influence of human standing positions on the feet-to-head transmission of vibrations.* Journal of Theoretical and Applied Mechanics, 2014. **52**(4): p. 1107-1114.
21. Matsumoto, Y. and M.J. Griffin, *Non-linear characteristics in the dynamic responses of seated subjects exposed to vertical whole-body vibration.* Journal of Biomechanical Engineering, 2002. **124**: p. 627-532.
22. Bovenzi, M., *Health effects of mechanical vibration.* Giornale Italiano de Medicina del Lavoro ed Ergonomia, 2005. **27**(1): p. 58-64.
23. Bovenzi, M., *Exposure-response relationship in the hand-arm vibration syndrome: an overview of current epidemiology research.* International Archives of Occupational and Environmental Health, 1998. **71**: p. 509-519.
24. Zhou, Z. and M.J. Griffin, *Response of the seated human body to whole-body vertical vibration: biodynamic responses to sinusoidal and random vibration.* Ergonomics, 2010. **57**(5): p. 693-713.
25. Mansfield, N.J. and M.J. Griffin, *Effects of posture and vibration magnitude on apparent mass and pelvis rotation during exposure to whole-body vertical vibration.* Journal of Sound and Vibration, 2002. **253**(1): p. 93-107.
26. Mansfield, N.J., *Review Article: Impedance methods (apparent mass, driving point mechanical impedance and absorbed power) for assessment of the biomechanical response of the seated person to whole-body vibration.* Industrial Health, 2005. **43**: p. 378-389.
27. Boileau, P.-E., Z. Wu, and S. Rakheja, *Definition of a range of idealized values to characterize seated body biodynamic response under vertical vibration.* Journal of Sound and Vibration, 1998. **215**(4): p. 841-862.
28. Randall, J.M., R.T. Matthews, and M.A. Stiles, *Resonant frequencies of standing humans.* Ergonomics, 1997. **40**(9): p. 879-886.
29. Morioka, M. and M.J. Griffin, *Thresholds for the perception of hand-transmitted vibration: Dependence on contact area and contact location.* Somatosensory and Motor Research, 2005. **22**(4): p. 281-297.
30. Leduc, M., et al., *Examination of vibration characteristics, and reported musculoskeletal discomfort for workers exposed to vibration via the feet.* Low Frequency Noise, Vibration and Active Control, 2011. **30**(3): p. 197-206.
31. Bovenzi, M. and C.T.J. Hulshof, *An updated review of epidemiologic studies on the relationship between exposure to whole-body vibration and low back pain (1986-1997).* International Archives of Occupational and Environmental Health, 1999. **72**: p. 351-365.
32. Bovenzi, M., I. Pinto, and N. Stacchini, *Low back pain in port machinery operators.* Journal of Sound and Vibration, 2002. **253**(1): p. 3-20.
33. Pope, M., et al., *Guidelines for whole-body vibration health surveillance.* Journal of Sound and Vibration, 2002. **253**(1): p. 131-167.
34. Alem, N., *Application of the new ISO 2631-5 to health hazard assessment of repeated shock un U.S. army vehicles.* Industrial Health, 2005. **43**: p. 403-412.

35. Bovenzi, M., et al., *An epidemiological study of low back pain in professional drivers.* Journal of Sound and Vibration, 2006. **298**: p. 514-539.
36. Bovenzi, M., *A follow up study of vascular disorders in vibration-exposed forestry workers.* International Archives Occupational and Environmental Health, 2008. **81**: p. 401-408.
37. Seidel, H., *Review Article: On the relationship between whole-body vibration exposure and spinal health risk.* Industrial Health, 2005. **43**: p. 361-377.
38. Griffin, M.J., *Measurement, evaluation, and assessment of peripheral neurological disorders caused by hand-transmitted vibration.* International Archives of Occupational and Environmental Health, 2008. **81**(5): p. 559-573.
39. Hagberg, M., et al., *Incidence of Raynaud's phenomenon in relation to hand-arm vibration exposure among male workers at an engineering plant a cohort study.* Journal of Occupational Medicine and Toxicology, 2008. **3**(13): p. 1-6.
40. Murata, K., S. Araki, and K. Maeda, *Autonomic and peripheral nervous system dysfunction in workers exposed to hand-arm vibration: a study of R-R interval variability and distribution of nerve conduction velocities.* International Archives of Occupational and Environmental Health, 1991. **63**: p. 205-211.
41. Noel, B., *Pathophysiology and classification of the vibration white finger.* International Archives of Occupational and Environmental Health, 2000. **73**: p. 150-155.
42. Egan, C.E., et al., *Acute effects of vibration on peripheral blood flow in healthy subjects.* Occupational and Environmental Medicine, 1996. **53**(10): p. 663-669.
43. Rakheja, S., et al., *A comparison of biodynamic models of the human hand-arm system for applications to hand-held power tools.* Journal of Sound and Vibration, 2002. **249**(1): p. 55-82.
44. Griffin, M.J. and M. Bovenzi, *The diagnosis of disorders caused by hand-transmitted vibration: Southampton Workshop 2000.* International Archives of Occupational and Environmental Health, 2002. **75**: p. 1-5.
45. Welcome, D.E., et al., *An investigation on the biodynamic foundation of a rat tail vibration model.* Journal of Engineering in Medicine, 2008. **222**: p. 1127-1141.
46. Krajnak, K., et al., *Long-term daily vibration exposure alters current perception threshold (CPT) sensitivity and myelinated axons in a rat-tail model of vibration-induced injury.* Journal of Toxicology and Environmental Health, 2016. **79**(3): p. 101-111.
47. Krajnak, K., et al., *Characterization of frequency-dependent responses of the vascular system to repetitive vibration.* American College of Occupational and Environmental Medicine, 2010. **52**(6): p. 584-594.
48. Laeger, U., *Vibration-induced white toes.* Herning Centralsygehus, arbejdsmedicinsk klinik, 1994. **156**(34): p. 879-886.
49. Toibana, N., et al., *Raynaud's phenomenon of fingers and toes among vibration-exposed patients.* Nagoya J. Med. Sci., 1994. **57**: p. 121-128.
50. Dickey, J.P., et al., *Multi-axis sinusoidal whole-body vibrations: Part 1 - How long should the vibration and rest exposures be for reliable discomfort measures?* Journal of Low Frequency Noise, Vibration and Active Control, 2006. **25**(3): p. 175-184.
51. Hashiguchi, T., et al., *Pathological changes of finger and toe in patients with vibration syndrome.* Nagoya J. Med. Sci., 1994. **57**: p. 129-136.

52. Hedlund, U., *Raynaud's phenomenon of fingers and toes of miners exposed to local and whole-body vibration and cold.* International Archives of Occupational and Environmental Health, 1989. **61**: p. 457-461.
53. Sakakibara, H., et al., *Correlation between vibration-induced white finger and symptoms of upper and lower extremities in vibration syndrome.* International Archive of Occupational and Environmental Health, 1988. **60**: p. 285-289.
54. Sakakibara, H., et al., *Circulatory disturbances of the foot in vibration syndrome.* International Archives of Occupational and Environmental Health, 1991. **63**: p. 4.
55. Thompson, A.J.L. and M.J. Griffin, *Effect of the magnitude and frequency of hand-transmitted vibration on finger blood flow during and after exposure to vibration.* International Archives on Occupational and Environmental Health, 2009. **82**: p. 1151-1162.
56. Furuta, M., et al., *Effect of vibration frequency on finger blood flow.* International Archives of Occupational and Environmental Health, 1991. **63**: p. 221-224.
57. Schweigert, M., *The relationship between hand-arm vibration and lower extremity clinical manifestations: a review of literature.* International Archives of Occupational and Environmental Health, 2002. **75**: p. 179-185.
58. Murata, K., et al., *Effects of occupational use of vibrating tools in the autonomic, central and peripheral nervous system.* International Archives of Occupational and Environmental Health, 1997. **70**: p. 94-100.
59. Tingsgard, I. and K. Rasmussen, *Vibration-induced white toes.* Ugeskr Laeger, 1994. **156**(34): p. 4836-4838.
60. Singh, P., et al., *Evaluation of gender differences in foot-transmitted vibration.* Canadian Acoustics, 2011. **39**(2): p. 62-63.
61. 2002/44/EC, E.D., *Directive 2002/44/EC of the European Parliament and of the council on the minimum health and safety requirements regarding the exposure of workers to the risks arising from physical agents (vibration)*. 2002, Official Journal of the European Communities. p. 13-19.
62. ISO-5349-1, *Mechanical vibration and shock – Guidelines for the measurement and the assessment of human exposure to hand-transmitted vibration*. 2004, International Organization for Standardization: Geneva, Switzerland.
63. Dawe, E.J.C. and J. Davis, *(vi) Anatomy and biomechanics of the foot and ankle.* Orthopaedics and Trauma, 2011. **25**(4): p. 279-286.
64. Cummings, B., *Anatomy Library*, F.b.l. #628241, Editor. 2001, Addison Wesley Longman Inc.: https://anatomy-library.com/img/foot-bones-labeled-14.html.
65. Creative, C., *Plantar Fascia*, P. Fascia, Editor. 2018, Orthoquest Pedorthics and Rehabilitation Inc.: https://www.orthoquestpedorthics.com/resources/blog/news/Blog-Entries/2018/02/03/50:top-10-tools-we-offer-for-plantar-fasciitis.
66. Kirby, K.A., *Biomechanics of the normal and abnormal foot.* Journal of the American Podiatric Medical Association, 2000. **90**(1): p. 1-5.
67. Paddan, G.S. and M.J. Griffin, *A review of the transmission of translational seat vibration to the head.* Journal of Sound and Vibration, 1998. **215**(4): p. 863-882.
68. Harazin, B. and J. Grzesik, *The transmission of vertical whole-body vibration to the body segments of standing subjects.* Journal of Sound and Vibration, 1998. **215**(4): p. 775-787.

69. Kiiski, J., et al., *Transmission of vertical whole body vibration to the human body.* Journal of Bone and Mineral Research, 2008. **23**(8): p. 1318-1325.
70. Wee, H. and A. Voloshin, *Transmission of vertical vibration to the human foot and ankle.* Annals of Biomedical Engineering, 2013. **41**(6): p. 1172-1180.
71. Palm III, W.J., *System Dynamics*. 3rd ed, ed. I. McGraw-Hill Companies. 2013, 1221 Avenues of the Americas, New York, NY. 907.
72. Dong, R.G., et al., *Theoretical foundation, methods, and criteria for calibrating human vibration models using frequency response functions.* Journal of Sound and Vibration, 2015. **356**: p. 195-216.
73. Smith, S.D. and L.E. Kazarian, *The effects of acceleration on the mechanical impedance response of a primate model exposed to sinusoidal vibration.* Annals of Biomedical Engineering, 1994. **22**: p. 78-87.
74. Wei, L. and M.J. Griffin, *Mathematical models for the apparent mass of the seated human body exposed to vertical vibration.* Journal of Sound and Vibration, 1998. **212**(5): p. 855-874.
75. Fairley, T.E. and M.J. Griffin, *The apparent mass of the seated human body: Vertical vibration.* Journal of Biomechanics, 1989. **22**(2): p. 81-94.
76. Barauskas, R. and R. Krusinskiene, *On parameters identification of computational models of vibrations during quiet standing of humans.* Journal of Sound and Vibration, 2007. **308**: p. 612-624.
77. Coe, T.E., et al., *A simplified 3-D human body-seat interaction model and its applications to the vibration isolation design of high-speed marine craft.* Ocean Engineering, 2009. **36**: p. 732-746.
78. Muksian, R. and C.D. Nash Jr, *A model for the response of seated humans to sinusoidal displacements of the seat.* Journal of Biomechanics, 1974. **7**: p. 209-215.
79. Wan, Y. and J.M. Schimmels, *A simple model that captures the essential dynamics of a seated human exposed to whole body vibration.* Advances in Bioengineering, 1995. **31**.
80. Boileau, P.-E. and S. Rakheja, *Whole-body vertical biodynamic response characteristics of the seat vehicle driver: Measurement and model development.* International Journal of Industrial Ergonomics, 1998. **22**: p. 449-472.
81. Matsumoto, Y. and M.J. Griffin, *Modelling the dynamic mechanisms associated with the principal resonance of the seated human body.* Clinical Biomechanics, 2001. **16**(1): p. S31-S44.
82. Subashi, G.H.M.J., Y. Matsumoto, and M.J. Griffin, *Apparent mass and cross-axis apparent mass of standing subjects during exposure to vertical whole-body vibration.* Journal of Sound and Vibration, 2006. **293**(1-2): p. 78-95.
83. Zadpoor, A.A. and A.A. Nikooyan, *Modeling muscle activity to study the effects of footwear on the impact forces and vibrations of the human body during running.* Journal of Biomechanics, 2010. **43**: p. 186-193.
84. Subashi, G.H.M.J., Y. Matsumoto, and M.J. Griffin, *Modelling resonances of the standing body exposed to vertical whole-body vibration: Effects of posture.* Journal of Sound and Vibration, 2008. **317**: p. 400-418.
85. Liu, W. and B.M. Nigg, *A mechanical model to determine the influence of masses and mass distribution on the impact force during running.* Journal of Biomechanics, 2000. **33**: p. 219-224.

86. Noorloos, D., et al., *Does body mass index increase the risk of low back pain in a population exposed to whole body vibration?* Applied Ergonomics, 2008. **39**: p. 779-785.
87. Muksian, R. and C.D. Nash Jr, *On frequency-dependent damping coefficients in lumped-parameter models of human beings.* Journal of Biomechanics, 1976. **9**: p. 339-342.
88. Kubo, M., et al., *An investigation into a synthetic vibration model for humans: An investigation into a mechanical vibration human model constructed according to the relations between the physical, psychological and physiological reactions of humans exposed to vibration.* International Journal of Industrial Ergonomics, 2001. **27**: p. 219-232.
89. Gao, J., et al., *Vertical vibration characteristics of seated human bodies and the biodynamic model with two degrees of freedom.* Science China Technological Sciences, 2011. **54**(10): p. 2776-2784.
90. Zhou, Z. and M.J. Griffin, *Response of the seated human body to whole-body vertical vibration: biodynamic responses to sinusoidal and random vibration.* Ergonomics, 2014. **57**(5): p. 693-713.
91. JiangHua, G., et al., *Vertical vibration characteristics of seated human bodies and a biodynamic model with two degrees of freedom.* Science China: Technological Sciences, 2011. **54**(10): p. 2776-2784.
92. Boileau, P.-E., S. Rakheja, and X. Wu, *A body mass dependent mechanical impedance model for applications in vibration seat testing.* Journal of Sound and Vibration, 2002. **253**(1): p. 243-264.
93. Nawayseh, N. and M.J. Griffin, *A model of the vertical apparent mass and the fore-and-aft cross-axis apparent mass of the human body during vertical whole-body vibration.* Journal of Sound and Vibration, 2009. **319**: p. 719-730.
94. Wang, Y. and S. Rahmatalla, *Human head-neck models in whole-body vibration: Effect of posture.* Journal of Biomechanics, 2013. **46**: p. 702-710.
95. Nikooyan, A.A. and A.A. Zadpoor, *Effects of muscle fatigue on the ground reaction force and soft-tissue vibrations during running: A model study.* IEEE Transactions on Biomedical Engineering, 2012. **59**(3): p. 797-804.
96. Smith, S.D., *Technical note: Modeling differences in the vibration response characteristics of the human body.* Journal of Biomechanics, 2000. **33**: p. 1513-1516.
97. Choi, S.-B. and Y.-M. Han, *Vibration control of electrorheological seat suspension with human-body model using sliding mode control.* Journal of Sound and Vibration, 2007. **303**: p. 391-404.
98. Kim, T.-H., Y.-T. Kim, and Y.-S. Soon, *Development of a biomechanics model of the human body in a sitting posture with vibration transmissibility in the vertical direction.* International Journal of Industrial Ergonomics, 2005. **35**: p. 817-829.
99. Zheng, G., Y. Qui, and M.J. Griffin, *An analytic model of the in-line and cross-axis apparent mass of the seated human body exposed to vertical vibration with and without a backrest.* Journal of Sound and Vibration, 2011. **330**: p. 6509-6525.
100. Cho, Y. and Y.-S. Yoon, *Biomechanical model of human on seat with backrest for evaluating ride quality.* International Journal of Industrial Ergonomics, 2001. **27**: p. 331-345.

101. Harsha, S.P., et al., *Measurement and bio-dynamic model development of seated human subjects exposed to low frequency vibration environment.* 2014: p. 1-21.
102. Qassem, W., M.O. Othman, and S. Abdul-Majeed, *The effects of vertical and horizontal vibrations on the human body.* Medical Engineering and Physics, 1994. **16**: p. 151-161.
103. Liang, C.-C. and C.-F. Chiang, *Modelling of a seated human body exposed to vertical vibrations in various automotive postures.* Industrial Health, 2008. **46**: p. 125-137.
104. Reynolds, D.D. and W. Soedel, *Dynamic response of the hand-arm system to sinusoidal input.* Journal of Sound and Vibration, 1972(21): p. 339-353.
105. Mishoe, J.W. and C.W. Suggs, *Hand-arm vibration part II: Vibrational responses of the human hand.* Journal of Sound and Vibration, 1977. **53**(4): p. 545-558.
106. Wood, L.A., C.W. Suggs, and C.F. Abrams, *Hand-arm vibration part III: A distributed parameter dynamic model of the human hand-arm system.* Journal of Sound and Vibration, 1978. **57**(2): p. 157-169.
107. Miwa, T., et al., *Vibration isolators for portable vibrating tools Part 1. A grinder.* Industrial Health, 1979. **17**: p. 85-101.
108. Reynolds, D.D. and R.J. Falkenberg, *Three- and four-degrees-of-freedom models of the vibration response of the human hand*, in *3rd International Symposium on Hand-Arm Vibration*, A.J. Brammer and W. Taylor, Editors. 1982, John Wiley & Sons, Inc.: Ottawa, ON, Canada. p. 117-132.
109. Daikoku, M. and F. Ishikawa. *Mechanical impedance and vibration model of hand-arm system*. in *Fifth International Conference on Hand-Arm Vibration*. 1990. Kanzawa, Japan.
110. Gurram, R., S. Rakheja, and A.J. Brammer, *Driving-point mechanical impedance of the human hand-arm system: Synthesis and model development.* Journal of Sound and Vibration, 1995. **180**(3): p. 437-458.
111. Dong, R.G., et al., *Modeling of biodynamic responses distributed at the fingers and the palm of the human hand-arm system.* Journal of Biomechanics, 2007. **40**: p. 2335-2340.
112. Reynolds, D.D. and E.N. Angevine, *Hand-arm vibration, Part II: Vibration transmission characteristics of the hand and arm.* Journal of Sound and Vibration, 1977. **51**(2): p. 255-265.
113. Dong, J.H., et al., *A method for analyzing absorbed power distribution in the hand and arm substructures when operating vibrating tools.* Journal of Sound and Vibration, 2008. **311**: p. 1286-1304.
114. Panaitescu-Liess, R. and F. Basic. *A 6-DOF human hand dynamic model*. in *SISOM Acoustics and Robotics*. 2013. Bucharest, Romania.
115. Adewusi, S., S. Rakheja, and P. Marcotte, *Biomechanical models of the human hand-arm to simulate distributed biodynamic responses for different postures.* International Journal of Industrial Ergonomics, 2012. **42**(2): p. 249-260.
116. Bausic, F. and R. Panaitescu-Liess. *A 8 DOF hand-arm dynamic model*. in *SISOM, Acoustics and Robotics*. 2013. Bucharest.
117. Gefen, A., *The in vitro elastic properties of the plantar fascia during the contact phase of walking.* Foot & Ankle International, 2003. **24**(3): p. 238-244.
118. Kim, W. and A.S. Voloshin, *Role of plantar fascia in the load bearing capacity of the human foot.* Journal of Biomechanics, 1995. **28**(9): p. 1025-1033.

119. Simkin, A. and I. Leichter, *Role of the calcaneal inclination in the energy storage capacity of the human foot - a biomechanical model.* Medical & Biological Engineering & Computing, 1990. **28**: p. 149-152.
120. Salathe Jr, E.P., G.A. Arangio, and E.P. Salathe, *A biomechanics model of the foot.* Journal of Biomechanics, 1986. **19**(12): p. 989-1001.
121. Kim, W., A.S. Voloshin, and S.H. Johnson, *Modeling of heel strike transients during running.* Human Movement Sciences, 1994. **13**: p. 221-244.
122. Wee, B.H., *The dynamic model of the foot and ankle system*, in *Mechanical Engineering*. 2012, Lehigh University: Lehigh Preserve. p. 176.
123. Shen, S.C. and R.A. House, *Clinical Review: Hand-arm vibration syndrome - What family physicians should know.* Canadian Family Physician, 2017. **63**: p. 206-210.
124. House, R., et al., *Vasospasm in the feet in workers assessed for HAVS.* Occupational Medicine, 2010: p. 1-6.
125. Ji, X., T.E. Eger, and J.P. Dickey, *Optimizing seat selection for LHDs in the underground mining environment.* The Journal of the Southern African Institute of Mining and Metallurgy, 2016. **116**: p. 785-792.
126. Gunaselvam, J. and J.L. van Niekerk, *Seat selection guidelines to reduce whole-body vibration exposure levels in the SA mining industry.* The Journal of The South African Institute of Mining and Metallurgy, 2005. **105**: p. 675-686.
127. Donati, P., *Survey of technical preventative measures to reduce whole-body vibration effects when designing mobile machinery.* Journal of Sound and Vibration, 2002. **253**(1): p. 169-183.
128. ISO-10819, *Mechanical vibration and shock – Hand-arm Vibration – Measurement and evaluation of the vibration transmissibility of gloves at the palm of the hand*. 2013, International Organization for Standardization: Geneva.
129. Dong, R.G., et al., *Vibration energy absorption (VEA) in human fingers-hand-arm system.* Medical Engineering and Physics, 2004. **26**: p. 483-492.
130. Tarabini, M., et al., *Analysis of non-linear response of the human body to vertical whole-body vibration.* Ergonomics, 2014. **57**(11): p. 1711-1723.
131. Polytec. *Laser Doppler vibrometry*. 2019 [cited 2019 March 1]; Available from: https: //www.polytec.com/us/vibrometry/basic-principles-of-vibrometry.
132. Drabenstedt, A., *Quantification of displacement and velocity noise in vibrometer measurements on transversely moving or rotating surfaces.* Proceedings of SPIE - The International Society for Optical Engineering, 2007. **6616**.
133. Smith, S.W., *The Scientist and Engineer's Guide to Digital Signal Processing*. Second ed. 1999, San Diego, California: California Technical Publishing. 688.
134. Welcome, D.E., et al., *The effects of vibration-reducing gloves on finger vibration.* International Journal of Industrial Ergonomics, 2014. **44**: p. 45-59.
135. Welcome, D.E., et al., *An examination of the vibration transmissibility of the hand-arm system in three orthogonal directions.* International Journal of Industrial Ergonomics, 2015. **45**: p. 21-34.
136. Xu, X.S., et al., *An examination of an adapter method for measuring the vibration transmitted to the human arms.* Measurement, 2015. **73**: p. 318-334.
137. Orlando, S., B. Peeters, and G. Coppotelli, *Improved FRF estimators for MIMO sine sweep data*, in *International Conference on Noise and Vibration Engineering*. 2008: Leuven, Belgium. p. 1-15.

138. Dong, R.G., et al., *Review and Evaluation of Hand–Arm Coordinate Systems for Measuring Vibration Exposure, Biodynamic Responses, and Hand Forces.* Safety and Health at Work, 2015. **6**(3): p. 159-173.
139. Adewusi, S., et al., *Vibration transmissibility characteristics of the human hand–arm system under different postures, hand forces and excitation levels.* Journal of Sound and Vibration, 2010. **329**(14): p. 2953-2971.
140. Xu, X.S., et al., *The vibration transmissibility and driving-point biodynamic response of the hand exposed to vibration normal to the palm.* International Journal of Industrial Ergonomics, 2011. **41**(5): p. 418-427.
141. Goggins, K., et al., *Biomechanical response of the human foot when standing in a natural position exposed to vertical vibration from 10-200 Hz.* Ergonomics, 2018.
142. Saggin, B., D. Scaccabarozzi, and M. Tarabini, *Metrological performances of a plantar pressure measurement system.* IEEE Transactions on Instrumentation and Measurement, 2013. **62**(4): p. 766-776.
143. Rothman, K.J., *No adjustments are needed for multiple comparisons.* Epidemiology, 1990. **1**(1): p. 43-46.
144. Aldien, Y., et al., *Influence of hand-arm posture on biodynamic response of the human hand-arm exposed to zh-axis vibration.* International Journal of Industrial Ergonomics, 2006. **36**: p. 45-59.
145. Xu, X.S., et al., *Vibrations transmitted from human hands to upper arm, shoulder, back, neck, and head.* International Journal of Industrial Ergonomics, 2016.
146. Almagirby, A., J.A. Rongong, and M.J. Carre, *The development of a new artificial model of a finger for assessing transmitted vibration.* Journal of the Mechanical Behavior of Biomedical Materials, 2018. **78**: p. 20-27.
147. Goggins, K., et al. *Standing centre of pressure alters the vibration transmissibility response of the foot*. in *7th American Conference on Human Vibration*. 2018. Cedarbrooke Lodge, Seattle, Washington.
148. Qui, Y. and M.J. Griffin, *Biodynamic responses of the seated human body to single axis and dual-axis vibration.* Industrial Health, 2010. **48**: p. 615-627.
149. Chaudhary, D.K., et al., *Whole-body vibration exposure of drill operators in iron ore mines and role of machine-related, individual, and rock-related factors.* Safety and Health at Work, 2015. **6**: p. 268-278.
150. Le Roux, B. and H. Rouanet, *Multiple Correspondence Analysis*. Quantitative Applications in the Social Sciences, ed. S. John Fox, McMaster University. Vol. 163. 2010, California, United States: SAGE Publications Inc. 115.
151. Pearson, R.H. and D.J. Mundform, *Recommended sample size for conducting exploratory factor analysis on dichotomous data.* Journal of Modern Applied Statistical Methods, 2010. **9**(2): p. 359-368.
152. Abdi, H. and D. Valentine, *Multiple Correspondence Analysis.* 2007: p. 1-13.
153. Wearing, S.C. and J.E. Smeathers, *The heel fat pad: mechanical properties and clinical applications.* Journal of Foot and Ankle Research, 2011. **4**: p. I14.
154. Fontanella, C.G., et al., *Biomechanical behaviour of plantar fat pad in healthy and degenerative foot conditions.* Med Biol Eng Comput, 2016. **54**: p. 653-661.
155. Morales-Orcajo, E., J. Bayod, and E. Barbosa de Las Casas, *Computational Foot Modeling: Scope and Applications.* Arch Computat Methods Eng, 2016. **23**: p. 389-416.

156. Gurram, R., S. Rakheja, and G.J. Gouw, *Mechanical impedance of the human hand-arm system subject to sinusoidal and stochastic excitations.* International Journal of Industrial Ergonomics, 1995. **16**: p. 135-145.
157. MacQueen, J. *Some methods for classification and analysis of multivariate observations*. in *5th Berkeley Symposium on Mathematical Statistics and Probability*. 1965. University of California . Berkeley, CA: University of California Press.
158. Isman, R.E. and V.T. Inman, *Anthropometric studies of the human foot and ankle.* Bulletin of Prosthetics Research, 1969: p. 97-129.
159. Aruin, A.S. and V.M. Zatsiorsky, *Biomechanical characteristics of human ankle-joint muscles.* European Journalists of Applied Physiology and Occupational Physiology, 1984. **52**(400-406).
160. Zatsiorsky, V.M., *Kinetics of Human Motion*. 2002, Champaign, IL: Human Kinetics. 657.
161. Scott, S.H. and D.A. Winter, *Biomechanical model of the human foot: Kinematics and kinetics during the stance phase of walking.* Journal of Biomechanics, 1993. **26**(9): p. 1091-1104.
162. Lemmon, D., et al., *The effect of insoles in therapeutic footwear - A finite element approach.* Journal of Biomechanics, 1997. **30**(6): p. 615-620.
163. Tarabini, M., et al., *Effect of work boot characteristics on vibration transmitted to workers' feet and subjective discomfort.*, in *International Ergonomics Association 20th Congress*. 2018: Florence, Italy. p. 1043-1051.
164. (NIOSH), N.I.f.O.S.a.H., *Workplace Safety and Health Topics: Hierarchy of Controls*. 2018.
165. House, R., et al. *Vascular symptoms and digital plethysmography abnormalities in the feet of workers with HAVS*. in *Third American Conference on Human Vibration*. 2010. Iowa City, IA: University of Iowa.
166. O'Rahilly, et al., *Basic Human Anatomy*, T.a.o.t.s.a.d.o.t. foot, Editor. 2009, O'Rahilly: https://www.dartmouth.edu/~humananatomy/figures/chapter_17/17-3.HTM.
167. Mayo Clinic, S. *Electromyography (EMG)*. 2018 [cited 2019 January 3rd].
168. Tarabini, M., *Experimental characterization of mechanical systems: A guide for engineers and technicians*, in *Course book for undergraduate mechanical engineers*. 2016: Politechnico de Milano, Lecco, Italy. p. 1-238.

APPENDICES

Appendix A. Laurentian University research ethics certificate

APPROVAL FOR CONDUCTING RESEARCH INVOLVING HUMAN SUBJECTS
Research Ethics Board – Laurentian University

This letter confirms that the research project identified below has successfully passed the ethics review by the Laurentian University Research Ethics Board (REB). Your ethics approval date, other milestone dates, and any special conditions for your project are indicated below.

TYPE OF APPROVAL / New X / Modifications to project / Time extension

Name of Principal Investigator and school/department	Katie Goggins, Engineering, supervisor, Tammy Eger, Human Kinetics
Title of Project	Transmissibility of vibration at the toes and foot when standing in a natural, forward lean and backward lean posture
REB file number	2016-05-17
Date of original approval of project	July 15, 2016
Date of approval of project modifications or extension *(if applicable)*	
Final/Interim report due on: *(You may request an extension)*	July 15, 2017
Conditions placed on project	

During the course of your research, no deviations from, or changes to, the protocol, recruitment or consent forms may be initiated without prior written approval from the REB. If you wish to modify your research project, please refer to the Research Ethics website to complete the appropriate REB form.

All projects must submit a report to REB at least once per year. If involvement with human participants continues for longer than one year (e.g. you have not completed the objectives of the study and have not yet terminated contact with the participants, except for feedback of final results to participants), you must request an extension using the appropriate LU REB form. In all cases, please ensure that your research complies with Tri-Council Policy Statement (TCPS). Also please quote your REB file number on all future correspondence with the REB office.

Congratulations and best wishes in conducting your research.

Rosanna Langer, PHD, Chair, *Laurentian University Research Ethics Board*

Appendix B. An outline of the twenty-four reflective marker numbers, names, and location descriptions to be used on the right foot for vibration transmissibility measurement

Marker #	Marker Name	Marker Location Description
1	T1P1	Place marker on the middle of the nail bed of each toe
2	T2P1	
3	T3P1	
4	T4P1	
5	T5P1	
6	T1P2	Palpate phalanges (toes) to feel the bony joint processes, place the marker in between the first and 2nd joint
7	T2P2	
8	T3P2	
9	T4P2	
10	T5P2	
11	T1P3	Palpate the first metatarsal (big toe) for joint between metatarsal and phalange, place the marker directly on the top of the joint.
12	T2P3	Palpate phalanges (toes) to feel the bony joint processes, place the marker in between the second and third joint.
13	T3P3	
14	T4P3	
15	T5P3	
16	M1	Viewing the foot from the top, locate metatarsal 2 and place this marker in a vertical line with toe 2 and in a horizontal line with T1P3
17	M2	Viewing the foot from the top, M2 should be approximately 2.5-4 cm from M1. If an imaginary horizontal line is drawn across the foot from T1P3 and another at the crease of the ankle/foot M2 should be located midway between these two lines.
18	M3	Viewing the foot from the top, locate metatarsal 2, place marker in vertical line with M2 at the crease of the foot/ankle.
19	M4	Palpate the medial portion of the ankle for the head of the fibula, place marker on the most protruding portion of the bone.
20	L1	Viewing the foot from the top, locate metatarsal 3 and 4, place this marker in the space between Toe 3 and 4 in line with M1 and T1P3 in the horizontal direction.
21	L2	Viewing the foot from the top, L2 should be approximately 2.5-4 cm from L1. If an imaginary horizontal line is drawn across the foot from T1P3 and another at the crease of the ankle/foot L2 should be located midway between these two lines and in the same horizontal plane as M2
22	L3	Viewing the foot from the top, place marker in vertical line with L2 at the crease of the foot/ankle (on the same vertical line as M3)
23	L4	Palpate the lateral portion of the ankle for the lateral malleolus, place marker on most protruding portion of the bone.
24	H1	Locate the marker on the head of the calcaneus back of the heel). Palpate for the bony landmark at the insertion point of the Achilles Tendon

Appendix C. Laser point (LP) locations (1-4) for 21 participants at 24 anatomical locations.

Anatomical Location	Participant #																				
	1	2	3	4	5	6	7	8	9	10	11	12	13	14	15	16	17	18	19	20	21
T1P1	1	1	1	2	2	2	1	1	1	1	1	1	1	1	1	1	1	1	1	1	1
T2P1	1	1	1	2	2	2	1	1	1	1	1	1	1	1	1	1	1	1	1	1	1
T3P1	1	1	1	2	2	2	1	1	1	1	1	1	1	1	1	1	1	1	1	1	1
T4P1	1	1	1	2	2	2	1	1	1	1	1	1	1	1	1	1	1	1	1	1	1
T5P1	1	1	1	2	2	2	1	1	1	1	1	1	1	1	1	1	1	1	1	1	1
T1P2	1	1	1	2	2	2	1	1	1	1	1	1	1	1	1	1	1	1	1	1	1
T2P2	1	1	1	2	2	2	1	1	1	1	1	1	1	1	1	1	1	1	1	1	1
T3P2	1	1	1	2	2	2	1	1	1	1	1	1	1	1	1	1	1	1	1	1	1
T4P2	1	1	1	2	2	2	1	1	1	1	1	1	1	1	1	1	1	1	1	1	1
T5P2	1	1	1	2	2	2	1	1	1	1	1	1	1	1	1	1	1	1	1	1	1
T1P3	1	1	1	2	2	2	1	1	1	1	1	1	1	1	1	1	1	1	1	1	1
T2P3	1	1	1	2	2	2	1	1	1	1	1	1	1	1	1	1	1	1	1	1	1
T3P3	1	1	1	2	2	2	1	1	1	1	1	1	1	1	1	1	1	1	1	1	1
T4P3	1	1	1	2	2	2	1	1	1	1	1	1	1	1	1	1	1	1	1	1	1
T5P3	1	1	1	2	2	2	1	1	1	1	1	1	1	1	1	1	1	1	1	1	1
M1	2	2	1	2	2	2	1	1	2	2	2	1	2	1	1	1	1	1	2	2	2
M2	2	2	2	2	2	2	2	4	2	2	2	2	2	2	2	2	2	2	2	2	2
M3	2	2	2	2	2	4	2	4	2	2	2	2	2	2	2	2	2	2	2	3	2
M4	4	4	4	4	4	4	4	4	4	3	4	4	4	4	4	4	4	4	4	3	3
L1	2	2	1	2	2	2	1	1	2	2	2	2	2	1	1	1	2	2	1	2	1
L2	2	2	2	2	2	2	2	4	2	2	4	2	2	2	2	2	2	2	2	2	2
L3	2	2	2	4	2	3	2	4	2	2	4	2	2	2	2	2	2	2	2	2	2
L4	2	2	2	2	4	2	2	4	4	3	4	3	2	4	3	2	2	3	4	2	3
H1	3	3	3	3	3	3	3	4	4	3	4	3	3	4	3	2	3	3	4	4	3

Appendix D. Outline of derivation of equations to calculate the power-spectral density transfer function, the cross-spectral density function, and the H_1 frequency response estimator

Power Spectral Density Transfer Function

Fourier Transform (FT)	$FT(f) = \int_{-\infty}^{+\infty} f(t) \cdot e^{-i2\pi ft} dt$	m/s^2	(1)
Where: $f(t)$ is the time domain function of the measurement signal. Note: The FT is the decomposition of any periodic signal to the superposition of potentially infinite number of sine waves with different amplitudes and magnitudes.			
Discrete Fourier Transform (DFT)	$DFT(b) = \left(\frac{1}{N}\right) \sum_{n=0}^{N-1} f(n) \cdot e^{-i2\pi bn/N}$	m/s^2	(2)
Where: N is the number of samples; $f(n)$ is the measured signal; and b is the observations of the system. Note: The DFT is the basis of all computer-based computations of the FT.			
Power Spectrum (PS)	$PS = \lvert DFT(b)\rvert^2 = \left[\left(\frac{1}{N}\right) \sum_{n=0}^{N-1} f(n) \cdot e^{-i2\pi bn/N}\right]^2$	(m/s^2)^2	(3)
Where: $G(k)$ is the DFT; N is the number of samples; $f(n)$ is the measured signal; and b is the observations of the system. Note: The PS is defined as the squared modulus of the Discrete Fourier Transform. The PS indicates the energy of each frequency component.			
Power Spectral Density (PSD)	$PSD = \frac{\lvert DFT(b)\rvert^2}{\Delta f} = \frac{N}{f_s}\left[\left(\frac{1}{N}\right) \sum_{n=0}^{N-1} f(n) \cdot e^{-i2\pi bn/N}\right]^2$	(m/s^2)^2/Hz	(4)
Where: $\lvert G(k)\rvert^2$ is the PS, f_s is the sampling frequency; N is the number of samples; $f(n)$ is the measured signal; and b is the observations of the system. Note: The PSD is defined as the ratio between the power spectrum and the frequency resolution. Using the PSD of random components does not depend on the frequency resolution (e.g. observing the signal for a longer time does not averagely lower the PSD). On the contrary, in the presence of harmonic components not affected by leakage, the PSD increases with the observation time, since a constant power is divided by smaller values. A signal is correctly sampled if fs is at least 2x larger than the maximum frequency of the signal (Shannon Theorem).			

Power Spectral Density (PSD) Transfer Function	$PSD\ transfer\ function\ (f) = \sqrt{\frac{PSD_{output}\ (f)}{PSD_{input}\ (f)}}$	unitless	(5)
Where: $PSD_{output}(f)$ is the PSD of the output; and $PSD_{input}(f)$ is the PSD of the input.			

Cross-Spectral Density Function

The Fourier Transform of correlation functions are:

Auto-spectral density (ASD) function of input	$S_{aa}(f) = \int_{-\infty}^{+\infty} FT_{aa}\ (\tau) e^{-i2\pi f\tau} d\tau$	m/s^2	(6)
Where: $FT_{aa}(\tau)$ is the Fourier Transform of the input.			
Auto-spectral density (ASD) function of output	$S_{vv}(f) = \int_{-\infty}^{+\infty} FT_{vv}\ (\tau) e^{-i2\pi f\tau} d\tau$	m/s^2	(7)
Where: $FT_{vv}(\tau)$ is the Fourier Transform of the output.			
Cross-spectral density (CSD) function	$S_{av}(f) = \int_{-\infty}^{+\infty} FT_{av}\ (\tau) e^{-i2\pi f\tau} d\tau$	m/s^2	(8)
Where: $FT_{av}(\tau)$ is the Fourier Transform of the input/output cross-correlation relationship (e.g. product $x(t) \cdot y(t + \tau)$).			

Modulus of CSD	$\lvert S_{av}(f)\rvert^2 = S_{aa}(f) S_{vv}(f)$	m/s^2	(10)
Where: $S_{aa}(f)$ is the ASD function of the input; and $S_{vv}(f)$ is the ASD function of the output.			

H_1 Frequency Response Function Estimator

The H_1 frequency response function (FRF) estimator is used if the measurement noise on the input signal is negligible.

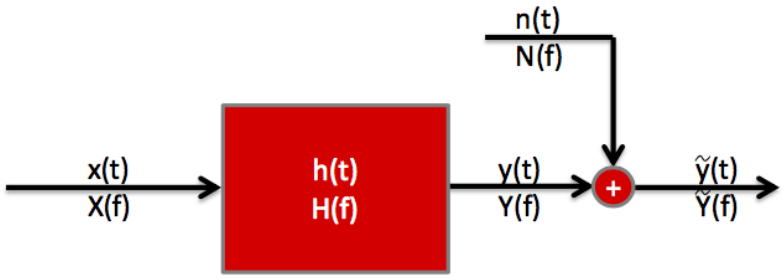

Figure 1: Schematic of a linear system whose output measurement is contaminated by random noise [168].

Averaged cross-spectral density including input signal and noise	$S_{av}(f) = H(f) \cdot S_{aa}(f) + S_{na}(f)$	m/s^2	(11)
Where: $H(f)$ is the Fourier Transform of the impulse response; $S_{aa}(f)$ is the auto-spectral density function of the input signal; and $S_{na}(f)$ is the auto-spectral density function of the noise input. Note: The average cross-spectral density between the noise and input is zero because input and noise are not generally correlated.			
H_1 Frequency Response Function (FRF) Estimator	$\tilde{H}_1(f) = \frac{S_{av}(f)}{S_{aa}(f)}$	unitless	(12)
Where: $S_{av}(f)$ is the averaged cross-spectral density; and $S_{aa}(f)$ is the auto-spectral density function of the input signal.			
Coherence	$\gamma^2(f) = \frac{\lvert S_{av}(f)\rvert^2}{S_{aa}(f) \cdot S_{vv}(f)}$	unitless	(13)
Where: $\lvert S_{av}(f)\rvert^2$ is the modulus of the cross-spectral density function; $S_{aa}(f)$ is the auto-spectral density function of the input signal; and $S_{yy}(f)$ is the auto-spectral density function of the output signal.			

Appendix E. The individual transmissibility responses of 21 participants at 24 anatomical locations. Excluded measurements include: one participant at T2P1, T3P1, and H1 and two participants at M4.

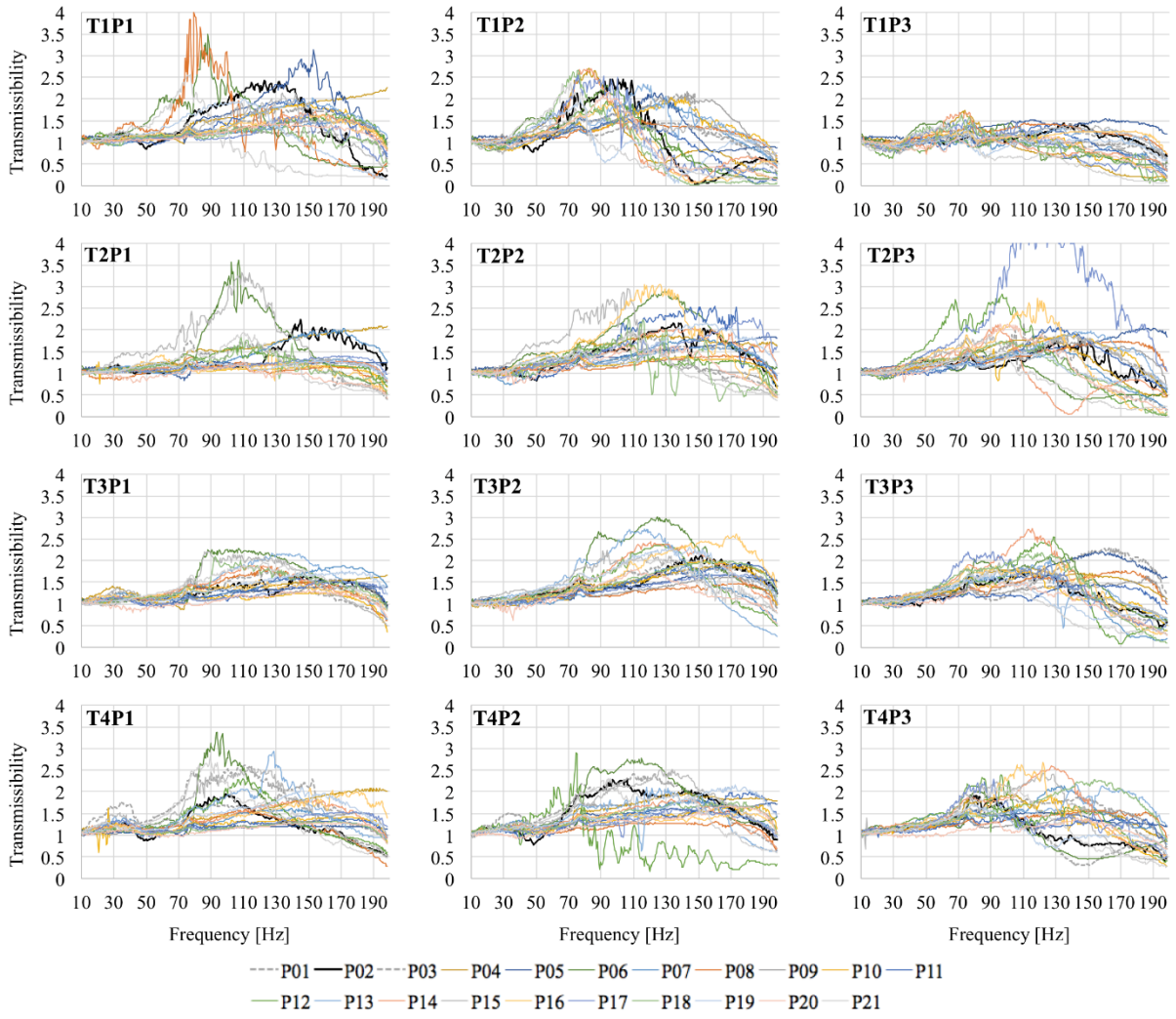

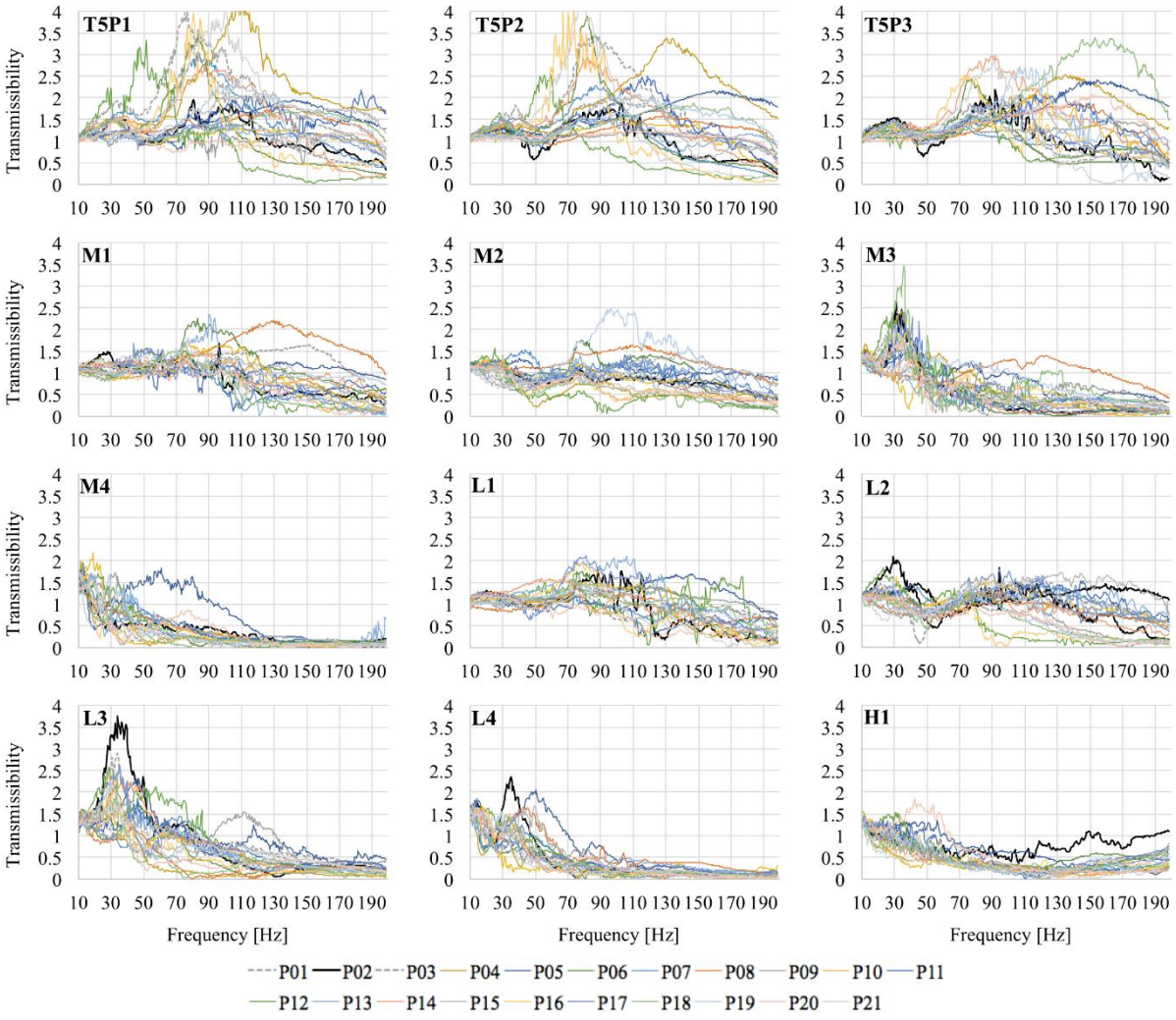
T5P1
T5P2
T5P3
M1
M2
M3
M4
L1
L2
L3
L4
H1
Transmissibility
Frequency [Hz]
P01 P02 P03 P04 P05 P06 P07 P08 P09 P10 P11
P12 P13 P14 P15 P16 P17 P18 P19 P20 P21

Appendix F. The average (black line) ± standard deviation (grey dotted line) of the entire transmissibility, phase and coherence responses of 21 participants for 24 anatomical locations while in the natural COP position.

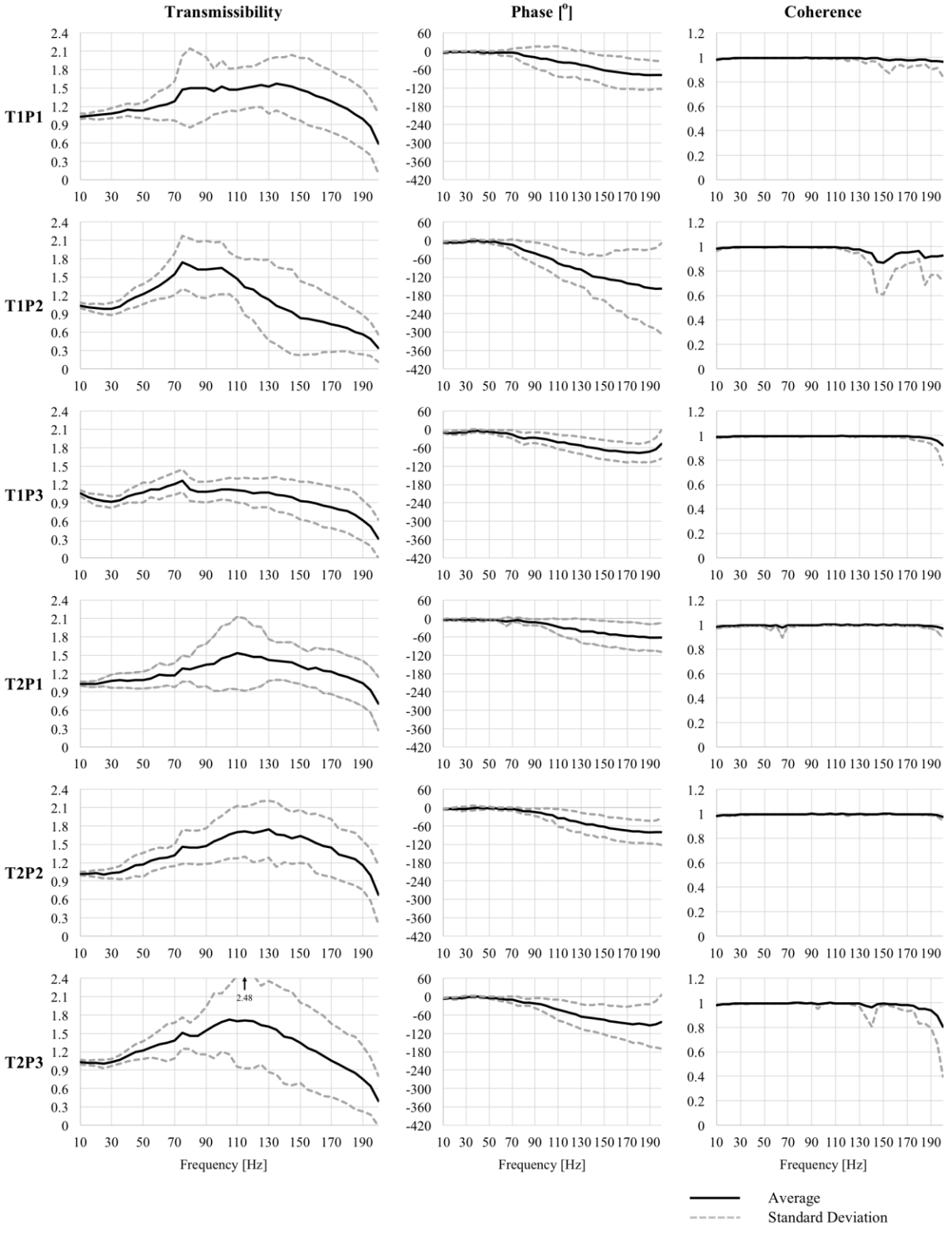

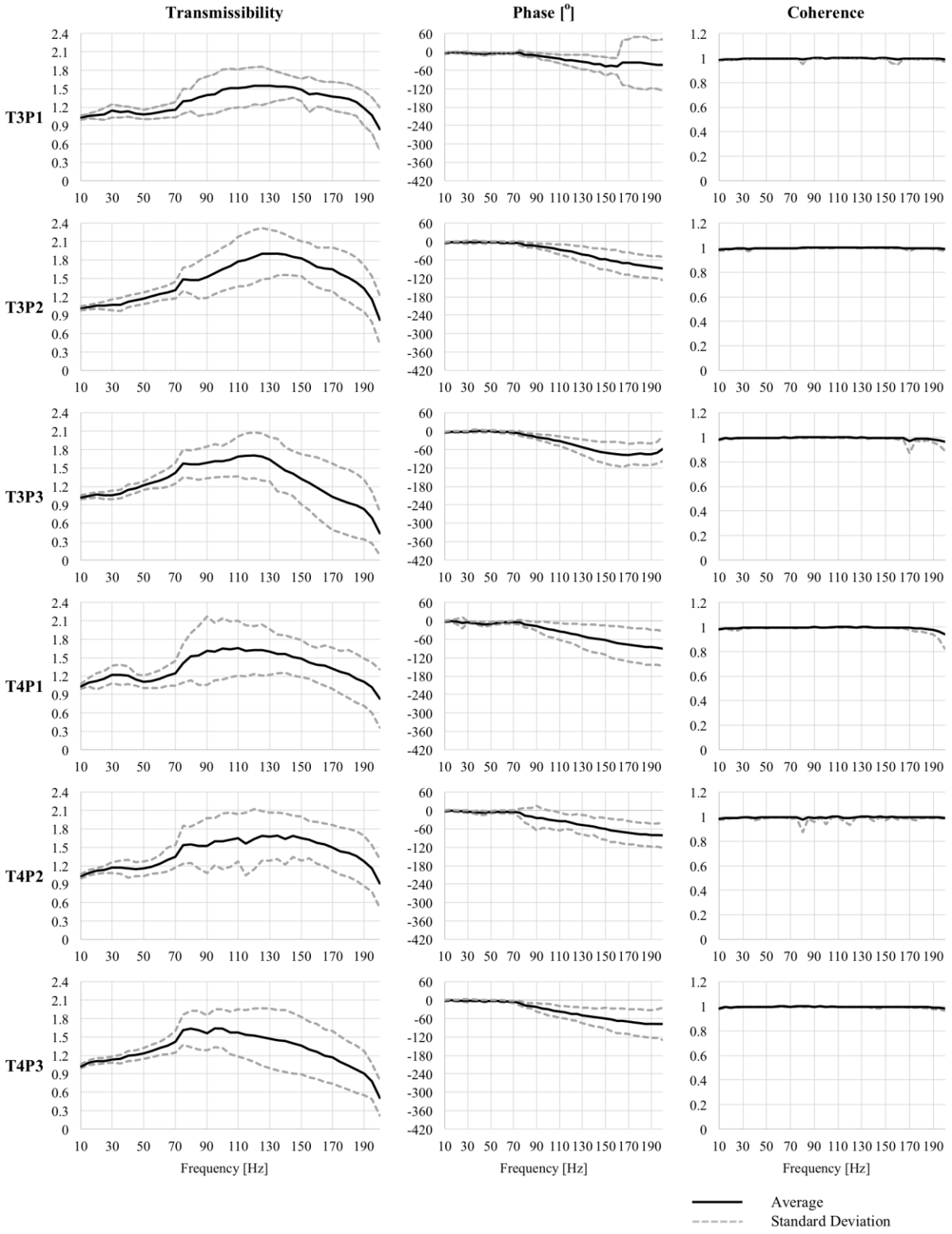
Transmissibility
Phase [°]
Coherence
T3P1
T3P2
T3P3
T4P1
T4P2
T4P3
Frequency [Hz]
Frequency [Hz]
Frequency [Hz]
Average
Standard Deviation

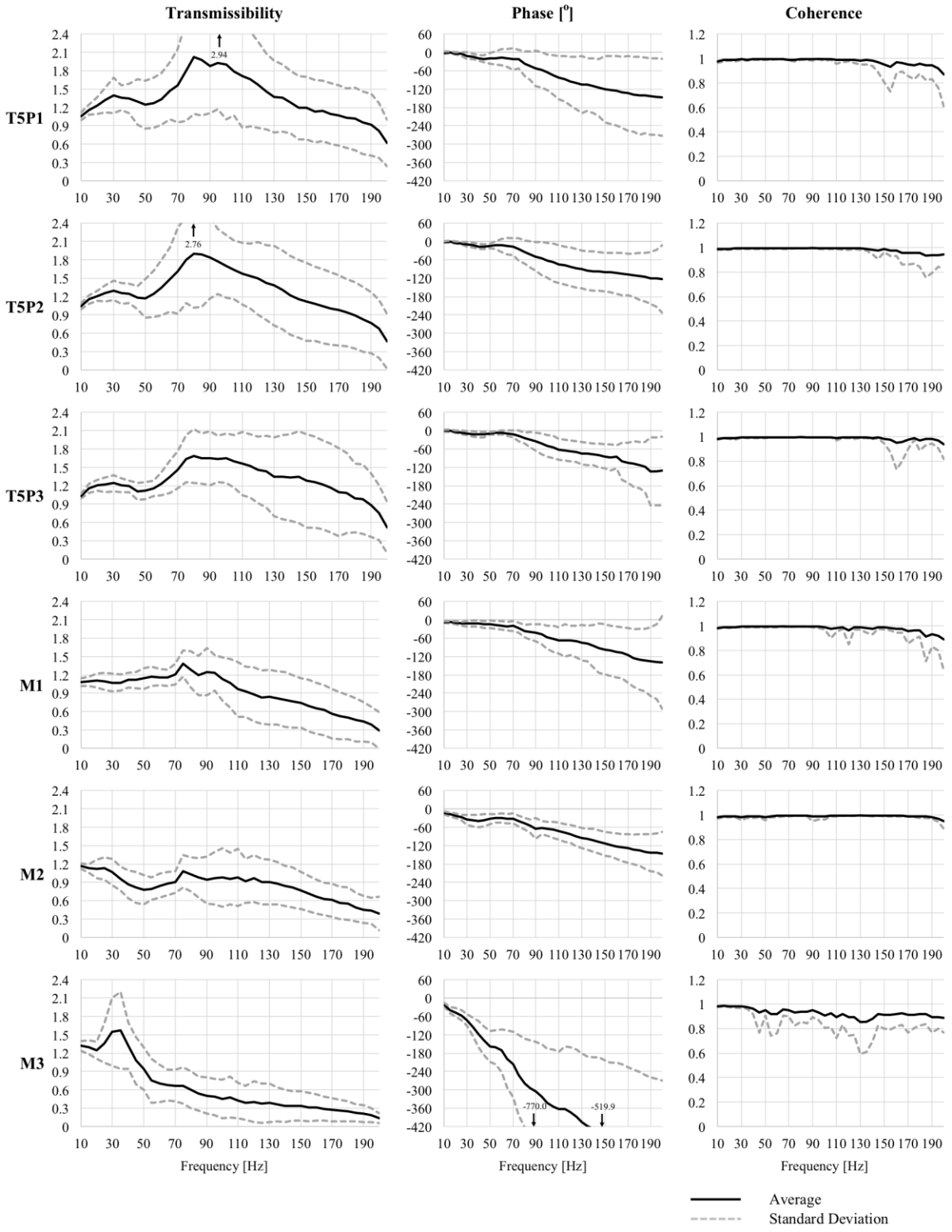
Transmissibility
Phase [°]
Coherence
T5P1
T5P2
T5P3
M1
M2
M3
2.94
2.76
-770.0
-519.9
Frequency [Hz]
Average
Standard Deviation

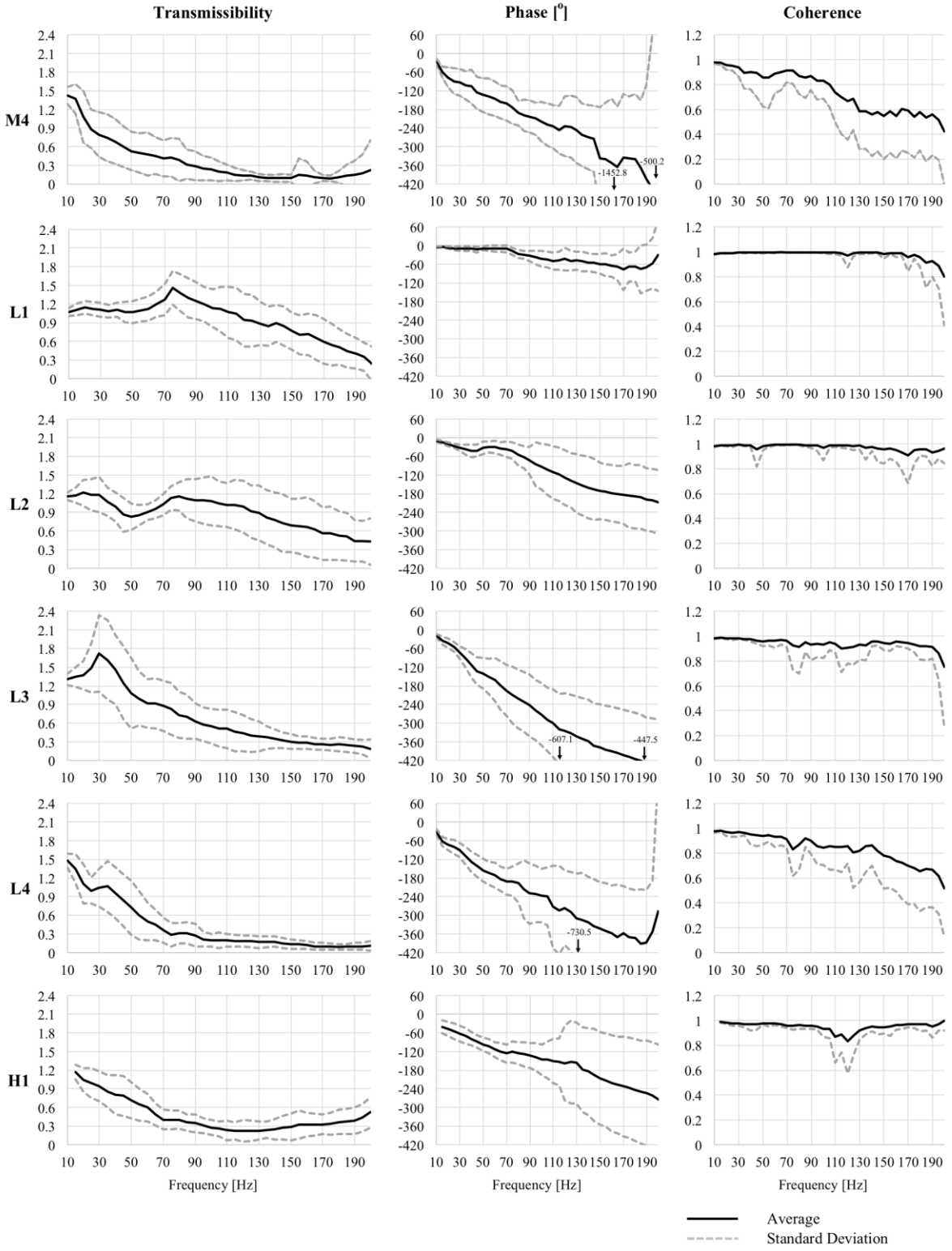
Transmissibility
Phase [°]
Coherence
M4
L1
L2
L3
L4
H1
-1452.8
-500.2
-607.1
-447.5
-730.5
Frequency [Hz]
Average
Standard Deviation

Appendix G. Laser point (LP) locations (1-4) for 21 participants at 24 anatomical locations in the forward and backward COP position.

Forward COP Position

Anatomical Location	Participant #																				
	1	2	3	4	5	6	7	8	9	10	11	12	13	14	15	16	17	18	19	20	21
T1P1	2	2	2	2	2	2	2	4	1	1	1	1	2	2	2	4	2	2	2	2	1
T2P1	2	2	2	2	2	2	2	4	1	1	2	2	2	2	2	4	2	2	2	2	1
T3P1	2	2	2	2	2	2	2	4	1	1	2	2	2	2	2	4	2	2	2	2	1
T4P1	2	2	2	2	2	2	2	4	1	1	2	2	2	2	2	4	2	2	2	2	1
T5P1	2	2	2	2	2	2	2	4	1	1	2	2	2	2	2	4	2	2	2	2	1
T1P2	2	2	2	2	2	2	2	4	1	1	2	1	2	2	2	4	2	2	2	2	1
T2P2	2	2	2	2	2	2	2	4	1	1	2	2	2	2	2	4	2	2	2	2	1
T3P2	2	2	2	2	2	2	2	4	1	1	2	2	2	2	2	4	2	2	2	2	1
T4P2	2	2	2	2	2	2	2	4	1	1	2	2	2	2	2	4	2	2	2	2	1
T5P2	2	2	2	2	2	2	2	4	1	2	2	2	2	2	2	4	2	2	2	2	1
T1P3	2	2	2	2	2	2	2	4	1	1	2	1	2	2	2	4	2	2	2	2	1
T2P3	2	2	2	2	2	2	2	4	1	1	2	2	2	2	2	4	2	2	2	2	1
T3P3	2	2	2	2	2	2	2	4	1	1	2	2	2	2	2	4	2	2	2	2	1
T4P3	2	2	2	2	2	2	2	4	1	1	2	2	2	2	2	4	2	2	2	2	1
T5P3	2	2	2	2	2	2	2	4	1	2	2	2	2	2	2	4	2	2	2	2	1
M1	2	2	2	2	2	2	2	4	1	2	2	2	2	2	2	4	2	2	2	2	1
M2	2	2	2	4	2	2	4	4	2	2	2	2	2	2	2	4	2	2	2	2	2
M3	4	2	2	4	2	4	4	4	4	2	2	4	2	2	4	4	2	2	4	2	2
M4	4	4	4	4	4	4	4	4	4	4	4	4	4	4	4	4	3	4	4	3	3
L1	2	2	2	2	2	2	2	4	2	2	2	2	2	2	2	4	2	2	2	2	1
L2	2	2	2	4	2	2	4	4	2	2	2	2	2	2	2	4	2	2	2	2	2
L3	4	2	2	4	2	4	4	4	4	2	2	4	2	2	4	4	2	2	4	2	2
L4	4	2	2	4	2	4	4	4	4	4	4	4	4	4	4	4	3	4	4	3	3
H1	3	3	3	3	3	3	4	4	4	4	4	3	3	4	3	4	3	4	4	3	3

Backward COP Position

Anatomical Location	Participant #																				
	1	2	3	4	5	6	7	8	9	10	11	12	13	14	15	16	17	18	19	20	21
T1P1	2	2	2	2	2	2	1	4	1	1	1	1	2	2	2	4	1	2	2	2	1
T2P1	2	2	2	2	2	2	1	4	1	1	1	1	2	2	2	4	1	2	2	2	1
T3P1	2	2	2	2	2	2	1	4	1	1	1	1	2	2	2	4	1	2	2	2	1
T4P1	2	2	2	2	2	2	1	4	1	1	1	1	2	2	2	4	1	2	2	2	1
T5P1	2	2	2	2	2	2	1	4	1	1	1	1	2	2	2	4	1	2	2	2	1
T1P2	2	2	2	2	2	2	1	4	1	1	1	1	2	2	2	4	1	2	2	2	1
T2P2	2	2	2	2	2	2	1	4	1	1	1	1	2	2	2	4	1	2	2	2	1
T3P2	2	2	2	2	2	2	1	4	1	1	1	1	2	2	2	4	1	2	2	2	1
T4P2	2	2	2	2	2	2	1	4	1	1	1	1	2	2	2	4	1	2	2	2	1
T5P2	2	2	2	2	2	2	1	4	1	1	1	1	2	2	2	4	1	2	2	2	1
T1P3	2	2	2	2	2	2	1	4	1	1	1	1	2	2	2	4	1	2	2	2	1
T2P3	2	2	2	2	2	2	1	4	1	1	1	1	2	2	2	4	1	2	2	2	1
T3P3	2	2	2	2	2	2	1	4	1	1	1	1	2	2	2	4	1	2	2	2	1
T4P3	2	2	2	2	2	2	1	4	1	1	1	1	2	2	2	4	1	2	2	2	1
T5P3	2	2	2	2	2	2	1	4	1	1	1	1	2	2	2	4	1	2	2	2	1
M1	2	4	2	2	2	2	1	4	2	2	4	1	2	2	2	4	1	2	2	2	1
M2	4	4	2	2	4	4	2	4	2	2	4	2	2	2	2	4	2	2	2	2	2
M3	4	4	2	4	4	4	2	4	4	2	4	2	2	2	2	4	2	2	2	2	2
M4	4	4	3	4	2	4	4	4	4	3	4	4	4	4	4	4	4	4	4	3	3
L1	2	4	2	2	2	2	1	4	2	2	4	1	2	2	2	4	1	2	2	2	2
L2	4	4	2	2	4	2	2	4	2	2	4	2	2	2	2	4	2	2	2	2	2
L3	4	4	2	4	4	4	2	4	4	2	4	2	2	2	2	4	2	2	2	2	2
L4	4	4	3	2	3	4	4	4	4	2	4	2	2	2	3	4	4	4	2	3	3
H1	3	3	3	3	3	3	3	4	4	3	4	4	4	2	3	4	4	4	4	3	3

Appendix H. Excluded measurements (black) based on coherence, noise presence, or signal quality

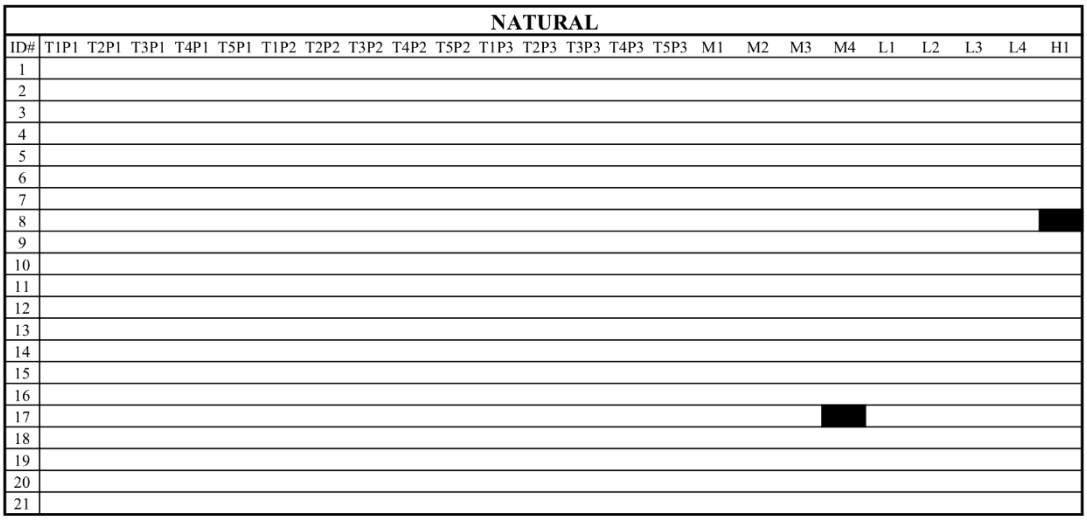

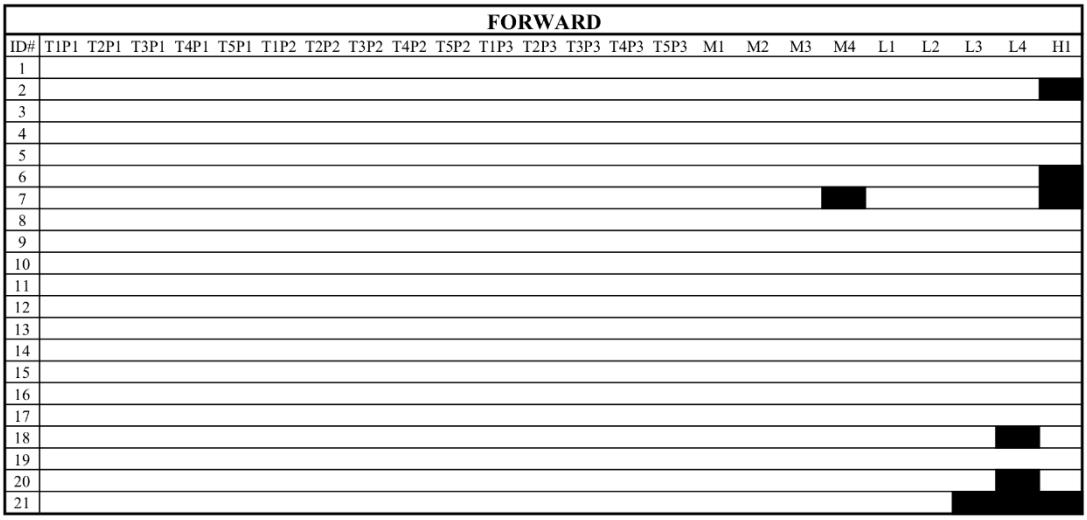

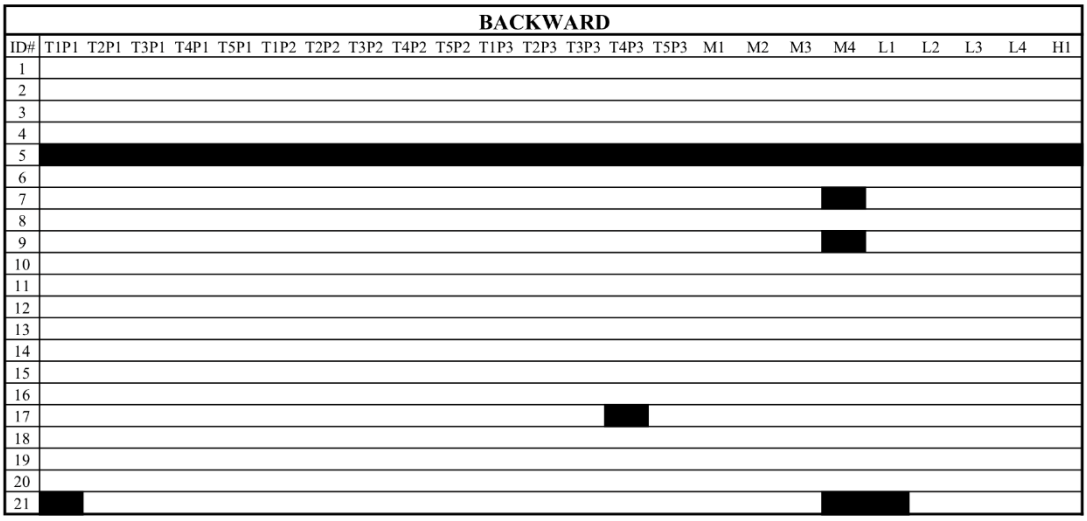

Appendix I. Summary of participant anthropometric information measured using the Pedar Expert (11.3.12) insole measurement system

Participant #	Height [cm]	Weight [kg]	Foot Length [cm]	Position	Maximum Force [N]		COP Position [cm]		Mean Pressure [kPa]	
					Left	Right	x	y	Left	Right
1	173	74	25.5	P1	318.0	290.4	5.15	4.42	79.5	75.7
				P2	266.2	257.7	5.18	12.0	46.3	42.1
				P3	323.3	258.1	4.84	6.95	58.0	47.7
2	187	93	28.5	P1	327.8	357.5	5.65	11.0	51.0	64.1
				P2	293.9	297.0	4.21	15.7	41.2	37.9
				P3	192.8	473.0	5.49	3.72	44.4	108.6
3	186	83	29	P1	331.7	319.6	5.22	5.69	59.5	57.3
				P2	298.2	259.0	4.20	16.0	42.7	43.7
				P3	342.6	342.9	5.27	6.44	70.1	70.2
4	165.5	75	23.5	P1	294.4	256.4	5.03	8.69	48.2	44.6
				P2	277.1	290.6	5.28	16.7	54.8	52.0
				P3	337.1	254.8	5.00	6.83	77.3	60.9
5	166.3	63	24.5	P1	278.6	276.9	5.38	7.84	69.5	63.5
				P2	272.0	241.3	4.83	11.4	47.3	46.0
				P3	292.2	283.4	5.70	4.42	79.8	70.7
6	192	94	29.5	P1	399.1	432.0	5.35	5.77	45.7	65.0
				P2	376.9	405.3	4.32	19.3	67.5	70.6
				P3	497.2	372.0	5.55	3.06	71.2	112.4
7	173	64	24.7	P1	256.5	241.0	5.15	3.17	40.8	40.6
				P2	225.9	247.8	3.86	15.9	43.2	41.8
				P3	246.8	280.4	4.92	4.78	50.6	69.9
8	170	54	25.2	P1	101.4	96.8	4.61	9.90	32.3	37.0
				P2	218.3	149.5	2.20	19.6	56.9	45.4
				P3	134.3	138.2	4.11	2.92	77.1	88.0
9	170	65	25.8	P1	326.9	255.8	4.57	16.2	55.2	44.5
				P2	327.0	293.9	3.82	20.1	69.9	45.8
				P3	391.1	258.0	4.67	4.81	112.3	78.0
10	178	59	25	P1	332.8	189.1	4.90	8.68	61.6	43.3
				P2	235.7	258.8	4.13	16.6	45.1	47.7
				P3	349.2	204.2	5.18	4.42	95.4	69.0
11	186	70	27.3	P1	44.0	74.7	4.36	7.95	28.0	26.7
				P2	99.9	203.9	2.87	19.5	38.1	50.8
				P3	164.4	140.2	5.51	2.21	67.4	73.5
12	187	85	26.9	P1	73.7	216.5	4.91	6.57	38.6	73.0
				P2	191.2	177.6	3.36	19.7	49.8	48.4
				P3	179.8	363.2	5.19	2.95	86.1	122.7
13	178	84	26.0	P1	371.9	457.9	6.11	11.0	59.2	65.8
				P2	383.0	485.1	3.70	15.9	61.0	60.5
				P3	385.1	503.7	4.91	6.51	71.1	80.3
14	185	72	27.0	P1	76.4	53.4	5.42	8.75	33.7	27.7
				P2	74.8	160.6	2.86	21.7	48.1	54.2
				P3	106.4	210.8	5.20	3.46	50.8	71.2

Participant #	Height [cm]	Weight [kg]	Foot Length [cm]	Position	Maximum Force [N]		Area [cm^2]		Mean Pressure [kPa]	
					Left	Right	Left	Right	Left	Right
15	180	73	26.2	P1	433.1	339.8	5.23	5.76	75.2	54.2
				P2	409.4	372.5	4.37	12.5	60.2	50.9
				P3	380.5	449.9	5.24	3.53	109.2	123.0
16	158	41	21.0	P1	130.8	163.2	5.30	8.34	34.1	42.6
				P2	157.8	169.9	4.13	15.9	39.2	40.5
				P3	177.7	182.4	4.85	4.29	51.1	65.5
17	170	52	25.0	P1	248.8	191.7	4.48	10.1	49.3	45.9
				P2	204.2	221.5	3.89	15.2	35.6	35.3
				P3	219.6	288.3	4.72	3.35	74.2	110.4
18	165	53	23.5	P1	169.1	176.8	3.40	8.28	42.3	35.0
				P2	145.1	181.6	5.58	16.4	46.5	52.1
				P3	164.5	281.5	5.82	4.49	72.8	62.2
19	165	53	23.5	P1	308.5	349.2	4.75	9.45	53.8	52.7
				P2	271.2	309.7	5.32	15.4	52.1	48.0
				P3	306.4	358.5	5.08	5.39	67.7	76.1
20	170	74	24.6	P1	341.5	407.9	4.98	8.42	57.6	75.5
				P2	318.1	380.3	4.73	13.9	48.0	49.6
				P3	330.2	503.3	5.42	4.86	82.5	90.1
21	170	62	25.0	P1	261.8	241.1	4.35	9.79	45.5	40.6
				P2	217.2	308.9	3.36	19.8	41.7	52.3
				P3	307.1	324.0	5.30	3.72	93.0	80.9

*Note: P1 = Natural, P2 = Forward Lean, P3 = Backward Lean

Appendix J. Individual transmissibility responses of 21 participants in two positions (forward lean, backward lean) at 24 anatomical locations.

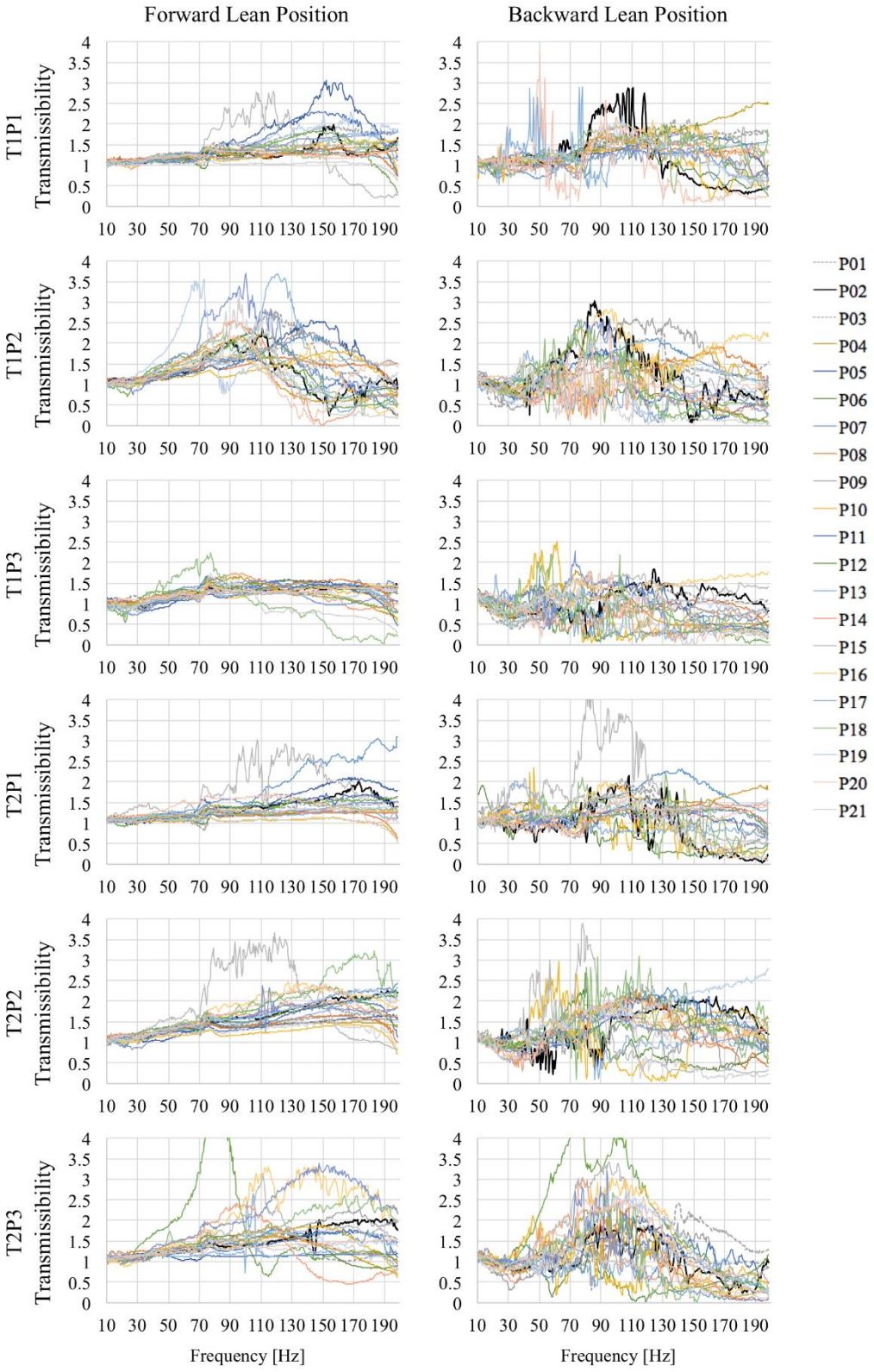

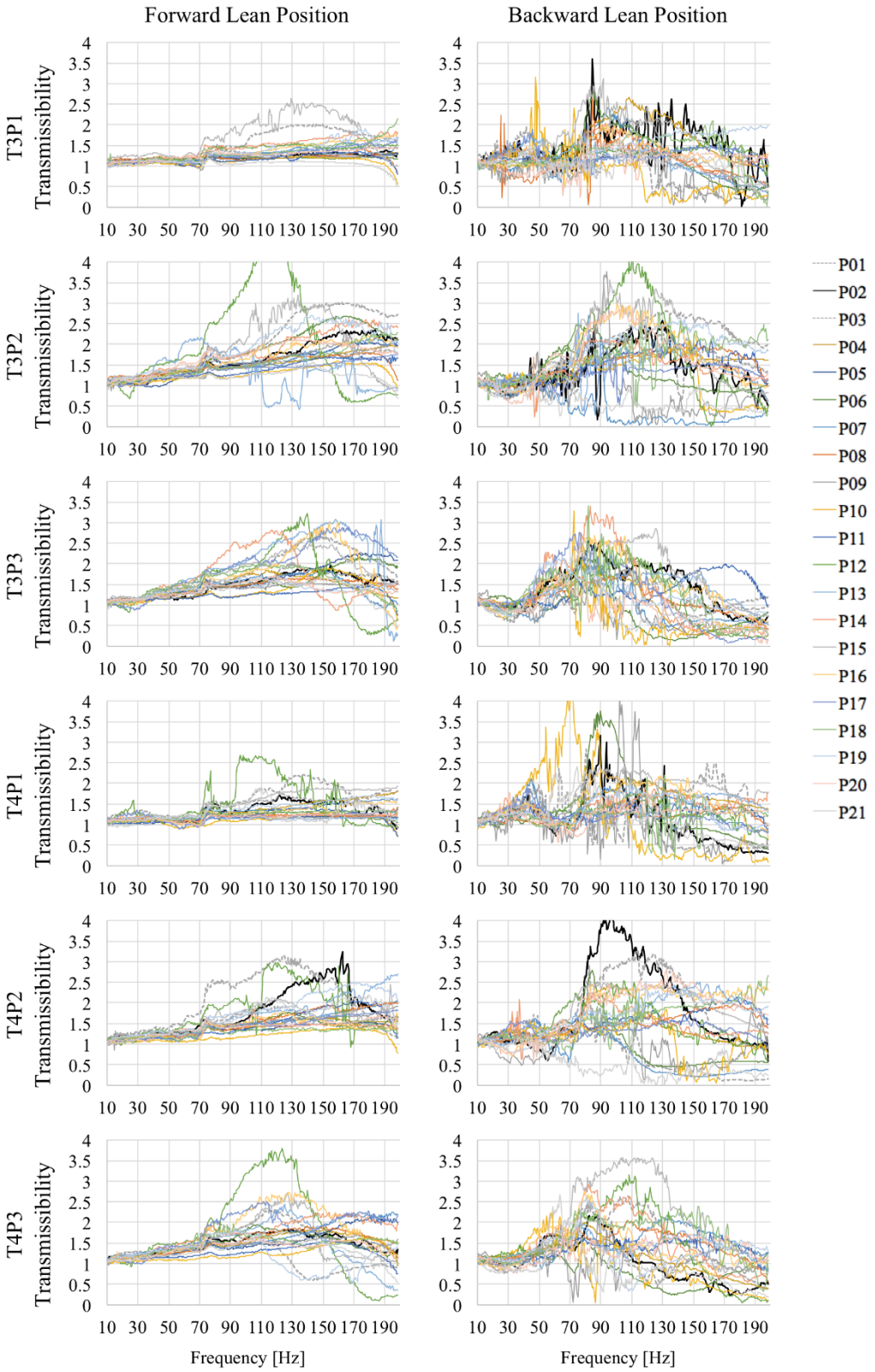
Forward Lean Position
Backward Lean Position
T3P1
T3P2
T3P3
T4P1
T4P2
T4P3
Transmissibility
0
0.5
1
1.5
2
2.5
3
3.5
4
10 30 50 70 90 110 130 150 170 190
Frequency [Hz]
P01
P02
P03
P04
P05
P06
P07
P08
P09
P10
P11
P12
P13
P14
P15
P16
P17
P18
P19
P20
P21

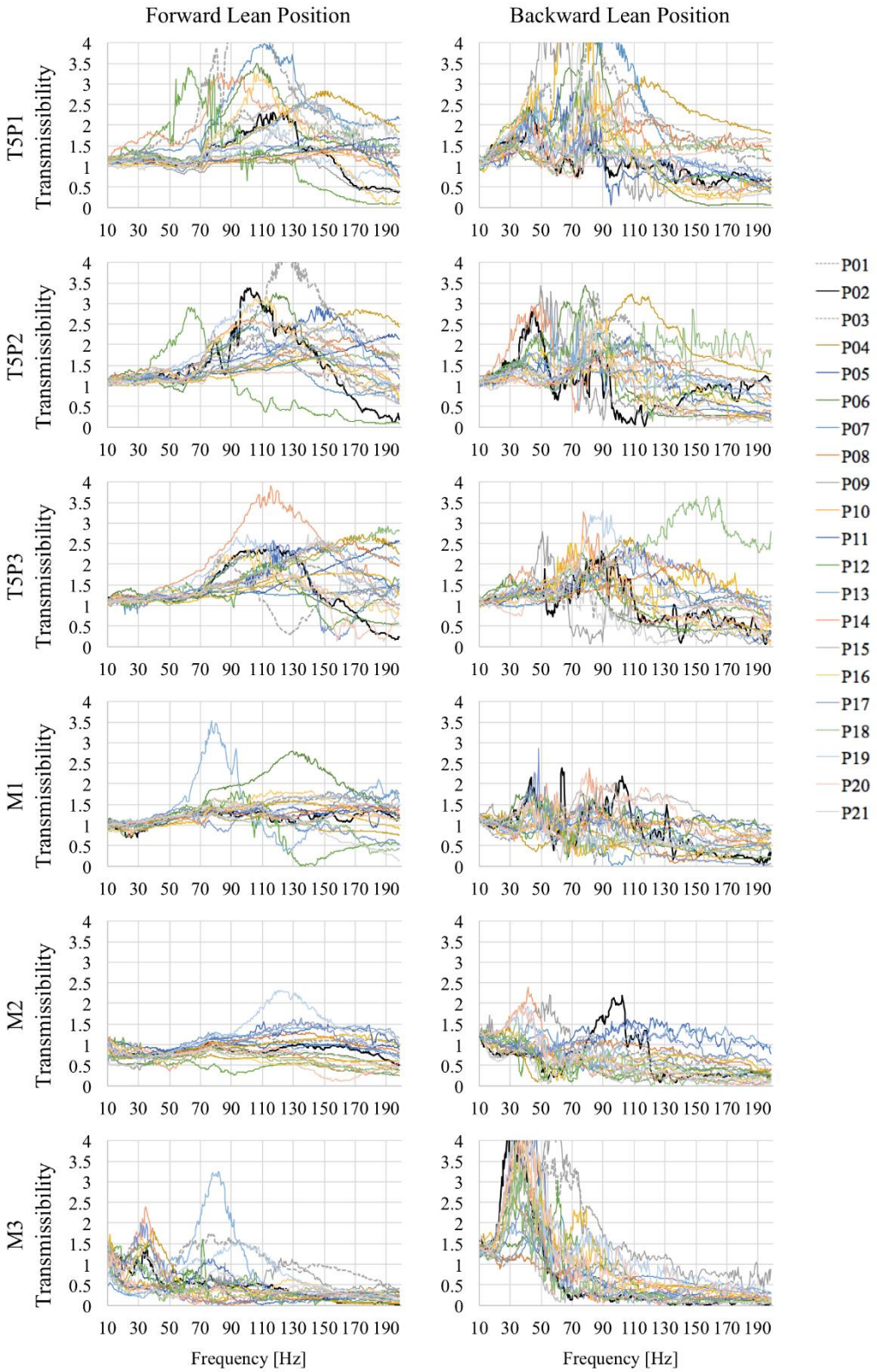
Forward Lean Position
Backward Lean Position
T5P1
T5P2
T5P3
M1
M2
M3
Transmissibility
0
0.5
1
1.5
2
2.5
3
3.5
4
10 30 50 70 90 110 130 150 170 190
Frequency [Hz]
P01
P02
P03
P04
P05
P06
P07
P08
P09
P10
P11
P12
P13
P14
P15
P16
P17
P18
P19
P20
P21

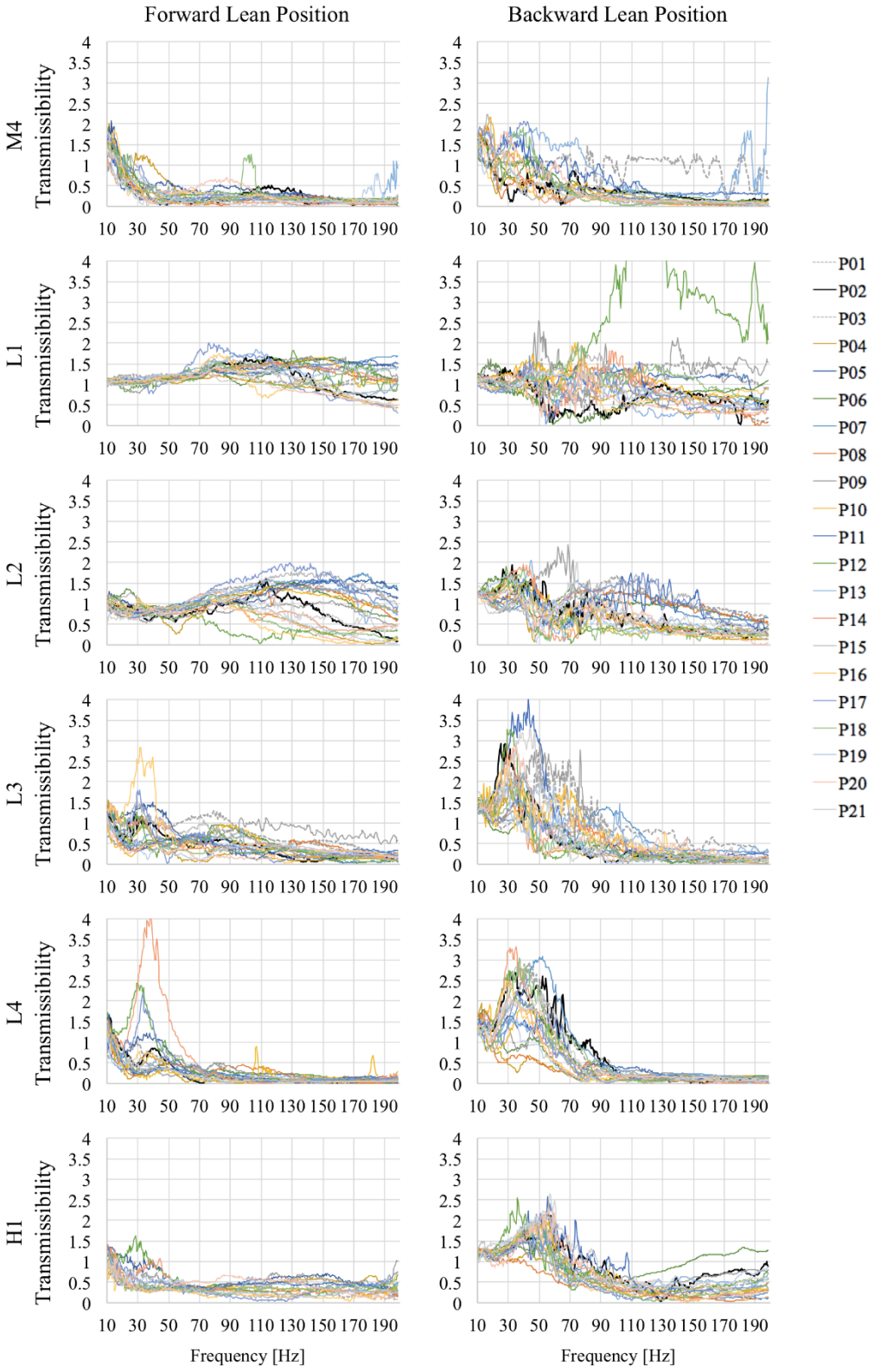
Forward Lean Position
Backward Lean Position
M4
L1
L2
L3
L4
H1
Transmissibility
0
0.5
1
1.5
2
2.5
3
3.5
4
10 30 50 70 90 110 130 150 170 190
Frequency [Hz]
P01
P02
P03
P04
P05
P06
P07
P08
P09
P10
P11
P12
P13
P14
P15
P16
P17
P18
P19
P20
P21

Appendix K. The average (black line) ± standard deviation (grey dotted line) transmissibility, phase and coherence of 21 participants for 24 anatomical locations in the forward COP position.

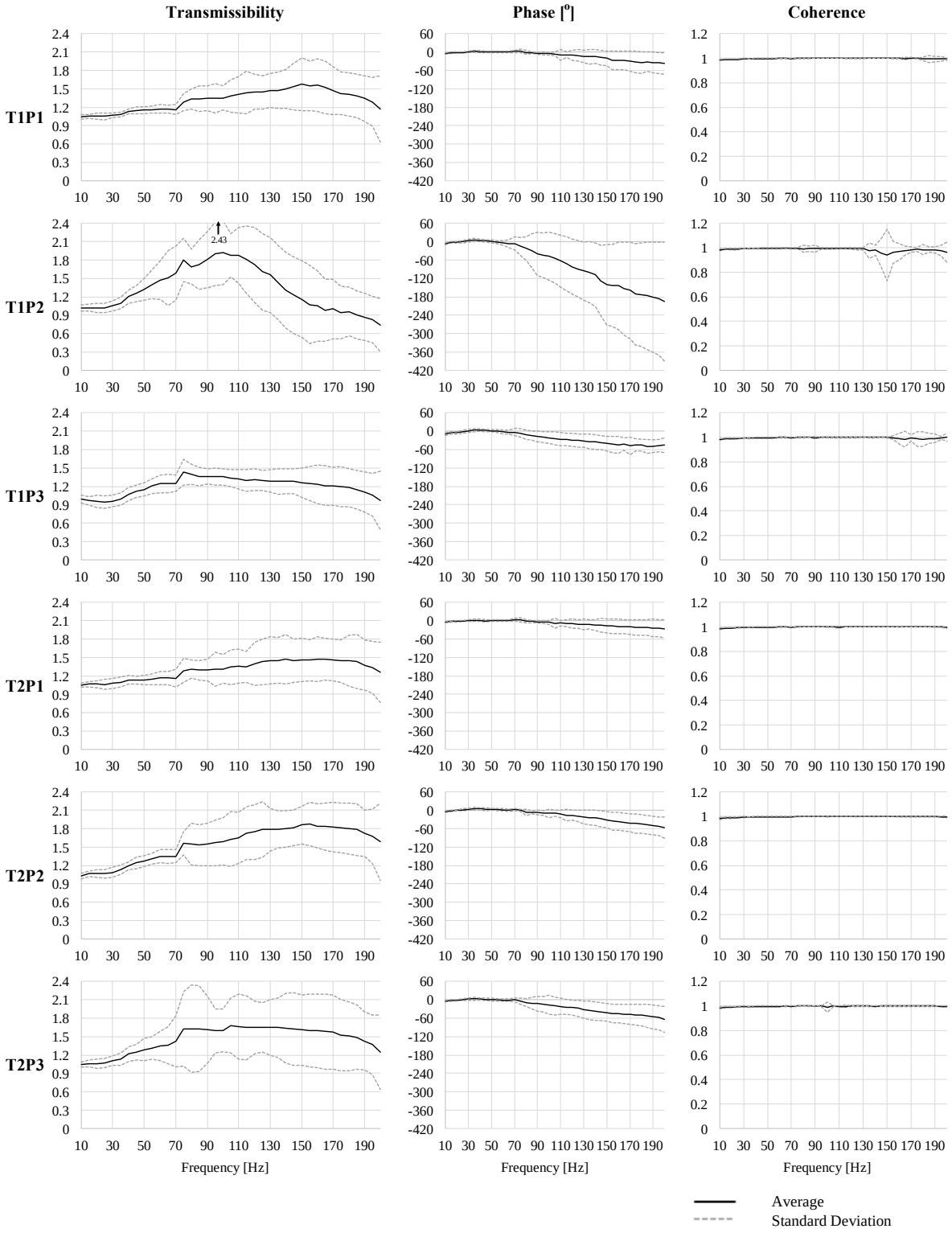

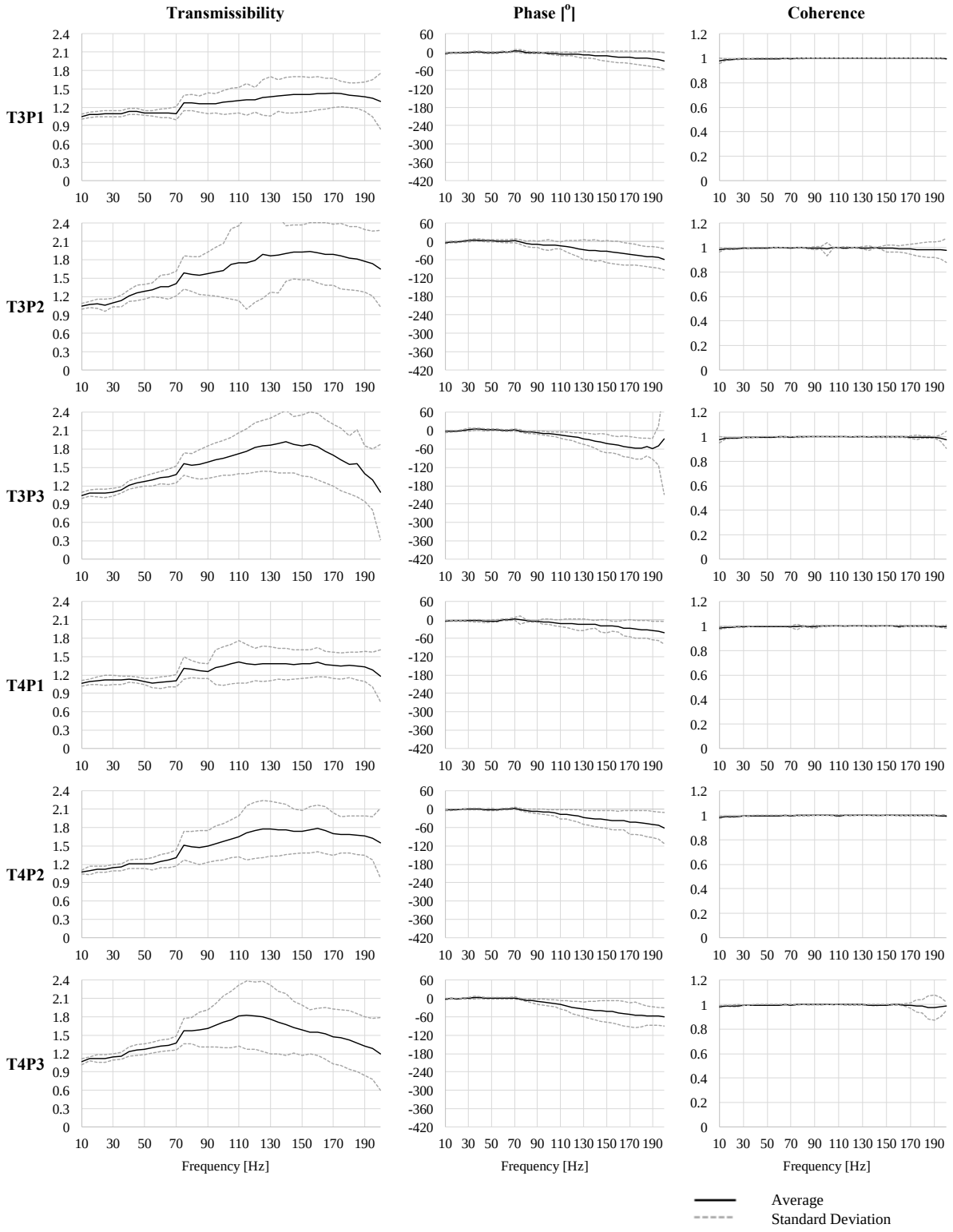
Transmissibility
Phase [°]
Coherence
T3P1
T3P2
T3P3
T4P1
T4P2
T4P3
Frequency [Hz]
Frequency [Hz]
Frequency [Hz]
Average
Standard Deviation

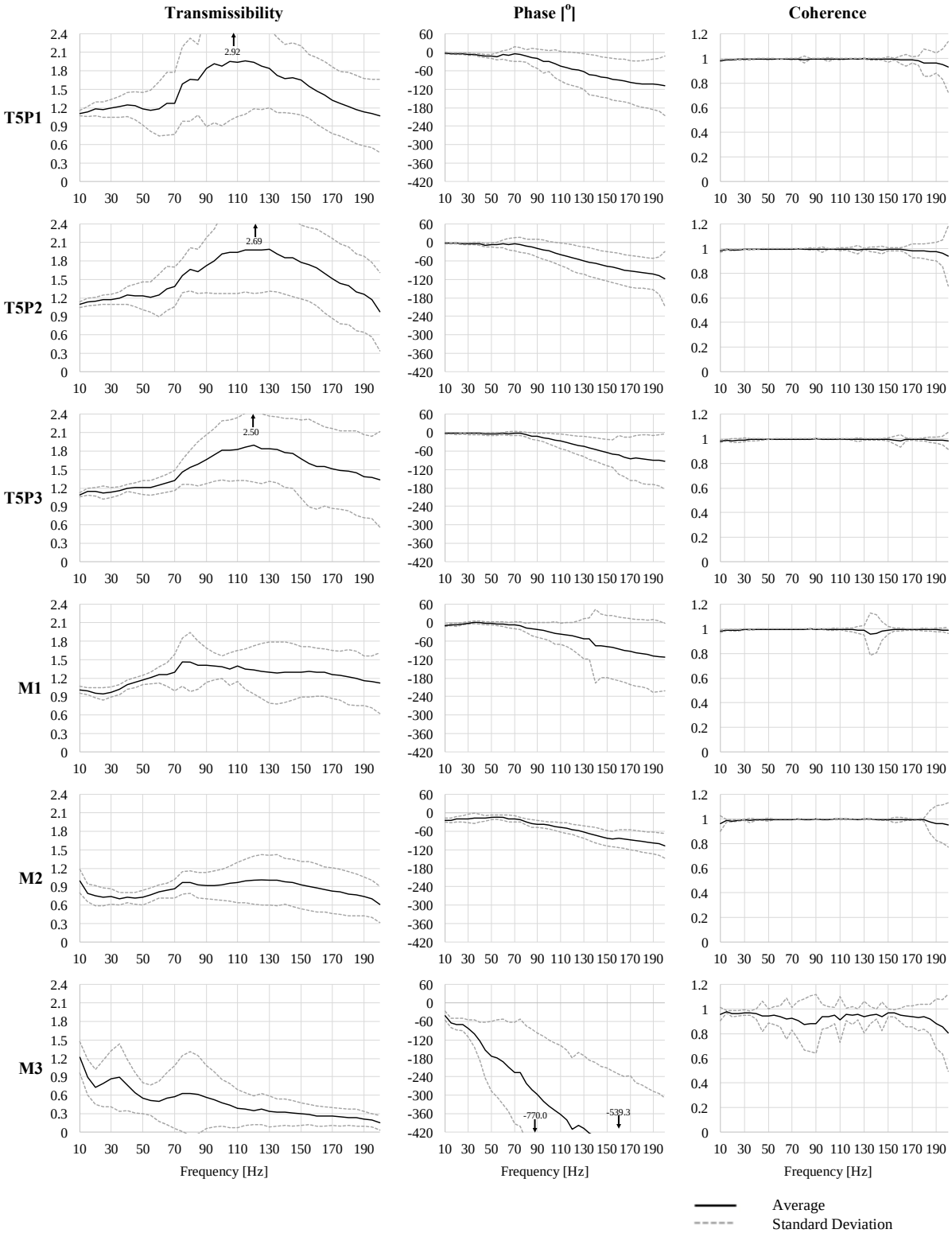
Transmissibility
Phase |°|
Coherence
T5P1
T5P2
T5P3
M1
M2
M3
2.92
2.69
2.50
-770.0
-539.3
Frequency [Hz]
Frequency [Hz]
Frequency [Hz]
Average
Standard Deviation

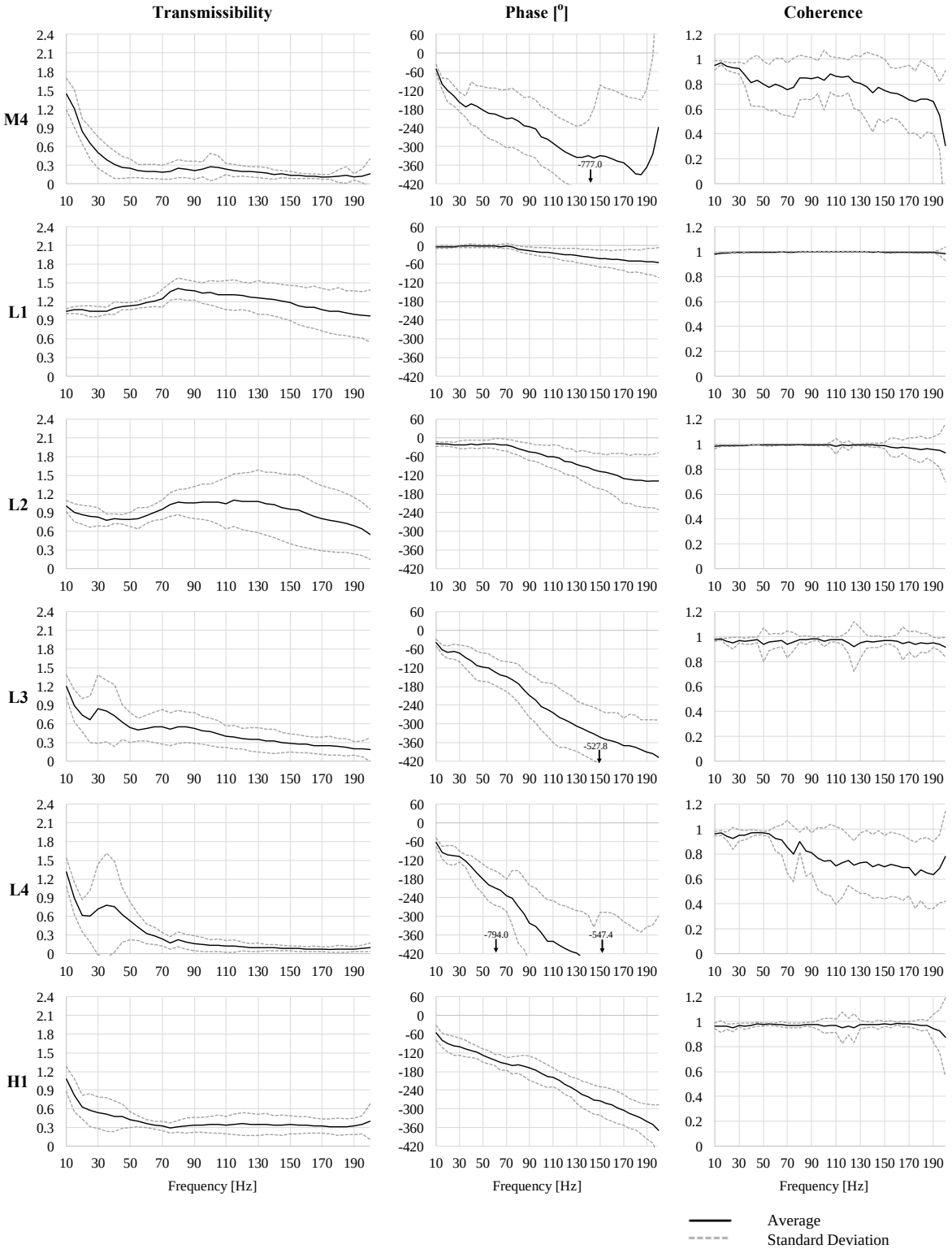
Transmissibility
Phase [°]
Coherence
M4
L1
L2
L3
L4
H1
-777.0
-527.8
-794.0
-547.4
Frequency [Hz]
Frequency [Hz]
Frequency [Hz]
Average
Standard Deviation

Appendix L. The average (black line) ± standard deviation (grey dotted line) transmissibility, phase and coherence of 21 participants for 24 anatomical locations in the backward COP position.

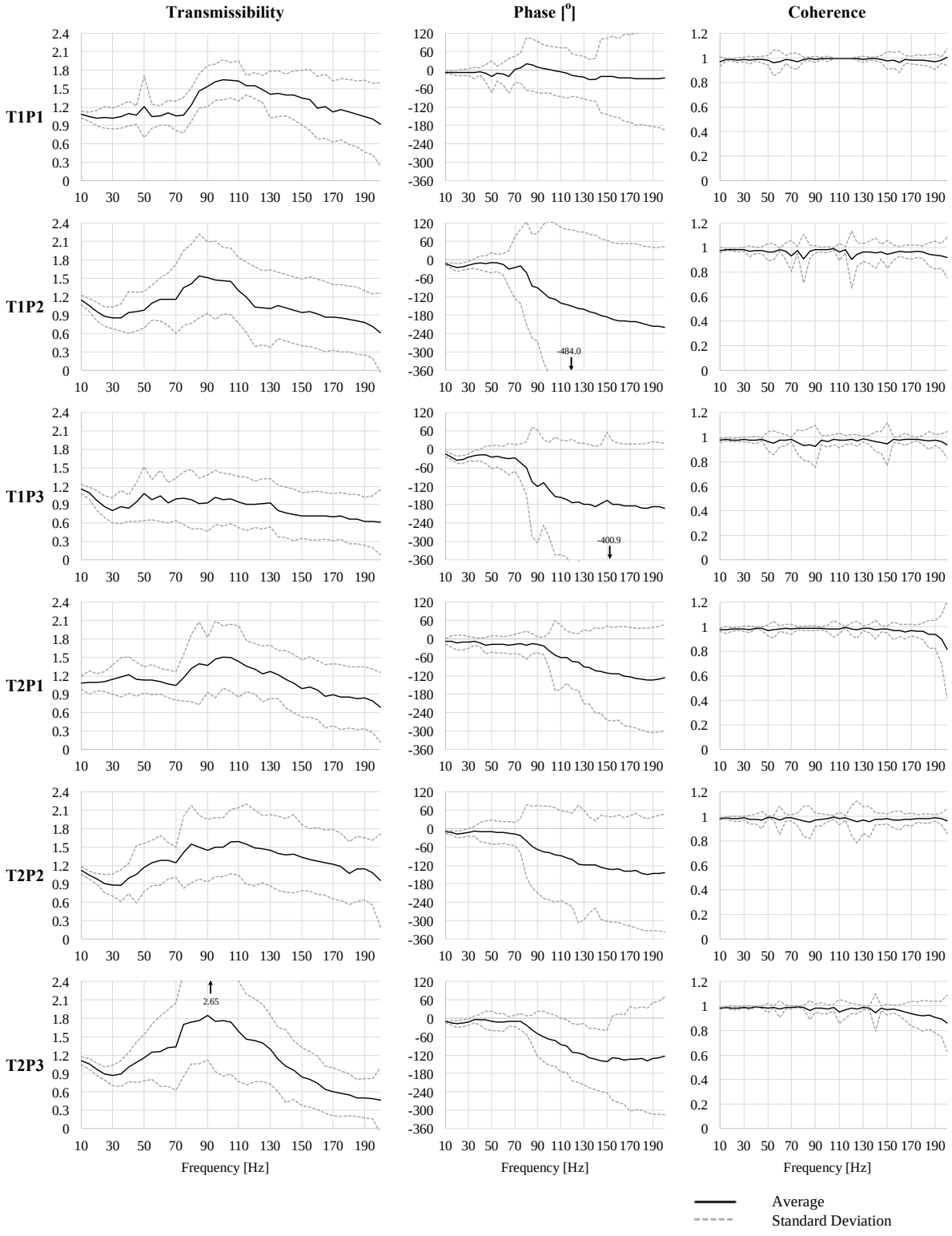

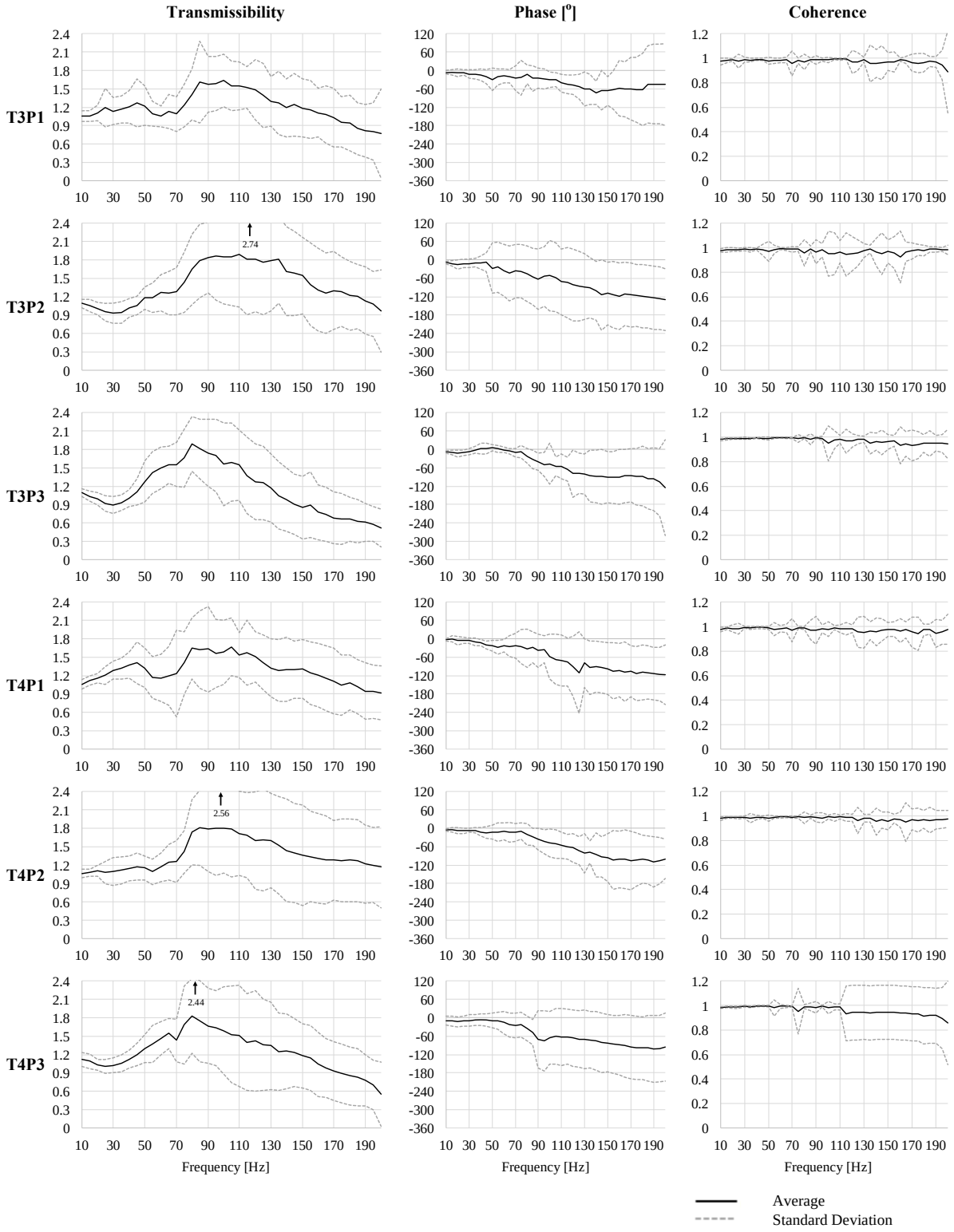
Transmissibility
Phase [°]
Coherence
T3P1
T3P2
T3P3
T4P1
T4P2
T4P3
2.74
2.56
2.44
Frequency [Hz]
Frequency [Hz]
Frequency [Hz]
Average
Standard Deviation

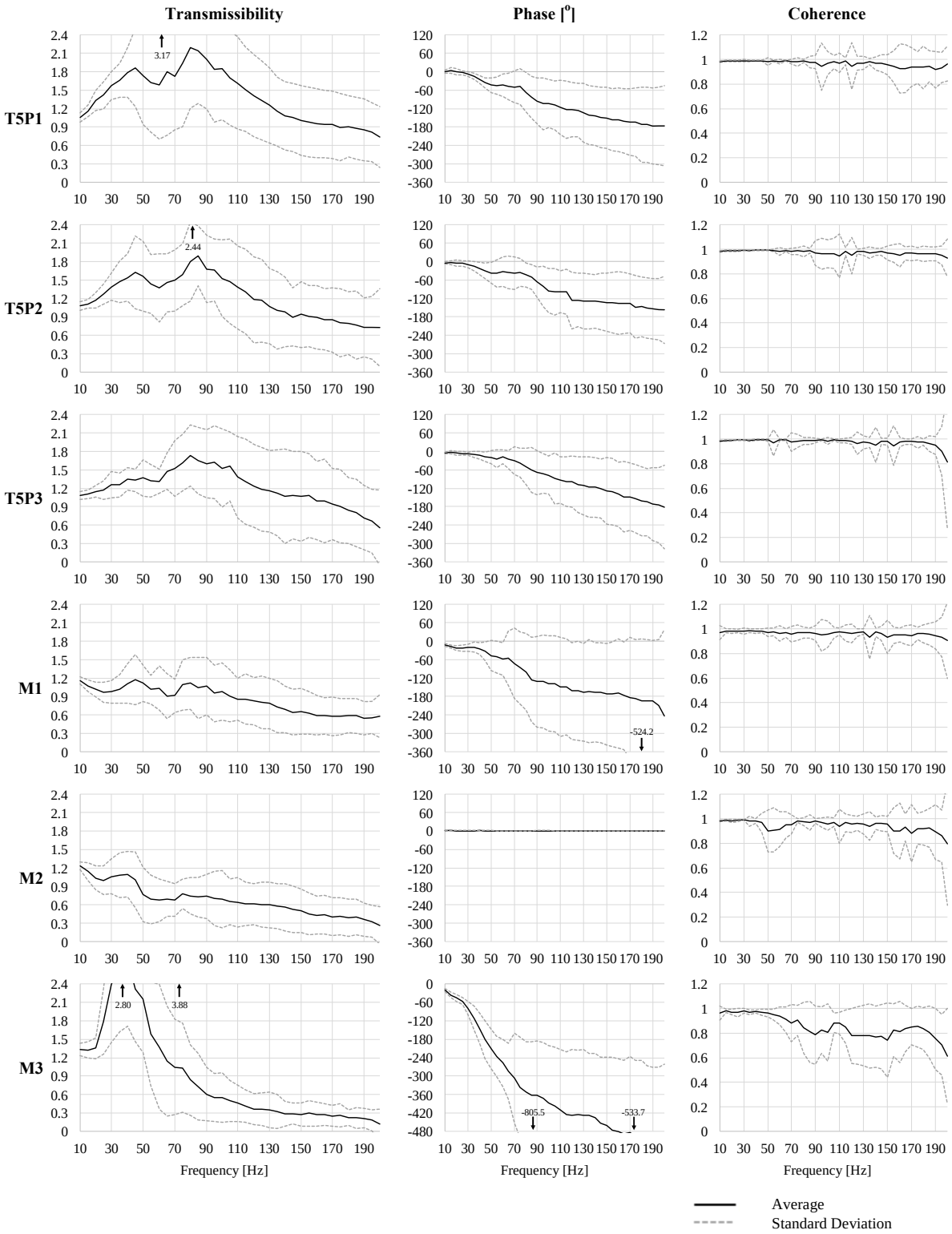
Transmissibility
Phase [°]
Coherence
T5P1
T5P2
T5P3
M1
M2
M3
3.17
2.44
-524.2
2.80
3.88
-805.5
-533.7
Frequency [Hz]
Frequency [Hz]
Frequency [Hz]
Average
Standard Deviation

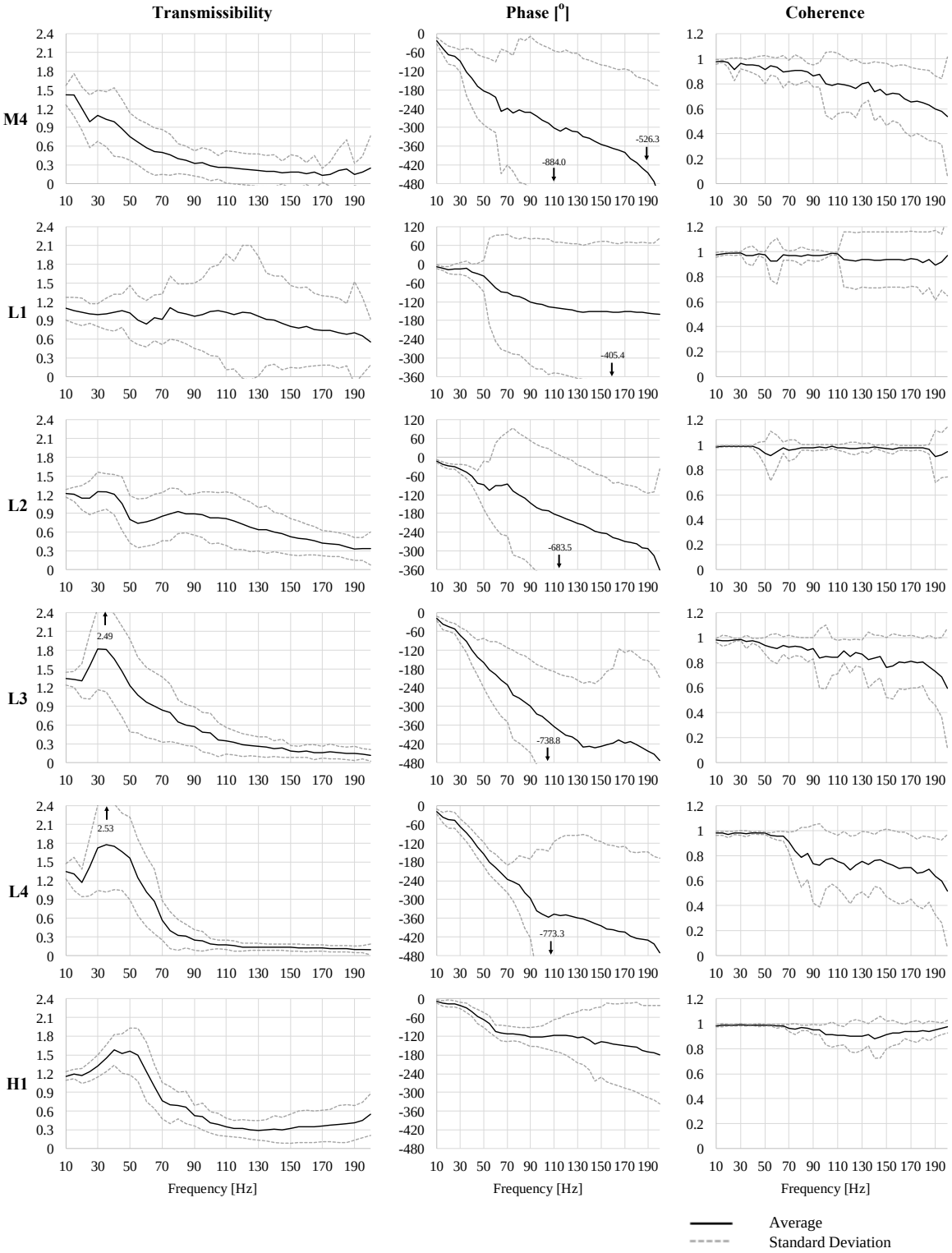
Transmissibility
Phase [°]
Coherence
M4
L1
L2
L3
L4
H1
-884.0
-526.3
-405.4
-683.5
-738.8
-773.3
2.49
2.53
Frequency [Hz]
Frequency [Hz]
Frequency [Hz]
Average
Standard Deviation

Appendix M. Derivation of the generalized mass matrix $\boldsymbol{M}$

$$\boldsymbol{M} = \begin{bmatrix} \left(\frac{\partial y_1}{\partial y_3}\right)^2 m_1 & 0 & 0 & 0 & 0 \\ 0 & \left(\frac{\partial \oplus_{y_{m_2}}}{\partial y_3}\right)^2 m_2 + \left(\frac{\partial \oplus_{y_{m3}}}{\partial y_3}\right)^2 m_3 & \left(\frac{\partial \oplus_{y_{m_2}}}{\partial y_3} \cdot m_2\right)\frac{\partial \oplus_{y_{m_2}}}{\partial \theta_1} & \left(\frac{\partial \oplus_{y_{m_3}}}{\partial y_3} \cdot m_3\right)\frac{\partial \oplus_{y_{m_3}}}{\partial \theta_2} & 0 \\ 0 & \left(\frac{\partial \oplus_{y_{m_2}}}{\partial \theta_1}\right)^2 m_2 & \left(\frac{\partial \oplus_{x_{m_2}}}{\partial \theta_1}\right)^2 m_2 + \left(\frac{\partial \oplus_{y_{m_2}}}{\partial \theta_1}\right)^2 m_2 + \left(\frac{\partial I_{\theta_1}}{\partial \theta_1}\right)^2 I_{m_2} & 0 & 0 \\ 0 & \left(\frac{\partial \oplus_{y_{m_3}}}{\partial \theta_2} \cdot m_3\right)\frac{\partial \oplus_{y_{m_3}}}{\partial y_3} & 0 & \left(\frac{\partial \oplus_{x_{m_3}}}{\partial \theta_2}\right)^2 m_3 + \left(\frac{\partial \oplus_{y_{m_3}}}{\partial \theta_2}\right)^2 m_3 + \left(\frac{\partial I_{\theta_2}}{\partial \theta_2}\right) I_{m_3} & 0 \\ 0 & 0 & 0 & 0 & 0 \end{bmatrix}$$

$$\boldsymbol{M}` = \begin{bmatrix} m_1 & 0 & 0 & 0 & 0 \\ 0 & m_2 + m_3 & m_2\left(\frac{\partial \oplus_{y_{m_2}}}{\partial \theta_1}\right) & m_3\left(\frac{\partial \oplus_{y_{m_3}}}{\partial \theta_2}\right) & 0 \\ 0 & \left(\frac{\partial \oplus_{y_{m_2}}}{\partial \theta_1}\right)^2 m_2 & \left(\frac{\partial \oplus_{x_{m_2}}}{\partial \theta_1}\right)^2 m_2 + \left(\frac{\partial \oplus_{y_{m_2}}}{\partial \theta_1}\right)^2 m_2 + I_{m_2} & 0 & 0 \\ 0 & \frac{\partial \oplus_{y_{m_3}}}{\partial \theta_2} \cdot m_3 & 0 & \left(\frac{\partial \oplus_{x_{m_3}}}{\partial \theta_2}\right)^2 m_3 + \left(\frac{\partial \oplus_{y_{m_3}}}{\partial \theta_2}\right)^2 m_3 + I_{m_3} & 0 \\ 0 & 0 & 0 & 0 & 0 \end{bmatrix}$$

$$\boldsymbol{M} = \begin{bmatrix} (1)^2 35 & 0 & 0 & 0 & 0 \\ 0 & (1)^2 0.294 + (1)^2 0.686 & (1 \cdot 0.294)0.0371 & (1 \cdot 0.686)0.0493 & 0 \\ 0 & (-0.0371)^2 0.294 & (-0.0139)^2 0.294 + (0.0371)^2 0.294 + (1)^2 0.00028 & 0 & 0 \\ 0 & (0.0493 \cdot 0.686)\ 1 & 0 & (0.0196)^2 0.686 + (0.0493)^2 0.686 + (1)0.00000555 & 0 \\ 0 & 0 & 0 & 0 & 0 \end{bmatrix}$$

$$\boldsymbol{M} = \begin{bmatrix} 35 & 0 & 0 & 0 & 0 \\ 0 & 0.98 & 0.0109 & 0.0338 & 0 \\ 0 & 0.0109 & 0.00741 & 0 & 0 \\ 0 & 0.0338 & 0 & 0.00193 & 0 \\ 0 & 0 & 0 & 0 & 0 \end{bmatrix}$$

Appendix N. Derivation of the generalized damping matrix $\boldsymbol{C}$

$$\boldsymbol{C}=\begin{bmatrix} \left(\frac{\partial\delta_3}{\partial y_1}\right)^2 c_3 & \left(\frac{\partial\delta_3}{\partial y_1}\cdot c_3\right)\frac{\partial\delta_3}{\partial y_3} & 0 & 0 & 0 \\ \left(\frac{\partial\delta_3}{\partial y_3}\cdot c_3\right)\frac{\partial\delta_3}{\partial y_1} & \left(\frac{\partial\delta_3}{\partial y_3}\right)^2 c_3+\left(\frac{\partial\delta_2}{\partial y_3}\right)^2 c_2+\left(\frac{\partial\delta_4}{\partial y_3}\right)^2 c_4 & \left(\frac{\partial\delta_2}{\partial y_3}\right)^2 c_2 & \left(\frac{\partial\delta_4}{\partial y_3}\cdot c_4\right)\frac{\partial\delta_4}{\partial\theta_2} & \left(\frac{\partial\delta_2}{\partial y_3}\cdot c_2\right)\frac{\partial\delta_2}{\partial y_2}+\left(\frac{\partial\delta_4}{\partial y_3}\cdot c_4\right)\frac{\partial\delta_4}{\partial y_4} \\ 0 & \left(\frac{\partial\delta_2}{\partial\theta_1}\cdot c_2\right)\frac{\partial\delta_2}{\partial y_3} & \left(\frac{\partial\delta_1}{\partial\theta_1}\right)^2 c_1+\left(\frac{\partial\delta_2}{\partial\theta_1}\right)^2 c_2 & \left(\frac{\partial\delta_1}{\partial\theta_1}\right)^2 c_1 & \left(\frac{\partial\delta_2}{\partial\theta_1}\cdot c_2\right)\frac{\partial\delta_2}{\partial y_2} \\ 0 & \left(\frac{\partial\delta_4}{\partial\theta_2}\cdot c_4\right)\frac{\partial\delta_4}{\partial y_3} & \left(\frac{\partial\delta_1}{\partial\theta_2}\cdot c_1\right)\frac{\partial\delta_1}{\partial\theta_1} & \left(\frac{\partial\delta_1}{\partial\theta_2}\right)^2 c_1+\left(\frac{\partial\delta_1}{\partial\theta_2}\right)^2 c_4 & \left(\frac{\partial\delta_4}{\partial\theta_2}\cdot c_4\right)\frac{\partial\delta_4}{\partial y_4} \\ 0 & \left(\frac{\partial\delta_2}{\partial y_2}\cdot c_2\right)\frac{\partial\delta_2}{\partial y_3}+\left(\frac{\partial\delta_4}{\partial y_4}\cdot c_4\right)\frac{\partial\delta_4}{\partial y_3} & \left(\frac{\partial\delta_2}{\partial y_2}\cdot c_2\right)\frac{\partial\delta_2}{\partial\theta_1} & \left(\frac{\partial\delta_4}{\partial y_4}\cdot c_4\right)\frac{\partial\delta_4}{\partial\theta_2} & \left(\frac{\partial\delta_2}{\partial y_2}\right)^2 c_2+\left(\frac{\partial\delta_4}{\partial y_4}\right)^2 c_4 \end{bmatrix}$$

$$\boldsymbol{C}=\begin{bmatrix} (0)^2 c_3 & (1\cdot c_3)(-1) & 0 & 0 & 0 \\ (-1\cdot c_3)(1)^2 & (-1)^2 c_3+(1)^2 c_2+(1)^2 c_4 & (1)^2 c_2 & (1\cdot c_4)(0.0986) & (1\cdot c_2)(-1)+(1\cdot c_4)(-1) \\ 0 & (0.0742\cdot c_2)(1) & (0.0742)^2 c_1+(0.0742)^2 c_2 & (0.0279)^2 c_1 & (0.0742\cdot c_2)(-1) \\ 0 & (0.0986\cdot c_4)(1) & (0.03992\cdot c_1)(0.0279) & (0.0279)^2 c_1+(0.0986)^2 c_4 & -0.0986 c_4 \\ 0 & (-1\cdot c_2)(1)+(-1\cdot c_4)(1) & (-1\cdot c_2)(0.0742) & (-1\cdot c_4)0.0986 & (-1)^2 c_2+(-1)^2 c_4 \end{bmatrix}$$

$$\boldsymbol{C}=\begin{bmatrix} c_3 & -c_3 & 0 & 0 & 0 \\ -c_3 & c_3+c_2+c_4 & c_2 & 0.0986 c_4 & -c_2-c_4 \\ 0 & 0.0742 c_2 & 0.00551 c_1+c_2 & 0.000778 c_1 & -0.0742 c_2 \\ 0 & 0.0986 c_4 & 0.00109 c_1 & 0.000778 c_1+0.00972 c_4 & -0.0986 c_4 \\ 0 & -c_2-c_4 & -0.0742 c_2 & -0.0986 c_4 & c_2+c_4 \end{bmatrix}$$

Appendix O. Derivation of the generalized stiffness matrix $\boldsymbol{K}$

$$\boldsymbol{K}=\begin{bmatrix} \left(\frac{\partial\delta_3}{\partial y_1}\right)^2 k_3 & \left(\frac{\partial\delta_3}{\partial y_1}\cdot k_3\right)\frac{\partial\delta_3}{\partial y_3} & 0 & 0 & 0 \\ \left(\frac{\partial\delta_3}{\partial y_3}\cdot k_3\right)\frac{\partial\delta_3}{\partial y_1} & \left(\frac{\partial\delta_3}{\partial y_3}\right)^2 k_3+\left(\frac{\partial\delta_2}{\partial y_3}\right)^2 k_2+\left(\frac{\partial\delta_4}{\partial y_3}\right)^2 k_4 & \left(\frac{\partial\delta_2}{\partial y_3}\right)^2 k_2 & \left(\frac{\partial\delta_4}{\partial y_3}\cdot k_4\right)\frac{\partial\delta_4}{\partial\theta_2} & \left(\frac{\partial\delta_2}{\partial y_3}\cdot k_2\right)\frac{\partial\delta_2}{\partial y_2}+\left(\frac{\partial\delta_4}{\partial y_3}\cdot k_4\right)\frac{\partial\delta_4}{\partial y_4} \\ 0 & \left(\frac{\partial\delta_2}{\partial\theta_1}\cdot k_2\right)\frac{\partial\delta_2}{\partial y_3} & \left(\frac{\partial\delta_1}{\partial\theta_1}\right)^2 k_1+\left(\frac{\partial\delta_2}{\partial\theta_1}\right)^2 k_2 & \left(\frac{\partial\delta_1}{\partial\theta_1}\right)^2 k_1 & \left(\frac{\partial\delta_2}{\partial\theta_1}\cdot k_2\right)\frac{\partial\delta_2}{\partial y_2} \\ 0 & \left(\frac{\partial\delta_4}{\partial\theta_2}\cdot k_4\right)\frac{\partial\delta_4}{\partial y_3} & \left(\frac{\partial\delta_1}{\partial\theta_2}\cdot k_1\right)\frac{\partial\delta_1}{\partial\theta_1} & \left(\frac{\partial\delta_1}{\partial\theta_2}\right)^2 k_1+\left(\frac{\partial\delta_1}{\partial\theta_2}\right)^2 k_4 & \left(\frac{\partial\delta_4}{\partial\theta_2}\cdot k_4\right)\frac{\partial\delta_4}{\partial y_4} \\ 0 & \left(\frac{\partial\delta_2}{\partial y_2}\cdot k_2\right)\frac{\partial\delta_2}{\partial y_3}+\left(\frac{\partial\delta_4}{\partial y_4}\cdot k_4\right)\frac{\partial\delta_4}{\partial y_3} & \left(\frac{\partial\delta_2}{\partial y_2}\cdot k_2\right)\frac{\partial\delta_2}{\partial\theta_1} & \left(\frac{\partial\delta_4}{\partial y_4}\cdot k_4\right)\frac{\partial\delta_4}{\partial\theta_2} & \left(\frac{\partial\delta_2}{\partial y_2}\right)^2 k_2+\left(\frac{\partial\delta_4}{\partial y_4}\right)^2 k_4 \end{bmatrix}$$

$$\boldsymbol{K}=\begin{bmatrix} (0)^2k_3 & (1\cdot k_3)(-1) & 0 & 0 & 0 \\ (-1\cdot k_3)(1)^2 & (-1)^2k_3+(1)^2k_2+(1)^2k_4 & (1)^2k_2 & (1\cdot k_4)(0.0986) & (1\cdot k_2)(-1)+(1\cdot k_4)(-1) \\ 0 & (0.0742\cdot k_2)(1) & (0.0742)^2k_1+(0.0742)^2k_2 & (0.0279)^2k_1 & (0.0742\cdot k_2)(-1) \\ 0 & (0.0986\cdot k_4)(1) & (0.03992\cdot k_1)(0.0279) & (0.0279)^2k_1+(0.0986)^2k_4 & -0.0986k_4 \\ 0 & (-1\cdot k_2)(1)+(-1\cdot k_4)(1) & (-1\cdot k_2)(0.0742) & (-1\cdot k_4)0.0986 & (-1)^2k_2+(-1)^2k_4 \end{bmatrix}$$

$$\boldsymbol{K}=\begin{bmatrix} k_3 & -k_3 & 0 & 0 & 0 \\ -k_3 & k_3+k_2+k_4 & k_2 & 0.0986k_4 & -k_2-k_4 \\ 0 & 0.0742k_2 & 0.00551k_1+k_2 & 0.000778k_1 & -0.0742k_2 \\ 0 & 0.0986k_4 & 0.00109k_1 & 0.000778k_1+0.00972k_4 & -0.0986k_4 \\ 0 & -k_2-k_4 & -0.0742k_2 & -0.0986k_4 & k_2+k_4 \end{bmatrix}$$

Appendix P. Final mass ($\boldsymbol{M}$), stiffness ($\boldsymbol{K}$), and damping ($\boldsymbol{C}$) matrices of the free (F) and constrained (C) degrees-of-freedom.

Mass Matrices

$$\boldsymbol{M}_{FF} = \begin{bmatrix} 35 & 0 & 0 & 0 & 0 \\ 0 & 0.98 & 0.0109 & 0.0338 & 0 \\ 0 & 0.0109 & 0.00741 & 0 & 0 \\ 0 & 0.0338 & 0 & 0.00194 & 0 \end{bmatrix}$$

$$\boldsymbol{M}_{FC} = \begin{bmatrix} 0 \\ 0 \\ 0 \\ 0 \end{bmatrix}$$

$$\boldsymbol{M}_{CF} = [0 \quad 0 \quad 0 \quad 0 \quad 0]$$

Stiffness Matrices

$$\boldsymbol{K}_{FF} = \begin{bmatrix} k_3 & -k_3 & 0 & 0 & 0 \\ -k_3 & k_3 + k_2 + k_4 & k_2 & 0.0986k_4 & -k_2 - k_4 \\ 0 & 0.0742k_2 & 0.00551k_1 + k_2 & 0.000778k_1 & -0.0742k_2 \\ 0 & 0.0986k_4 & 0.00109k_1 & 0.000778k_1 + 0.00972k_4 & -0.0986k_4 \end{bmatrix}$$

$$\boldsymbol{K}_{FC} = \begin{bmatrix} 0 \\ -k_2 - k_4 \\ -0.0742k_2 \\ -0.0986k_4 \end{bmatrix}$$

$$\boldsymbol{K}_{CF} = [0 \quad -k_2 - k_4 \quad -0.0742k_2 \quad -0.0986k_4 \quad k_2 + k_4]$$

Damping Matrices

$$\boldsymbol{C}_{FF} = \begin{bmatrix} c_3 & -c_3 & 0 & 0 & 0 \\ -c_3 & c_3 + c_2 + c_4 & c_2 & 0.0986c_4 & -c_2 - c_4 \\ 0 & 0.0742c_2 & 0.00551c_1 + c_2 & 0.000778c_1 & -0.0742c_2 \\ 0 & 0.0986c_4 & 0.00109c_1 & 0.000778c_1 + 0.00972c_4 & -0.0986c_4 \end{bmatrix}$$

$$\boldsymbol{C}_{FC} = \begin{bmatrix} 0 \\ -c_2 - c_4 \\ -0.0742c_2 \\ -0.0986c_4 \end{bmatrix}$$

$$\boldsymbol{C}_{CF} = [0 \quad -c_2 - c_4 \quad -0.0742c_2 \quad -0.0986c_4 \quad c_2 + c_4]$$